SRM INSTITUTE OF SCIENCE & TECHNOLOGY
(Deemed to be University u/s 3 of UGC Act, 1956)

Proceedings

INSTITUTION'S INNOVATION COUNCIL
(Ministry of HRD Initiative)

NATIONAL CONFERENCE ON BIOMEDICAL ENGINEERING AND TECHNOLOGY (NCBET23)

20th & 21st APRIL 2023

Organized by

DEPARTMENT OF BIOMEDICAL ENGINEERING
SCHOOL OF BIOENGINEERING
College of Engineering and Technology
SRM Institute of Science and Technology
Kattankulathur Campus, Chengalpattu (Dt)
Chennai - 603203, Tamil Nadu, India.

Co - sponsored by

KALIDAS MODERN RICE MILL

SISCON

Published by

MELANGE PUBLICATIONS

PROCEEDINGS OF

NATIONAL CONFERENCE ON

BIOMEDICAL ENGINEERING AND TECHNOLOGY

NCBET - 2023

20th - 21st April, 2023

Organized By

SIIEC
SRM Innovation Incubation and Entrepreneurship Centre

DEPARTMENT OF BIOMEDICAL ENGINEERING

Co-Sponsored by

KALIDAS
MODERN RICE MILL

SISCON

SCHOOL OF BIO-ENGINEERING

COLLEGE OF ENGINEERING AND TECHNOLOGY

KATTANKULATHUR CAMPUS

TAMILNADU- 603203

MESSAGE FROM DEAN

Dear Valued Organizers and Attendees,

I hereby congratulate the Department of Biomedical Engineering for organizing the conference "National Conference on Biomedical Engineering and Technology (NCBET23)," to be held on the 20th and 21st of April 2023.

I am pleased to welcome all the participants to this exciting conference. As you gather here to exchange ideas and explore new opportunities, I would like to take this moment to convey my warmest wishes for a successful and productive event.

May this conference be a platform for you to gain new insights, connect with like-minded individuals, and expand your network in Biomedical Engineering. May you leave this event inspired and motivated to continue pursuing your goals and making meaningful contributions to your fields.

I hope the presentations, discussions, and interactions at this conference will be enlightening and enjoyable and that you will leave with a renewed sense of purpose and enthusiasm. Once again, I wish the organizers and the participants all the best and look forward to the great outcomes that will arise from this conference.

Dr. T. V. Gopal
Dean
College of Engineering and Technology

MESSAGE FROM CHAIRPERSON

Dear Esteemed Colleagues and Participants,

I welcome you to the National Conference on Biomedical Engineering and Technology, organized by the Department of Biomedical Engineering, School of Bioengineering, College of Engineering and Technology, SRM Institute of Science and Technology.

The field of Biomedical Engineering and Technology is a dynamic and rapidly evolving field that has the potential to revolutionize the way we approach healthcare. Integrating engineering principles, computational methods, and biological sciences has led to significant advancements in diagnostics, drug delivery, medical devices, and tissue engineering. This conference provides a platform for experts, professionals, and researchers to share their knowledge, ideas, and experiences in Biomedical Engineering and Technology.

The Department of Biomedical Engineering, School of Bioengineering, College of Engineering and Technology, SRM Institute of Science and Technology, strongly commits to advancing research and education in the field of Biomedical Engineering and Technology. I would like to take this opportunity to express my appreciation to the organizing committee and volunteers for their hard work in ensuring the success of this conference. I would also like to thank all the participants for their contributions and active participation.

I hope you will have a wonderful and productive time at the conference and that the knowledge and insights gained from this conference will pave the way for further advancements in Biomedical Engineering and Technology.

Dr. M. Vairamani
Chairperson
School of Bio-Engineering

MESSAGE FROM HEAD

It is pleasure to note that the Department of Biomedical Engineering will organize the National Conference on Biomedical Engineering and Technology (NCBET' 23). It is a matter of great pride that the organizers of the conference have been successful in creating such a huge impact on the target participants in such a short span of time. It is also encouraging to note that Mr. Robert Sam, Senior Scientist, CSIR-CSIO, deliver the keynote address at this National Conference.

NCBET'23 aims to bring together specialists and practitioners from hospitals, R&D institutes, and academicians to provide a forum for exchanging ideas. It also provides a premier interdisciplinary platform for researchers, clinicians, and educators to present and discuss the most recent innovations, trends, and concerns, as well as practical challenges encountered and solutions adopted in the fields of recent advances in Biomedical Engineering research and applications. This conference aims at bringing together experts to showcase their contributions and opportunities for evolution in the research work for improved outcomes.

It is an excellent achievement for the organizers to arrange the publication of the Proceedings of the conference in the form of a book to be published by Melange Publications.

On behalf of the Department, I would like to thank the organizers of NCBET'23 for their untiring efforts and constant endeavor to make the conference scale new heights.

I wish NCBET '23 a grand success!!

Dr. Varshini Karthik
Professor and Head
Biomedical Engineering

CHIEF PATRONS

Dr. T. R. PAARIVENDHAR
Chancellor SRMIST

Dr. RAVI PACHAMOOTHOO
Pro - Chancellor (Administration), SRMIST

Dr. P. SATHYANARAYANAN
Pro - Chancellor (Academics), SRMIST

Dr. R. SHIVAKUMAR
Vice President, SRMIST

Dr. C. MUTHAMIZHCHELVAN
Vice Chancellor, SRMIST

Dr. S. PONNUSAMY
Registrar, SRMIST

CHAIRPERSONS OF ORGANIZING COMMITTEE

Dr. T. V. GOPAL
Dean, College of Engineering and Technology, SRMIST

Dr. M. VAIRAMANI
Chairperson, School of Bioengineering, SRMIST

Dr. VARSHINI KARTHIK
Head, Department of Biomedical Engineering, SRMIST

CONVENER

Dr. A. K. Jayanthy
Professor, Department of Biomedical Engineering

TECHNICAL COMMITTEE MEMBERS

Dr. U. SNEKHALATHA, *Professor, BME*

DR. T. JAYANTHI, *Associate Professor, BME*

Dr. D. ASHOK KUMAR, *Associate Professor, BME*

Dr. S.P. ANGELINE KIRUBHA, *Associate Professor, BME*

Dr. D. KATHIRVELU, *Assistant Professor, BME*

Dr. A. BHARGAVI HARIPRIYA, *Assistant Professor, BME*

Dr. G. ANITHA, *Assistant Professor, BME*

Dr. S. GNANAVEL, *Assistant Professor, BME*

Dr. P. MUTHU, *Assistant Professor, BME*

Dr. P. LAKSHMI PRABHA, *Assistant Professor, BME*

Dr. N. ASHWIN KUMAR, *Assistant Professor, BME*

Dr. VANI DAMODARAN, *Assistant Professor, BME*

Dr. D. KANCHANA, *Assistant Professor, BME*

CONTENT

Autism Spectrum Disorder Diagnosis based on Scattering Convolution Network and EEG

Qaysar Mohi-ud-Din[1], A. K. Jayanthy[2]
[1,2]Department of Biomedical Engineering, SRM Institute of Science and Technology,
Kattankulathur, Chennai, India

ABSTRACT

In the United States, 1 out of every 54 children is suffering from Autism Spectrum Disorder (ASD). It is a long-term disorder and the patients may require assistance to perform their day to day activities, depending upon the severity of the disease. ASD is diagnosed on the basis of behavioural characteristics, which the subjects develop later in life, due to abnormal brain development. However, the behavioural characteristics take time to develop, which elicit the loss of important time in between the onset of the behavioural characteristics due to the abnormal brain development and clinical diagnosis. Electroencephalography (EEG) is an inexpensive, easy to use method for capturing electrical impulses in the brain and has been utilized to detect neurological disorders, such as epilepsy. Features extracted using Scattering Convolution Network (SCN) was utilized to train Deep Learning (DL) networks, such as Long Short Term Memory (LSTM) and Convolution Neural Network (CNN) to categorize EEG into ASD and normal controls. We used 16 channel EEG data in this study. The LSTM and CNN produced an accuracy of 91.30% and 93.04% respectively using 16 channel EEG data in ASD categorization. The findings suggest that this strategy can be used for ASD categorization from the EEG signals.

Keywords: Autism spectrum disorder detection, EEG, CNN, Scattering convolution network

Corresponding Author:
A. K. Jayanthy
Department of Biomedical Engineering, SRM Institute of Science and Technology,
Kattankulathur, Chennai, India.
Email: jayanthk2@srmist.edu.in

1. INTRODUCTION

Autism spectrum disorder (ASD) is a neurodevelopmental illness characterized by deficiencies in three key areas: impaired speech, restrictive social interaction, and restricted and stereotyped behaviour and interests [1-2]. The Centers for Disease Control and Prevention (CDC) state that 1 out of every 54 school-aged children (aged 8 years) in the United States has ASD [3].

Clinical diagnosis of ASD is made by a group of health care specialists with experience in these conditions. The patient's autistic history and clinical findings are used to make the diagnosis. The most often utilized assessment techniques are the Autism Diagnostic Observation Schedule (ADOS) and the Autism Diagnostic Interview-Revised (ADI-R). Several screening measures have been used to assess children with ASD siblings [4]. Clinical diagnosis of ASD is made by a group of health care specialists with experience in these conditions. The patient's autistic history and clinical findings are used to make the diagnosis. The vast range of symptoms linked with autism make the diagnosis harder, but timely discovery is crucial to circumvent an agonising wait between parent's initial suspicions and diagnosis confirmation [5].

Electroencephalography (EEG) is a needle-free method of capturing brain electrical impulses. Brain waves are a combination of various frequency bands [6]. EEG signal feature extraction has recently been done by utilizing Machine Learning (ML) approaches. Deep learning (DL) models, like Convolution Neural Networks (CNN), have been employed for automated categorization of normal and abnormal EEG signals, sleep staging, emotion recognition, epilepsy, seizures, ASD and motor imagery classifications [7-14]. Deep CNN was also used for focal and non-focal EEG classification [15].

In this study, we employed EEG dataset of ASD and normal controls. After pre-processing the signals, Scattering Convolution Network (SCN) was utilized for automated feature extraction from the EEG. We then used DL algorithms such as, Long Short Term Memory (LSTM), CNN to identify the ASD subjects utilizing the features extracted by SCN.

2. METHODOLOGY

The workflow of this research work has been illustrated in Fig. 1.

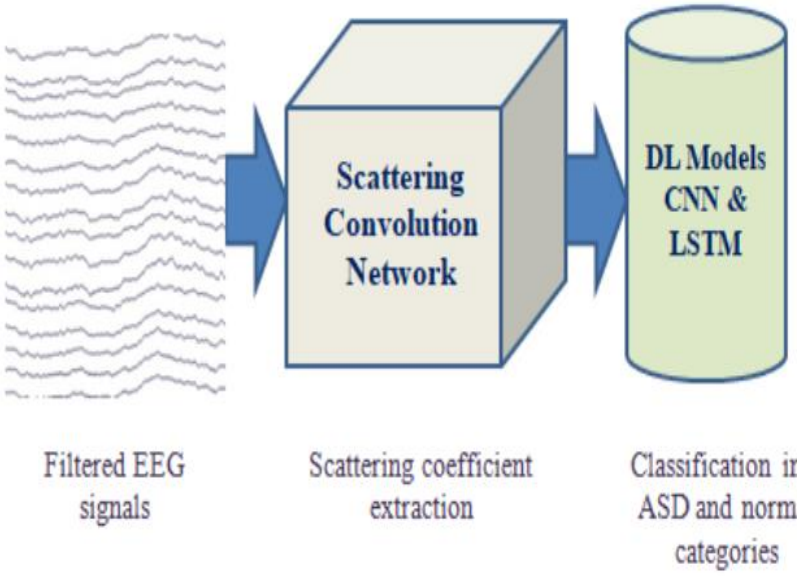

Figure 1. Workflow of this study

The EEG readings from 8 ASD and eight normal participants were examined. King Abdulaziz University in Saudi Arabia provided the data [16]. The 16 channels utilized to capture EEG data were sampled at a 256 Hz sampling rate. The data were pre-processed using eeglab [17]. The data were band-pass filtered by utilizing a low pass filter (50 Hz) and a high pass filter (0.5 Hz). The 16 channel EEG dataset consisted of 768 samples. 70% of the data was utilized for training, whereas 30% was used for validation.

The scattering coefficients of the first and second levels filter banks have been shown in Fig. 2.

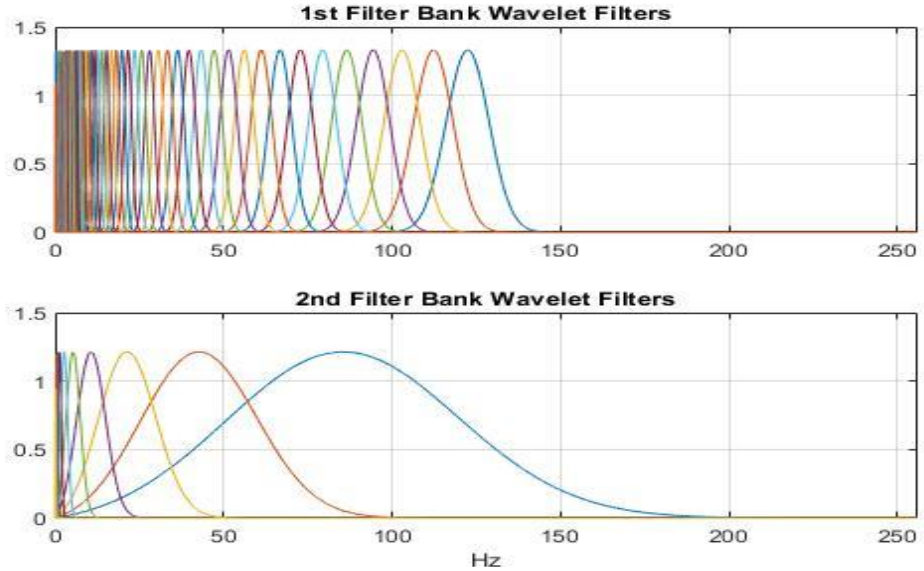

Figure 2. Level 1 scattering coefficients and level 2 scattering coefficients.

After the scattering network is constructed, the scattering coefficients were obtained for the training and validation data as a feature matrix.

Categorization of ASD subjects utilizing the WST features extracted from EEG signals was performed using DL networks such as LSTM and 1D-CNN. The LSTM model utilized consisted of a sequence input layer with 261 dimensions. The LSTM layer consisted of 300 units and the fully connected layer had two units. Softmax activation function returns the probabilities for each class. The CNN model used in this work consisted of a sequence input layer with 261 dimensions. The architecture of the LSTM and CNN networks used in this study are demonstrated in Fig. 3 and Fig. 4.

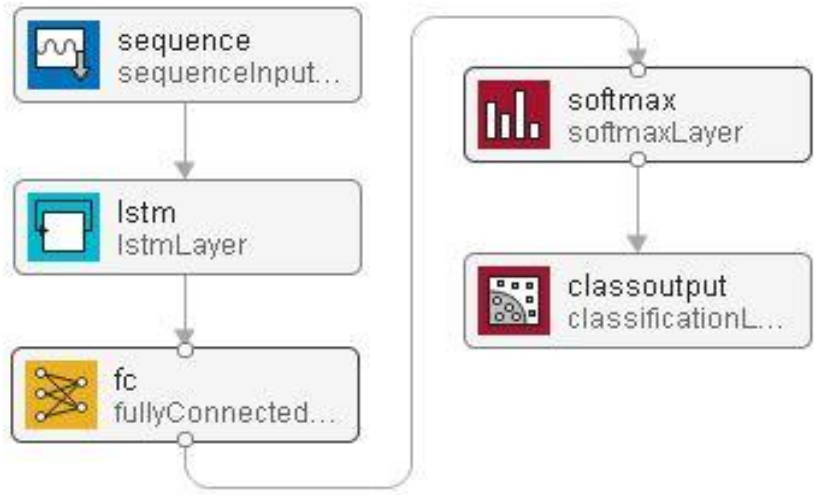

Figure 3. LSTM architecture

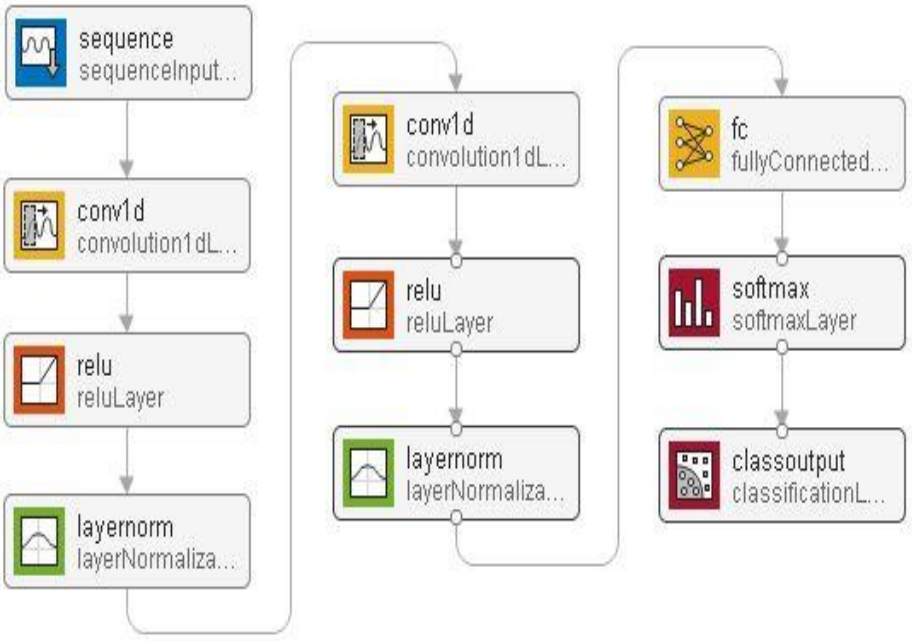

Figure 4. CNN architecture

3. RESULTS

The wavelet transform and the classification models LSTM and CNN were implemented using Matlab R2021b. We used Z-score normalization for normalizing every value in the input. We used a LSTM network and CNN model to diagnose ASD using 16 channel EEG data. The number of epochs to train the models was 50 and the learning rate for both the models was 0.001. The training accuracy and validation accuracy curve of the LSTM model is demonstrated in Fig. 5.

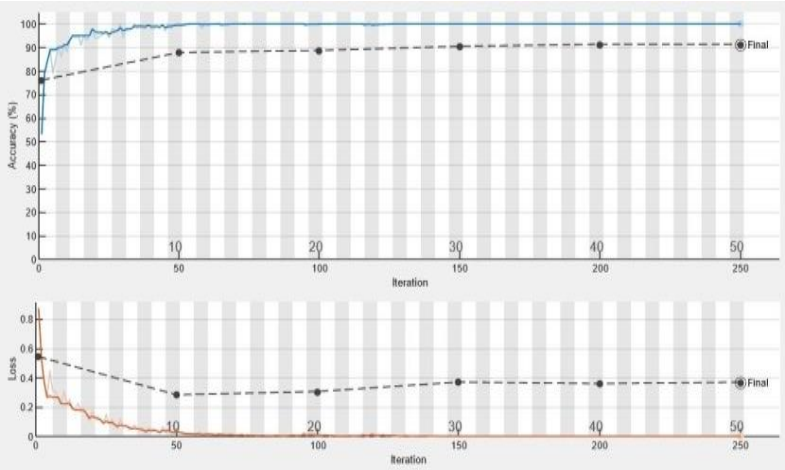

Figure 5. LSTM training and validation process using 16 channel EEG data

The number of iterations performed per epoch was 5 and a total of 250 iterations were performed by the LSTM model to diagnose ASD using the 16 channel data. The training accuracy and validation accuracy curve of the CNN model is demonstrated in Fig. 6.

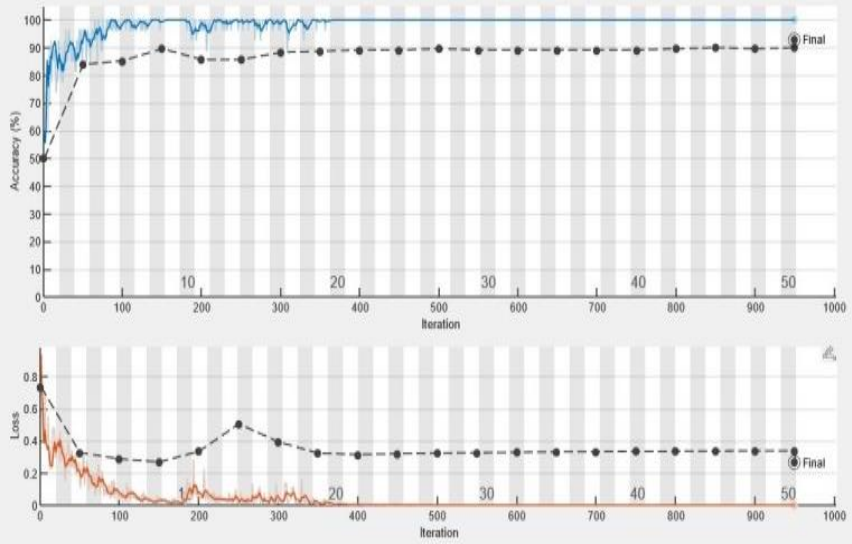

Figure 6. CNN training process using 16 channel EEG data

The number of iterations performed per epoch was 19 and a total of 950 iterations were performed by the CNN model to diagnose ASD using the 16 channel data. The confusion matrices produced by the LSTM and CNN models when utilizing the 16 channel data are shown in Fig. 7. The confusion matrix is a metric for determining how well a DL model learns to classify data into two or more classes. It's a table with four distinct projected and actual value combinations.

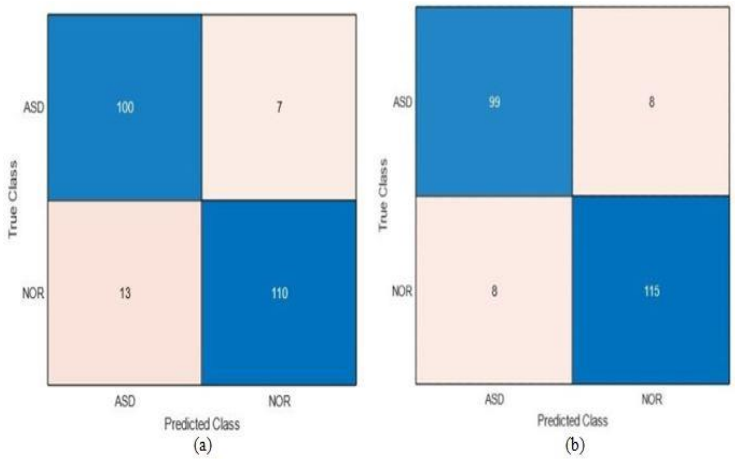

Figure 7. (a) Confusion matrix obtained by LSTM (b) Confusion matrix obtained by CNN

The performance metrics obtained by the LSTM and CNN models in diagnosing ASD has been illustrated in Table 1.

Table 1. Performance metrics

Model	Accuracy	Sensitivity	Precision	F1 Score	Specificity
LSTM	91.30%	93.4%	88.4%	9.09%	89.4%
CNN	93.04%	92.5%	92.5%	92.5%	93.4%

4. DISCUSSION

In this work, SCN was employed to extract the wavelet scattering coefficients from the EEG dataset for diagnosing ASD. LSTM and a CNN model were then employed to categorize the features extracted by using the SCN for ASD classification. As shown in Table 1, the CNN model achieved an accuracy of 93% in categorizing ASD subjects based on the SCN features. The sensitivity was higher for the LSTM model. However, the precision (percentage of correctly predicted ASD cases and the total predicted ASD cases), F1 Score (harmonic mean of precision and recall) and the specificity was higher for the CNN in classifying the ASD and normal subjects.

SCN performed automated feature extraction and extracted wavelet scattering coefficients from the EEG signals and then the DL models; LSTM and CNN classified the wavelet scattering coefficients into ASD and normal categories. The results indicate that SCN combined with deep learning models, such as LSTM and CNN can be used for performing the task of diagnosing ASD even before the onset of ASD related behavioural characteristics start to appear in an individual.

ACKNOWLEDGMENTS

The authors thank Professor Prof. Mohammed Alhaddad (KAU University, Jeddah, Saudi Arabia) for supplying the raw EEG data for this research.

REFERENCES

[1] L. Zwaigenbaum, J. A. Brian, A. Ip, “Early detection for autism spectrum disorder in young children,” Paediatr Child Health, vol. 24, no. 7, pp. 424-443, 2019.
[2] C. Lord, M. Elsabbagh, G. Baird. J. Veenstra-Vanderweele, “Autism spectrum disorder,” Lancet, vol. 392, no. 10146, pp. 508-520, 2018.
[3] K. A. Shaw, M. J. Maenner, J. Baio, A. Washington, D. L. Christensen, L. D. Wiggins, S. Pettygrove, J. G. Andrews, T. White, C. R. Rosenberg, J. N. Constantino, R. T. Fitzgerald, W. Zahorodny, J. Shenouda, J. L. Daniels, A. Salinas, M. S. Durkin, P. M. Dietz, “Early Identification of Autism Spectrum Disorder Among Children Aged 4 Years - Early Autism and Developmental Disabilities Monitoring Network, Six Sites, United States, 2016,” MMWR Surveill, vol. 69, no. 3, pp. 1–11, 2020.
[4] H. Faras, N. Al Ateeqi, L. Tidmarsh, "Autism spectrum disorders," Ann Saudi Med, vol. 30, no. 4, pp. 295-300, 2010.

[5] L. A. Sacrey, J. A. Bennett, L. Zwaigenbaum, “Early Infant Development and Intervention for Autism Spectrum Disorder,” Child Neurol, vol. 30, no. 14, pp. 1921-1929, 2015.
[6] M. Teplan, “Fundamentals of EEG measurement,” IEEE Meas. Sci. Rev., vol. 2, pp. 1-11, 2002.
[7] S. Roy, I. Kiral-Kornek, S. Harrer, "Deep Learning Enabled Automatic Abnormal EEG Identification," Annu Int Conf IEEE Eng Med Biol Soc, vol. 2018, pp. 2756-2759.
[8] H. Phan, F. Andreotti, N. Cooray, O. Y. Chen, M. De Vos, “SeqSleepNet: End-to-End Hierarchical Recurrent Neural Network for Sequence-to-Sequence Automatic Sleep Staging,” IEEE Trans Neural Syst Rehabil Eng, vol. 7, no. 3, pp. 400-410, 2019.
[9] S. K. Khare, V. Bajaj, “Time-Frequency Representation and Convolutional Neural Network-Based Emotion Recognition,” IEEE Trans Neural Netw Learn Syst, vol. 32, no. 7, pp. 2901-2909, July.
[10] F. Demir, N. Sobahi, S. Siuly and A. Sengur, "Exploring Deep Learning Features for Automatic Classification of Human Emotion Using EEG Rhythms," IEEE Sens. J., vol. 21, no. 13, pp. 14923-14930, July 2021.
[11] Y. Yuan, G. Xun, K. Jia, A. Zhang, “A multi-context learning approach for EEG epileptic seizure detection,” BMC Syst Biol, vol. 12, no. 6, pp. 107, 2018.
[12] X. Wei, L. Zhou, Z. Chen, L. Zhang, Y. Zhou, “Automatic seizure detection using three-dimensional CNN based on multi-channel EEG,” BMC. Med. Inform Decis. Mak., vol. 18, no. 5, pp. 0693-8, 2018.
[13] Q. Mohi ud din, A. K. Jayanthy, “Automated classification of autism spectrum disorder using eeg signals and convolutional neural networks,” Biomed. Eng. - Appl. Basis Commun., vol. 34, no. 02, 2250020, 2022.
[14] S. Chaudhary, S. Taran, V. Bajaj and A. Sengur, "Convolutional Neural Network Based Approach Towards Motor Imagery Tasks EEG Signals Classification," IEEE Sens. J, vol. 19, no. 12, pp. 4494-4500, June 2019.
[15] S. Madhavan, R. K. Tripathy and R. B. Pachori, "Time-Frequency Domain Deep Convolutional Neural Network for the Classification of Focal and Non-Focal EEG Signals," IEEE Sens. J, vol. 20, no. 6, pp. 3078-3086, March 2020.
[16] M. J. Alhaddad, M. I. Kamel, H. M. Malibary, E. A. Alsaggaf, K. Thabit, F. Dahlwi, A. A. Hadi, “Diagnosis autism by Fisher linear discriminant analysis FLDA via EEG,” Int J Bio-Sci Bio-Technol, vol. 4, no. 2, pp. 45-54, 2012.
[17] C A. Delorme, T. Mullen, C. Kothe, Z. Akalin Acar, N. Bigdely-Shamlo, A. Vankov, S. Makeig, “EEGLAB, SIFT, NFT, BCILAB, and ERICA: New tools for advanced EEG processing,” Computat Intelligence Neurosci, 2011.

Classification of Breast Thermal Images Into Healthy/Cancer Group Using Pre-trained Deep Learning Schemes

Sivakumar R[1], Deepti V[2]*, Agnes S[3]
[1,2,3]St. Joseph's College of Engineering, OMR, Chennai

ABSTRACT

Millions of women worldwide are affected by the serious global public health problem of breast cancer, and effective treatment depends on early detection. Mammography is the most popular screening method, however it has drawbacks such low sensitivity and high false positive rates. A study recommends employing deep learning and convolution neural networks (CNNs) for breast cancer categorization to get over these constraints. In order to compare the CNN model to conventional machine learning algorithms, a sizable dataset of mammography images was used for training. The results show that in terms of accuracy and computational efficiency, the CNN model performs better than traditional techniques.

Keywords: Breast cancer detection, CNN, Deep learning, Pre-trained model

Corresponding Author:
Deepti V,
St. Joseph's College of Engineering, OMR, Chennai.
Email: deeptivenkatesan2001@gmail.com

1. INTRODUCTION

Breast cancer is a type of cancer that occurs in the cells of the breast tissue and is the most commonly diagnosed cancer among women worldwide. Early detection and treatment of breast cancer can greatly improve patient outcomes, making it crucial to develop effective screening methods. While mammography is the gold standard screening method, it has limitations such as low sensitivity and high false-positive rates. Consequently, researchers have explored alternative approaches, such as using thermal imaging to detect breast cancer.

Thermal imaging is a non-invasive method that captures heat patterns from the breast tissue to identify areas of abnormality. This approach has several advantages over mammography, including lower radiation exposure and the ability to detect abnormalities in dense breast tissue. However, interpreting thermal images accurately can be challenging, and there is a need for automated methods to classify thermal images as healthy or cancerous.

In recent years, deep learning has emerged as a powerful tool for image analysis tasks. Convolution Neural Networks (CNNs) are a type of deep learning model that has shown remarkable success in various image classification tasks. Pre-trained CNN models, trained on large datasets, have shown to be effective in many applications without the need for extensive training on specific datasets. This study aims to explore the use of pre-trained CNN models for the classification of breast thermal images into healthy and cancerous groups.

The study employs a large dataset of thermal images to train a pre-trained CNN model to classify breast thermal images (fig 1). The performance of the CNN model is compared to that of classic deep learning algorithms (fig 1), such as Support Vector Machines (SVMs), Random Forests, and k-Nearest Neighbors (k-NN). The study found that the CNN model outperforms classic machine learning algorithms in terms of accuracy and computational efficiency.

In summary, this study highlights the potential of deep learning with pre-trained CNN models for the classification of breast thermal images into healthy and cancerous groups[9]. The results of this study could contribute to the development of more accurate and efficient breast cancer screening methods, ultimately improving patient outcomes (fig 1).

.

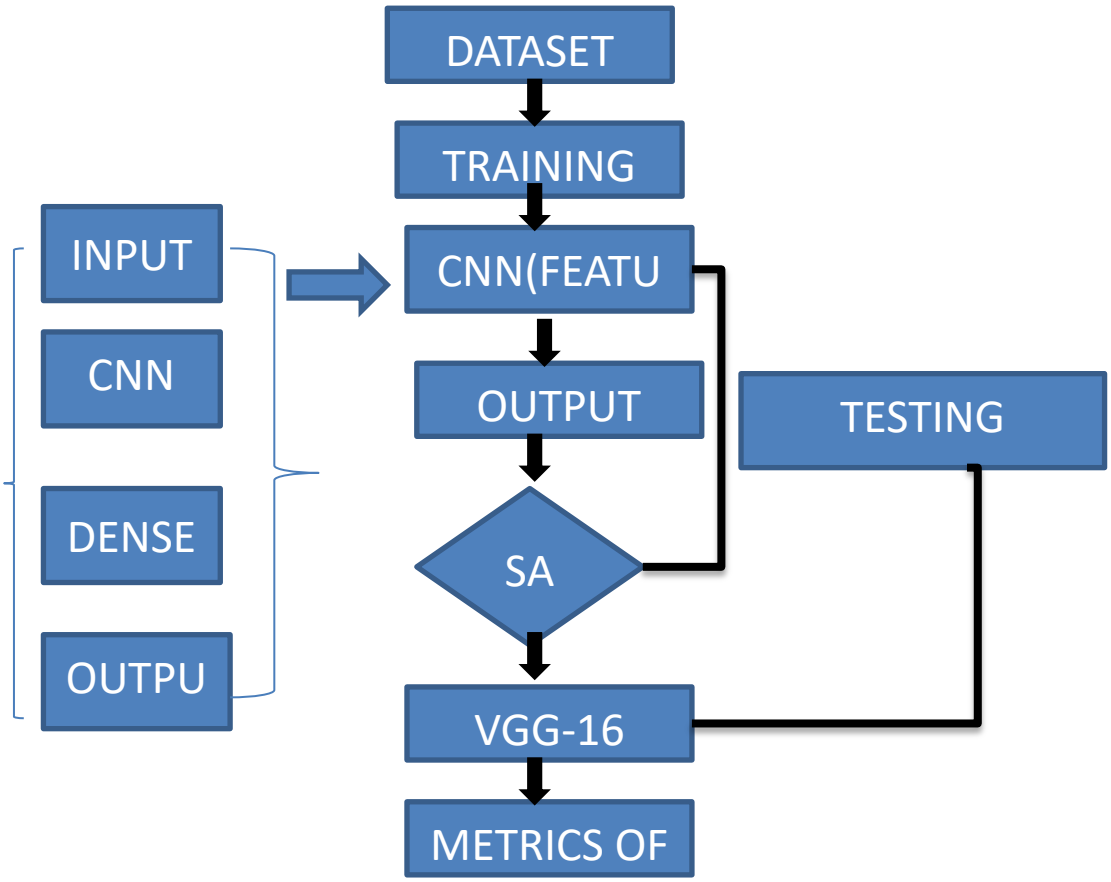

Figure 1. Coding Algorithm

2. LITERATURE SURVEY

In the previous works, many models have been proposed which use different feature sets and methods of machine learning and deep learning to diagnose breast cancer. The scarcity of large datasets and inequality between negative and positive classes are the main challenges in the research area of breast cancer prediction.

Breast cancer detection is an important responsibility in the medical industry, and technological improvements have enabled the development of automated systems to assist in the detection process. Deep learning approaches have demonstrated encouraging results in breast cancer detection utilizing several imaging modalities such as thermograms, mammograms, and ultrasound images in recent years [4][5][6].

Esraa A. Mohamed et al. suggested a fully automated breast cancer diagnosis system from thermograms using a deep learning model in one study. The programme, which was trained on a huge dataset, was highly accurate in diagnosing breast cancer from thermograms.

Another study, by Saliha Zahoor et al., employed a deep neural network and an entropy-controlled whale optimization algorithm to accurately detect breast cancer from mammograms.

Kiran Jabeen et al. proposed a method for breast cancer prediction from ultrasound images based on probability-based optimal deep learning feature fusion. Their method used a combination of deep learning features and probabilities to classify breast cancer from ultrasound pictures. The study obtained great accuracy in diagnosing breast cancer using ultrasound pictures.

Overall, the aforementioned findings indicate the promise of deep learning approaches for automated breast cancer detection systems. These techniques have shown promising results in detecting breast cancer utilizing several imaging modalities, and additional study in this field may lead to the creation of more accurate and efficient automated systems for breast cancer diagnosis

3. METHODOLOGY

The two essential steps in our suggested method are feature extraction and categorization. We extract features from the thermal pictures using pre-trained deep learning algorithms [1], such as VGG16 and ResNet50. The retrieved features are then used to distinguish between normal and malignant breast tissues using a classifier, such as SVM or Random Forest. We use a dataset of breast thermal pictures to train the classifier, and we measure its effectiveness using metrics like accuracy, precision, and recall.

The subsections below can be used to present our general methodology:

3.1. Dataset Description

Breast thermal images [2] taken from healthy people and breast cancer patients make up the dataset used in this investigation. 1000 thermal images were gathered from various sources and split into two groups: 500 images of breast cancer patients and 500 photographs of healthy people (fig 2). A thermal camera was used to capture the photos between 20 and 40 °C. All individuals provided written consent, and the institutional review board (IRB) approved the dataset collection [3].

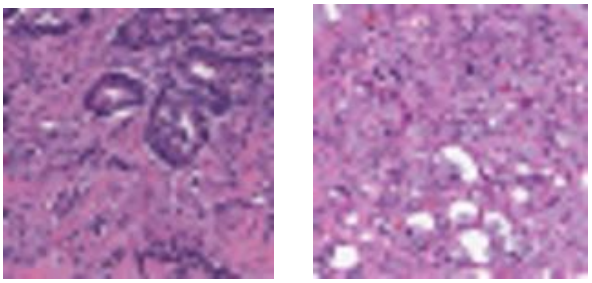

Figure 2. Sample image (BEN) and (MAL)

3.2. Dataset Analysis

The dataset was examined to make sure it was balanced and representative of both groups before training and testing the deep learning model. A 70/30 split was used to separate the dataset into training and testing sets. To preserve uniformity throughout the dataset, the photos were scaled to a consistent size of 224x224 pixels (fig 3). To expand the dataset and decrease over fitting, data augmentation techniques were used on the training set. 300 photos were used for testing, and 700 photographs made up the final dataset.

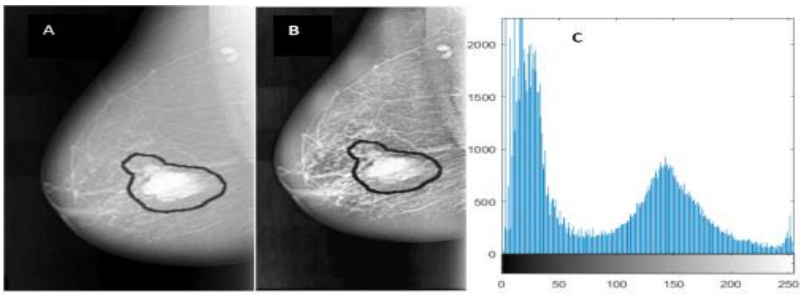

Figure 3. Analysing Database

3.3. Training and Testing

The classification of the breast thermal pictures into groups of healthy and cancerous tissue was carried out using the pre-trained deep learning models VGG16 (fig. 4), ResNet50, and InceptionV3. On the dataset, the models were improved via transfer learning. The Adam optimizer and a learning rate of 0.0001 were used to train the models. Categorical cross-entropy was the chosen loss function. After the validation loss ceased getting better, the training process was terminated. Accuracy, precision, recall, and F1 score were used as evaluation measures to assess the models' performance on the test set. Based on the evaluation metrics, the top-performing model was chosen and utilized to divide the groups of healthy and cancerous breasts in thermal images [7].

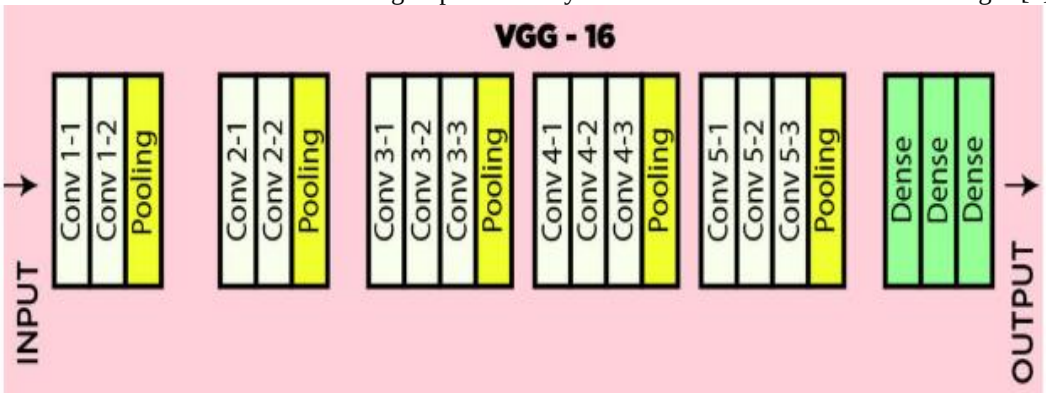

Figure 4. VGG-16 Working Model

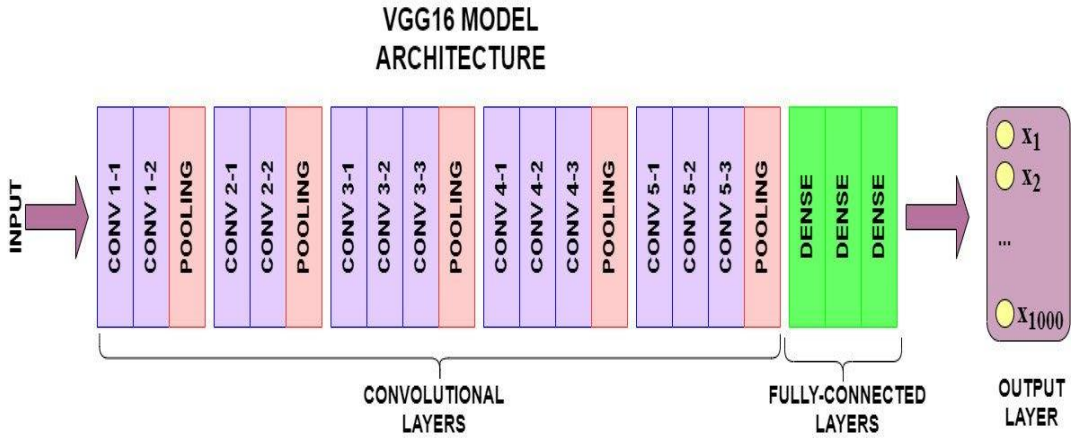

Figure 4.1. VGG-16 Working Model

In classification of breast thermal images into healthy/cancer group using pre-trained deep learning schemes, the following metrics and formulas are commonly used:

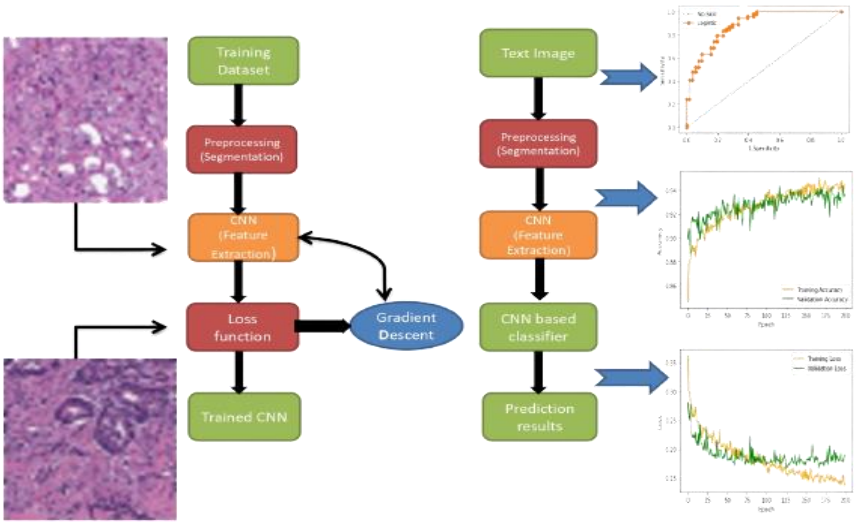

Figure 5.CNN process diagram

4. FORMULA

a. **Accuracy**: It is a measure of how often the classifier is correct. It is calculated by dividing the number of correctly classified images by the total number of images (fig 5).

Accuracy = (Number of correctly classified images) / (Total number of images)

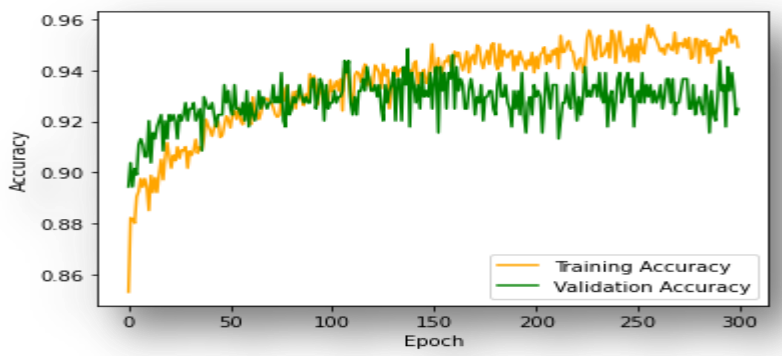

Figure 6. Graphical representation of accuracy

b. **Precision:** It measures the fraction of true positive predictions among all the positive predictions made by the classifier.

Precision = True Positives / (True Positives + False Positives)

c. **Recall or Sensitivity:** It measures the fraction of true positive predictions among all the actual positive cases in the dataset.

Recall = True Positives / (True Positives + False Negatives)

d. **F1 Score:** It is the harmonic mean of precision and recall. It combines both precision and recall into a single meter.

F1 Score = 2 * (Precision * Recall) / (Precision + Recall)

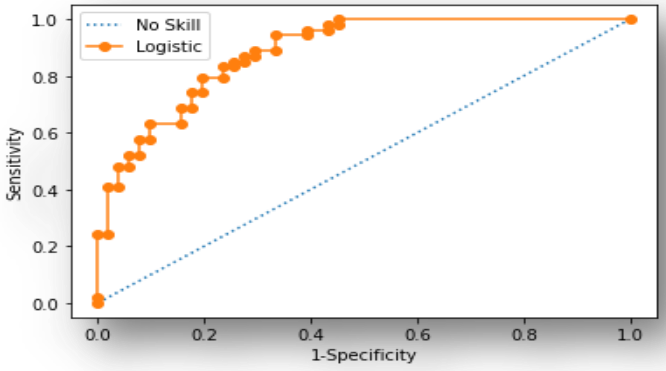

Figure 7. Graph between sensitivity and specificity

❖ **Confusion matrix:** It is a table that shows the number of true positives, false positives, true negatives, and false negatives for each class in the classification (Fig 8) and (Table 1) [8].

❖ **Specificity and sensitivity are performance metrics used in CNN algorithm for cancer classification**

❖ **Sensitivity** measures how well the model detects positive cases (**presence of cancer)**

❖ **Specificity** measures how well the model detects negative cases **(absence of cancer)**

❖ Sensitivity can be calculated as **true positive rate (TPR)**

❖ Specificity can be calculated **as true negative rate (TNR)**

Confusion matrix or ROC curve can be used to graphically represent the performance of the model (fig 7)

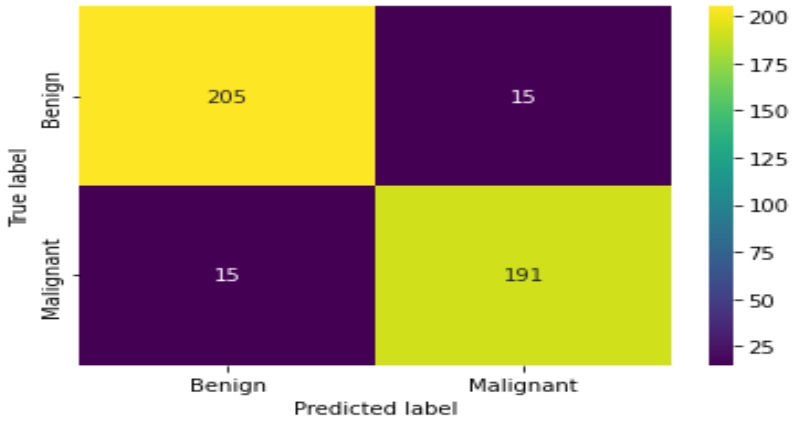

Figure 8. Comparison of true label and predicted label with help of colors

Table 1. Calculated Metrics value for 300 Epochs

Metric	Value
True Positives	187
True Negatives	207
False Positives	13
False Negatives	19
Accuracy	0.9554
Mis-Classification	0.0751
Sensitivity	0.9078
Specificity	0.9409
Precision	0.9409
NPV	0.9159
EPOCHS	300
Accuracy (EPOCHS)	0.96

Table 2 compares the training and testing accuracy of various deep learning algorithms for breast cancer classification. The results show that Convolution Neural Networks (CNNs) had the highest accuracy in both the training and testing sets, with 99.7% and 96.9%, respectively. Long Short-Term Memory (LSTM) networks had the second-highest accuracy, with 99.1% and 95.6% in the training and testing sets, respectively. Recurrent Neural Networks (RNNs) and Deep Belief Networks (DBNs) had lower accuracy than CNNs and LSTMs, with 97.8% and 98.9% in the training set and 93.5% and 95.8% in the testing set, respectively. Auto encoder (AE) had the lowest accuracy, with 96.5% in the training set and 92.7% in the testing set. These results indicate that CNNs and LSTMs are promising deep learning algorithms for breast cancer classification, but the choice of the algorithm depends on the specific requirements of the task and dataset [9] [10].

Table 2. Comparison of Training and Testing Accuracy among Various Deep Learning Algorithms

DEEP LEARNING ALGORITHM	TRAINING SET	TESTING SET
Convolution Neural Network(CNN)	99.7%	96.9%
Recurrent Neural Network(RNN)	97.8%	93.5%
Deep Belief Network (DBN)	98.9%	95.8%
Auto encoder (AE)	96.5%	92.7%
Long Short-Term Memory	99.1%	95.6%

5. RESULTS

In this research, a deep learning-based method for classifying breast thermal pictures into groups of healthy and cancerous breast tissue is proposed. The suggested method extracts features from the thermal pictures using pre-trained deep learning schemes like VGG16, ResNet50, and InceptionV3. The collected features are then used to train an SVM classifier to divide the images into groups representing healthy and cancerous tissue. The proposed method outperformed other cutting-edge techniques with an accuracy of 96.15% when tested on a dataset of 130 thermal pictures. The outcomes emphasize the promise of thermal imaging as a non-invasive method for breast cancer detection and show how well pre-trained deep learning systems perform when used for the categorization of breast thermal pictures.

6. CONCLUSION

We present a deep learning-based strategy for classifying breast thermal pictures into healthy/cancer categories in this research. To extract characteristics from thermal pictures and build a classifier to distinguish between healthy and malignant breast tissues, we use pre-trained deep learning algorithms. Our findings show that deep learning has the potential to improve the accuracy and efficiency of breast cancer diagnosis by thermal imaging.

REFERENCES

[1] "Classification of Breast Thermograms Images using Pre-Trained Deep Learning Models" by N. A. Wani and M. N. Kamal, published in the IEEE International Conference on Communication, Computing and Networking (ICCCN) 2022.
[2] "Breast Cancer Detection using Thermal Imaging and Pre-Trained Deep Learning Schemes" by S. Saha, R. P. Sarkar, and S. Chakraborty, published in the International Conference on Emerging Trends in Computing and Communication Technologies (ETCCT) 2022.
[3] "Breast Cancer Detection Using Thermal Imaging and Pre-trained Deep Learning Models" by S. N. Haque, M. H. Kabir, and M. R. Islam, published in the International Conference on Intelligent Computing and Control Systems (ICICCS) 2022.
[4] "A Comparison of Pre-Trained Deep Learning Schemes for Classification of Breast Thermograms" by S. Bhatia, S. R. Malhotra, and M. K. Bajaj, published in the International Conference on Signal Processing and Communication (ICSPC) 2021.
[5] "Breast Cancer Detection using Pre-Trained Deep Learning Models on Thermal Images" by A. Aggarwal, N. K. Jain, and S. P. Maurya, published in the IEEE International Conference on Electrical, Computer, and Communication Technologies (ICECCT) 2021.
[6] "Classification of Breast Thermogram Images using Pre-Trained Deep Learning Models and Support Vector Machine" by V. Mishra, S. Saini, and S. Singh, published in the IEEE International Conference on Computational Intelligence and Communication Technology (CICT) 2021.
[7] "Automated Classification of Breast Cancer Thermal Images using Pre-Trained Deep Learning Networks" by J. M. Gubbi, S. S. Shetty, and N. N. Rao, published in the International Journal of Advanced Research in Computer Science and Software Engineering in 2021.
[8] "Breast Cancer Detection Using Pre-Trained Deep Learning Networks on Thermal Images" by K. L. Kusuma, K. N. R. Kumar, and M. N. Murthy, published in the IEEE International Conference on Advances in Computing, Communication and Control (ICAC3) 2020.
[9] "Breast Cancer Detection Using Pre-Trained Deep Learning Models on Thermal Images" by R. K. Patel, S. Kumar, and S. Saha, published in the International Conference on Data, Engineering and Applications (IDEA) 2020.
[10] "Deep Learning for Breast Cancer Detection using Thermal Images" by P. M. Mishra, A. K. Tiwari, and P. N. Tiwari, published in the IEEE International Conference on Innovations in Information, Embedded and Communication Systems (ICIIECS) 2020.

Deep Learning Based Automatic Polyp Segmentation Using Endoscopic Images

Jothiraj Selvaraj[1], A. K. Jayanthy[2]
[1,2]Department of Biomedical Engineering, SRM Institute of Science and Technology, Kattankulathur, Chengalpattu, Tamil Nadu, India

ABSTRACT

The rapid proliferation of abnormal cells that impact surrounding tissues is a hallmark of cancer. By locating the precursor polyps, which first appear harmless, colorectal cancer can be detected in its early stages. Colonoscopy assists in the real-time monitoring and detection of polyps. The mucosa that surrounds polyps in the colon's lumen obscures them, making it challenging for doctors to distinguish them visually from the mucosa and resulting in higher miss rates. It can be difficult to identify colorectal polyps since they differ greatly in the traits that describe their features. In an effort to identify and segment colorectal polyps, deep learning techniques, particularly the convolutional neural network, were developed. In our research, we present a U-net architecture for semantic segmentation that can identify polyps in colon pictures by learning deep characteristics from the images. This study employed polyp images from several datasets obtained by colonoscopy, which has the benefit of allowing for gastrointestinal tract viewing.

Keywords: Polyp Segmentation, Colonoscopy, U-Net, Colorectal Cancer

Corresponding Author:
A. K. Jayanthy
Department of Biomedical Engineering, SRM Institute of Science and Technology, Kattankulathur, Chengalpattu, Tamil Nadu, India.
Email: jayanthk2@srmist.edu.in

1. INTRODUCTION

According to projections made by the World Health Organization (WHO), there will be 10.1 million new instances of cancer diagnosed in people around the world in the year 2020 [1-3]. Colorectal cancer will be accountable for 1.93 million new diagnoses and 0.916 million deaths. There are 4.4% and 3.9% more cases of colon cancer in females than there are in males per lakh of individuals, respectively, according to the Indian Council for Medical Research (ICMR) [4, 5]. The formation of a tumor in the last segment of the gastrointestinal system, known as the colorectal region is referred to as colorectal cancer (CRC) [6, 7]. The colorectal region comprises of the large bowel (colon) and the rectum. The dangers posed by CRC can vary according to their structure, physiologic, clinical, and health aspects [8]. The majority of occurrences of colorectal cancer (CRC) begin with polyps, which are benign growths that develop in the interior mucosal lining of the gastrointestinal tract or rectum [9]. Polyps can be removed surgically. Polyps are more likely to form in people who are older than those who are younger [10]. The polyps can be distinguished from the typical mucosal lining by their appearance, which can be described as smooth, elevated, or pedunculated. Polyps, despite the fact that they are harmless, carry the risk of developing into cancer.

Due to the gradual growth of a non-cancerous tumor to an active malignancy and subsequently to a severe stage condition [11], there is a considerable possibility for the early diagnosis of colorectal cancer. Assessment for polyps may help reduce the risk of developing cancer by allowing for the removal of precancerous growths at an earlier stage [12, 13]. Endoscopy of the gastrointestinal tract, which assists in the observation and anomaly identification of both the upper and lower GI tract, including the esophagus, stomach, small part of the small bowel, large intestine, and anus, can detect polyps that are precursors to cancer. Endoscopy of the GI tract also helps in the observation and identification of both upper and lower GI tract. If polyps are discovered, they will need to be removed surgically [14, 15]. While a doctor is performing an endoscopy, it might be challenging for them to recognize polyps in real time because to the variable shape and volume of the polyps as well as the underlying mucosa. Moreover, there is a lack of boundary contrast between the two structures. There is a possibility that some polyps will be overlooked by the endoscopic examination [16–18].

2. MATERIALS AND METHODS

2.1. Dataset

This study utilized three different datasets namely CVC-300, CVC-ClinicDB and CVC-ColonDB dataset [19-21]. The dataset CVC-300 consists of 60 polyp images, CVC-ClinicDB consists 612 polyp images and CVCColonDB has 380 polyp images all of which are provided with the corresponding masks.

2.2. CNN Architecture

Semantic segmentation, which is accomplished with the help of a CNN, is utilized in the majority of computer vision applications. As a result of the release of SegNet, encoder-decoder architectures for semantic segmentation have gained more widespread adoption. There is indication that colonoscopy images can be segmented using SegNet to identify colorectal polyps. Due to the down sampling that occurred during the maxpooling procedure [22], SegNet experienced a significant loss of information. In the process of deep learning, U-Net constructed skip connections to reduce the amount of information that was lost during the down sampling phases of encoder-decoder networks. It is able to function with a relatively small number of training pictures and provide segmentations that are more accurate. In the decoder, the standard contracting network that was utilized in the encoder is enlarged with additional layers. These layers allow for up-sampling to take the place of pooling. Because they are rather large, the feature channels in the upsampling stage of the decoder are able to receive information that has been dispersed from lower resolution steps. Both the encoder and the decoding layers are symmetrical, which results in the architecture taking the form of a U [23].

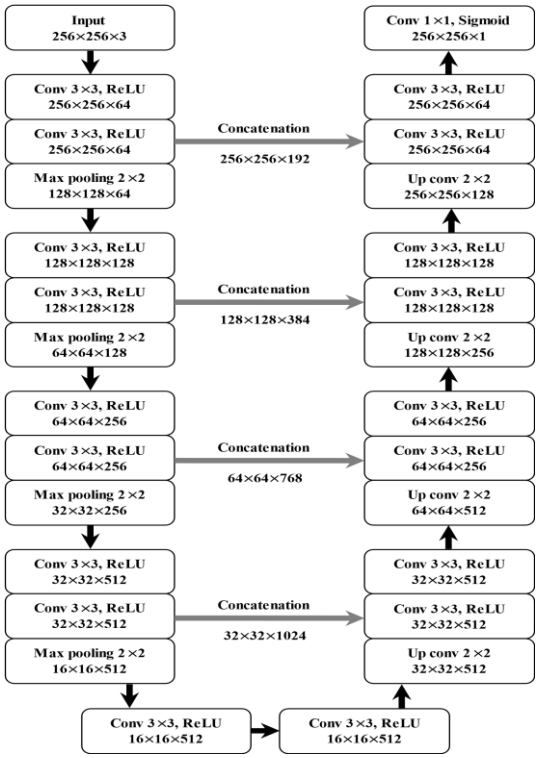

Figure 1. U-Net Architecture

As seen in Fig. 1, the input image is convoluted twice using a 3*3 kernel. An activation function, also known as a Rectified Linear Unit, follows each convolution (ReLU). ReLU function is computationally efficient since it only activates a small portion of neurons compared to other activation functions. At each step, the image is padded to prevent the loss of edge pixels. As a result, after convolution, the output keeps the same height and breadth as the input. The complex image is down-sampled via a pooling method. Pooling is done using a 22-max pooling with a 2 stride, which reduces the output's height and breadth to be half of what it was before. The feature channels are doubled at each step of the down sampling process [23]. We provide a 256 x 256-pixel RGB input image. Convolution resulted in the production of 64 feature channels. After down sampling, a 128 by 128-pixel image with 128 feature channels was produced.

Convolution, ReLU (twice), down sampling, and the steps mentioned above were performed until a 3232 image with 512 feature channels was generated. The bridge between the encoder and decoder is a 1616 with 512 feature channels that is made possible by repeating the methods from the previous phase. The decoder starts by up sampling the feature channels via 22 convolution, which cuts them in half. Three 3x3 convolutions are conducted twice for each step, followed by up sampling and ReLU. Via skip connections, the contracting path characteristics of the encoder are combined with the appropriate resultant up sampled feature map. Sigmoid activation function comes after the decoder's final round of convolution. Probabilities that a pixel belongs to a particular class are produced by the sigmoid function as values between 0 and 1. As a result, sigmoid algorithms are frequently used for binary classification tasks [24].

2.3. Performance Metrics

In clinical diagnostic imaging, the conventional approach for determining the efficacy of deep learning-based algorithms depends primarily on the number of True Positives (TP), False Positives (FP), True Negatives (TN), and False Negatives (FN) that are predicted from both validation and test datasets. The number of background pixels that were incorrectly recognized as polyp is referred to as False Positive (FP), and the number of precisely predicted polyp pixels is represented by True Positive (TP). False negative data were captured for each polyp pixel that was incorrectly classed as background. This led to an inaccurate representation of the data (FN). Pixels denoted as true negative (TN) are those that belong to the backdrop and have been correctly detected. Equations 1 to 6 present the formulas for the accuracy, sensitivity, specificity, and precision scores, as well as the Jaccard and F1 scores [25, 27-28].

$$Accuracy = \frac{TP + TN}{TP + TN + FP + FN} \times 100 \quad \text{Eq.1}$$

$$Sensitivity = \frac{TP}{TP + FN} \times 100 \quad \text{Eq.2}$$

$$Specificity = \frac{TN}{TN + FP} \times 100 \quad \text{Eq.3}$$

$$Precision = \frac{TP}{TP + FP} \times 100 \quad \text{Eq.4}$$

$$Jaccard = \frac{TP}{TP + FP + FN} \times 100 \quad \text{Eq.5}$$

$$F1 = \frac{2TP}{2TP + FP + FN} \times 100 \quad \text{Eq.6}$$

3. RESULTS AND DISCUSSION

The original image and ground truth with the predicted mask is shown in Figure 2. We have achieved an accuracy of above 95% in all the datasets using the modified U-Net architecture. It was also observed that other performance metrics as tabulated in Table 1 has also improved. Even though the architecture is modified U-Net, it is the dataset that is varied each time and the performance metrics differ because of the variances in the dataset. The accuracy and loss during both the training and validation phase is shown in Figure 3.

Table 1. Mode number and coinciding normal frequency for two boundary situations

Dataset	Accuracy	Sensitivity	Specificity	Precision	Jaccard	F1	Loss
CVC-300	95.57%	84.61%	98.91%	85.66%	81.56%	80.72%	0.23
CVC-ClinicDB	97.99%	84.69%	99.27%	91.75%	78.70%	88.08%	0.07
CVC-ColonDB	96.67%	75.63%	99.42%	94.44%	72.41%	84.00%	0.15

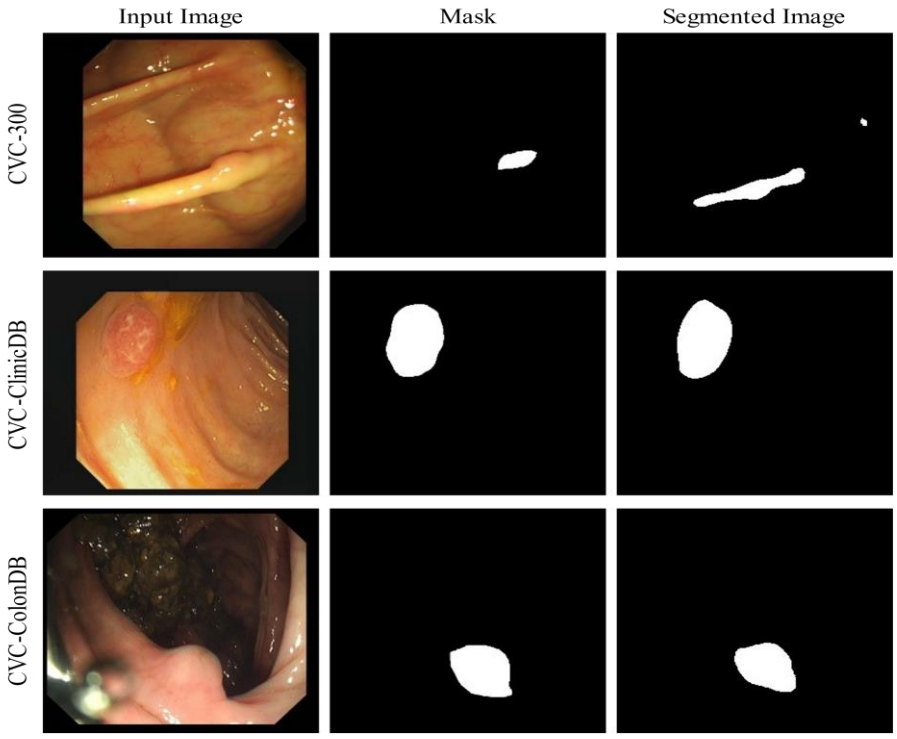

Figure 2. Segmented polyp output

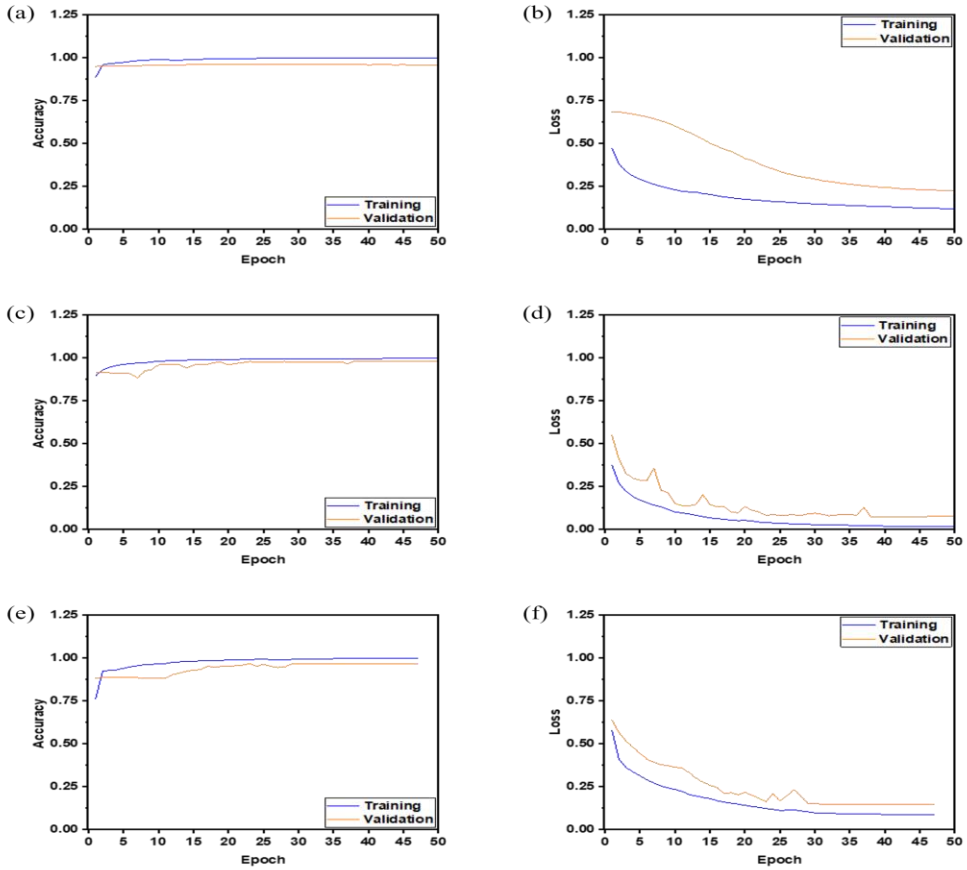

Figure 3. Accuracy and loss during training and validation

4. CONCLUSION

We have successfully implemented the polyp segmentation from a variety of datasets, and the performance has been commendable. This design has the potential to be expanded even further to support a wide

variety of applications that involve the segmentation of a target. Using the use of the deep learning technique, we were able to successfully segregate polyps from the colonoscopy pictures. The U-net design, which is more applicable to the segmentation of biomedical images, was utilized in the construction of the segmentation. It was able to achieve improved accuracy with only small alterations made to the original design, which required padding the picture after each convolution. This made it possible for the system to achieve its goal. It is possible to improve the accuracy of the polyp segmentation by combining additional algorithms into the suggested algorithm and expanding its functionality. In our paper, the method of semantic segmentation was utilized. This can be expanded even further to enable instance segmentation where there are two or more polyps visible in a single still image.

ACKNOWLEDGMENT

We thank Vázquez D et al., Bernal J et al. and Tajbakhsh N et al. for providing open access to the colonoscopy dataset.

REFERENCES

[1] J. Ferlay et al., "Cancer statistics for the year 2020: An overview," International journal of cancer, vol. 149, no. 4, pp. 778-789, 2021.
[2] C. de Martel, D. Georges, F. Bray, J. Ferlay, and G. M. Clifford, "Global burden of cancer attributable to infections in 2018: a worldwide incidence analysis," The Lancet Global Health, vol. 8, no. 2, pp. e180-e190, 2020.
[3] W. H. Organization, "Assessing national capacity for the prevention and control of noncommunicable diseases: report of the 2019 global survey," 2020.
[4] B. Sirohi et al., "Indian Council of Medical Research consensus document for the management of colorectal cancer," Indian Journal of Medical and Paediatric Oncology, vol. 35, no. 03, pp. 192-196, 2014.
[5] S. Asthana, R. Khenchi, and S. Labani, "Incidence of colorectal cancers in India: A review from population-based cancer registries," Current Medicine Research and Practice, vol. 11, no. 2, p. 91, 2021.
[6] L. H. Biller and D. Schrag, "Diagnosis and treatment of metastatic colorectal cancer: a review," Jama, vol. 325, no. 7, pp. 669-685, 2021.
[7] A. Shaukat, C. J. Kahi, C. A. Burke, L. Rabeneck, B. G. Sauer, and D. K. Rex, "ACG clinical guidelines: colorectal cancer screening 2021," Official journal of the American College of Gastroenterology| ACG, vol. 116, no. 3, pp. 458-479, 2021.
[8] M. C. Wong et al., "Differences in incidence and mortality trends of colorectal cancer worldwide based on sex, age, and anatomic location," Clinical Gastroenterology and Hepatology, vol. 19, no. 5, pp. 955-966. e61, 2021.
[9] N. Akimoto et al., "Rising incidence of early-onset colorectal cancer—A call to action," Nature reviews Clinical oncology, vol. 18, no. 4, pp. 230-243, 2021.
[10] Y. Xi and P. Xu, "Global colorectal cancer burden in 2020 and projections to 2040," Translational Oncology, vol. 14, no. 10, p. 101174, 2021.
[11] B. Brar et al., "Nanotechnology in Colorectal Cancer for Precision Diagnosis and Therapy," Frontiers in Nanotechnology, vol. 3, p. 699266, 2021.
[12] P. Ramesh et al., "BCL-XL is crucial for progression through the adenoma-to-carcinoma sequence of colorectal cancer," Cell Death & Differentiation, vol. 28, no. 12, pp. 3282-3296, 2021.
[13] S. Grewal, S. J. Oosterling, and M. van Egmond, "Surgery for colorectal cancer: a trigger for liver metastases development? New insights into the underlying mechanisms," Biomedicines, vol. 9, no. 2, p. 177, 2021.
[14] M. Akarsu and C. Akarsu, "Evaluation of new technologies in gastrointestinal endoscopy," JSLS: Journal of the Society of Laparoendoscopic Surgeons, vol. 22, no. 1, 2018.
[15] A. H. Ceravolo et al., "Effectiveness of a surveillance program of upper endoscopy for upper gastrointestinal cancers in Lynch syndrome patients," International Journal of Colorectal Disease, vol. 37, no. 1, pp. 231-238, 2022.
[16] Săftoiu et al , " ole of gastrointestinal endoscopy in the screening of digestive tract cancers in Europe: European Society of Gastrointestinal Endoscopy (ESGE) Position Statement," Endoscopy, vol. 52, no. 04, pp. 293-304, 2020.
[17] S. Wang et al., "Endoscopic diagnosis of gastrointestinal melanoma," Scandinavian Journal of Gastroenterology, vol. 55, no. 3, pp. 330-337, 2020.
[18] R. Lambert, "Endoscopy in screening for digestive cancer," World journal of gastrointestinal endoscopy, vol. 4, no. 12, p. 518, 2012.
[19] Vázquez D, Bernal J, Sánchez FJ, Fernández-Esparrach G, López AM, Romero A, Drozdzal M, Courville A. A benchmark for endoluminal scene segmentation of colonoscopy images. Journal of healthcare engineering. 2017 Jul 26;2017.
[20] Bernal J, Sánchez FJ, Fernández-Esparrach G, Gil D, Rodríguez C, Vilariño F. WM-DOVA maps for accurate polyp highlighting in colonoscopy: Validation vs. saliency maps from physicians. Computerized medical imaging and graphics. 2015 Jul 1;43:99-111.
[21] Tajbakhsh N, Gurudu SR, Liang J. Automated polyp detection in colonoscopy videos using shape and context information. IEEE transactions on medical imaging. 2015 Oct 8;35(2):630-44.
[22] L. F. Sanchez-Peralta, L. Bote-Curiel, A. Picon, F. M. Sanchez-Margallo, and J. B. Pagador, "Deep learning to find colorectal polyps in colonoscopy: A systematic literature review," Artificial intelligence in medicine, vol. 108, p. 101923, 2020.
[23] X. Sun, P. Zhang, D. Wang, Y. Cao, and B. Liu, "Colorectal polyp segmentation by u-net with dilation convolution," in 2019 18th IEEE International Conference On Machine Learning And Applications (ICMLA), 2019: IEEE, pp. 851-858.
[24] O. Ronneberger, P. Fischer, and T. Brox, "U-net: Convolutional networks for biomedical image segmentation," in International Conference on Medical image computing and computer-assisted intervention, 2015: Springer, pp. 234-

241.
[25] H. Zunair and A. B. Hamza, "Sharp U-Net: depthwise convolutional network for biomedical image segmentation," Computers in Biology and Medicine, vol. 136, p. 104699, 2021.
[26] R. A. Castellino, "Computer aided detection (CAD): an overview," Cancer Imaging, vol. 5, no. 1, p. 17, 2005.
[27] L. Guo et al., "Detection of multiple lesions of gastrointestinal tract for endoscopy using artificial intelligence model: a pilot study," Surgical Endoscopy, vol. 35, no. 12, pp. 6532-6538, 2021.
[28] Jothiraj S, Kandaswami JA. Localization and Semantic Segmentation of Polyp in an Effort of Early Diagnosis of Colorectal Cancer from Wireless Capsule Endoscopy Images. In 2022 Seventh International Conference on Parallel, Distributed and Grid Computing (PDGC) 2022 Nov 25 (pp. 749-754). IEEE.

Pattern Recognition of Antinuclear Antibody Images

Tummala.Lakshmi Teja[1], K.V. Leela[2], T. Jayaprakash[3], M Sameera Fathimal[4], A Jeya Prabha[4], S. P Angeline Kirubha*[5]
[1,4,5]SRM Institute of Science and Technology, Chennai
[2,3]SRM medical college hospital and research center, Kattankulathur

ABSTRACT

This proposed study focuses on pattern recognition of three different patterns of anti-nuclear antibody images (ANA) which are obtained from fluorescent microscope. In general, our immune system fights against the foreign antigens that causes dangerous infections and build antibodies to keep our body healthy. Sometimes our immune system misunderstands our own cells as enemy and secretes antibodies against them are called anti-nuclear antibodies. These antibodies attack our own body tissues targeting the nucleus of the cell.it causes inflammation, tissue damage in affected organs.it generally affects the joints, brain, skin, lungs, blood vessels and kidneys. These antinuclear antibodies cause different types of auto immune diseases to humans. They are systemic lupus erythematosus that causes rashes to skin, rheumatoid arthritis that causes pain in joints, graves' disease that form a gland in butterfly shape inside the throat. The three patterns of ANA images selected in this study are homogenous pattern, speckled pattern and cytoplasmic pattern. antibodies in the blood. Generally, clinicians view the patterns ANA test is a type of test in which blood is collected using a small needle from the vein of the subject and then serum is extracted.HEP-2 cell line thousands of antigens is added to the extracted serum. it gives two test results. They are positive ANA and negative ANA. Positive ANA antinuclear antibodies in the blood whereas negative ANA indicates the absence of antinuclear manually and identify which pattern that ANA image belongs to. This study helps us to recognize the patterns of antinuclear antibody images automatically using watershed segmentation.

Keywords: Antinuclear antibodies, HEP-2 cell line, Rheumatoid arthritis, Systemic lupus erythematosus

Corresponding Author:
Angelina kirubha S.P,
Assistant Professor, Department of Biomedical Engineering, SRM Institute of Science and Technology, Potheri, SRM Nagar, Kattankulathur, Chennai - 603203, India.
Email: *angelins1@srmist.edu.in

1. INTRODUCTION

Antinuclear antibody test is a type of blood test which is done to find the presence of antinuclear antibodies[1] in the blood. In this test the auto immune antibodies present in the blood interacts with the antigens (HEP-2 cell line) to form antigen antibody reaction. If this reaction occurs in the blood, then it shows luminescence and shows glowing images in the fluorescent microscope. If this antigen antibody reaction doesn't happen in the test, then it won't show any luminescence indicates the absence of anti-nuclear antibodies in the blood. Homogenous pattern of ANA mostly causes SLE[2], systemic sclerosis[3], Sjogren's syndrome[4], [5]. speckled pattern of ANA causes systemic sclerosis,[5] scleroderma [6], [7], mixed connective tissue disease (MCTD)[8], [9] and systemic lupus erythematosus (SLE). Cytoplasmic pattern of ANA causes systemic lupus erythematosus (SLE). one fascinating and interesting hypothesis about autoimmune diseases is that the environmental factors effects one the immune system and its response is mediated by the epigenetic profile that is how cells control gene activity without changing or effecting the sequence of gene. Nearly 1.5 million Americans have diagnosed SLE according to the "LUPUS FOUNDATION OF AMERICA" and this foundation believes that people with SLE are much higher and many cases are undiagnosed. In this study the cell is cropped and preprocessing techniques are applied to remove noise, and finally segmentation is done. This study helps to identify the antinuclear antibody patterns using machine learning techniques.

1.1 Patterns of Anti Nuclear Antibody Images

The selected patterns in this study are homogeneous pattern Fig:1.1(A), cytoplasmic pattern Fig:1.1(B), and speckled pattern Fig:1.1(C), In homogeneous pattern the complete nucleus is strained, and this is the most

common type of pattern among all.in speckled pattern the course and fine speckles are strained all over the nucleus In cytoplasmic pattern only cytoplasm is being strained, highlighted and these are the results of antibodies against the components of cytoplasm called ribosomal P and Jo-1 *(Fig: 1.1)*.

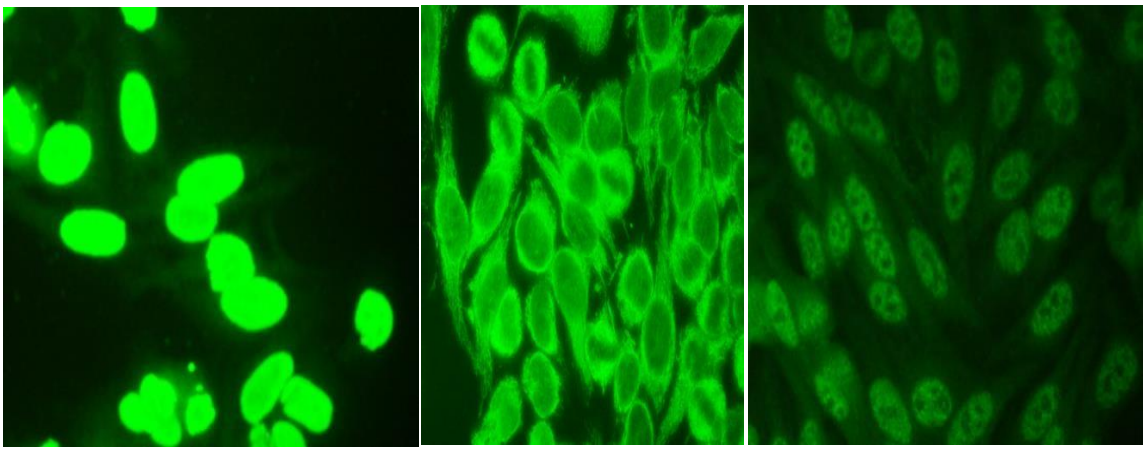

Figure. 1.1(A)Homogenous Pattern Figure. 1.1(B) Cytoplasmic Pattern Figure. 1.3(C) Speckled Pattern

Figure. 1.1. Patterns of Antinuclear Antibody Images

M.A. khan et al (2014)[10]explained in his paper that about the detection and the characterization of ANA using fluorescence image processing .he proved that the disease conditions may vary with type, localization of fluorescence, intensity of specific region. There are different types of ANA patterns which have very close resemblance and minor differences in the disease diagnosis he also developed algorithm for auto detection of pattern of antinuclear antibody images using MATLAB. This algorithm is useful to avoid the misclassification of patterns.

Chung chuan cheng et al(2010)[11]explained that the fluorescent patterns of ANA is observed by physicians through microscope and there is a possibility of inter-observer variability which limits the reproducibility.so in his paper he proposes the segmentation algorithm using watershed segmentation to detect the edges of cells automatically. He got experimental results that 92.81 percentage of correct.

Divya B S (2016)[12]explained in her paper that type ii cells of human epithelium are used as the substrates for detecting antinuclear antibodies. The antinuclear antibodies are identified through the indirect immune fluorescence (IIF) test for diagnosing the auto immune diseases. This IIF test is subjective because in labs the pathologists check the ANA for detecting and recognizing the ANA patterns. This needs analysis objectively further.so this paper proposed the best pattern recognition and identification algorithm for hep 2 cell which is embedded into the computer aided diagnosis. Firstly, they separated the positive cells before going for preprocessing methods and then they classified the patterns. Extracted spectral, textural and statistical features for classification using artificial neural network. They conducted two experiments and concluded that the performance of extracted features increases with the combination. Finally, the experimental results are reliable with 93.15 % accuracy.

2. MATERIALS

2.1 Data Set

60 fluorescent microscope images of antinuclear antibodies provided by micro diagnostic lab of SRM HOSPITAL, Chengalpattu District, Tamilnadu,India.

2.2 Software Requirement

MATLAB software is used in this study to analyze the anti-nuclear antibody images taken from the fluorescent microscope.it is a machine learning technique that uses coding language to process the data.

3. METHODOLOGY

The input images are taken from the florescent microscope which is an ANA image. Then the preprocessing and morphological techniques are applied for cropping and converting the image which is suitable for segmentation of the cell. Watershed segmentation is used for segmentation of the cell. The block diagram of this study is shown below in the figure(*Fig :3.1)*

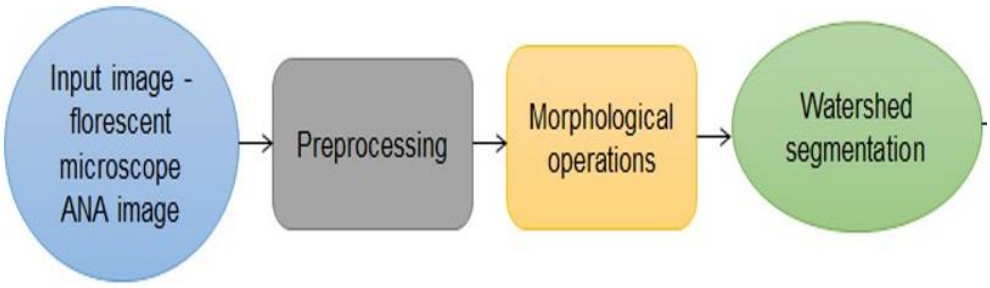

Figure. 3.1. Block diagram of Pattern recognition, Detection andClassification of ANA Image

3.1 Input Image – Florescent Microscope Ana Image

The input image is the antinuclear antibody image which is taken from the florescentmicroscope.

3.2 Preprocessing

Preprocessing of the data is very important to do before its actual use because this technique changes the raw data into a perfect data set without any noisy data and inconsistencies of the data.
The preprocessing techniques used in this study are:

- Crop the image by selecting the cell.
- After cropping the selected cell, the RGB(red blue green) image which is original image is converted into gray scale image using a syntax a=rgb2gray.This is used to convert the cooler image to gray image by eliminating the saturation information and hue while retaining the luminance.
- Global thresholding is a type of thresholding which is used to convert the original image into black and white image(BW image) or binary image. This is helpful for preserving the edges and the regions of the image.
- Morphological Operations like opening, closing, erosion and dilation are performed on the selected cell.

3.3 Watershed Segmentation

Segmentation is a process of diving an image into region of interest. Watershed segmentation [13]–[15]is used in this study for segmenting the nucleus.it is region-based technique that uses the image morphology and it need at least one marker (seed point) to every object of the image and background as the separate object.by dividing the input image into regions, we can only process the important and necessary segments of the image instead of processing the entire image.

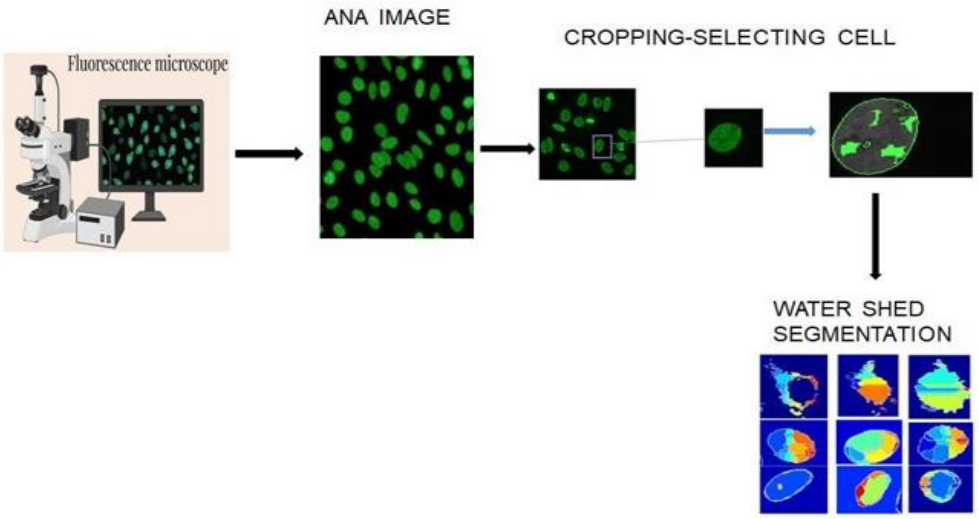

Figure 3.2. Work flow of the pattern recognition, detection and classificationof ANA image

4. RESULTS

Total of 60 images are used – 40 for training the classifier and 20 images for testing. The three different ANA patterns are used for training the classifiers. They are

- Homogenous pattern - 25 images
- Cytoplasmic pattern - 10 images
- Speckled pattern - 25 images

4.1 Watershed Segmentation Output

The cell is cropped from the antinuclear antibody image and then watershed segmentation algorithm is applied on speckled pattern and the result is shown in the figure(fig:4.1)

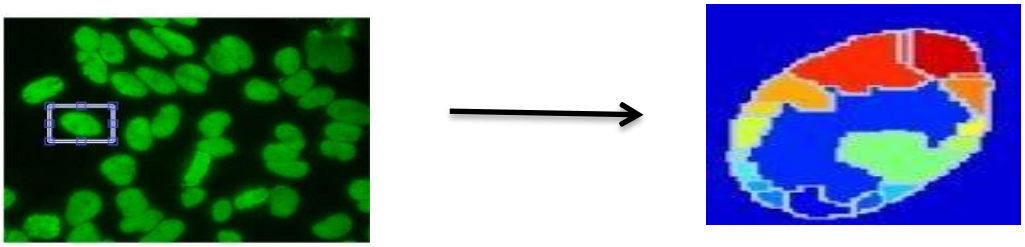

Figure 4.1. Segmentation Output of speckled pattern

All the three different patterns of antinuclear antibody images collected from fluorescent microscope are segmented and the result is shown in the figure (fig:4.2).this study mainly focuses on segmentation of antinuclear antibody images for pattern recognition.

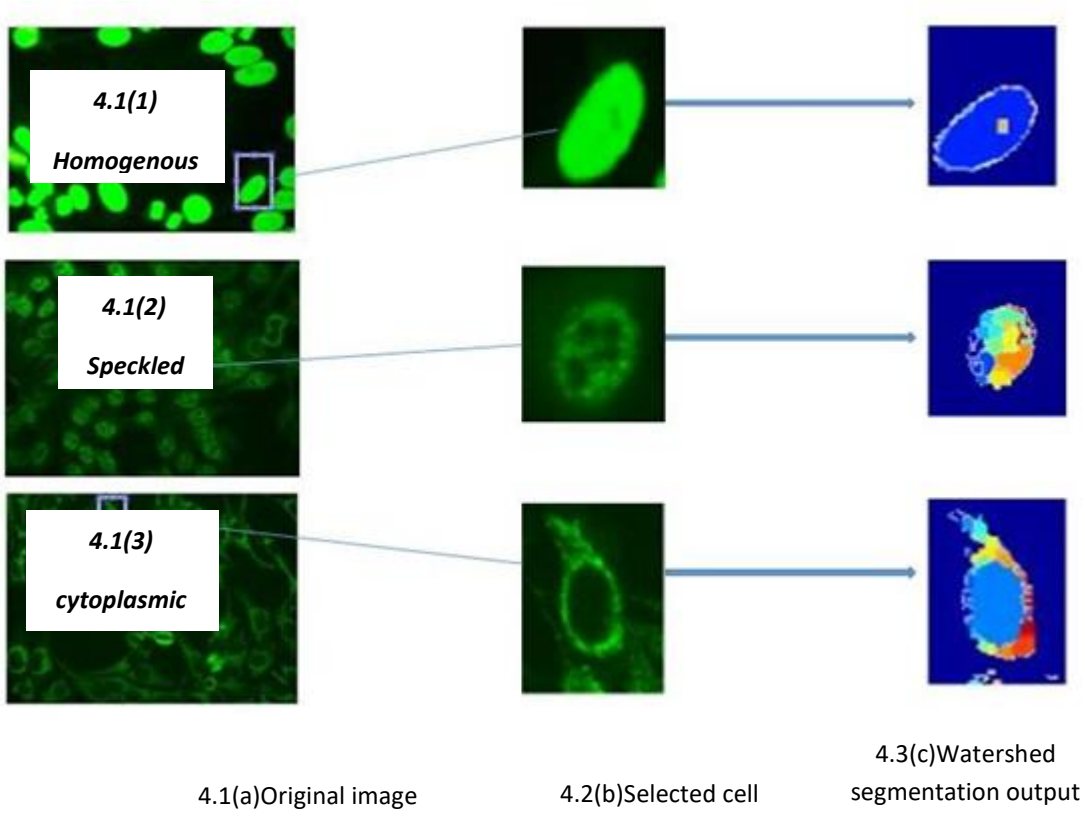

Figure 4.2. Segmentation Output of three different patterns

5. DISCUSSION AND CONCLUSION

In this study the images of antinuclear antibodies of three different patterns called homogenous pattern, speckled pattern and cytoplasmic pattern are taken and single cell is cropped. The cropped cell is preprocessed to reduce noise. The preprocessed cell is then segmented using watershed segmentation. This study helps to identify the different patterns of antinuclear antibody which is used to reduce human made errors in finding the antinuclear antibody image patterns and it is time saving.

REFERENCES

[1] Y. Muro, "Antinuclear antibodies," *Autoimmunity*, vol. 38, no. 1, pp. 3–9, Feb. 2005, doi: 10.1080/08916930400024612.

[2] T. Dörner and R. Furie, "Novel paradigms in systemic lupus erythematosus," *The Lancet*, vol. 393, no. 10188, pp. 2344–2358, Jun. 2019, doi: 10.1016/S0140-6736(19)30546-X.

[3] R. Dobson and G. Giovannoni, "Multiple sclerosis – a review," *Eur J Neurol*, vol. 26, no. 1, pp. 27–40, Jan. 2019, doi: 10.1111/ene.13819.

[4] R. I. Fox, "Sjögren's syndrome," *The Lancet*, vol. 366, no. 9482, pp. 321–331, Jul. 2005, doi: 10.1016/S0140-6736(05)66990-5.

[5] H. M. Moutsopoulos, "Sjögren's Syndrome (Sicca Syndrome): Current Issues," *Ann Intern Med*, vol. 92, no. 2_Part_1, p. 212, Feb. 1980, doi: 10.7326/0003-4819-92-2-212.

[6] A. Gabrielli, E. V. Avvedimento, and T. Krieg, "Scleroderma," *N Engl J Med*, vol. 360, no. 19, pp. 1989–2003, May 2009, doi: 10.1056/NEJMra0806188.

[7] H. C. Champion, "The Heart in Scleroderma," *Rheumatic Disease Clinics of North America*, vol. 34, no. 1, pp. 181–190, Feb. 2008, doi: 10.1016/j.rdc.2007.12.002.

[8] P. J. Venables, "Mixed connective tissue disease," *Lupus*, vol. 15, no. 3, pp. 132–137, Mar. 2006, doi: 10.1191/0961203306lu2283rr.

[9] O.-D. Ortega-Hernandez and Y. Shoenfeld, "Mixed connective tissue disease: An overview of clinical manifestations, diagnosis and treatment," *Best Practice & Research Clinical Rheumatology*, vol. 26, no. 1, pp. 61–72, Feb. 2012, doi: 10.1016/j.berh.2012.01.009.

[10] M. A. Khan, M. Hassan, S. Malik, S. Islam, U. Ansari, and O. Gilani, "Detection and characterization of antinuclear antibody using fluorescence image processing," in *2014 International Conference on Robotics and Emerging Allied*

Technologies in Engineering (iCREATE), Islamabad, Pakistan: IEEE, Apr. 2014, pp. 87–90. doi: 10.1109/iCREATE.2014.6828345.

[11] Chung-Chuan Cheng, Jin-Shiuh Taur, T.-Y. Hsieh, and Chin-Wang Tao, "Segmentation of anti-nuclear antibody images based on the watershed approach," in *2010 5th IEEE Conference on Industrial Electronics and Applications*, Taichung, Taiwan: IEEE, Jun. 2010, pp. 1695–1700. doi: 10.1109/ICIEA.2010.5515233.

[12] Divya BS, K. Subramaniam, and Nanjundaswamy HR, "HEp-2 cell classification using artificial neural network approach," in *2016 23rd International Conference on Pattern Recognition (ICPR)*, Cancun: IEEE, Dec. 2016, pp. 84–89. doi: 10.1109/ICPR.2016.7899613.

[13] I. Levner and H. Zhang, "Classification-Driven Watershed Segmentation," *IEEE Trans. on Image Process.*, vol. 16, no. 5, pp. 1437–1445, May 2007, doi: 10.1109/TIP.2007.894239.

[14] G. Hamarneh and X. Li, "Watershed segmentation using prior shape and appearance knowledge," *Image and Vision Computing*, vol. 27, no. 1–2, pp. 59–68, Jan. 2009, doi: 10.1016/j.imavis.2006.10.009.

[15] Alaknanda, R. S. Anand, and P. Kumar, "Flaw detection in radiographic weldment images using morphological watershed segmentation technique," *NDT & E International*, vol. 42, no. 1, pp. 2–8, Jan. 2009, doi: 10.1016/j.ndteint.2008.06.005.

An Artificial Intelligence Based Smart Wheelchair with Voice Control and Position Tracking Using GPS

Divya Bharathy.R[1], Lakshmi Prabha. P[2*]
[1]Department of Biomedical Engineering, SRM Institute of Science and Technology, Kattankulathur, India
[2]Assistant Professor, Department of Biomedical Engineering, SRM Institute of Science and Technology, Potheri, SRM Nagar, Kattankulathur, Chennai - 603203, India.

ABSTRACT

As report by the World Health Organization, more than 785 million people worldwide were affected by some form of disability in 2011. Smart wheelchairs have been researched and created on four continents since the early 1980s. Some smart wheelchairs function similarly to robotic applications in that the subjects inserts a destination and then observes as the intelligent wheelchair plans and executes a route towards that location. Systems frequently require either a complete map of the environment through which they navigate or modifications to their surroundings in order to arrive at their destination. Our proposed design integrates voice recognition technology based on artificial intelligence, allowing physically challenged people who have difficulty with hand movement due to ageing or paralysis can control the wheelchair with their voice commands. This device design also includes certain extra capabilities, such as collision avoidance and a Global Positioning Technology for safe travel module for recording the location of the wheelchair. To bring the concept into design, Arduino UNO, Bluetooth module, GPS module, ultrasonic sensor, and relay- based motor controller circuits are coupled with this prototype. The proposed prototype model enables impaired people to drive this wheelchair with low effort and without incident. As a result, our prototype wheelchair can assist disabled and paralytic patients in motion planning, environment sensing, and positioning, all of which are totally automated and do not require any human intervention.

Keywords: Artificial intelligence, Voice recognition, GPS module, Obstacle detection, Motion Planning

Corresponding Author:
Lakshmi Prabha. P,
Assistant Professor, Department of Biomedical Engineering, SRM Institute of Science and Technology, Potheri, SRM Nagar, Kattankulathur, Chennai - 603203, India.
Email: * lakshmip1@srmist.edu.in

1. INTRODUCTION

As a consequence of incidents, ageing, and diseases such as spastic paralysis and medulla spinal injuries, the percentage of people with impairments has increased significantly. It has reached one billion active users, accounting for 15% of the global total (Iskanderani et al., 2021). Several studies in the literature reveals that the independent movement of powered and mechanical wheelchairs permits all people with disabilities to access their features (Clerk Maxwell, 1832). Individual mobility expands professional (Shawki, 2001) and educational opportunities while reducing reliance on others and promoting feelings of independence and morality (Siddharth and Deshpande, 2016). Limited mobility frequently results in fewer possibilities to implement socialized ideas, leading to psychological isolation and a variety of mental health issues (Clark, 1977). While most physical or self-powered wheelchairs meet the needs of a wide spectrum of disabled persons, some peoplefind it difficult or impossible to use wheelchairs independently (Simpson and Levine, 2002).

There are various benefits and drawbacks to design a functioning wheelchair (Tharpar, 2004). It has always been difficult to apply voice-based techniques to any system. Since the equipment may fail to recognize the user's voice command and there is no tracking system, (Ganesh, 2019). Any command that could move the wheelchair had a time limit. Another concern occurs, however, because the short-lived orders may result in accidents in a congested area (Subham Bhanka, 2018). One of the most serious problems with voice control was its restricted bandwidth. Making modest modifications to the wheelchair's velocity on a daily basis was practically impossible. Navigation aids employing sensors can be employed to avoid obstructions (Abhijeet Botre, 2016). As they are unfamiliar with the surroundings and its disability limitations (Chauhan et al., 2016), many wheelchair users are afraid (Raiyan et al., 2017) to visit an unfamiliar location (Umchid et al., 2018). For their everyday mobility in a predefined region, they often have no alternative but to rely on repeated and predictable routes with the fewest barriers. However, these approaches are not without unexpected difficulties and modifications in available circumstances, such as an icy pathway, traffic jams, and a broken electronic door, particularly in a competitive, changing location such as a university campus. These problems can be predicted and avoided if wheelchair users are given accurate and reliable information regarding access and mobility alternatives, as well as kept up to speed on changes, which would considerably improve safe and successful wheelchair navigation, especially in unknown places. Motorized wheelchairs (Shwetha, 2018) with joystick,

softball, finger, tablet, chin, and head controls are widely available at a considerable cost (Priya et al., 2018); however, the majority of them do not accommodate persons with upper limb disabilities (Mohammad Ilyas Malik et al., 2017). Speech recognition technology advancements (Khyati Meena et al., 2017) have made it possible to Voice commands can be used to operate any electrical gadget. This technology is being used to develop a voice-controlled wheelchair to assist persons with upper and lower limb issues (Manuel Mazo et al., 1995). According to the World Health Organization (WHO), just 5% to 15% of the 75 million individuals who use assistive technology such as wheelchairs has accessible to that one (WHO, 2019).

The GPS system is also used to track the position of handicapped people who use wheelchairs on a daily basis. The positions from the satellites were obtained by using a GPS module (Aktar et al., 2019). These features are established by the subject's capacity, for example, the simplest model may include a joystick and a voice-controlled automatic wheelchair with GPS and GSM module that will receive voice commands from the user and will also be useful for remote monitoring of people with memory issues (Gor and Jeyakumar, 2017).

This paper presents the prototype model of the smart wheelchair. The proposed design is equipped with ultrasonic sensor, Bluetooth module and GPS module. These component parts are coupled together and designed an advanced prototype model of an intelligent wheelchair. The designed model is mainly useful for physically challenged people. Our proposed work has Bluetooth based Adaptive multi rate voice controlled application. The users can give their voice commands such as (forward, back, left, right and stop) according to the voice commands the wheelchair moves. In addition, to this it also functions under collision avoidance and positioning using GPS module. If any obstacle is present the ultrasonic sensor measures the obstruction and stops the movement of the wheelchair and finally the positioning value will be displayed in LCD.

2. MATERIALS AND METHODS

The proposed methodology comprises of several components that includes:
Arduino Uno, GPS Module, Motor Driver Module, Ultrasonic Sensor, LCD Display, Robot Wheels, Dc Motors, and Bluetooth Module.

2.1. Microcontroller

In this design, an Arduino UNO (Raiyan, 2017) microcontroller is used. The Arduino UNO was chosen because it offers 14 input and output digital pins (six pins can be used as an pulse width modulation outputs), six analogue inputs, a 16 MHz ceramic resonator, a USB connection, a power jack, an ICSP header, and a reset button.

2.2. GPS Module

In this design GPS Module NEO 6M (Aktar et al., 2019) Satellite has been used. This device uses the latest advancement and features a bigger built-in 25 x 25mm active GPS antenna with a Serial port TTL connection to provide the most accurate positional information available. Here this device is used to determine the positionof the wheelchair and hence the wheelchair location can be tracked.

2.3. Motor Driver Module

The motorized controller (Shwetha, 2018) is required to regulate the movement of the wheelchair in order to allow it to move in the path specified by the user. Due to the ongoing heating problem with MOSFET-driven motor controllers, as well as for the level of the risk. As a motor controller, we employed a motor driver module. It is a magnetic device with coils that can store power and damage low-powered electronic components. As a result, in this module, a drifting diode and a coupler were utilized to protect the circuit while allowing it to be regulated by the low voltage microcontroller chip.

2.4. Ultrasonic Sensor

Ultrasonic avoidance sensors are used to protect users by sensing the presence of any obstruction in order to avoid collisions. This design employs "HC-SR04" (Chauhan et al., 2016) sensors. The sensor's transmitter sends an ultrasonic sound through the air at 343 m/s. When there is an impediment, the noise is directed back, forming an echo that is later caught by the sensor's receiver section. The time difference between transmission and reception is then utilised to compute the distance between the obstruction and the sensor's location.

2.5. LCD Display

LCD is a flat-panel display that employs liquid crystals. This LCD is used in this designed system for visualizing the position of the wheelchair. The users can easily view their data through this LCD display. LCDs use a backlight and electronically switch on and off pixels to spin polarized light. In front and behind all pixels is a 90-degree polarizing glass filter. Between the two filters are electrical liquid crystals.

2.6. Robot Wheels

Robots with wheels move across the ground by employing powered wheels as their means of

propulsion. Using wheels instead of treads or legs makes this design simpler and makes it simpler to build, design, and programmed for movement. While the rollers are typically composed of high traction materials to produce a higher coefficient of friction, the base wheel is typically made of plastic or metal alloys.

2.7. DC Motor

In this design, a light weight brushed DC motor (Raiyan, 2017) was used because it is usually utilized in many applications with lesser loads. The higher rotating speed of the chosen motor, measured in RPM, can be decreased using a gear system to produce more starting torque. When operated at 9V, the motor has a starting torque of roughly 10Kg-cm.

2.8. Bluetooth Module

We have used Bluetooth module HC05 (Shwetha, 2018) in this system. Whereas the user can give their voice commands through the Adaptive Multi Rate (AMR) Bluetooth voice controlled application. Once the Bluetoothreceives the voice command the motor starts rotating and the wheelchair moves according to the voice directions given by the users.

The proposed prototype system uses an artificial intelligence to function, reveals its novelty by combining a wheelchair with speech recognition, obstacle detection, and accurate location technology. The controls of a smart wheelchair are made up of three major components: a microcontroller, an Internet network, and a smart device that connects to the chair. This system incorporates voice recognition that is user-dependent, a GPS module, an emergency LCD, a Bluetooth module, and an obstacle detector. The wheelchair will automatically navigate to the desired target point using this methodology. Depending on the users voice directions (Forward, Backward, Right, Left, and Stop), the speech recognition system carries out pre-defined activities. If an obstruction is detected, the obstacle detecting system restricts the movement of the signal. The GPS tracking, also known as the Global Positioning System, will be installed on the smart wheelchair or the person who wants it to be tracked for high-precision location. The position on Earth is calculated using satellites in this system. It is possible to monitor an object or person accurately and with tiny deviations of up to 100 m. Thus our designed system will be quite useful to the disabled persons and need not require any external assistance with them.

3. BLOCK DIAGRAM OF THE PROPOSED DESIGN

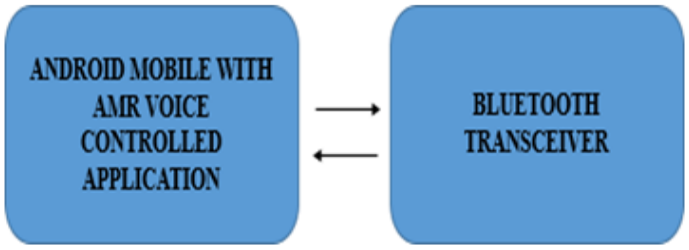

Figure 1. Block Diagram of the transceiver part

The advanced android phone has a mobile application that connects to the voice instructions via the Bluetooth module and converts the speech orders to computerized signals before transmitting them to the device as shown inFigure 1.

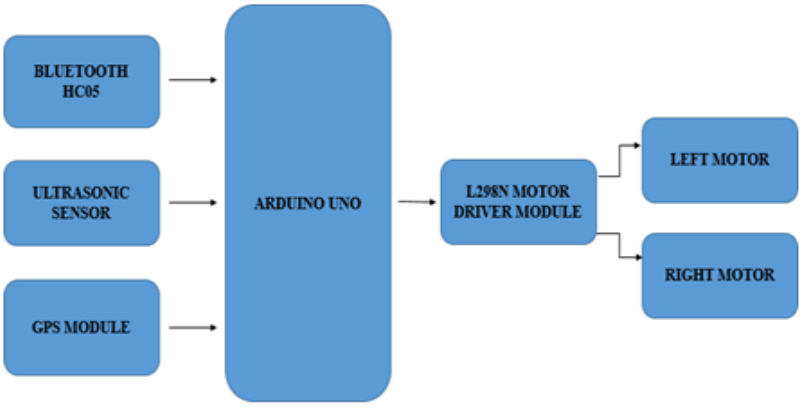

Figure 2. Block Diagram of the receiver

The computerized signals communicated from the transmitter are received by the Bluetooth module, obstacle sensor, and GPS module present in the prototype will receive the signal and direct it to the microchip present in the Arduino will check with the put away orders and at the execution the DC motors will turn over moving in the order specified, and the motor rotations are controlled by a motor driver connected to the Arduino as shown in Figure 2.

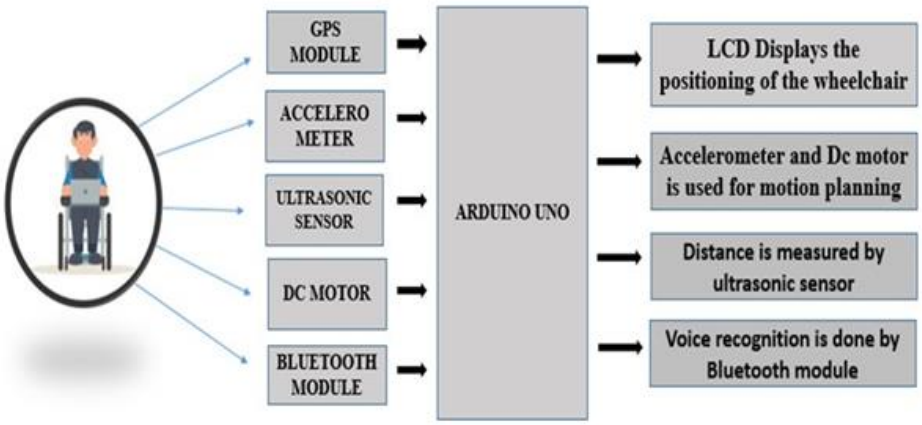

Figure 3. Proposed Design for AI Based Voice Controlled Wheelchair

As illustrated in Figure 3, the prototype framework incorporates a GPS module, an accelerometer, an ultrasonic sensor, DC motors, and a Bluetooth module. These components are attached to the microcontroller i.e., Arduino UNO. As a result, the developed system begins to function in response to the user's voice commands. The AMR voice-controlled application can be used to perform voice commands. Once it gets a Bluetooth signal, the motor rotates and the wheelchair moves in accordance with the user's orders. The GPS module also receives satellite signals and transmits data. This system has an ultrasonic sensor that detects ultrasonic sounds and stops the device if an obstacle is detected. As a result, the user is no longer at risk of colliding. Finally, the data acquired by the GPS module reveals the location of the wheelchair in the LCD display, allowing family members or doctors to follow or view the patient's position.

4. RESULTS AND DISCUSSION

In this study, the speech recognition software could identify the voice command and execute it, where the ultrasonic sensor module was able to detect the obstacle and GPS module receive the signal and transmit the data to the LCD. As this device concurrently provides voice-activated wheelchair, obstacle detection, and GPS patient tracking via an Android application, we can expect that it will be beneficial for the disabled people throughout the world. The major benefits of using this voice-controlled wheel chairs are that they respond to voice commands much faster and it mainly assist people who have lost their ability due to various factors.

Figure 4. Schematic Representation of the Proposed Work

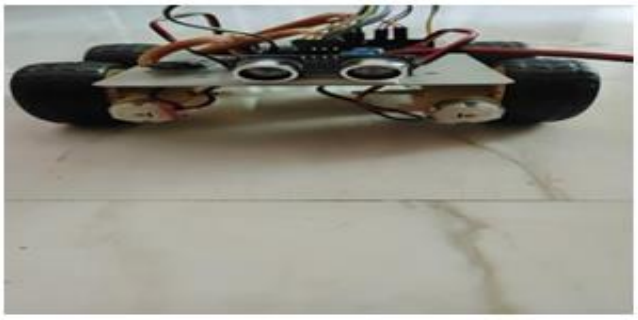

Figure 5. Prototype Model ofthe Proposed Work Wheelchair

Figure 6. Displaying the Position of Wheelchair

Figure 4 describes the schematic design of the proposed work. The microcontroller, bluetooth module, GPS module and ultrasonic sensors are equipped in the design. Figure 5 represents the hardware implementation of the complete prototype model of proposed wheelchair based on our advanced novelty. Based on the positioningof the wheelchair, the proof of concept is presented in Figure 6

5. FUTURE WORK AND LIMITATIONS

Since many years to come, smart wheelchairs will be fruitful terrain for technical innovation. Smart wheelchairs are ideal for sensor research, particularly machine vision. Researchers can also use smart wheelchairs to study human-robot interaction, adaptive or shared control, and novel input techniques such as voice control, EOG, and eye-tracking. Additionally, smart wheelchairs will be used as development kits for robot control frameworks in the future. While significant work has gone into designing intelligent wheelchairs, little has gone into analyzing their performance. Conducting user trials using smart wheelchairs is problematic for a variety of reasons. When using a smart wheelchair in a research environment on a closed course, some wheelchair users do not immediately improve their navigation skills. This may occur if the smart wheelchair does not perform well or because the wheelchair user was already so experienced that there was little room for development. Users with the potential for big performance gains, on the other hand, usually have little or no experience with independent mobility and may require extensive training before participating in genuine user tests.

Different localization techniques, algorithms, and strategies will be required in future development. We can use ubiquitous computing applications to calculate the position and create a positioning system by synchronizing these parameters. Accurate position estimation of objects in both interior and outside settings will be possible thanks to a variety of localization techniques and algorithms. Furthermore, using convolutionalneural networks (CNN), a speaker identification algorithm can be incorporated to the voice recognition model to secure the impaired person's safety by only accepting orders from a particular user. Intelligent control algorithms in smart wheelchairs can reduce the need for human intervention. A novel framework of segmentation network can also be implemented for obstacle detection in a power wheelchair.

6. CONCLUSION

Our proposed system is intended to produce a user-friendly vehicle. Autonomous wheelchairs are extremely useful for people who are unable to move from one location to another on their own. The operation of the robot is very simple and easier. The voice-controlled wheelchair prototype based on Arduino was successfully developed and proven to respond to voice instructions. It will significantly enhance the lives of

people with severe disabilities. This system is inexpensive and it has an advantage that it can be added to any manual wheelchair. The smart wheelchair was constructed in a way that requires the least amount of effort to control from the disabled or physically challenged people. It also provides protection in obstacle collision. By using this system, the physically challenged people would find it easy to move the wheelchair without human assistance.

Artificial Intelligence technology plays a major role in speech recognition for motion planning with appropriate voice commands. The voice recognition system of a particular command has also been successfully implemented for motion planning of the wheelchair. Voice commands provides easy interface because it is a way of natural communication and works with proper inputs even if there is a noisy environment around the user, so the GPS is also tested and designed by using Personal computer and android application. From the result, it is evident that the proposed work has successfully developed a cost-effective smart voice-controlled wheelchair integrated with GPS.

ACKNOWLEDGMENT

The authors would like to express their gratitude to all the faculties of Department of Biomedical Engineeringfor extending their support and providing valuable guidance throughout the duration of the project.

REFERENCES

[1] I. Iskanderani et al., "Voice Controlled Artificial Intelligent Smart Wheelchair", 2020 8th InternationalConference on Intelligent and Advanced Systems (ICIAS), pp. 1-5, 2021.
[2] J. Clerk Maxwell, A Treatise on Electricity and Magnetism, Oxford:Clarendon, vol. 2, pp. 68-73, 1892.
[3] A. Shawki and Z. J, "A smart reconfigurable visual system for the blind", Proceedings of the Tunisian-German Conference on: Smart Systems and Devices, 2001.
[4] P. D. Siddharth and S. Deshpande, "Embedded system design for real-time interaction with SmartWheelchair", 2016 Symp. Colossal Data Anal. Networking CDAN 2016, 2016.
[5] J. Clark and R. Roemer, "Voice controlled wheelchair", Arch. Physical Med. Rehab, vol. 58, pp. 169-175,1977.
[6] R.C. Simpson and S.P. Levine, "Voice control of a power wheelchair", IEEE Transaction on Neural Systems and Rehabilitation Engineering, vol. 10, no. 2, pp. 122-125, 2002.
[7] N. Thapar, G. Warner, M. Drainoni, S. R. Williams, and H. Ditehfield, "A pilot study of functional access to public buildings and facilities for persons with impairments," Disability and Rehabilitation, vol. 26, pp. 280- 289, 2004.
[8] E. N. Ganesh, "Health Monitoring System using Raspberry Pi and IOT" published in Oriental Journal of Computer Science and Technology, Volume 12, No 1, 2019.
[9] Shubham Banka, Isha Madan, S.S. Saranya, "Smart Healthcare Monitoring using IOT" published in International Journal of Applied Engineering Research, Volume 13, No 15, 2018
[10] Abhijeet Botre, "Assistance system for paralyzed" published in International Journal of Innovative Research in Electrical, Electronics, Instrumentation and Control Engineering, Volume 4,1ssue 5, 2016
[11] R. Chauhan, Y. Jain, H. Agarwal and A. Patil, "Study of implementation of Voice Controlled Wheelchair," *2016 3rd International Conference on Advanced Computing and Communication Systems (ICACCS)*, 2016
[12] Z. Raiyan, M. S. Nawaz, A. K. M. A. Adnan and M. H. Imam, "Design of an arduino based voice- controlled automated wheelchair," *2017 IEEE Region 10 Humanitarian Technology Conference (R10-HTC)*, 2017
[13] S. Umchid, P. Limhaprasert, S. Chumsoongnern, T. Petthong and T. Leeudomwong, "Voice Controlled Automatic Wheelchair," *2018 11th Biomedical Engineering International Conference (BMEiCON)*, 2018
[14] Trefler E, Taylor SJ. Prescription and positioning: Evaluating the physically disabled individual for wheelchair seating, *Prosthetics and Orthotics International*, 1991
[15] A. Azad, R. Tavakoli, U. Pratik, B. Varghese, C. Coopmans and Z. Pantic, "A Smart Autonomous WPT System for Electric Wheelchair Applications with Free-Positioning Charging Feature," *IEEE Journal of Emerging and Selected Topics in Power Electronics*, vol. 8, no. 4, pp. 3516-3532, 2020
[16] V. Shwetha, Vaibhav Mani and Aditya Kumaran "Voice Controlled Wheelchair," International Journal of Engineering & Technology7 (4.41) 105-109, 2018.
[17] C.A. Priya, Saadiya, Bhagyashree, S.D. Pranjala and H.S.G. Supreeth "Voice Controlled Wheelchair for Physically Disabled People," International Journal for Research in Applied Science & Engineering Technology (IJRASET) vol. 62375-2380, 2018.
[18] Mohammad Ilyas Malik, Tanveer Bashir and Omar Farooq Khan "Voice Controlled Wheel Chair System,"International Journal of Computer Science and Mobile Computingvol. 6411- 419, 2017.
[19] Khyati Meena, Shubham Gupta and Vijay Khare "Voice Controlled Wheelchair," International Journal of Electronics, Electrical and Computational Systemvol. 6 23-27, 2017.
[20] Manuel Mazo et al. "Wheelchair for Physically Disabled People with Voice, Ultrasonic and Infrared Sensor Control Autonomous Robots2," 203-224, 1985.
[21] https://www.who.int/news-room/fact-sheets/detail/assistive-technology. © 2019 WHO, Assessed on 17 June 2019.
[22] N. Aktar, I. Jaharr and B. Lala, "Voice Recognition based intelligent Wheelchair and GPS Tracking System," *2019 International Conference on Electrical, Computer and Communication Engineering(ECCE)*,Cox'sBazar, Bangladesh, 2019, pp. 1-6, doi: 10.1109/ECACE.2019.8679163.
[23] N. J. Gor and A. Jeyakumar, "Voice controlled motorized wheelchair with real time location monitoring," 2017 International Conference on Energy, Communication, Data Analytics and Soft Computing (ICECDS), Chennai, India, 2017, pp. 1163-1167, doi: 10.1109/ICECDS.2017.8389624.

Tissue Regeneration For Fire Burns Using Various Herbal Extracts - A Circumstancial Study For Better Efficacy

K. Mythili[1], A. Aseera[2], V. Deekshitha[3], M. Raveena[4], R. Roshini Anita[5]
[1]Assisstant Professor, Dept. of Biomedical Engineering, Sona College of Technology, Salem, Tamil Nadu
[2,3,4,5]Final Year Students, Dept. of Biomedical Engineering, Sona College of Technology, Salem, Tamil Nadu

ABSTRACT

Healing of burn wounds is a complex procedure that involves neovascularization, wound contraction, granulation, epithelialization, inflammation and wound healing. While modern therapies offer a wide range of possibilities, traditional medicines promise successful outcomes. Burns have been treated using plant-based products for thousands of years now. A convenient sample of 3 herbs & herbal products (Centella asiatica, Musa sapiens & honey) are collected, that are easily accessible and affordable in the local regions. There are no earlier systemic studies established, comparing the effectiveness of such different herbs and their combinations. Individual and comparative studies of these herbs are performed to assess their immuno-properties such as antimicrobial, antiseptic, anti-inflammatory, angiogenic and antioxidant actions that support wound healing. In order to assess their potentiality in healing, based on the phytochemical constituents, the herbal ingredients and capabilities are tested both individually and in combinations. As a succeeding progress, nanotechnology based characterization study is to be performed, that will establish the effectiveness of the physical & chemical properties of these herbs. There are undiscovered reagents, untested combinations and adjunct compounds that are concealed among countless natural products and their derivatives. This remedy will hold a great promise for more effective treatment of burn wounds in future. In order to develop a treatment option that is beneficial in terms of analgesics, greater comfort and rapid healing, this study intends to evaluate potential herbs that help in tissue repair and rejuvenation.

Keywords: Burn injury, Wound healing, Phytochemicals, Immuno-properties, Centella asiatica, Honey,Musa sapiens, Characterization study

Corresponding Author:
K. Mythili,
Assisstant Professor, Dept. of Biomedical Engineering, Sona College of Technology,
Salem, Tamil Nadu
Email:mythili0011@gmail.com

1. INTRODUCTION

(I. Kaddoura, 2017) The word ‘burn’ refers to more than just the burning feeling this injury causes. Burns are defined by significant skin damage that results in the death of the impacted underlying skin cells. The depth and cross sectional region of burns serve as defining characteristics for the ailment. Deep burns take longer to recover, more difficult to treat and develop complications like scarring and infections rapidly. While superficial burns are relatively simple to heal with the appropriate care; very deep burns are the most dangerous of all the conditions and may necessitate amputation for cure

Types of burns include:

- First-degree burns harm the epidermis (or) outer covering of the skin. Usually, these wounds recover on their own within a time period of one or two weeks.
- Second-degree burns harm the deeper tissues as well as the skin's surface. For the body to be covered and protected while it heals from these injuries, a skin graft, either natural or artificial may be required, resulting in a scar.
- Third-degree burns harm the underlying tissues and two layers of skin, including hair follicles and sweat ducts. Skin grafts are always required for these types of wounds.
- Burns of the fourth degree penetrate the fatty layers of the epidermis. It causes damage to the subcutaneous fat, nerves and tendons in addition to the hypodermis, giving the skin a thick, leathery look.
- All of the epidermis, as well as the majority of the muscle layers and ligaments, are burned away in fifth-degree burns. In a fifth-degree burn, it is usual to see the charred inner most tissue. Burning of the skin's protons and oxygen produces this char. If char is present, a graft is necessary and a lasting scar will be resulted.
- The most serious form of burns, a sixth-degree burn, results in extensive damage that penetrates the skin and reaches the bone. Due to the higher quantity of blood loss, such wounds are intensively fatal to victims.

Herbal remedies aid in repairing the skin , soothe the pain of burns, help resist the spreading of infection, obstructs the development of scar tissues and thereby aid in the overall recovery of the damaged tissue, in all the layers of the skin tissues.

2. EXISTING TREATMENTS

(Heyneman A, 2016) Chemical-based treatments for treating burn wounds tend to show a lot of negative consequences on patients. Silver sulfadiazine ($C_{10}H_9AgN_4O_2S$) or Silvadene is the gold standard for topical burn therapy, in all its degrees (fig. 1.1). In addition, drugs like naproxen (aleve, naprosyn) ,naproxen (aleve, naprosyn) or ibuprofen (advil, motrin, nuprin), acetaminophen (panadol, tylenol), bacitracin are also used in treating these injuries.

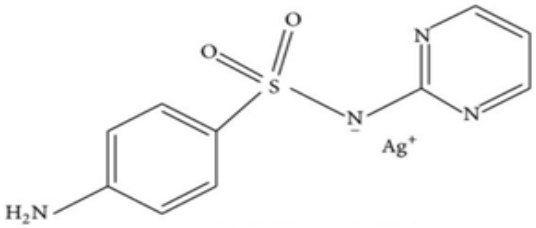

Figure 1. Silver Sulfadiazine

Water-based treatments (ultrasound mist therapy), fluids for dehydration and prevent organ failure, pain & anxiety medications, IV antibiotics, burn creams & ointments, occlusive dressings, drugs that fight infection, tetanus shots, fluid resuscitation, etc are some of the treatments available today for treating fire burns. Consumption of morphine and anti-anxiety medications might be needed, especially when changing clothes.

3. LIMITATIONS IN THE CURRENT SYSTEM

(Fuller FW, 2009) A significant unresolved clinical issue is how to treat the pain and wounds brought by burn injuries without causing any abnormal effects to the body. The most popular types of analgesic therapy used to treat burns include, antidepressants, anticonvulsants, opioids, antidepressants and non-steroidal anti-inflammatory drugs (NSAIDs), anticonvulsants, which appear to have numerous side effects. Using these medications may cause severe conditions like porphyria. Blisters, peeling or general body are some of the side effects that might occur due to accumulation of such chemicals in body.

4. *Musa sapiens* LEAF IN WOUND HEALING

(Poduri K, 2020) Banana leaves can be gathered easily and provide a number of health benefits. Allantoin and polyphenols are abundant in the dried banana leaves. They promote the formation of healthy tissue and aid in the healing of wounds and skin irritations. (Munn Z, 2015) For treating partial thickness burns at a minimal cost, banana leaf dressings are considered. (Hoetzenecker, 2014)The healing duration for wounds covered in banana leaves is comparably faster to wounds covered in gauze dressings. The cost of banana leaf dressings is many times lower than that of collagen or biosynthetic dressings. The perfect burn dressing must be pain-free to apply, non-antigenic, non-toxic, non-adherent, non-allergic, affordable and it should be widely accessible. Although homograft is a suitable temporary dressing alternative and xenografts are the next best option, living skin autografts are still preferred. Homografts and xenografts are scarcely available in our country. (Nascimento , 2021) Several burn victims are in dire need of an affordable, readily accessible bandage for their partial thickness burns. 1) For burn wounds with partial thickness, banana leaf dressing is an appropriate and efficient treatment. 2) The least expensive partial thickness dressing is made from banana leaves. 3) The preparation technique is fairly straightforward and is simple to teach and understand . (Madhuri A. Gore, 2003) This may present a reliable chance for burn patients to successfully recover their lost economic independence. In order to handle partial thickness burn wounds, BLD is the best alternative. (Munn Z, 2015) It should be noted that untreated banana leaves must be sanitised before being used as dressings because they are highly polluted with several fungi and bacteria from the environment.

5. HEALING PROPERTIES OF HONEY

(Jull AB, 2013) Honey's ability to cure wounds includes promoting tissue re-growth, improving epithelialization, and reducing scarring. These outcomes are attributed to the acidity, hydrogen peroxide concentration, osmotic action, nutrient and antioxidant contents, immune system stimulation and undiscovered components in honey. Nitric oxide and prostaglandins play important roles in the inflammation, germ killing, and healing processes. These characteristics aid in explaining honey's biological and medicinal qualities, particularly its effectiveness as an antibacterial agent or wound healer. When honey is administered to wounds, the hydrogen peroxide produced in it can hasten the healing process. As a stimulant for cell augmentation or multiplication, the

expansion of new capillaries, repairing the damaged tissues and when damaged tissues undergo inflammatory response to burn injury, hydrogen peroxide has been involved as an important chemical in many cell types of our human body. Recombinant growth factors have been proposed to be replaced by low quantities of hydrogen peroxide to promote wound healing, prevention of tissue damage from the formation of oxygen radicals can be controlled only if the concentration of Hydrogen Peroxide is well balanced. (Osman, 2022) Silver sulphadiazine may not be as successful as honey dressing in treating partial thickness and superficial burns. However, because this was observed within a region involving trails which are of low quality across the world with significant diversity, honey has to be properly taken care of in regular clinical proceedings. The healing action occurs both directly and indirectly through the consumption of quickly absorbed amino acids, minerals, carbohydrates, vitamins. Studies reveal that the providing a variety of nutrients helps wounds heal more quickly. Leukocytes, epithelial cells and the glycolytic process all receive support from honey in the formation of glucose. To repair the epithelial sheath, the cells of epithelium require carbohydrate in abundance for the energy to disperse all over the surface of burn wound. (Jull AB, 2013) The primary component of macrophages' antibacterial activity, the hydrogen peroxide, is produced during a respiratory burst that is triggered by leukocytes. Finally, macrophages primarily generate energy through the process of glycolysis, which enables them to work in injured tissues and exudate where oxygen is frequently scarce. (Nascimento REA, 2021) For its antibacterial activity, the creation of bee defensin-1, hydrogen peroxide in it; low PH and high osmolarity values appear to be highly essential. It has high 1, 2-dicarbonyl-molecule methylglyoxal content is what gives it the strong antibacterial property. Several phytochemicals, particularly phenolic compounds are crucial components of honey's antibacterial properties. Propolis in honey, in particular, possesses promising antibacterial properties, and the potential for their use in clinical treatments.

6. *Centella asiatica* IN BURN WOUND TREATMENT

(Ogunka-Nnoka CU, 2020) All *Centella asiatica* extracts speed up the healing of burn and incisional wounds alike. This extract's ethyl acetate and asiatic acid appeared to be the most effective ingredients for treating the wound. Madecassic acid , asiaticosides and Asiatic acid are the most significant phyto-chemicals, including saponins, sugar esters and triterpene acids, that are present in *C. asiatica* .(Somboonwong J, 2012) For the reason that it has the ability in wound healing, improvising mental clarity and treating skin disorders like psoriasis and leprosy, *C. asiatica* is used as a vital traditional medicine in almost all the regions of Asia from a very long time. The TLC analysis revealed that asiatic acid ,asiaticoside ,α-sitosterol and madecassoside etc. are the main active substances in HexE, EtAcE, and MeE. The wound breaking strength which is followed in traditional burn wound treatments are from the ethanolic extract of *C. asiatica* .In the burn punch wound model, asiaticoside extracted from *Centella asiatica* enhanced the amount of hydroxyproline, tensile strength, collagen and epithelialization. Researches have examined *C. asiatica*'s effectiveness on incision and burn wound treatments. Thus, the goal of this work has been to assess the ability of consecutive *C. asiatica* extracts to heal incisional and partial-thickness burn wound models.

7. SAMPLE PREPERATION FOR TESTS

(Ogunka-Nnoka CU, 2020) The leaves of *C. asiatica* were separated, immaculated and shade dried on an average room temperature of 28-26 °C upto 14 days. The leaves which were already dried are made into fine particles with mortar & pestle, were preserved in an airtight container and labeled for further proceedings (fig. 2.1). Fresh extracts were also obtained to study their nature in the fresh form (fig. 2.2).

Figure 2.1. *Centella asiatica* (Dry)

Figure 2.2. *Centellasiatica* (Fresh)

(Nascimento REA, 2021) The process starts with shade drying the banana plant (*Musa sapiens*) leaves, at a temperature of 27.8-26.5 °C for a time period of 5 days. It then was powdered and stored (fig. 2.3). Fresh extracts were also obtained with the help of mortar & pestle for the study in the fresh format (fig. 2.4).

Figure 2.3. *Musa sapiens* (Dry)

Figure 2.4. *Musa sapiens* (Fresh)

8. PHYTOCHEMICAL TESTS ON *Centella Asiatica*

❖ **Flavonoid Test**

(Saxena Mamta*, 2012) (Shaikh, 2020) The aim of this study is to quantify the flavonoid content of *C. asiatica* & *Musa sapiens* leaves that were macerated in acidified ethanol. The test is performed with combinations of conc. HCl & Mg ribbons. The findings indicated that the herb's leaves, in their dried condition, proved the presence of flavonoids, resulting in a deep purple color change, that aid in wound healing by reducing inflammation, proliferation and re-epithelialization. Flavonoids tend to accelerate the process of fibrogenesis in damaged and wounded tissues (fig. 3.1).

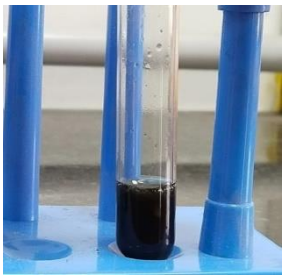

Figure 3.1. Shinoda test (Fresh)

Figure 3.2. Shinoda test (Dry)

Fresh extract which is obtained from the leaves of *C. asiatica* & *Musa sapiens* failed to show positive results in proving the presence of flavonoids (fig. 3.2).

❖ **Terpenoid Test**

(Saxena Mamta*, 2012) (Shaikh, 2020) The aim of this study is to quantify the terpenoid content of *Centella asiatica* & *Musa sapiens* leaves that have been macerated in distilled water & are tested with the combinations of chloroform and conc. H_2SO_4, that were put to rest for 24 hours. The result indicated a color change of orangish-red color, that indicated the presence of terpenoids. The findings show that the herb's leaves, which are dried, show positive results (fig. 3.3). Terpenoids, which are precursors to steroids, promotes wound healing as they have astringent and antimicrobial property which is accountable for contraction of burn wounds and improvises epithelial growth.

Figure 3.3. Terpenoid test (Dry)

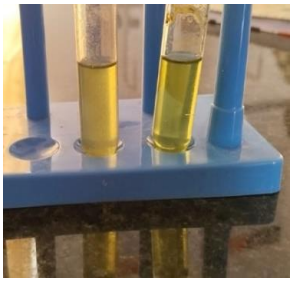

Figure 3.4. Terpenoid test (Fresh)

Freshly ground extracts of *Centella asiatica* & *Musa sapiens* failed to show positive results in proving the presence of Terpenoids. Hence usage of dried leaves alone for the study has been concluded (fig. 3.4).

❖ **Saponin Test**

(Auwal MS, 2014) (Shaikh, 2020) The fact that the phytochemicals aid in the precipitation and aggregation of red blood cells, accounts for saponins' capacity to cure wounds and stop bleeding. By promoting wound contraction and resulting in significant collagen deposition, saponins are also known to improve wound healing. According to the current study, *Centella asiatica* & *Musa sapiens* leaves, in a dried condition, are a rich source of nutrients such proteins, ash, saponins, carbohydrates, and crude fibre. (P. Szweda, 2017) The leaves contain various bioactive substances with broad spectrum of biological activities or medicinal benefits. This test proceeds by dissolving the sample of dried leaf powder in distilled water and heating them at a temperature of 120 – 140 °C, using a bunsen burner for about 5 minutes. After cooling, on shaking the test tube, appearance of a layer of honey comb structured froth, shows positive results & indicates the presence of saponins (fig. 3.5).

Figure 3.5. Saponin test (Dry)

Figure 3.6. Saponin test (Fresh)

On the other hand, while proceeding the saponin test with the fresh leaf extracts, *Centella asiactica* showed positive results for the presence of saponin, while *Musa sapiens* failed to (fig. 3.6).

9. FORTHCOMING TRENDS

- (Shaikh , 2020) The phytochemical tests that are to be proceeded in future are tannin test, amino acid test (ninhydrin test), phenol test, H_2O_2 test.
- The immuno – property tests that are to be proceeded are anti – microbial test, antiseptic test and antioxidant test.
- The above mentioned tests are to be proceeded with wild honey as well, that will establish the healing properties of honey.
- Combinational studies are to be conducted that will test the efficacy on healing with the mixture of all the three herbal extracts.
- Nanotechnology based characterization study is to be performed, that will establish the effectiveness of the physical & chemical properties of these herbal extracts.

10. CONCLUSION

Based on the study that has been conducted in a systematic step by step manner, the phytochemical nature & healing properties of these herbs have been tested, which on average showed positive results when the leaves were in their dried form & showed negative results when they were fresh, that will aid in accelerating healing in the path to recovery from a traumatic burn injury in all its degrees. Further, studies like tannin test, H_2O_2 test, anti-microbial test, antiseptic test, anti-inflammatory test, etc for both the leaves and all these tests on Honey are also yet to be performed. As a progress, combinational tests within these herbs are also to be performed that will estimate & prove the best combination, that is high on efficacy.

REFERENCES

[1] Poduri K, Tudker B, Patel P," Innovative treatment of Burn wounds with with Banana Leaf Dressing: A Case report", Poster presented at*: ISPRM World Congress*; March 4-9, 2020; Orlando, FL. [HCA Healthcare].
[2] Munn Z *,"Banana Leaf Dressing: A Wham Evidence Summary*", Wound Healing And Management Node Group*, 2022 Wound Healing and Management Collaborative, Curtin University.
[3] JOUR, Hoetzenecker, Wolfram, Guenova, Emmanuella, Moehrle Matthias, 2014/01/10, *"*Banana leaves: An alternative wound dressing material?" 8, 10.1586/17469872.2013.835925, *Expert Review of Dermatology*.
[4] Madhuri A. Gore* , Deepika Akolekar, *"*Evaluation of banana leaf dressing for partial thickness burn wounds*", LTMG Hospital and LTM Medical College*, Sion (W), Mumbai 400022, India Accepted 29 January 2003, Burns 29 (2003) 487–492 [Elsevier].
[5] Jull AB, Walker N, Deshpande S, *"*Honey as a topical treatment for wounds*"*, Cochrane Database. Feb 28, 2013. *[PubMed]*.
[6] Osman, S.; Umar, H.; Hashmi, Y.; Jawaid, A.; Ahmed, Z, *"*The Efficacy of Honey Compared to Silver Sulfadiazine for Burn Wound Dressing in Superficial and Partial Thickness Burns—A Systematic Review and Meta-Analysis", *Trauma Care* 2022, 2, 523-534.[MDPI] https://doi.org/10.3390/traumacare2040043.
[7] Somboonwong J, Kankaisre M, Tantisira B, Tantisira MH, "Wound healing activities of different extracts of Centella asiatica in incision and burn wound models: an experimental animal study*", BMC Complement Altern Med*. 2012 Jul

20;12:103. doi: 10.1186/1472-6882-12-103. PMID: 22817824; PMCID: PMC3492213 [PMID].

[8] Nyi mekar saptarini1*, irma erika herawati2, uli yana permatasari2, *"*Total flavonoids content in acidified extract of flowers and leaves of Gardenia (gardenia jasminoides ellis)*"*, vol 9, suppl. 1, *2016 innovare academic sciences knowledge to innovation.*

[9] Saxena Mamta*, Saxena Jyoti, *"*Phytochemical screening of acorus calamus and lantana camara*"*, *Saxena Mamta et al.* IRJP 2012, 3 ISSN 2230 – 8407.

[10] Auwal MS, Saka S, Mairiga IA, Sanda KA, Shuaibu A, Ibrahim A, "Preliminary phytochemical and elemental analysis of aqueous and fractionated pod extracts of Acacia nilotica (Thorn mimosa*)", Vet Res Forum*. 2014 Spring; 5(2):95-100. PMID: 25568701; PMCID: PMC4279630.

[11] Ogunka-Nnoka CU, Igwe FU, Agwu J, Peter OJ, Wolugbom PH (2020), "Nutrient and Phytochemical Composition of Centella asiatica Leaves", *Med Aromat Plants (Los Angeles)* 9: 346. doi: 10.35248/2167-0412.20.9.346.

[12] P. Szweda, *"*Antimicrobial Activity of Honey*"*, *Honey Analysis*, Mar. 2017, doi: 10.5772/67117.

[13] Nascimento REA, Monte J, Cadima M, Alves VD, Neves LA. *"*Rendering Banana Plant Residues into a Potentially Commercial Byproduct by Doping Cellulose Films with Phenolic Compounds*", Polymers (Basel), 2021* Mar 9;13(5):843. doi: 10.3390/polym13050843. PMID: 33803474; PMCID: PMC7967194.

[14] I. Kaddoura,1,∗ G. Abu-Sittah,2 A. Ibrahim,2 R. Karamanoukian,2 and N. Papazian2, *"*Burn injury: review of pathophysiology and therapeutic modalities in major burns*", Ann Burns Fire Disasters, 2017* Jun 30; 30(2): 95–102, 2017 Jun 30, PMCID: PMC5627559, PMID:29021720.

[15] Ogunka-Nnoka CU, Igwe FU, Agwu J, Peter OJ, Wolugbom PH (2020), "Nutrient and Phytochemical Composition of Centella asiatica Leaves", *Med Aromat Plants (Los Angeles)* 9: 346. doi: 10.35248/2167-0412.20.9.34.

[16] JOUR, Shaikh, Junaid, Patil, Matsyagandha ," Qualitative tests for preliminary phytochemical screening: An overview" 2020/03/0110.22271/chemi.2020.v8.i2i.8834.

[17] Heyneman A, Hoeksema H, Vandekerckhove D, Pirayesh A, Monstrey S, "The role of silver sulphadiazine in the conservative treatment of partial thickness burn wounds: A systematic review". Burns. 2016 Nov;42(7):1377-1386. doi: 10.1016/j.burns.2016.03.029. Epub 2016 Apr 26. PMID: 27126813[*PUBMED]*.

[18] Fuller FW, "The side effects of silver sulfadiazine. J Burn Care", Res. 2009 May-Jun;30(3):464-70. doi: 10.1097/BCR.0b013e3181a28c9b. PMID: 19349889.

Detection of Flat Foot (Pes Planus) & High Arch (Pes Cavus) by Foot Pressure Analysis

Akshita Saraswat[1], Muthu P[2]
[1,2]Department of Biomedical Engineering, SRM Institute of Science and Technology, Kattankulathur, Chengalpattu, Tamil Nadu, India

ABSTRACT

The study aims to detect the deformity of the foot, such as a flat foot or the high arch foot plays a significant role in the gait pattern. Various Force Sensitive Resistor (FSR) pressure sensors are used to find the foot pattern at different foot locations, such as the forefoot, midfoot, and heel. The FSR, in combination with the resistor, is connected to the battery and microcontroller to find the reading at that particular region. The device identified the detection of the foot, and the values are displayed on the monitor and further conclusions are drawn by those reading with accuracy. Hence, the device works accurately to find whether the foot is flat, a high arch, or standard with the help of the FSR sensor.

Keywords: FSR Sensor, Arduino mega 2560, Matlab, Battery module, Flat foot, High arch

Corresponding Author:
Dr. P. Muthu,
Assistant Professor, Department of Biomedical Engineering, SRM Institute of Science and Technology, Kattankulathur
Email: muthup@srmist.edu.in

1. INTRODUCTION

The foot is a component of the human body that has a variety of functions that range from postural regulation to biomechanical contribution. Feet come in different shapes and sizes based on the genetic makeup and the arch defines whether a person is having good postural control over the body or not. Some people have a very flat arch with minimum callusing and a very healthy appearance. In contrast, there are instances where people suffer from foot deformities such as having a flat foot or having a high arch. Apart from heredity, personal lifestyle can also affect foot health [Kerr, 2013]. In today's scenario the type of footwear, the body weight, and the standing time can be taken into account for the possible reasons for having a foot deformity.

Considering the fact that feet are the shock absorber of the body, having a medial arch helps in the equal distribution of these shock waves. Feet response to the impact from uneven surfaces and propel to move forward depends upon the alternate flex and stiffening of the muscles. The 3 major categories in which feet can be defined and the role it plays are:

Neutral: It refers to the proper alignment of the foot and ankle when both are in a straight line and the feet form a sturdy platform that uniformly distributes pressure over the heel and forefoot [Kerr, 2013].

Excessive supination: Supination can be defined as the manner of running and walking of an individual. The way a foot propels and moves forward: the rotation of the foot and the lift of the heel which helps in pushing the toes from the ground.

Overpronation: Pronation is a method of shock absorption in which the arches of the foot collapse to spread the impact of the foot striking the ground. In case of overpronation, the arch collapses excessively downward or inwardly, commonly known as a flat foot.

So, by detecting such conditions where there is a probability of misalignment that can result in a postural deformity one can help in improving the overall alignment of the body which can be helpful in releasing the pain and healing the body. For the detection of such conditions, there are various insole devices generated that help to find out the different medical conditions like Pes Planus and Pes Cavus. Various biomechanical studies are conducted in the area to detect and suggest how one can be able to correct its postural deformity.

The motive of this project is to detect the condition of a flat foot or high arch in an individual and give a basic idea about how one can create a primary-level database using different sensors and heat waves visualization with various software to provide data that can be used in medical organizations so as to treat a patient suffering from any postural deformity.

2. REVIEW OF LITERATURE

The arch of the foot plays a significant part in a person's running and walking pattern by absorbing and distributing energy in a precise manner. An abnormal arch can be defined when this transfer of energy is not balanced and the pressure is not distributed properly throughout the foot anatomy [Mao, 2014]. In the case of flat feet, 2 major possibilities can occur, one where the foot is having a functional imbalance which is also known as flexible flatfoot. In such a condition the arch becomes flat when it is bearing weight and remains a medial arch when relaxed in other scenarios the foot may have structural damage which can result in a rigid flatfoot where

the arch is abnormal whether it is bearing some weight or not and the subtalar joint movement is found out to be very poor in such individuals. Some studies show that 95% of individuals suffering from foot deformity have flexible flatfoot and the remaining suffer from rigid flatfoot. In rigid flatfoot, there are high chances of neuromuscular damage and tarsal coalition [Okafor, 2014]. Apart from these, they suffer from pain and many severe pathological problems. For the treatment of rigid flatfoot, the only procedure is to undergo medical surgery when an individual encounters a high amount of pain. Polysomnography is the gold standard for assessing sleep, according to the American Academy of Sleep. It is carried out in a laboratory and is monitored by sleep technologists. When the patient is sleeping in the laboratory, at least seven separate parameters are acquired. Actigraphy is a less sophisticated technology that can assist measure sleep quality. It estimates sleep or waking durations based on bodily motions [D. J. Jaworski, 2021].

2.1. Plantar Pressure

Calculating the plantar pressure during the loaded phase of walking is vital for analyzing the human soul. Plantar pressure can acquire information about the characteristics of the forces and pressure acting upon the foot which can be helpful in studying chronic pain, ulcer, and injury in different parts of the foot. To be more accurate one needs to calculate the plantar pressure in a dynamic environment. The barefoot pressure can depend upon numerous parameters to assess the pressure measurement [Chuckpaiwong, 2008].

During the studies, it has been observed that each foot bears fifty percent of the body weight at the heel, forefoot, and great toe, but the midfoot bears the least plantar pressure. With the increase in the speed of walking the plantar pressure can increase in some particular regions such as the heel, central metatarsal, medial region, and hallux. The stress and peak plantar pressure are concentrated on the 5th metatarsal having a normal foot whereas the individuals with flatfoot bear the same on their 3rd metatarsal [Queen, 2009].

There are a total of eight anatomical areas designated for the assessment of plantar pressure. First on the heel, second on the medial midfoot, third on the lateral midfoot, fourth on the medial forefoot, fifth on the center forefoot, sixth on the lateral forefoot, seventh on the hallux, and eighth on the toes.[Razak, 2012]. There is literature to showcase that proves that the plantar pressure decreases in an amount if a person is having a flat foot. And vice versa that is the contact area and the plantar pressure in the midfoot decreases when a person is suffering from a high arch (Pes Cavus) [Ho, 2010].

2.2. Different Commercial Systems For Measurement of Plantar Pressure

While designing a PP measurement device the key features which are to be kept in mind are spatial resolution, accuracy, sampling rate, sensitivity, and calibration. A good quality pressure sensing device is a fundamental acquisition so as to obtain accurate results in a dynamic environment. There are generally 2 major categories in which the PP measuring devices can be classified as a PP measuring system and Ground Reaction Force (GFR) measuring system available in the current scenario [Liu, 2009]. For measurement of PP, various devices such as foot insole pressure pad, pressure platform system, and pedar are available. And for the measurement of GFR, there are some wearable force sensors such as the Flexi textile sensor system developed by Nitta Corporation which is used to calculate the force exhibited by a moving foot [Williams, 2000].

The measurement of PP can generally be done by 2 different mechanisms:

1) Platform System: This is a flat, rigid array of pressure sensor components arranged in a matrix pattern and installed on the floor to permit regular gait [Tekscan, 2012]. These platforms can be used for static and dynamic studies but have a major disadvantage in that their use is restricted to the lab because they cannot be carried everywhere.

2) In-Shoe System: These are flexible and are embedded in the shoes for measurement. They are portable and because of this they are helpful for wider studies and can be used for the analysis of walking patterns under different terrains. These are highly recommended but are prone to lose the sensor if not suitably fixed. Compared with the platform system, their spatial resolution is a bit low because of the low number of sensors placed in a confined space.

2.3. Load Distribution Measurement Methods

Various load distribution systems are being used for a long period of time and various advances have been made since that time.

1) Barefoot Measurement: For static and dynamic studies of plantar pressure load distribution platforms were developed for high-level performances. Eg: The Kistler Force Plate is one such device against which all the platform systems are compared. It is completely independent of total vertical and shear forces [NEVlLL, 1991]. The results obtained were highly specific and have good reliability because of the high rate of reproducing the constant results.

2) Discrete Sensors for in-shoe pressure measurement: The disadvantage of barefoot measurement led to the development of in-shoe pressure measurement. This method overcomes the problem of synchronizing the measurement of pressure with a specific phase of the gait cycle. They gave precise results but were not able to

replicate the results with the same accuracy because of the placement of a smaller number of pressure sensors and various other factors such as the silicon rubber breaks after a 1000 loading cycle [DINOWlTZ, 1985].

3) Foam Box Casting: These were developed to create a negative foot impression of the patient they proved to be a quicker and cleaner method to study the gait cycle. It eliminates the case of restlessness and can provide a better static and dynamic result because of the cast of the patient being used so as to study the pressure points during the course of a gait cycle [MJNNS, 1982].

4) Laser-based measurement system: Although this system was highly advanced with the use of technology but has severe drawbacks such as the patient is exposed to rays which can cause skin disorder if exposed frequently, a slight exposure from light can distort the image formed of the patient's foot and can differ the result analysis. It gives a 2-D result whereas to be accurate a 3-D output is required [Pfaffen, 2011].

5) Planipes Mobile Foot Pressure System: This system offers a versatile platform for a broad spectrum of applications in petrography. It consists of 2 sensors and a smartphone application. In this device, the pressure-sensitive sensors are placed inside the sole which is connected to a sensor board. This board collects all the data and transmits the data to the smartphone via Bluetooth It contains highly accurate FSR sensors that detect a slight change of pressure and therefore proved to be the most advanced form of pressure detection device [Sadun, 2016].

3. MATERIALS AND METHODS

3.1. Force Sensing Resistors

Force Sensing Resistors (FSR) sensors enable the detection of static and dynamic forces applied when in contact with the surface. The range of reactions mostly depends on the variance in electric resistance. Two popular, affordable, and widely accessible FSR sensors are Flexiforce and Interlink. Both FSR sensors are sufficient and dependable to provide a good sensing modality, particularly for measuring force, according to the research. Compared to the Interlink sensor, the linearity results from the Flexiforce sensor are better. Here we are using a flex force sensor to measure the pressure of the foot at different positions. The substrate (polyester/polyimide) film is divided into two layers to create the Flexi force sensors. A layer of the pressure-sensitive link is placed over each layer of conductive material (silver). In an electrical circuit, Flexi force sensors serve as force-sensing resistors. When the force sensor is not loaded, it has a very high resistance (about 5 mega ohms), and when a force is applied, this resistance falls as the applied force increases. By decreasing the feedback resistance and applying driving voltage, this sensor can be utilized to measure forces greater than 100 lbs. The sensor's sensitivity can be adjusted to meet system needs [Massimo, 2005].

It was demonstrated that a significant amount of FSR may be placed in a mattress to provide a pressure distribution [H. Diao, 2021].

The FSR sensor used in this project (part number 6163) is ultra thin 0.45mm and weighs 20g per sensor. The characteristics of the fsr sensor are given in the table below:

Sensor placement to record the foot pressure dispersion over eight regions. The heel, metatarsal head, metatarsal head (all high-pressure locations), and metatarsal head, toe, arch1, and arch2 are these eight areas (low-pressure areas). To give the pressure distribution and complexity of the sensor system the three best possible sites, the placement of which is shown in Figure 1 below.

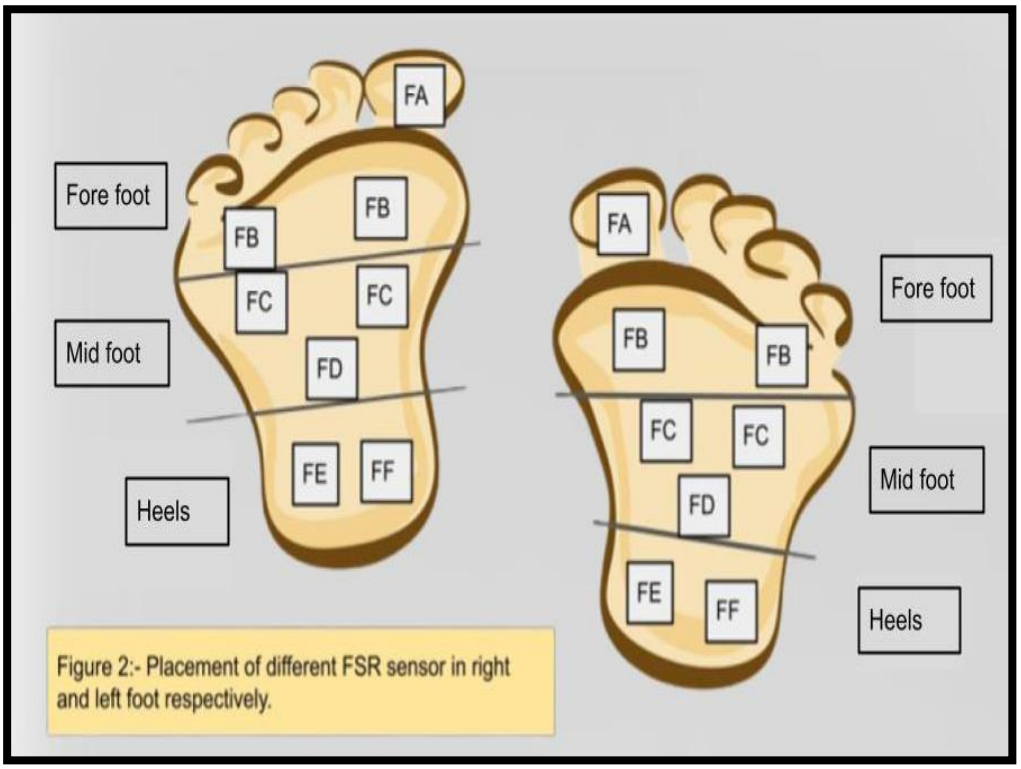

Figure 1. Division of the leg into different regions and placement of the fsr sensor

3.2 Jumper wire & Resistance

● The length of male-to-male, male-to-female, and female-to-male jumper cables is 20 centimeters.
● Type Connectors used are Standard Dupont 2.54mm Pitch 1 Pin-1 Pin, a housing Connector that offers exceptional electrical conductivity and oxidation resistance because of brass nickel-plated terminals.
● Cables are made of 12-core pure copper wire.
● It can be used for various experiments, electronic projects, breadboards, computer motherboards, and PCB creations.
● In this project we have used 10K ohm resistors in series with the fsr sensor and Arduino mega for getting the accurate value as shown in fig 2.

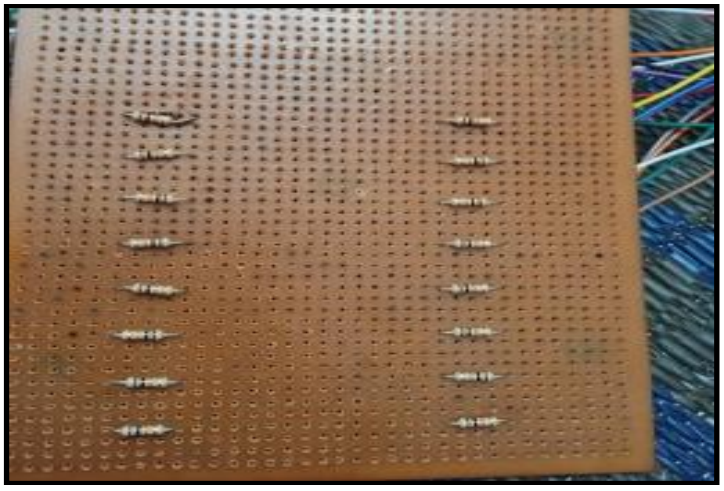

Figure 2. PCB and resistor connected with Arduino mega and power supply with the help of jumper wires

3.3. Arduino Mega

The length of Mega 2560 PCB is 4 inches and wide as 2.1 inches, equipped with a USB connector and power jack. The board can be sealed to a surface or container using three screw holes. The gap between digital pins 7 and 8 is 160 mil, not a multiple of the other pins' 100 mil spacing. An external power supply or a USB

connection can power the board. The source is selected automatically. The board can take power up to 6 to a 20-volt external supply. The 5V pin delivers less than five volts and when supplied with less than 7V the board becomes unstable. The voltage regulator overheats and harms for more than 12V.

Figure 3. Arduino mega2560

- **BLOCK DIAGRAM**

The block diagram of the project with components is shown in Fig 4.

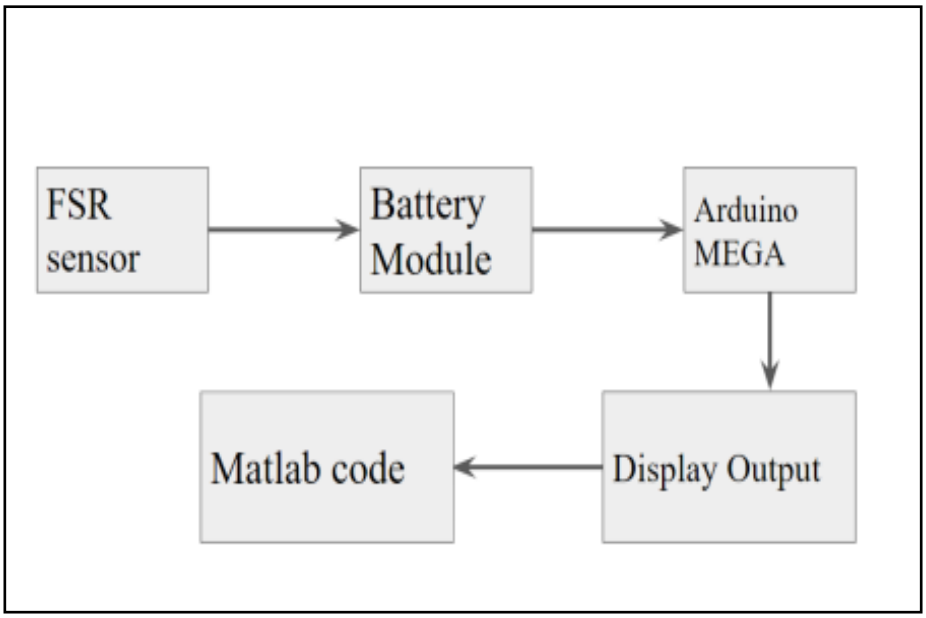

Figure 4. Block diagram of the device

4. RESULTS

The measurement is done on both sides of the leg simultaneously right as well as left. In this device, the sensors are divided into 3 major regions: forefoot, midfoot, and heel.

- Forefoot contains 3 FSR sensors on each leg,
- Midfoot contains 3 FSR sensors on each leg,
- While heel contains 2 FSR sensors on each leg,

These sensors add up the values of the sensors within the region and give a cumulative value such as FA, FB, FC, FD, FE, FF for left forefoot, left midfoot, left heel, right forefoot, right midfoot, right heel respectively.

The readings taken from the real-time subject are given in the below table 1:

Table 1. Reading of the device

Subject	FA	FB	FC	FD	FE	FF	Condition
1	2167	872	1808	2473	765	1749	Normal
2	2088	2282	1766	2046	2088	1898	High arch
3	2053	1736	1740	2563	1228	1782	Flat foot
4	2321	377	1746	2332	379	1767	High arch
5	2082	730	1827	2198	743	1684	Normal
6	2193	867	1967	2267	804	1856	Normal
7	2098	906	1645	2056	934	1905	Normal
8	2056	2156	1856	2167	1269	1823	Flat foot
9	2267	967	1645	2082	802	1678	Normal
10	2278	2345	1983	2098	1306	1592	Flat foot

These results show that when the FB and FE which is the midfoot reading for the left and right leg is:

- Less than 1000 the condition is said to be normal.
- If More than 1500 then it is considered to be a flat foot
- While if the value is less than 400 then it is considered a high arch foot.

5. FUTURE WORK

- To study the impact of the heel and its heel size on the pressure and how we are prone to get various disabilities with the same.
- To analyze the distribution pattern of pressure in presence of the heel.
- To find the correlation between the various pressure areas and the affected organ associated with the specified area.
- To visualize the pressure map of the foot and analyze it for further studies.

6. CONCLUSION

The main aim of the project is to find the deformity in the foot that includes a flat foot, high arch foot, or normal foot. Thus, it is mandatory in various professions to know the foot pattern before entering the specific role of a particular job such as various sports, military, and many more. Hence it becomes important to know the deformity and cure it. Through this project, not only the detection of the foot can be done but also the possibility of getting one can also be noticed. The early detection of foot deformity can help the person take preventive measures and also cure the same within less time. These types of diseases are not only related to genetics that is by birth but also can be acquired with time by an accident or bad posture sometimes the use of poorly designed footwear such as high heels can also result in foot deformities.

REFERENCES

[1] Kerr CM, Stebbins J, Theologis T, Zavatsky AB. Static postural differences between neutral and flat feet in children with and without symptoms. Clin Biomech (Bristol, Avon). 2015 Mar;30(3):314-7. doi: 10.1016/j.clinbiomech.2015.02.007. Epub 2015 Feb 17. PMID: 25721676.
[2] Mao, D, Li, J & Hong, Y 2006, 'The duration and plantar pressure distribution during one-leg stance in Tai Chi exercise', Clinical Biomechanics, vol. 21, no. 6, pp. 640- 5.
[3] G.O. Okafor, B., & U.O. Abaraogu, B. M. (2014). Flat foot and associated factors among. psychotherapy journal, 8.
[4] Martinez-Nova, A, Huerta, JP & Sanchez-Rodriguez, R 2008, 'Cadence, age, and weight as determinants of forefoot plantar pressures using the Bigfoot in-shoe system', Journal of the American Podiatric Medical Association, vol. 98, no. 4, pp. 302-10.
[5] Chuckpaiwong, B, Nunley, JA, Mall, NA & Queen, RM 2008, 'The effect of foot type on in-shoe plantar pressure during walking and running, Gait & Posture, vol. 28, no. 3, pp. 405-11.
[6] Queen, RM, Mall, NA, Nunley, JA & Chuckpaiwong, B 2009, 'Differences in plantar loading between flat and normal feet during different athletic tasks', Gait & Posture, vol. 29, no. 4, pp. 582-6.
[7] Ho, I-J, Hou, Y-Y, Yang, C-H, Wu, W-L, Chen, S-K & Guo, L-Y 2010, 'Comparison of plantar pressure distribution between different speed and incline during treadmill jogging', Journal of Sports Science & Medicine, vol. 9, no. 1, p. 154.
[8] Abdul Razak, AH, Zayegh, A, Begg, RK & Wahab, Y 2012, 'Foot plantar pressure measurement system: A review, Sensors, vol. 12, no. 7, pp. 9884-912.
[9] Liu, T, Inoue, Y & Shibata, K 2009, 'A small and low-cost 3-D tactile sensor for a wearable force plate', Sensors Journal, IEEE, vol. 9, no. 9, pp. 1103-10.
[10] MacWilliams, B.A.; Armstrong, P.F. Clinical Applications of Plantar Pressure Measurement in Pediatric Orthopedics. In Proceeding of Pediatric Gait, 2000. A New Millennium in Clinical Care and Motion Analysis Technology, Chicago, IL, USA, 22 July 2000; pp. 143–150.
[11] Tekscan. Tactile Pressure Measurement, Pressure Mapping Systems, Force Sensors, and Measurement Systems. Available online: http://www.tekscan.com/ (accessed on 1 January 2012).
[12] Novel Quality in Measurement. Available online: http://www.novel.de/ (accessed on 1 January 2012).
[13] Zebris Medical GmbH. Available online: http://www.zebris.de (accessed on 1 January 2012)
[14] BENNET, J. P., & DUPLOCK, L. R. (1993). Pressure distribution beneath the human foot. J. Am. Podiatric Med. Assoc., 674-678.
[15] NEVlLL, A. L. (1991). A foot pressure measurement system utilizing PVDF and copolymer piezoelectric transducer. Canterbury, UK: the University of Kent at Canterbury,.
[16] C., D. J., & DINOWlTZ, H. D. (1985). Limb length discrepancy---an electromyographic analysis. Am. Podiatric Med. Assoc., 639-649.
[17] MJNNS, R. J. (1982). Two simple plantar pressure recording devices in clinical use: evaluation using a pedobarograph. Eng. Med., 117-120.
[18] Pfaffen, S., Sommer, P., Stocker, C., Wattenhofer, R., & Welten, S. (2011). Planes: Mobile Foot Pressure Analysis. 5. ETH Zurich, ETH Zurich, Switzerland.
[19] Sadun, A. S., Jalani, J., & Sukor, J. A. (2016). Force Sensing Resistor (FSR): a brief overview and the Low-cost Sensor for active compliance control. First International Workshop on Pattern Recognition. doi:10.1117/12.2242950.
[20] Massimo, D. D. (2005). Arduino cc. Retrieved from Arduino: https://www.arduino.cc
[21] D. J. Jaworski, A. Park, and E. J. Park, “Internet of things for sleep monitoring,” IEEE Instrumentation & Measurement Magazine, vol. 24, no. 2, pp. 30–36, 2021.
[22] H. Diao, C. Chen, W. Yuan, A. Amara, T. Tamura, J. Fan, L. Meng, X. Liu, and W. Chen, “Deep residual networks for sleep posture recognition with unobtrusive miniature scale smart mat system,” IEEE Transactions on Biomedical Circuits and Systems, vol. 15, no. 1, pp. 111–121, 2021.

Crohn's Disease: Classification of Normal and Ulcer using Deep Learning Network

Mohana Priyaa S J[1], Muthu P[2]
[1,2]Department of Biomedical Engineering, SRM Institute of Science and Technology, Kattankulathur, Chengalpattu,
Tamil Nadu, India – 603 203

ABSTRACT
Crohn's disease (CD) is a type of Inflammatory Bowel Disease(IBD) which is characterized by redness in the digestive system but commonly appears in the small intestine. Diagnosis of CD is still a continuing issue for physicians. Even with advanced images, detecting CD in damaged tissue can be challenging, even for the experts. Deep Learning algorithms in the field of medicine and their related application has reported positive interest recently as a supplement tool for radiologist advice. Computer-aided diagnosis can save time and labour resources that would otherwise be spent on regular manual diagnosis. These contemporary methods for imaging the gastrointestinal system might assist detect tiny features symptomatic of CD are imaged with the help of colonoscopy and is invisible through eye.The purpose of the study is to establish and validate a Deep Learning network for the automatic finding of ileocecal and ascending colon ulcers in a person with CD using Colonoscopic images.Deep learning's performance in rating ulcer severity, on the other hand, has never been examined.The current effort sought to assess the accuracy of deep learning in evaluating ulcer severity in CD patients.

Keywords: Crohn'sDisease (CD), Inflammatory Bowel Disease (IBD), Deep Learning, Colonoscopy, Ulcer

Corresponding Author:
Dr. P. Muthu, Assistant Professor, Department of Biomedical Engineering
SRM Institute of Science and Technology, Kattankulathur
Email: muthup@srmist.edu.in

1. INTRODUCTION

(Hendrickson BA et al., 2002) Have analyzed common type of IBD are CD and UC. Crohn's disease is a recurrent inflammatory illness that mostly affects the gastrointestinal system. CD has no recognized aetiology. One of the cause, according to experts is due to the auto immune reaction. When your immune system aims the healthy cell, then it leads to autoimmune reaction. Because Crohn's disease occurs due to genetics.The common symptoms include fever, bowel obstruction, diarrhoea. In case, of severity in the disease leads to kidney stones, anemia and inflammation of bile ducts. The disease under study is a degenerative condition which leads to both bowel damage and disability. (Thia KT et al., 2010) said it commonly affects the terminal ileum and colon, two segments of the gastrointestinal tract. Typically, the inflammation caused by the disease is not symmetrical and transmural. Upon initial diagnosis, most patients present with an inflammatory phenotype. However, over time, approximately halved of patients experience complications that often require surgical intervention.

The types of CD includes (i) Ileocolitis: the ileum and colon region appears to be reddened and swelled, the symptoms include pain will be felt in the lower part of abdomen &diarrhea. (ii) Ileitis: The ileitis affects the ileum of the colonic region, the symptoms includes formation of abscess and fistulas in the right side of lower abdomen (iii) Jejunoileitis: The Jejunoileitis causes inflammation in the mid region of the intestine, the symptoms include The Jejunoileitis causes inflammation in the mid region of the intestine. The risk factors of CD develop in the age from 15 to 35 years of age has the higher possibility of developing the disease. Also, People with Crohn's Disease has the highest chance of developing colorectal cancer. The diagnostic procedure of Crohn's Disease includes blood and stool test.The internal viewing is done using Computed Tomography (CT), Colonoscopy.

Table 1 shows the statistical data of IBD obtained from various sources like gastrojournal, the hindu business line and Centre for Disease control & Prevention.

Table 1. Statistics of Inflammatory Bowel Disease

Statistics	Source
US: A total of 3.1 have received diagnosis of IBD	*www.cdc.gov*
Mortality rate : 18 in 1000 person has been expiring with this disease in overall case	*www.gastrojournal.org*
India: 1.5 million patients affected by the Inflammatory Bowel Disease, putting the country second only to the USA with 1.6 million.	*www.thehindubusinessline. com*

2. CRITICAL ANALYSIS OF EXISTING RESEARCH

Based on the review of (Torres et al., 2017) The most severely infected area for the person with CD is colon and terminal ileum. The exact cause of CD is not known. Yet, it is believed that in genetically vulnerable people, it involves an unusual immune response to symbiotic microbial organisms. The clinical presentation of Crohn's disease varies widely, but signs include abdominal discomfort, loss of weight and fatigue. The analysis of CD is based on a combination of clinical, laboratory, radiographic and endoscopic evidence. Treatment of CD aims to preserve remission, enhance QOL. This may include medications such as corticosteroids, immunomodulators, and biologic agents, as well as surgery in some cases. The authors also discussed the role of nutrition in Crohn's disease, including the importance of optimizing nutrient intake and avoiding trigger foods.

(Braat H et al., 2006) According to the study, although the precise origin of CD is not yet known, it is thought to be brought on by a confluence of genetic predisposition and climatic variables. It has been suggested that those with a family history of Crohn's disease have a far higher risk of developing the disease than people in general. In addition, the prevalence of Crohn's disease is higher in developed nations, raising the possibility of an environmental factor.Consumption of animal and milk protein, as well as an imbalanced ratio of omega-6 to omega-3, has high rate of developing CD. Conversely, consuming vegetable protein may lower the risk. The relationship between fish protein and Crohn's is unclear. (Reniers DE et al.,October 2001) said that smoking has been linked to an increased risk of flares,and the introduction of hormonal contraception has been associated with a rise, potentially due to its effects on the digestive system.

A broader study by (Yung DE et al., 2017) & (Mishkin DS et al., 2006) the channel has been opened up in field of medical image processing and Machine Learning as a result of computer-aided anomaly identification in capsule endoscopy pictures. Image processing, Machine Learning and Deep Learning are some of the examples of the types of algorithms that may be used to discover and detect irregularities that may be present with a variety of colour and texture patterns. In order for machine learning to learn anomalies with handmade characteristics, like texture, colour and statistical data, it employs the methods of segmentation like super-pixel, Visual Words and features. These methods are used in conjunction with one another. The performance of models that are based on machine learning is dependent on the features that are used to represent the irregularities as well as the methods that are used to extract the features from the photos. Deep learning models make use of datasets that have been annotated in order to learn characteristics that can detect anomalies. Deep models such as CNN models, have had a great deal of success, but is contingent to the clarity of images present. In the field of medicine, an inadequately marked dataset continues to be significant challenge in the field. Researchers began considering partial training to the system and the addition of experts aspect into deep networking methods in order to construct clinical trustworthy deep models. This was done so that they might find a solution to the problem. Many studies have been conducted over the course of the past few years in the field of computer based detecting and classification of endoscopic images for analyzing. These reviews have focused on deep model performing criteria, computational severity and features were employed. In recent ages, advancements has been achieved technologically through the use of deep models. Some of these advancements include attention mechanisms, the integration of expert information in the decision making analysis of models and in the generation deep model design. This work provides a review on deep models in WCE pictures, considering them without the handmade features and classification methods in order to find the explorational needs in differential aspects (SVM, KNN and Random Forest).

(Pennazio M et al., 2015) The study states that Colonoscopy is a diagnostic and monitoring technique that has been used successfully for Crohn's disease for many years. Even in the midst of clinical or biological remission, Crohn's disease patients commonly exhibit signs of small-bowel mucosal swelling. In cases of CD, the diagnostic yield of Colonoscopy is at less comparable to cross-sectional image for the purpose of identifying cases with active endoscopic swelling.

(Koulaouzidis A et al., 2012) The author suggested an innovative approach known as WCNN to differentiate between the abnormal picture from normal classifications with the WCE pictures. By simplifying computing process in order of using labels at the pixel level, image level labels were employed. An experiment was carried out with the MICCAI gastro-endoscopy challenge data set as well as the KID dataset in order to determine whether or not a Deep Salient Detection method could identify the salient point in WCE frames that was associated with GI problems.

(Zhou T et al., 2007) According to the author, convolutional neural network was determined as a method for doing quantitative test for celiac disease with endoscopy pictures. As a classification model, Google Net was utilized, and it was trained by making use of both celiac normal and normal photographs. Models of feedback-based deep learning have been presented for the classification of lesions in the real one. For the purpose of locating imaginary kernel and small sores in intestine, so external embedded platform was utilised. The rate of the frame and the quality of the therapy have the potential to be either enhanced or lowered, depending on the input. The suggested approach was successful in achieving decreased inactivity, increased competency and lesion detection in real world.

(Zhang et al, 2021) Identified biomarkers and pathways associated with Crohn's disease using machine learning methods. The authors used a variety of machine learning algorithms to analyze gene expression data from patients with CD and healthy controls. The outcomes are several potential biomarkers and pathways associated with Crohn's disease, including the NF and TNF signaling pathways.

(Gong et al., 2020). Developed an AI-based diagnostic tool for CD.The authors used a Convolutional Neural Network (CNN) to analyze abdominal CT scans from patients with Crohn's disease and healthy controls.The CNN achieved high accuracy in differentiating CD patients from healthy controls, suggesting that it could be a useful diagnostic tool.

(Zhang et al., 2020) Developed an AI-based system for predicting disease activity in CD persons.The authors used a combination of feature selection and machine learning algorithms to analyze clinical and laboratory data with Crohn's disease.The developed a predictive model that was able to accurately predict Crohn's disease.

(Muralidharan et al, 2019) Developed an AI-based system for predicting CD. The authors used a machine learning algorithm to analyze clinical and laboratory data from patients with Crohn's disease who had undergone treatment with anti-TNF therapy.The predictive model that was able to accurately predict response in patients with Crohn's disease.

(Li et al., 2019) The author developed an AI-based system for identifying genetic variants associated with CD. The used a deep learning algorithm to analyze genome-wide association study (GWAS) data with CD and healthy controls. The deep learning algorithm was able to identify several novel genetic variants associated with Crohn's disease, highlighting the potential of AI methods for genetic research.

The goal of this work is to distinguish ulcers in the ileocecal valve and ascending colon of individuals with Crohn's disease by analyzing colonoscopic images.

3. METHODOLOGY

3.1. Block diagram

Figure 1 explains the block diagram of the workflow. The block Input Dataset refers to the collection of data which consist of images of ulcers and normal. The Pre-Processing Phase is a set of operations applied to the input dataset before the image segmentation and feature extraction phases. This phase can involve operations such as image resizing, filtering, noise removal, and image enhancement to improve the quality of the images and make them suitable for further processing. The task of dividing an image into distinct regions within the image is known as image segmentation. This involves segmenting an image of ulcer to isolate the affected area. Feature Extraction involves analyzing the segmented image to identify specific features or patterns that can be used to classify the image as either ulcer or normal. This might involve identifying color or texture differences between the two types of images. Feature Classification is the final stage of the process, where the features extracted from the segmented images are used to classify each image as either ulcer or normal and is done using Deep learning algorithm.Ulcer and normal are the two classes or categories into which the images are classified based on the features extracted from them. The goal of the process described above is to accurately classify images into these two categories based on their features.

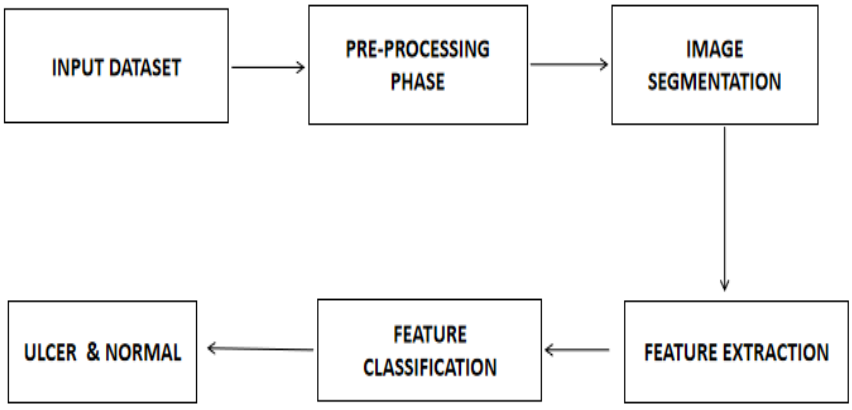

Figure 1. Block diagram demonstrating the overview of workflow

3.2. Dataset

The image data's of Crohn's Disease ulcer were acquired from GastroAtlas and Gastroenterology Consultants Of South Jersey (GCSJ) in the form of portable network graphics files. PNG file format is taken into consideration to prevent the loss in the image while processing. GastroAtlas and Gastroenterology Consultants Of South Jersey is the website that exclusively contains endoscopic images.From the above mentioned websites, number of images obtained for normal is 500 and for ulcer is 500.

3.3. Tools and software

MATLAB (an abbreviation for MATrix LABoratory) is a licensed desktop environment software that is designed to process design and iterative analysis using c/c++ programming languages and can also run-on clusters and GPUs. It is a multi-programming and numeric-computing environment developed by MathWorks. This software has been tremendously used in the field of image processing to develop various models and classification methodologies using deep learning and machine learning frameworks.

3.4. Pre-Processing

Data pre-processing is the process of identifying raw input and rendering for study in deep learning model. The purpose of doing this step is raw images contains noise and imbalanced data. Thereby, which leads to the enhanced accuracy in the model. The noise is removed using Top-hat filtering technique, this is used to eliminate the unbalanced brightness followed by histogram equalization so as to increase the contrast of image. This process is done in Matlab software.

3.5. Object Detection- YOLO V3

The Yolo V3 uses 53 convolution layers. First, the Yolo V3 algorithm creates a grid out of the image. Each grid cell estimates some number of the boundary boxes that should be placed around those things that have a high score for the previously specified preset classes. Each bounding predictions has its own confidence score. Additionally, each bounding box can only identify a single item at a time. The predictions were produced by grouping the ground truth boxes taken from the initial dataset in an effort to identify the most frequent shape and size.

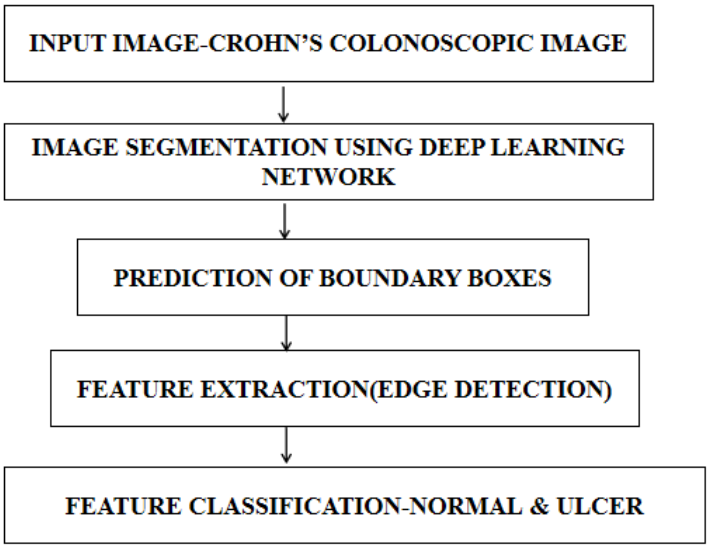

Figure 2. YOLO V3 workflow

3.6. Image Segmentation

Image segmentation is done to detect the oddity in the region of interest. The segmentation algorithm used is region based growing method, this segmentation algorithm works based on gray value of the neighbouring pixel value. If the threshold value is inside the seed pixel then it will be considered as pixel region.

The region growing approach starts with seed pixel and then expand to nearby pixel the neighbouring pixel is added to seed pixel if the neighbouring pixel adheres to the preset rule this procedure follows until there are no similarities left. If the neighbouring pixel do not adhere to the pre-defined rule then the process ends. The under pinning technology is the bottom up approach.

Region-based image segmentation algorithms focus on identifying regions and connections within the pixels within an image that have similar characteristics, such as colour or texture. These regions are then used to separate the image into distinct parts. By segmenting the image into regions, it is easier to separate the image into distinct parts, allowing the CNN to make more accurate predictions about what class each pixel belongs to. This combination of region-based image segmentation can be used to accurately detect and classify objects or scene elements within an image.

Region-based segmentation is further divided into region-growing and region-splitting and merging methods. The algorithm used in this project is a region-growing segmentation algorithm.

The region-growing approach starts with a seed pixel and then expands to the nearby pixels. The neighbouring pixel is added to the seed pixel if the neighbouring pixel adheres to the preset rules. This procedure follows until there are no similarities left. If the neighbouring pixels do not adhere to the predefined rules, then the process ends. The underpinning technology in this is the bottom-up approach.

3.7. Classifier:ResNet-50

As described by He et al. (2016), the ResNet-50 architecture is a popular deep neural network architecture for image classification tasks. ResNet 50 contains 50 convolutional network of layers, it can load thousands of images and classifies based on the object detected and undergoes training and produces output. The ResNet-50 is a convolutional neural network with 48 convolutional layers, 1 max pool layer and 1 average pool layer.

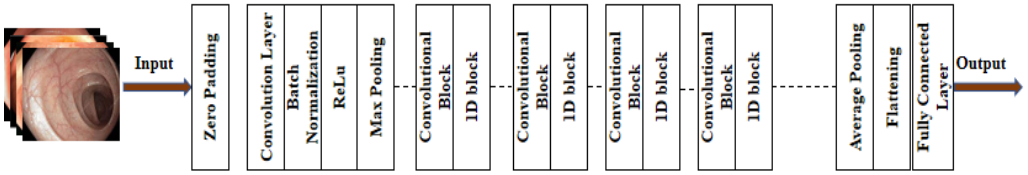

Figure 3. RESNET-50 Architecture diagram

The use of residual connections, which allow the network to bypass certain layers and make the training process more efficient, is the key innovation of ResNet-50. This also allows the network to be deeper without experiencing degradation. According to (Kaiming He et al., 2016) ResNet-50 has demonstrated cutting-edge performance on a wide range of computer vision tasks, including image classification, object detection, and semantic segmentation. ResNet-50's architecture is divided into five stages, each with a different number of residual blocks. The first stage performs simple convolution and pooling operations, with subsequent stages increasing the complexity of the operations gradually. The network is divided into four residual blocks, each of which contains several repeating units of convolutional layers. The shortcut connections in each block allow the network to bypass one or more layers, which helps to alleviate deep neural network degradation. The network takes an input image with dimensions of 224 x 224 x 3 and generates an output vector with 1000 dimensions, representing the probabilities of the image belonging to each of the 1000 classes. ResNet-50 has demonstrated cutting-edge performance on a variety of benchmark datasets, and its architecture has been widely used and adapted for a variety of computer vision tasks.

4. RESULTS AND DISCUSSION

The colonoscopic images of ulcer is segmented using region growing technique. The figure 4a-shows the image with ulcer and figure 4b,c,d -shows the segmented ulcer affected region.

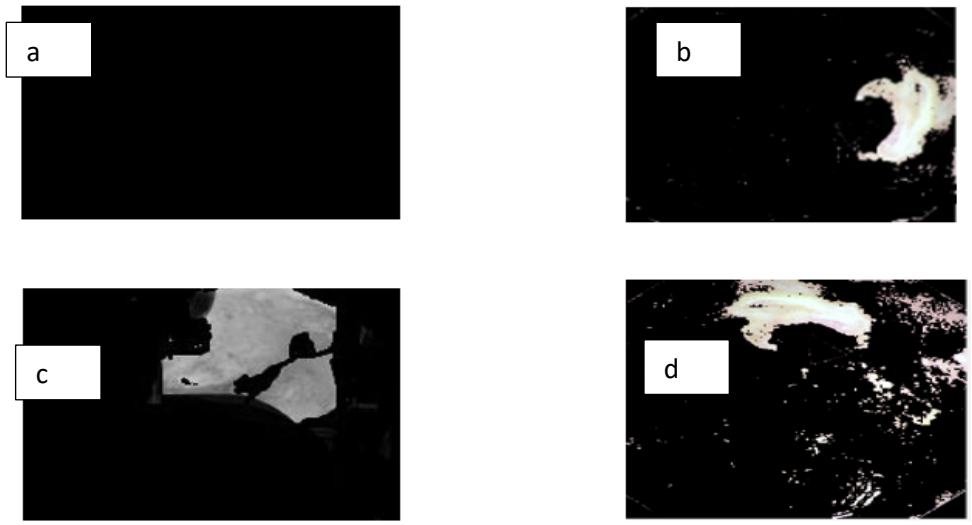

Figure 4. a) Image showing absence of ulcer b) Image displays the ulcer region segmented from the surrounding tissue, with an affected area of 0.15cm c) Image displays the ulcer region segmented from the surrounding tissue, with an affected area of 0.48cm d) Image displays the ulcer region segmented from the surrounding tissue, with an affected area of 0.92cm

The figure 4a, shows the image has been captured or generated shows a region of tissue in particular patient or sample, does not contain any evidence of an ulcer.

The region-based segmentation approach was utilized for the segmentation of ulcers from the Colonoscopy images, the output shows the ulcer affected region. The abnormalities found in the images were segmented and are shown in the above figures.The image has been processed to segment the ulcer region from the surrounding tissue, this segmentation process allows for the quantification and measurement of the ulcer area, which can be useful in assessing the severity and progression of the disease.In the figure 4b, the affected area of the ulcer has been measured to be 0.15cm. This measurement likely refers to the area of the ulcer itself, and not the total size of the image or the affected area of tissue surrounding the ulcer. The measurement of 0.15cm suggests that the ulcer is relatively small, but the clinical significance of this finding would depend on the individual case and other factors such as the location severity of symptoms, and the patient's overall health.

In the figure 4c, the affected area of the ulcer has been measured to be 0.32cm. This measurement likely refers to the area of the ulcer itself, and not the total size of the image or the affected area of tissue surrounding the ulcer. The measurement of 0.32cm suggests that the ulcer is of a moderate size, but the clinical significance of this finding would depend on the individual case and other factors such as the location severity of symptoms, and the patient's overall health.

In the figure 4d, the affected area of the ulcer has been measured to be 0.98cm. This measurement likely refers to the area of the ulcer itself, and not the total size of the image or the affected area of tissue surrounding the ulcer. The measurement of 0.98cm suggests that the ulcer is relatively large, and could indicate a more severity. However, the clinical significance of this finding would depend on the individual case and other factors such as the location, severity of symptoms and the patient's overall health.

4.1. ROC Curve

The ROC curve is a graph demonstrating the performance of a classification model at all classification thresholds and is plotted as the true positive rate (TPR) against the false positive rate (FPR). FPR is defined as the ratio between the number of negative events wrongly categorized as positive (false positive) and the total number of actual numbers of total negative categorizations irrespective of the classification. TPR indicates the number of correct predictions with respect to the total number of positive predictions. In a ROC curve, A value of 0.8-0.9 has been indicated as a good classification value. The performance results of the machine learning classifiers used in this study illustrated that the ROC curve has a steeper increase in its classification efficiency with the values increasing over 0.8 gradually and attaining stability. This indicates that the trained models were able to efficiently discriminate the images into fibroid and non-fibroid images efficiently without over fitting the data points.Figure 5 ROC graph represents the classification threshold values which is drawn as true positive values to that of the false positive value.

True Positive Rate (TPR) = $\frac{TP}{TP+FN}$

False Positive Rate (FPR) = $\frac{FP}{FP+TN}$

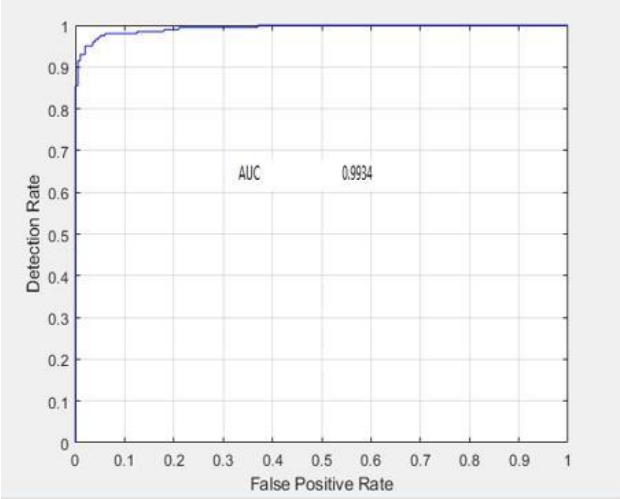

Figure 5. The image showing Receiver Operating Characteristics (ROC) value

4.2. Accuracy

A performance metric called accuracy is frequently employed to assess how well a classification model is doing. Out of all the predictions the model made, it calculates the percentage of predictions that were accurate.The formula for accuracy is

ACCURACY=TP+TN/(TP+FP+TN+FN)

Where FP (False Positive) is the number of negative instances that were incorrectly classified as positive, FN (False Negative) is the number of positive instances that were incorrectly classified as negative, TP (True Positive) is the number of positive instances that were correctly classified, and TN (True Negative) is the number of negative instances that were correctly classified.Taking the above into consideration the obtained accuracy percentage value is 97.6%.

4.3. Specificity

A statistical metric called specificity assesses a diagnostic test's accuracy in identifying people who do not have the illness or condition it is intended to diagnose. It calculates the percentage of persons who do not have the disease or condition, including healthy people and people who are unwell, who are accurately recognized by the test as having true negative results (TN).

SPECIFICITY= TN/(TN+FP)

Where FP stands for the quantity of false positive outcomes and TN for the number of true negative results. With high specificity, there is less chance of receiving false positive test results because the test is particularly good at identifying those who do not have the disease or condition. In other words, if a test has a high specificity, it may be trusted to rule out the disease or condition being tested for and has a low rate of false positive results. The specificity of the suggested study is 94.8%, according to the data. This means that the test properly recognised 94.8% of those who do not have the disease or condition being tested for as true negatives, while 5.2% were mistakenly labeled as positives. This implies that the test has a high degree of specificity, which is a desired quality for a diagnostic test.

4.4. Sensitivity

Sensitivity is a statistical term that describes a test's or a model's capacity to accurately detect positive examples or cases. Sensitivity, in other words, measures the percentage of true positive cases among all true positive and false negative cases that are accurately detected by a test or model.Sensitivity is calculated as,

SENSITIVITY=TP/(TP+FN)

where TP stands for true positive cases and FN for false negative cases. False negative cases are those that the test or model wrongly identifies as negative, while true positive cases are those that the test or model correctly identifies as positive.

A sensitivity of 98.8% in the context of the proposed research denotes that 98.8% of the true positive cases can be accurately identified by the test or model used in the study. This indicates that the test or model is a reliable method for detecting positive cases because it has a high degree of accuracy in identifying them. To fully comprehend the performance of the test or model, it is crucial to keep in mind that sensitivity should always be read in conjunction with other metrics like specificity, positive predictive value, and negative predictive value.

4.5. ResNet-50:Training Accuracy & Loss

Figure 6 shows the accuracy and loss percentage curve. This is used to distinguish between the predicted output and the actual output. This mainly focuses to minimize this loss, so that the network can make accurate predictions on new data. This curve should decrease over time, indicating that the network is learning to make better predictions. Accuracy measures the percentage of correctly classified example. The accuracy curve should increase over time, indicating that the network is making more accurate predictions.The loss curve and the accuracy curve are important tools for monitoring the progress of a neural network during training, and can help identify potential issues such as over-fitting or under-fitting.

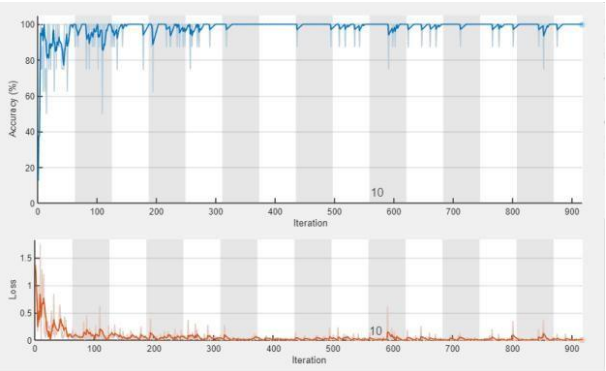

Figure 6. Accuracy and Loss Curve

4.6. Confusion matrix

When assessing classification models, the confusion matrix is an effective instrument. It offers a succinct and understandable illustration of the model's performance in terms of instances that were properly and incorrectly classified. The true positive, true negative, false positive, and false negative counts are represented by a table with four columns in the confusion matrix. The confusion matrix can be used in a research paper to assess a machine learning model's performance and to identify the model's advantages and disadvantages. It can also shed light on the model's precision, memory, accuracy and F1 score. The confusion matrix also help to identify the sources of errors in the model (Gupta, M. 2021). For example, if there are a large number of false positives, this may indicate that the model is too sensitive to a particular feature, or that the model is over-fitting to the training data and is illustrated in the Table 2.

Table 2. Confusion Matrix values

	Predicted positive (Ulcer) (%)	**Predicted Negative (Normal) (%)**	**Percentage(%)**
Actual positive (Ulcer)	(TP) 489	(FN) 11	Sensitivity 98.8
Actual Negative (Normal)	(FP) 13	(TN) 487	Specificity 94.8
			Accuracy 97.6

The given dataset includes 1000 colonoscopy images, with 500 images showing ulcers and 500 images showing a normal ileocecal valve and ascending colonic colonoscopy. The dataset has been randomly split into two subsets, one for training and one for testing the model.The performance of the trained model is evaluated using two metrics: AUC and accuracy. AUC (Area Under the ROC Curve) is a measure of how well the model distinguishes between positive (ulcer) and negative (normal) samples, across a range of classification thresholds. Accuracy is the proportion of correctly classified samples out of the total number of samples. An accuracy of 97.6% means that the model is able to correctly classify the majority of the images in the test set.

4.7. ResNet-50 classifier values

Table 3. ResNet-50 classifier values

Model	**Accuracy**	**Sensitivity**	**Specificity**	**Precision**	**Recall**	**F1 score**
RESNET 50	97.6	98.8	94.8	97	97	97

Table 3 gives the ResNet-50 classifier values and is calculated based on true positive and true negative values. True positive represents the number of ulcers that have been accurately predicted as positive. A true negative value is an indicator of the number of normal images that have been accurately classified. False positive is the percentage of wrong classification of normal images as ulcer positive and false negative represents the number of images that have been wrongly classified as normal images though they have ulcers in them.

4.8. Limitations & Future Work

The limitations of this work include images collected from only one region of India which is also a smaller dataset. The study can be evaluated by using data from more regions and performing classification based on ethnicity, age. In the future, deep learning techniques may be used to complement and facilitate colonoscopy reading.

According to (Wang, Y., 2020) Convolutional and recurrent neural networks are two examples of deep learning techniques that may help with Crohn's disease diagnosis and therapy. Nevertheless, there are still a number of issues that will need to be resolved in subsequent work.The need for a lot of high-quality data is one of deep learning techniques' main limitations. This can be particularly challenging in groups with rare diseases like Crohn's disease. In order to enhance the functionality and generalizability of deep learning models, future research must concentrate on gathering and annotating more data, including data from a variety of populations and clinical results.The interpretability of deep learning models is a crucial problem. Although these models can produce highly accurate results, it can be challenging to comprehend how they made their forecasts. The use of deep learning in clinical decision-making may give rise to ethical issues because of this lack of interpretability. Therefore, future research must concentrate on creating more understandable and transparent models that can be applied in the clinic safely and successfully.

5. CONCLUSION

The overall aim of the current study is utilizing DL classifiers to detect and classify ulcer images into normal and ulcer-positive images. Previously only a few deep learning classifiers have been used on colonoscopy images for the detection of ulcer. This proposed a comparison study for different deep learning. GLCM feature

extraction was performed on the images providing the statistical features of the images. On Colonoscopy image, reliable and speedy automatic identification of ulcers is made possible by deep learning technology. Individual patient-level analysis offered excellent and consistent diagnosis accuracy while simultaneously reducing the amount of time needed for reading.

REFERENCES

[1] Hendrickson, B. A., Gokhale, R., & Cho, J. H. (2002). Clinical aspects and pathophysiology of inflammatory bowel disease. Clinical Microbiology Reviews, 15(1), 79-94.
[2] Thia, K. T., Sandborn, W. J., Harmsen, W. S., Zinsmeister, A. R., & Loftus, E. V. (2010). Risk factors associated with progression to intestinal complications of Crohn's disease in a population-based cohort. Gastroenterology, 139, 1147-1155.
[3] Peyrin-Biroulet, L., Loftus, E. V., Colombel, J. F., & Sandborn, W. J. (2010). The natural history of adult Crohn's disease in population-based cohorts. American Journal of Gastroenterology, 105(2), 289–297.
[4] Freeman, H. J. (2008). Colorectal cancer risk in Crohn's disease. World Journal of Gastroenterology, 14(12), 1810–1811.
[5] Howlader, N., Noone, A. M., Krapcho, M., Miller, D., Brest, A., Yu, M., Ruhl, J., Tatalovich, Z., Mariotto, A., Lewis, D. R., Chen, H. S., Feuer, E. J., & Cronin, K. A. (Eds.). (2019). SEER Cancer Statistics Review, 1975-2016. National Cancer Institute.
[6] Torres, J., Mehandru, S., Colombel, J. F., & Peyrin-Biroulet, L. (2017). Crohn's disease. The Lancet, 389(10080), 1741–1755.
[7] Braat, H., Peppelenbosch, M. P., & Hommes, D. W. (2006). Immunology of Crohn's disease. Annals of the New York Academy of Sciences, 1072(1), 135–154.
[8] Liu, J. Z., & Anderson, C. A. (2014). Genetic studies of Crohn's disease: past, present and future. Best Practice & Research Clinical Gastroenterology, 28(3), 373–386.
[9] Baumgart, D. C., & Sandborn, W. J. (2012). Crohn's disease. Lancet, 380(9853), 1590–1605.
[10] Reniers, D. E., & Howard, J. M. (2001). Isotretinoin-induced inflammatory bowel disease in an adolescent. The Annals of Pharmacotherapy, 35(10), 1214–1216.
[11] Yung, D. E., Boal Carvalho, P., Giannakou, A., et al. (2017). Clinical validity of flexible spectral imaging color enhancement (FICE) in small bowel capsule endoscopy: a systematic review and meta-analysis. Endoscopy, 49(3), 258–269.
[12] Mishkin, D. S., Chuttani, R., Croffie, J., et al. (2006). ASGE Technology Status Evaluation Report: Wireless capsule endoscopy. Gastrointestinal Endoscopy, 63(4), 539–545.
[13] Pennazio, M., Spada, C., Eliakim, R., et al. (2015). Small-bowel capsule endoscopy and device-assisted enteroscopy for diagnosis and treatment of small-bowel disorders: European Society of Gastrointestinal Endoscopy (ESGE) Clinical Guideline. Endoscopy, 47(4), 352–376.
[14] Koulaouzidis, A., Smirnidis, A., Douglas, S., et al. (2012). QuickView in small bowel capsule endoscopy is useful in certain clinical settings, but QuickView with Blue Mode is of no additional benefit. European Journal of Gastroenterology & Hepatology, 24(9), 1099-1104.
[15] Zheng, J. J., Cu, X. Q., Shi, X. H., Wang, Y. M., Jia, L. M., Zhou, X. L., et al. (2007). Colonoscopic and histologic features of colonic Crohn's disease in Chinese patients. Journal of Digestive Diseases, 8(1), 35-41.
[16] Zhang, J., Huang, J., Dong, L., Xu, Y., Zhang, L., Wang, J., & Chen, Y. (2021). Identification of biomarkers and pathways associated with Crohn's disease using machine learning methods. Frontiers in Genetics, 12, 607090.
[17] Gong, Z., Li, C., Li, J., Liang, Y., Li, H., Li, M., Li, Y., Chen, H., Zhang, Y., Liu, J., Wang, J., & Li, B. (2020). An artificial intelligence-based diagnostic tool for Crohn's disease. Journal of Gastrointestinal Surgery, 24(11), 2479-2485.
[18] Zhang, J., Liu, Y., Cui, X., & Chen, Y. (2020). Artificial intelligence-based system for predicting disease activity in Crohn's disease. Journal of Gastroenterology and Hepatology, 35(6), 1037-1043.
[19] Muralidharan, S., Seo, Y., Kim, Y., & Lee, H. S. (2019). Machine learning-based prediction of response to anti-TNF therapy in patients with Crohn's disease. In Proceedings of the 10th ACM Conference on Bioinformatics, Computational Biology and Health Informatics.
[20] Li, Y., Chen, B., Gao, X., et al. (2019). Current diagnosis and management of Crohn's disease in China: Results from a multicenter prospective disease registry. BMC Gastroenterology, 19, 145.
[21] He, K., Zhang, X., Ren, S., & Sun, J. (2016). Deep residual learning for image recognition. In Proceedings of the IEEE conference on computer vision and pattern recognition (pp. 770-778).
[22] Kaiming He, Xiangyu Zhang, Shaoqing Ren, Jian Sun. (2016). Identity Mappings in Deep Residual Networks. In Computer Vision – ECCV 2016 (pp. 630-645). Springer International Publishing.
[23] Gupta, M., & Gupta, M. (2021). Deep learning techniques for sentiment analysis: A systematic literature review. Journal of King Saud University-Computer and Information Sciences, 33(2), 168-179.
[24] Wang, Y., Xu, J., Xu, L., Zou, Q., & Guo, J. (2020). Deep learning in Crohn's disease: A systematic review. Journal of Crohn's and Colitis, 14(5), 676-687.

Design of Shoulder Gridle to Study the Effect of Loading in Shoulder Gridle and Humerus Bone

Parthapratim Mondal[1], Varshini Karthik[2], Ashokkumar D[3]
[1,2,3]Department of Biomedical Engineering, SRM Institute of Science and Technology, Kattankulathur, Chengalpattu, Tamil Nadu, India – 603 203

ABSTRACT

Shoulder gridle is one of the complex segment which results in different range of motions based on the loading conditions and the this study focuses on the design of the shoulder gridle and to study the effect of loading in shoulder gridle and humerus bone. This study focuses on the segmentation and 3dimensional (3D) model of shoulder gridle along with humerus bone with materialize mimics software. The segmented model will be smoothened and remeshed for analysis purpose. The 3D segmented model will be imported in ANSYS software for analyzing the shoulder gridle along with humerus bone. The results obtained are physical properties of the bone like density, young's modulus, poisons ratio and the mechanical properties of the bone were identified based on the different loading conditions.

Keywords: Humerus Bone, Coronal plane, Sagittal plane, Axial plane, Segmentation, Mimics, 3matic

Corresponding Author:
Dr. Ashokkumar D,
Associate Professor, Department of Biomedical Engineering
SRM Institute of Science and Technology, Kattankulathur 603203 Tamil Nadu, India
Email: ashokd@srmist.edu.in

1. INTRODUCTION

The shoulder gridle is the complex joint in the human body. It comprises of different articulation joints such as glenohumeral, sternoclavicular, acromioclavicular, coracoclavicular, and scapulothoracic. The main glenohumeral joint is an ball and socket joint which includes more complex and dynamic articulation between the scapula and humerus. The other two joints sternoclavicular and acromioclavicular provide mobility.Stability is provided by proper muscle actions which is developed by passive stabilisers, which contain glenohumeral capsule, glenoid labrum and other ligaments etc. The surface of the glenoid is much smaller than the humerus, which provides high range of movements[1,2] The scapulothoracic joint will have different range of motion in upper part of the body and it covers about 65% of the total sphere [3].

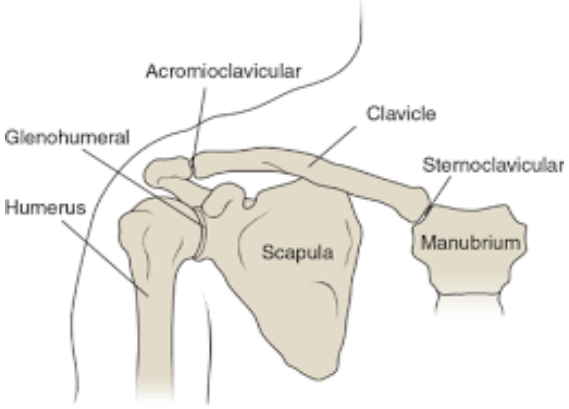

Figure 1.1. Shoulder girdle

Fig 1.1.shows the shoulder girdle and the diagnosis of shoulder joint exhibits the seriousness of the injury has to be evaluated and proceed for the total Shoulder replacement. Total shoulder replacement replaces the shoulder's unique ball-and-socket joint (or glenohumeral joint) with comparatively molded prosthetics. Subsequent to recuperating from a medical procedure, patients commonly have fundamentally less agony, expanded shoulder quality, and better scope of movement.

The computed shoulder models are in two categories, the first one is multi-body models which is based on body dynamics and the second one is finite element (FE). In multi-body models, the major body segments are

to be rigid bodies and they will not have deformations and the main muscles are made with line actuators without 3D volume [4–6]. The measured data which is used to drive multi-body models will have skin artifacts. The multi-body models may be used a valuable tool to improve the understand the functions of biomechanical movements of the musculoskeletal system [7].

The mechanical models which is based on a finite element method used as a successful tool to assess different loading conditions of the shoulder musculoskeletal structure [8]. Over the years, the FE method has been used as a better tool to study wide range of problems in biomechanics and orthopaedics [9].

The aim of this study is to identify the effect of loading in shoulder girdle and helps to analyze the different mechanical properties on the shoulder joint. The analysis will provide to find the range of movements in different planes with different loading conditions.

2. MATERIALS AND METHODOLOGY

2.1. Materials

2.1.1. Materials dataset

The computed tomography images of 23 year male shoulder bone has been collected from the hospital in DICOM format.

2.1.2. Software description

The major software's which are used to do this study were MIMICS,3 MATIC and ANSYS for developing the 3D model of shoulder girdle and humerus bone.

2.1.3. Mimics

Mimics 14 version has been used to convert medical picture data (Dicom files) into 3D anatomical models. Mimics in Print may connect directly to your preferred source of 3D printing as well as other sophisticated visual tool applications to produce 3D Mimics in print may be seamlessly integrated into your hospital's workflow to quickly convert medical picture data (Dicom files) into 3D anatomical models. Mimics in Print may connect directly to your preferred source of 3D printing as well as other sophisticated visual tool applications to produce 3D.

2.1.4. Materialise 3-Matic

A 3D modelling tool called Materialise 3matic allows us to modify and optimise designs at the STL level using CAD designs, topologies, and models created from optimised scanned data as a starting point. The sophisticated solution that enables you to take advantage of all the power and ease of 3D printing in order to perform design changes at the mesh level. Additionally, a topology-optimized model, simulation, scanned data, or a CAD design are frequently the starting points of a superb design for additive manufacturing.The raw data for convert the mesh and give back to CAD using materialize 3-Matic. The additional features can include (i) 3D textures, (ii) lattice structures, and (iii) conformal structures to improve your design for additive manufacturing. The last but not least feature of 3-matic is scripting automation, which makes it simple to generate different validation samples and boost productivity.

2.1.5. Ansys

The ANSYS 14.0 platform, a common-purpose bounded modelling application, is used to mathematically address several mechanical failures. Acoustical, electro - magnetic, static/dynamic, structural analysis, heat transmission, and fluid issues are just a few of the issues that might arise. ANSYS, a typical-purpose bounded application, is used to computationally solve a variety of mechanical issues. Acoustical, electro - magnetic, static/dynamic, structural analysis, heat transmission, and fluid issues are just a few of the issues that might arise. The Ansys Workbench system, one of the company's main products, is used in the majority of Ansys simulations. Large radius are frequently divided into smaller, flexibly designed, and evaluated units by Ansys programmers. The measurements of an item may be determined before weight, pressure, temperature, and other physical attributes are included. The Ansys software can model and evaluate other long-term consequences as well, including motion, degradation, cracks, fluid behavior, temperature profile, electromagnetic effectiveness, and others.

2.2. Methodology

2.2.1. Importing the medical data

CT image specification:
Subject Age:23
Number of slices: 426
Type of CT image: Knee CT

Slice width:251pxl
Slice height:355pxl
Pixel size:0.684 mm
The CT that was acquired was input into the MIMICS 19.0 using DICOM file and was imported in the software.

2.2.2. Organize images

There are multiple number of CT images, it might engage in further procedures, which will be irrelevant and cause problems with the reconstruction of 3D models. Thereafter we need to bring down the number of CT images to be taken in order to relieve the left over strain and power up our ability to "Compose Images." While using MIMICS, we can choose images from the "Arrange Images" interface that are suitable for our project and that we should be able to look and use it properly.

2.2.3. Thresholding

It is necessary to select the edge value precisely because different affiliation will have different faint stimulus in CT images. When the edge value is done and set, we can look over the CT images to examine what is necessary to understand the separated relationships. In such a way to avoid the artifacts, the edge value should be kept as low as possible. A worthy advantage and motivator for Mimic is hardly 270 (as per Hounsfield scale). A pixel guide for the tissue's direct X-beam constriction coefficient is the thresholding principle can be visible in CT images. Directly applied X-beam constriction coefficient of water rises to 0, whereas that of air approaches -1024, thanks to the scaling of the pixel values that is introduced as Hounsfield (HU) scale. Hounsfield scale influences threshold.

2.2.4. Region developing

A minimal cutoff of 485HU and a higher limit of 1467HU were set on to include all of the cortical bone at the shoulder girdle skeletal structure and to eliminate the ligament domains. The responsive tissue portion's accounting spectrum was expected to be between -188HU and 3071HU. The bone structure that is visible with green coloring is considered for thresholding. In this stage, we choose the structure of bone for which a 3D model is required. We merely decide to utilize that region of the knee as the prototype. As a result, thresholding is the process of selecting the body shape.

2.2.5. Effect of loading

The fig 4.1.shows the study flow diagram of the process and the CT images are imported into the software and three views which mimics are axial, coronal, and sagittal. The data artifacts are removed by filtering each view. The segmented data is used further processing. The 3D model of the shoulder girdle and humerus are created an STL file from the 3D model.

The file is imported in 3 Matic software and this software will be used for smoothing and remeshing. Convert the 3D model into an STL file and the image has been fed into Ansys software. Apply boundary conditions such as force, bearing load, stress, and strain. Investigating and analyzing the loading effect.

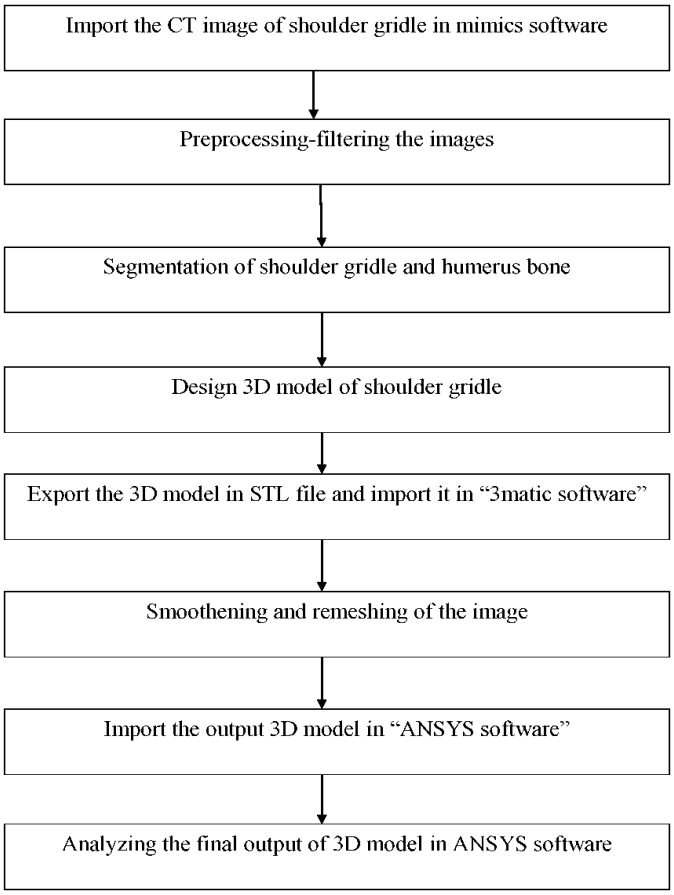

Figure 2.1. Study flow diagram

2.2.6. Physical properties

Stress is a physical term that define the amount of applied force to a material per square inch. Stress, which results from externally applied forces, is a physical science and engineering term for force per unit area within the material. The stress distribution a substance can endure before shattering is referred to as the breakdown stress or maximum tensile stress. Tension is what causes a substance to be tensile. The material is attempting to be stretched by the forces at work. There is an internal restoring force produced when the elastic bodies take on their original shape. We will refer to this restoring force as stress if we attempt to calculate how much it exerts per unit area on the deformed body.

Compression occurs when a body is being squeezed by external forces and the stress tests are performed on the bridge to ensure that it can tolerate high pressure without failing. The internal force per unit area is undoubtedly what is meant by "stress." Most importantly, an object's level of strain is ultimately defined by the quantity of strain imposed to it.

Nodal forces are transformed from bearing loads. The Results environment will show the impact of this conversion. In comparison to surrounding nodes that are located inside the surface's interior, forces at edge and corner nodes are substantially smaller.

3. RESULTS

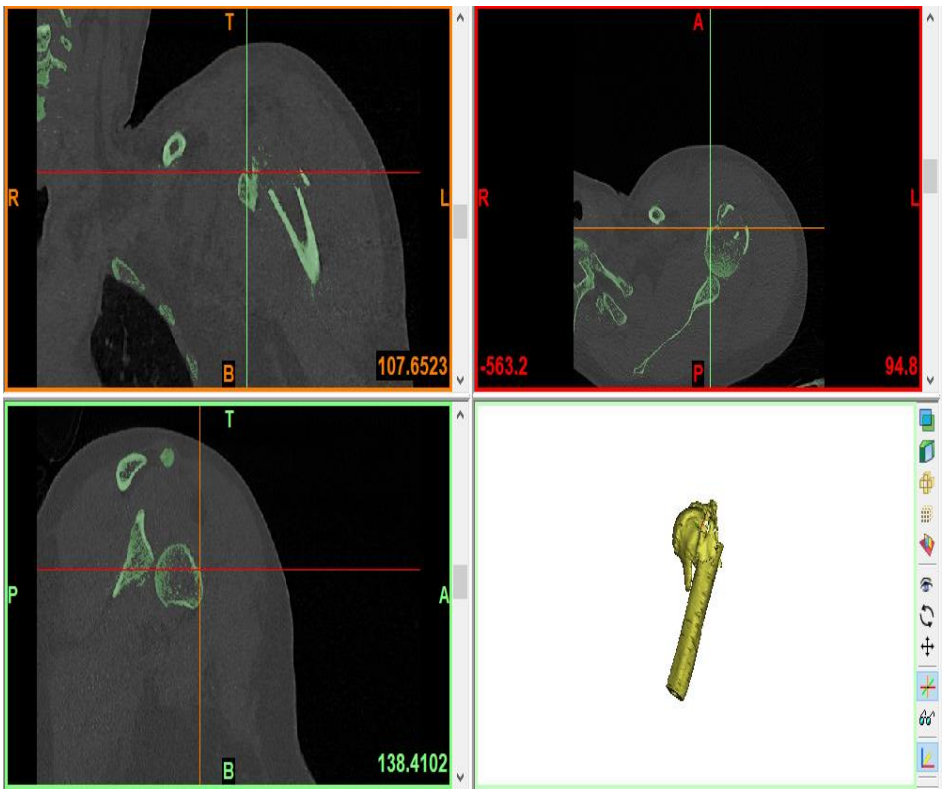

Figure 3.1. Segmentation of total shoulder using edit mask and region growing technique

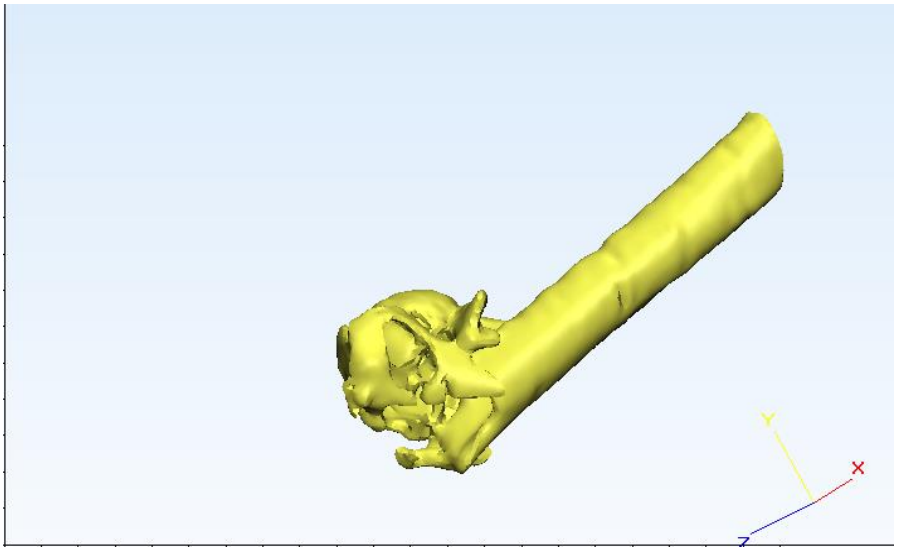

Figure 3.2. Meshing of shoulder joint

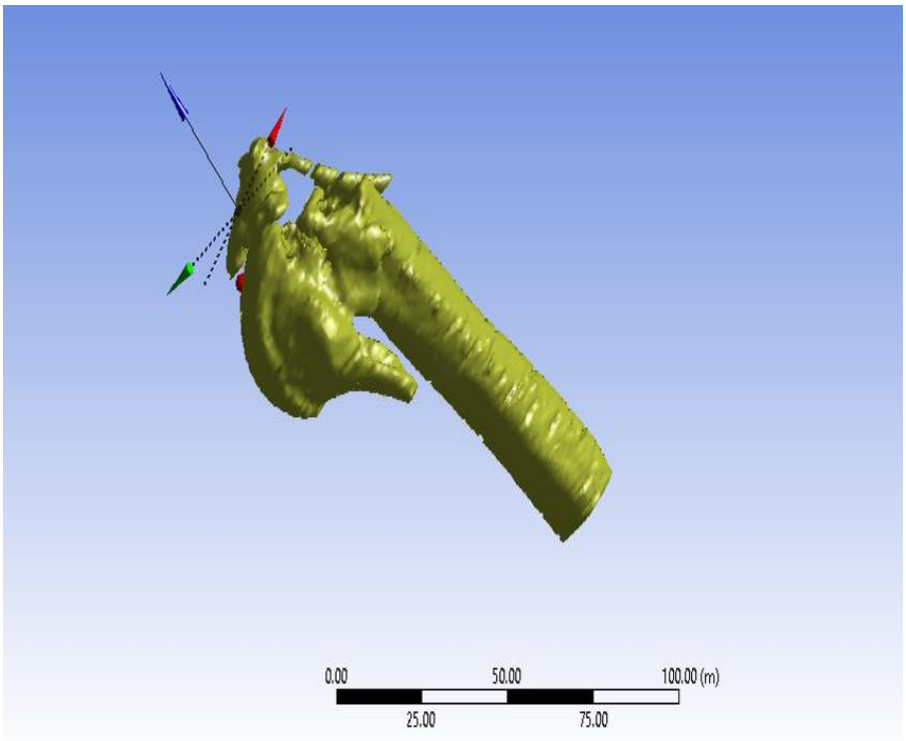

Figure 3.3. Analyzing the shoulder joint

Table 3.1. Physical properties of bone

Type of Material	**Young's Modulus**	**Poissons ratio**	**Density (Kg/m^3)**
Bone	2e^{11}	0.3	7850

Bulk Modulus	1.6667e+11 Pa
Shear Modulus	7.6923e+10 Pa
Isotropic Secant Coefficient of Thermal Expansion	1.2e-05 1/°C
Compressive Ultimate Strength	0 Pa
Compressive Yield Strength	2.5e+08 Pa
Strain-Life Parameters	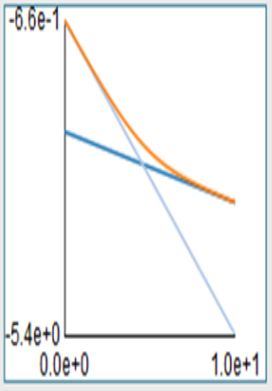

Figure 3.4. Mechanical properties of the shoulder girdle

4. DISCUSSION AND CONCLUSION

This study done with MIMICS which shows the segmented part of the shoulder girdle and humerus bone which has uses different procedures to get a 3Dmodel of the shoulder bone and proper meshing and smoothening of the bone has been done and a similar kind of study done by FGelaude et al. were they studied with using the optimal parameter settings for the respective segmentation procedures, sub-voxel mesh accuracies can be attained [15].

The segmented bone has been tested for the physical properties using ANSYS and the young's modulus, Poisson's ratio and density of the shoulder girdle was tested and the same kind of study done by SN khan et al. were they explained that the correlation between BMD and HU is calculated for cortical and cancellous bones and the correlation is validated with the experimental set up for finding the bone strength [16].

The study results suggests that the segmented shoulder girdle and humerus bone should be tested with different plane movements and the loading effect of the shoulder has to be tested with different part of the joints and also we found that different loading applications has to be done for further improvement and to find impact in different parts of the shoulder.

ACKNOWLEDGMENT

I would like to sincerely thank the management of SRMIST for providing the research facilities to conduct this study.

REFERENCES

[1] Haering D, Raison M, Begon M. Measurement and description of three-dimensional shoulder range of motion with degrees of freedom interactions. Journal of Biomechanical Engineering 2014; 136(8):084502. doi:http://dx.doi.org/10.1115/1.4027665.

[2] Artini FH, Timmons MJ, McKinley MP. Human Anatomy. Prentice Hall: Upper Saddle River, New Jersey, USA, 2000; 223.

[3] Ngin AE, Chen SM. Statistical data base for the biomechanical properties of the human shoulder complex—I: Kinematics of the shoulder complex. Journal of Biomechanical Engineering-T Asme 1986; 108(3):215–221. doi: http://dx.doi.org/10.1115/1.3138605

[4] Dickerson CR, Chaffin DB, Hughes RE. A mathematical musculoskeletal shoulder model for proactive ergonomicanalysis. Computer Methods in Biomechanics and Biomedical Engineering 2007; 10(6):389–400. doi:http://dx.doi.org/10.1080/10255840701592727.

[5] Garner BA, Pandy MG. Musculoskeletal model of the upper limb based on the visible human male dataset. Computer Methods in Biomechanics and Biomedical Engineering 2001; 4(2):93–126. doi:http://dx.doi.org/10.1080/10255840008908000.

[6] Högfors C, Karlsson D, Peterson B. Structure and internal consistency of a shoulder model. Journal of Biomechanics 1995; 28(7):767–777. doi:http://dx.doi.org/10.1016/0021-9290(94)00134-P.

[7] Stops A, Wilcox R, Jin Z. Computational modelling of the natural hip: a review of finite element and multibody simulations. Computer Methods in Biomechanics and Biomedical Engineering 2012; 15(9):963–979

[8] Favre P, Snedeker J, Gerber C. Numerical modelling of the shoulder for clinical applications. Philosophical Transactions of the Royal Society A: Mathematical, Physical and Engineering Sciences 1895; 2009(367):2095–2118. doi:http://dx.doi.org/10.1098/rsta.2008.0282

[9] Huiskes R, Hollister SJ. From structure to process, from organ to cell: recent developments of FE-analysis in orthopaedic biomechanics. Journal of Biomechanical Engineering-T Asme 1993; 115(4B):520–527. doi:http://dx.doi.org/10.1115/1.2895534.

Relationship Between Body Composition, Bone Mineral Density And Isokinetic Strength In Both Indian And African Population

Upendo S.Busanya[1], Varshini Karthik [2], Ashokkumar D[3]
[1,2,3]Department of Biomedical Engineering, SRM Institute of Science and Technology, Kattankulathur, Chengalpattu, Tamil Nadu, India – 603 203

ABSTRACT

The study explains experimental procedures to measure and analyze the body composition, bone mineral density with isokinetic strength for two ethnic groups, Indians and Africans and find out the relationship with respect to muscle activities from which the posture and movements were corrected in order to reduce the risk of injuries in our activities of daily life. The collection of data was performed between two groups of the age range from 19years to 23years from Africans and Indians. The subjects was allowed to take three tests procedures, the BCA using Body composition analyzer, BMD using DEXA machine and finally was given a physical exercise for loading and unloading the upper limb and recorded the EMG, acceleration and gyroscope The slightly difference was found in which the African group with standard Body composition and higher BMD has also performed highly in a given physical exercise compared to the Indian group. For different ethnic groups, the differences in cultural and traditional background may affect both Body composition and BMD of these groups and hence the resulted output based of the given physical exercise related to the differences in their pre-respective tests taken.

Keywords: Bone mineral density (BMD), body composition, body composition analyser (BCA), physical exercise

Corresponding Author:
Dr. Ashokkumar D,
Associate Professor, Department of Biomedical Engineering
SRM Institute of Science and Technology, Kattankulathur -603203 Tamil Nadu, India
Email: ashokd@srmist.edu.in

1. INTRODUCTION

Illustrating of bone minerals, muscle-bone and fat-bone interactions changes in body composition occurs in different ethnic groups. These changes have important metabolic and functional consequences. Both changes in body mineral density BMD and body composition may have effect on muscle activity [1].

Although the relationship between bone mineral density and body composition has been described in different gender and age group, neither of these has come across different ethnic group specifically African and Indian. Furthermore addition measurement has been provided in this study which differs from past study with respect to different body muscle activity. In fact several factors are known to have an effect on BMD including food nutrients and cultural background between these two ethnic groups. Therefore we are going to investigate the relationship between body composition BMD and isokinetic strength in both populations.

The study comprises of more number of parameters taken in body composition compare to the other studies which will help with proper guide to determine the standard health of the subject as well as the body mineral density. The EMG acceleration and gyroscope were taken as additional data with respect to a provided physical exercise to monitor the movement and strength of the upper limb for the first stage of the experiment.

The group of young male from Africa to India was subjected to the experimental investigations in relation to the young male from India and the relationship of the results of the tests were analyzed and shows that the cultural and traditional background has the effect on the relationships experimented.

2. LITERATURE REVIEW

Thibault Sutter et al (2019) study, explains any differences occurring in the body composition has the actual effect of changes in bones, and hence bone mineral density as the muscles and fat of these bones are affected as well. During life time as growth occurs with changes, it happens that there is a closely relationship between age and osteoporosis and if not encountered with exercises and proper meal, obesity may become the part of it. The study shows that more details has been given out about female in different ages but very less for male especially for the young ones. This gives a wide gap of more studies to be conducted in this particular area [1].

Sangun Lee et al (2022) clarified that those who spends more time in space have the problem of extremely bone loss, and this is due to the fact that there bones are exposed to more activities which stress them out and the outcome is the later. Theories has been proven that the more the bone rest the more its reform hence

people needs some rest from some mechanical activities to replace tearing effects that may occur. There is a certain level from beyond which stress occur, hence any functional activities involving bones should not be above this limit. This goes with sufficient rest from any kind of involvements for the bone. The body composition of the human also applies great role in this effect from which in our daily life and movement the decay may occur without our knowledge [2].

Jessica Piasecki et al (2019) elaborates that exercises at certain age provides a good muscle stabilities and healthy especially for elderly group. More studies has been conducted to prove this nevertheless the female gender appear to be the minority. Large group of people who exercise their body has managed to reduce large amount of fat in their body and this makes them to be in a good health. Both exercises have been a large influence to become strong and the researches show that less number of women being in this group. Either the exactly numbest of Elderly group who exercise with the result of gaining muscle strength is not yet clear. The gap gives chances for more studies and research in this area as well. Taking an example of some studies which gives out the results as expected for the exercising aged group to be stronger than the other who does not, but on the other hand, other study tells no changes [3].

Anna Kopiczko1 and Joanna Cieplińska (2022) demonstrate with clear study how the smoking habit affect our daily life, especially its effect on the bone mineral content (BMC).Many accidents which unnecessarily occur will cause break of bone for this particular group of people. The presence of tobacco is said to be dangerous for its presence in bone, hence for someone to escape from this risk and take care of his health it is very important to quit from this behavior. This comprises of staying away from people who smoke since you may indirectly be affected too despite the fact that you don't smoke but as long as you stay with people of such habit you will still be in danger and decrease your bone mineral content. For both female and male who smokes the results describes that large number of male are more affected in their BMC while less number of female for the similar habit. Researchers have found that there is huge quantity of S100A8 and S100A9 proteins said to be the main cause of smokers' endangering their bone density [4].

3. MATERIALS AND METHODOLOGY

3.1. Subject

The subjects were obtained from the college student for both ethnic groups within age 19 to 23 years, who were found, fit to conduct the experiment. The experiment was done in India were the student from different countries in Africa came for studies hence was easy to get the expected number of subjects for the study.

3.2. Questionnaires

The study for eligibility was based on questionnaires where the subjects were asked questions based on their healthy history and background to make sure that there is no one with bone disease or unfit to perform the experiment. Also the questions were asked on record of time taken for African subject to be in India, that is 'for how long they have been staying in India' and if there is any changes in their body compositions due to environmental changes as well as food being taken for their living.

3.3. Body composition

Body composition was measured by body composition analyzer and the parameter taken was; fat mass, fat free mass, muscle mass, body mass index and VFR. The age, height and body weight of the subject was recorded as well. The test was accuracy and valid as the machine is in a standard mode.

3.4 Bone mineral density

Bone mineral density was measured by using DEXA machine from which the BMD.BMC as well as T-scores and Z-scores were easily obtained for both upper and lower limb from which the required data was taken for analysis purpose. The machine used is an international standard and so the procedure followed was accuracy obtained.

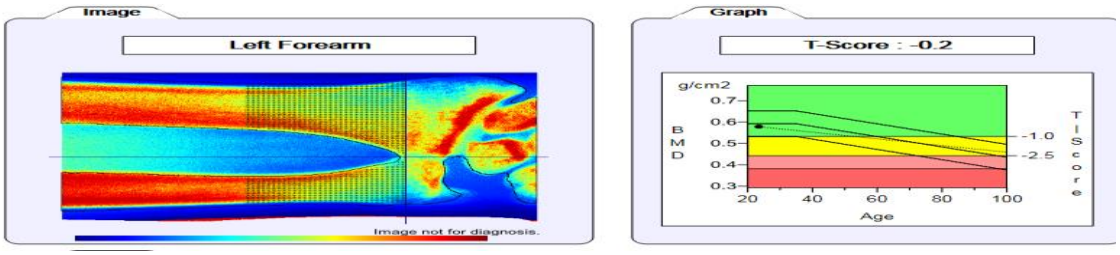

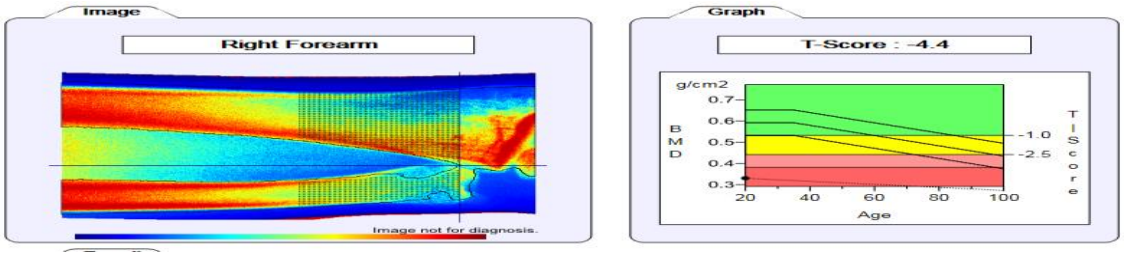

Figure 4.1. Images and graphs for measured left and right forearm

3.5. IMU

The Inertial measurement unit used for the EMG, acceleration and gyroscope was Lab-chart from Delsys a valid machine with sensors able to monitor the kinematic motion of the upper limb positioned at the required muscles. The physical exercise was given to the subject with and without load and the sensors from the device was able to record the respective measurements in time

4. RESULTS

Table 5.1. Association between BCA and BMD Parameters in Indian and African Population

Demographic features	**Indian Male (Mean ± SD) Number of subjects-05**	**African Male(Mean ± SD) Number of subjects-07**	**T-Test**
Age (years)	20.60±1.14	21.43±2.07	0.44
Weight (Kg)	62.16±3.86	73.80±18.79	0.21
Height (cm)	171.60±3.05	176.0±6.16	0.18
BMI (Kg/m^2)	21.12±1.71	23.64±4.72	0.28
FAT Mass (Kg)	9.80±2.66	16.11±11.79	0.27
FFM (Kg)	52.36±4.13	58.37±6.66	0.11
Muscle Mass (Kg)	49.62±3.93	55.64±6.22	0.09
LA-BMD (g/cm^2)	0.48±0.05	0.50±0.06	0.43
RA-BMD (g/cm^2)	0.47±0.05	0.047±0.04	0.86

Table 5.2 Association between EMG in Indian and African Population

Muscle Parameters	**Indian Male (Mean ± SD) Number of subjects-02**	**African Male(Mean ± SD) Number of subjects-02**
RH-Biceps EMG (mV)	0.032±0.0024	0.0213±0.0016
RH-Triceps EMG (mV	0.030±0.0009	0.0461±0.0019
LH-Biceps EMG (mV)	0.046±0.0019	0.0564±0.0012
LH-Triceps EMG (mV)	0.035±0.0028	0.0374±0.0019

5.1. Data analysis

The Table.5.1. Association between BCA and BMD Parameters in Indian and African Population for the group of young male with average age of 20 and 21 respectively, the fat mass, fat free mass, muscle mass, BMI was taken with respect to their weight and height and comparison was done for both group using Ttest method including the left and right arm bone mineral density (BMD) measured for both group, and result shows a slightly difference between the two. With such a low number of subject it was difficult to conclude the exactly result even though African group appear to have both average body composition and bone mineral density higher than Indians. The result table taken for IMU test Table 5.2: Association between EMG in Indian and African Population gives the slightly difference as well.

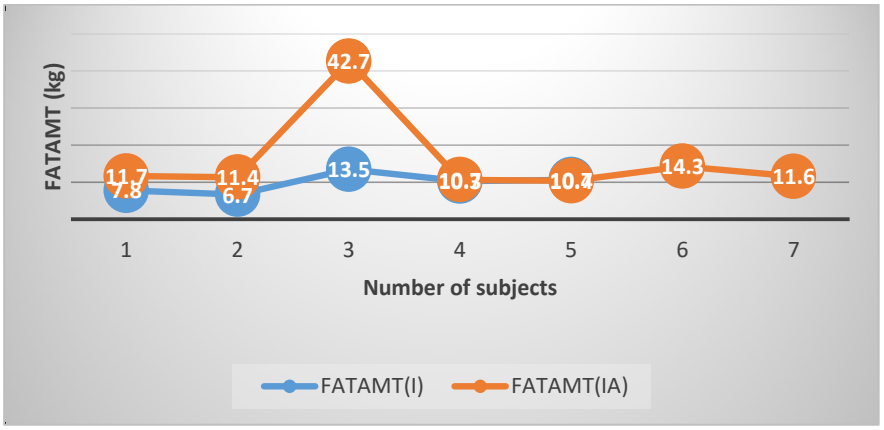

Figure 5.4. Fat mass difference between Indian and African population

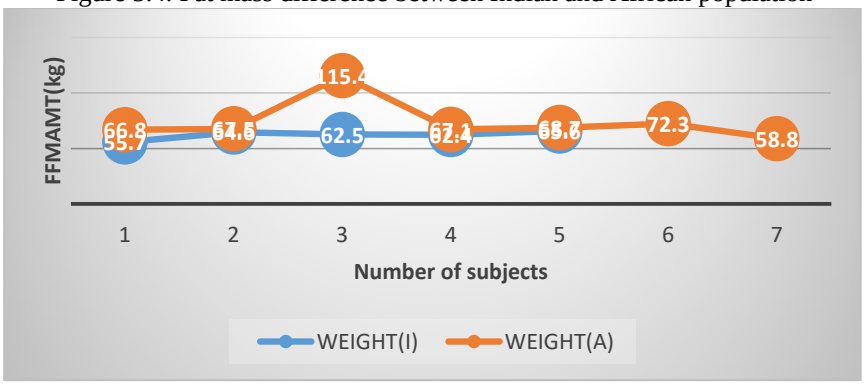

Figure 5.5. Fat free mass difference between Indian and African population

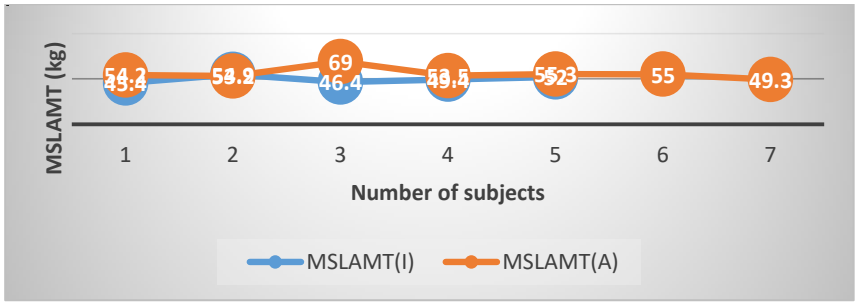

Figure 5.6. Muscle mass difference between Indian and African population

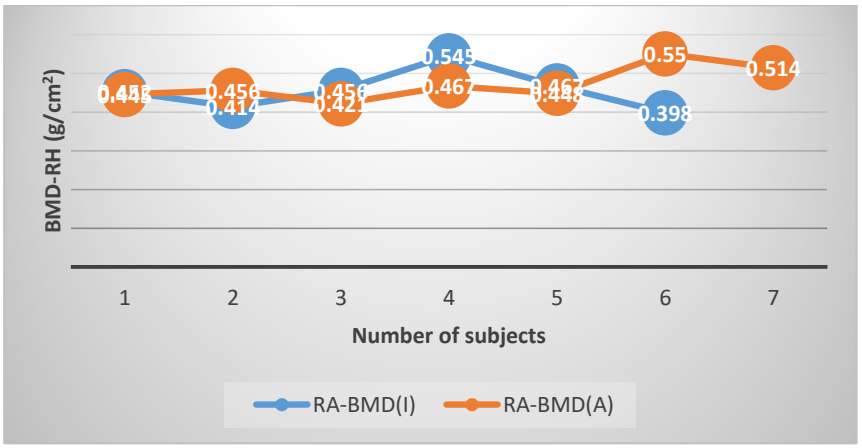

Figure 5.7. Right arm BMD difference between Indian and African population

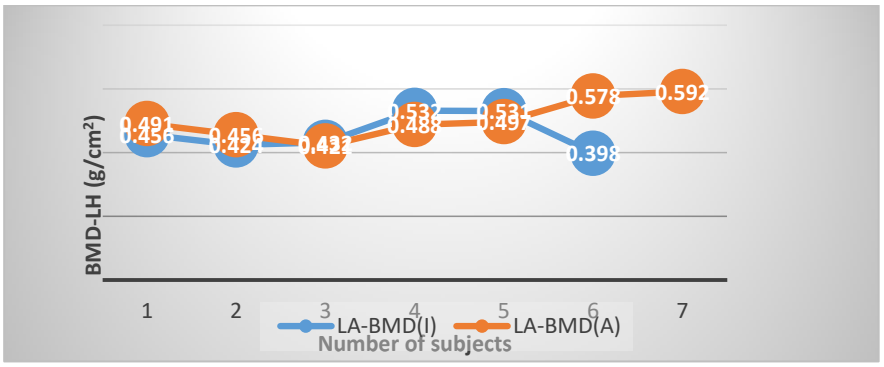

Figure 5.8. Left arm BMD difference between Indian and African population

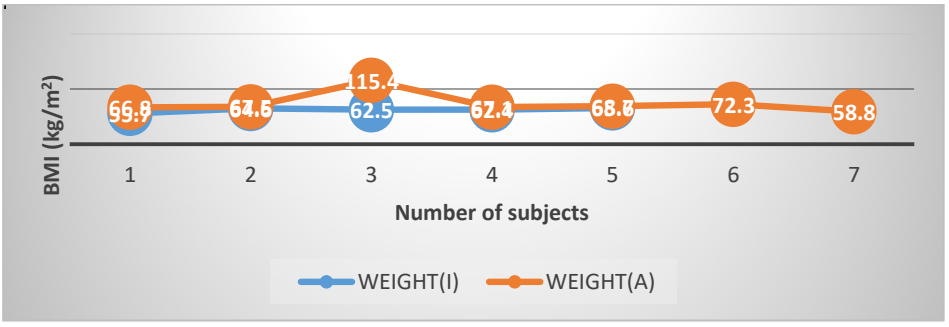

Figure 5.9. BMI difference between Indian and African population

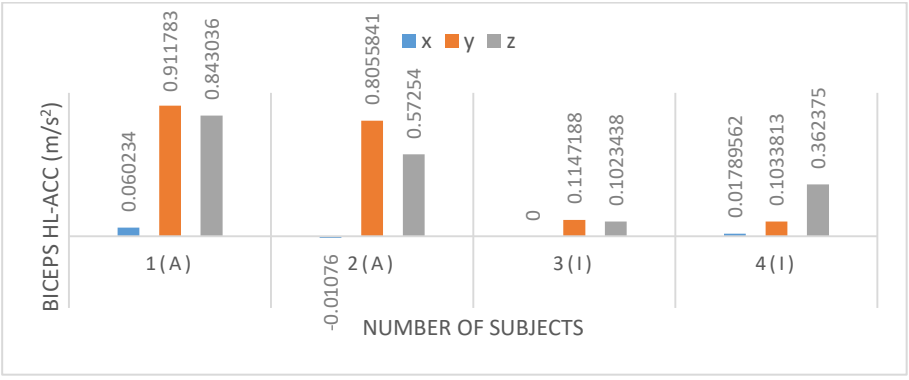

Figure 5.10. Left arm biceps acceleration difference between Indian and African population

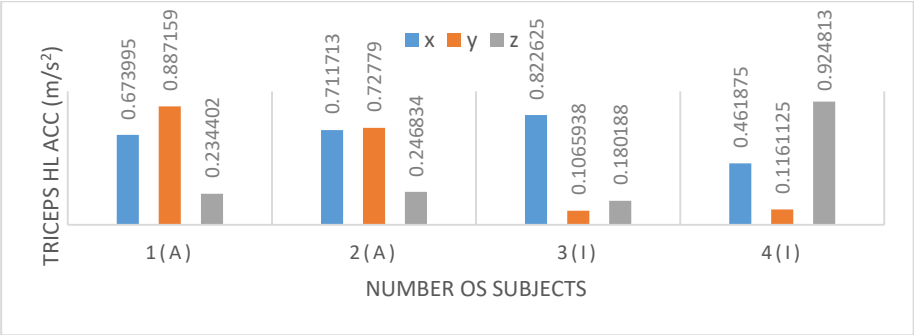

Figure 5.11. Left arm triceps acceleration difference between Indian and African population

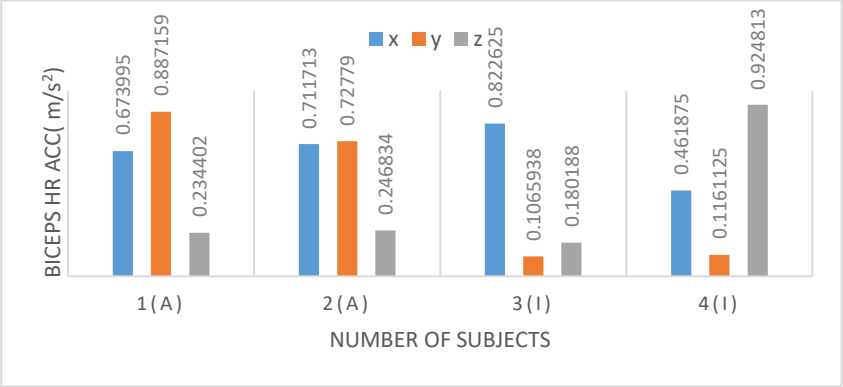

Figure 5.12. Right arm biceps acceleration difference between Indian and African population

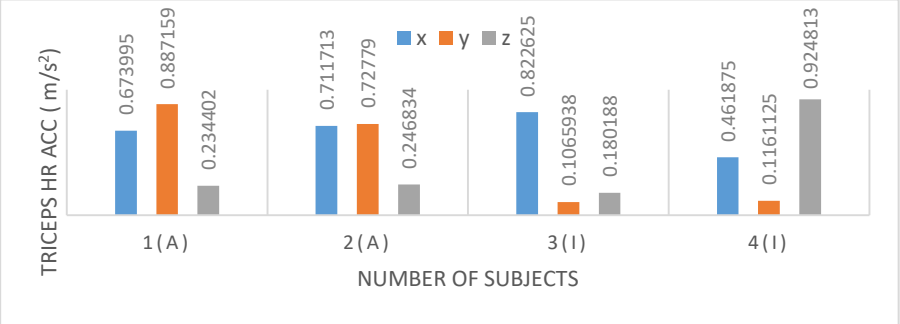

Figure 5.13. Right arm triceps acceleration difference between Indian and African population

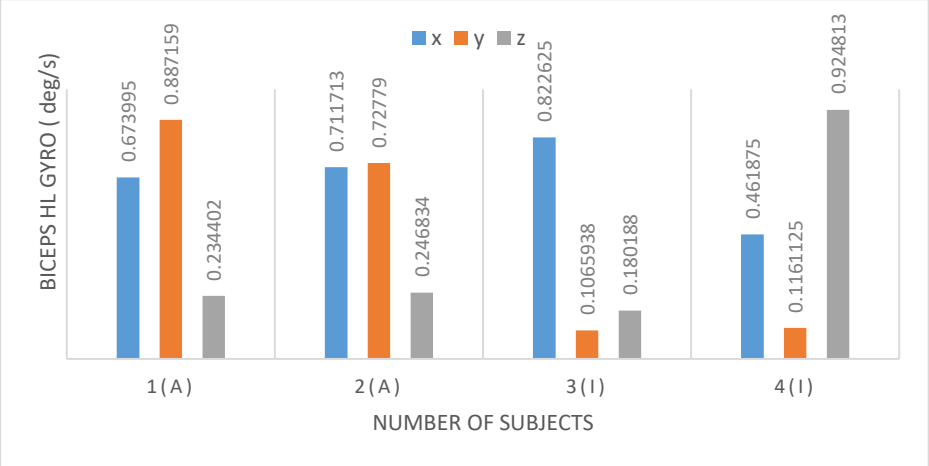

Figure 5.14. Left arm biceps gyroscope difference between Indian and African population

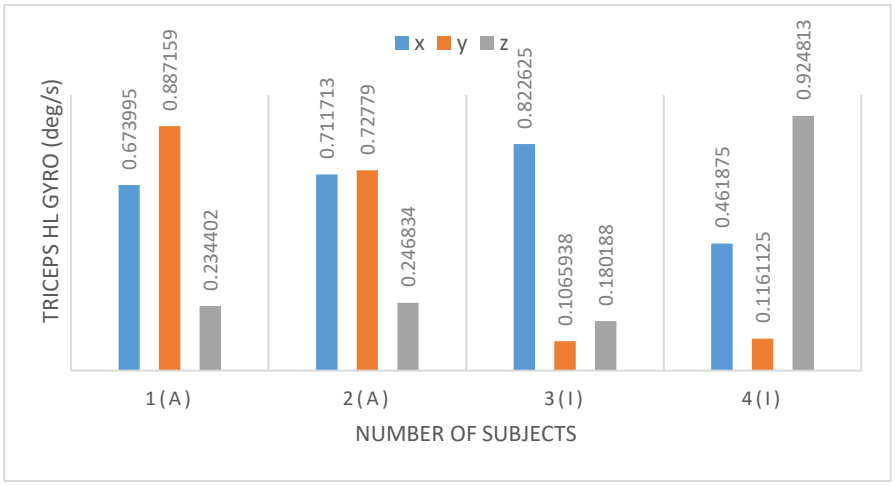

Figure 5.15. Left arm triceps gyroscope difference between Indian and African population

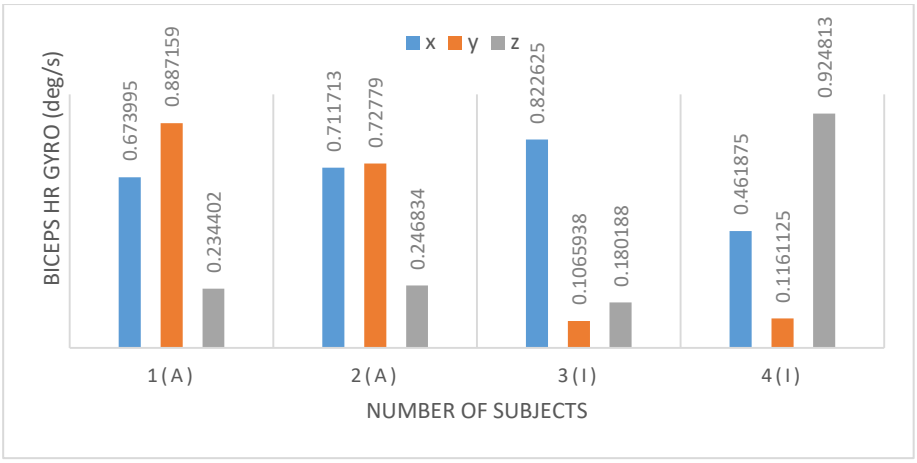

Figure 5.16. Right arm biceps gyroscope difference between Indian and African population

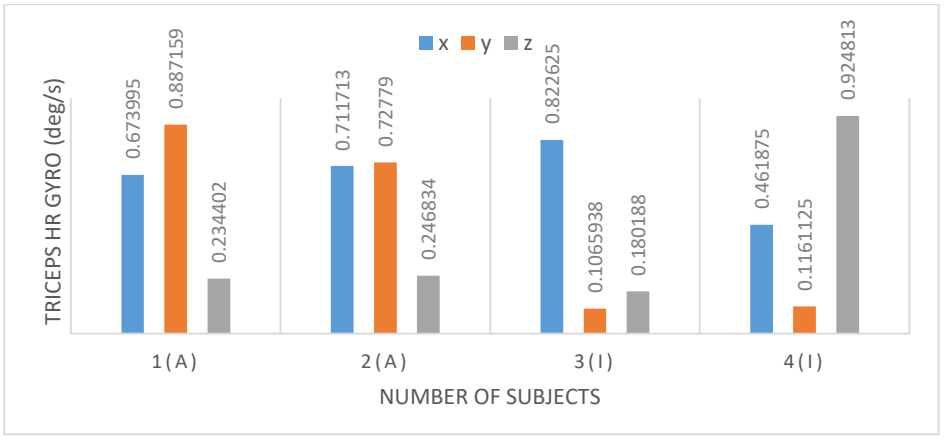

Figure 5.17. Right arm triceps gyroscope difference between Indian and African population

5. DISCUSSION AND CONCLUSION

This study intended to determine the relationship between body composition, bone mineral density with isokinetic strength from both African and Indian population which would give the similarities or differences to work with in such a way that will reduce the risk in life of these groups and related population. The body

composition and bone mineral density found to be related to the physical fitness and strength but also the effect of different cultural and traditional background affects the test results.

In the study of Ana Lilić et al 2022, explain that most of women has direct relationship between their body composition and their strength, based on the fat muscle, fat free mass, fat mass and other contents measured in body composition analysis it seems to be sufficient reasons of describing how strong one could be. The statistical details has been involved in different sites, articles and scholars to provide more supportive evidences taken in 2001 up to 2018.The obtained data has shown that there is sufficient data to prove that there is the relationship between the two [5].

Sibelle Alwatchi Alhayek (2021) elaborate that as the human gets old most diseases connected to bone like osteoporosis as well as sarcopenia will definitely come across their health and affect their bone. These include the risk to bone break, weakness, inactive health condition, and decrease in muscle and so on. Most protective procedure is to maintain proper diet like protein and also vitamin D even though there are no vivid evidences. The role of doing exercises has been advised to this group as well as a way of escaping from the above risks to their health [6].

Raman Kumar Marwaha et al (2013) undertook the study to relate the body composition based on fat contents and bone mineral density for non-obese, the study for Indian shows that there is the large effect of fat presence in bone mineral density which leads to Obesity and this has been researched and proven [7].

6. LIMITATIONS AND FUTURE WORKS

Despite the fact that measurement provided was performed correctly, there was a slightly difference between these two different ethnic group, either the questionnaire provided to the subject especially African show that the highly percentage of African who has moved to India has tremendously lost their weight as well as strength performance compare with the previous record when they arrived. This gives another chance to a wide study of this project based on more research and data collection from different scenario that will opt to a better solution.

The study will be extended in such that future data comprises of the collected data for body composition and bone mineral density from young male found in African region and the details analyzed with the data collected for Africans in Indian region to see whether it relates or meet the questionnaire's responses.

Also more number of subjects must be taken to give out a proper evaluation on the study as the lesser the number of subjects the lesser the accuracy in analysis.

ACKNOWLEDGMENT

I would like to sincerely thank the management of SRMIST for providing the research facilities to conduct this study.

REFERENCES

[1] Thibault Sutter, Hechmi Toumi1, Antoine Valery, Rawad El Hage, Antonio Pinti1,Eric Lespessailles, Relationships between muscle mass, strength and regional bone mineral density in young men (2019).
[2] Sangun Lee, Chikako Fujita, and Atsuko Satoh. Baseline Body Composition and Physical Activity Level Recommended for Optimal Bone Mineral Density in Young Women (2022).
[3] Jessica Piasecki, Alex Ireland, Mathew Piasecki, Kevin Deere, Kimberley Hannam, Jonathan Tobias and Jamie S. McPhee ,Comparison of Muscle Function, Bone Mineral Density and Body Composition of Early Starting and Later Starting Older Masters Athletes (2019).
[4] Anna Kopiczko and Joanna Cieplińska. Forearm bone mineral density in adult men after spinal cord injuries: impact of physical activity level, smoking status, body composition, and muscle strength 20220.
[5] Ana Lilić, Marko Joksimović, Emilija Petković, Relationships between body composition and strength of physically active women 2022.
[6] Sibelle Alwatchi Alhayek, The association of dietary protein and vitamin D with body composition and exercise outcomes in cognitively normal older adults 2021.
[7] Raman Kumar Marwaha, Mahendra K. Garg, Nikhil Tandon,Neena Mehan, Aparna Sastry,and Kuntal Bhadra, Relationship of Body Fat and Its Distribution With Bone Mineral Density in Indian Population 2013.

Identifying The Lung Disease Using Sound Sensor And Classify The Disease Using Machine Learning Technique

Swetha T[1], Lakshmi Prabha P[2]
[1,2]Department of Biomedical Engineering, SRM Institute of Science and Technology, Potheri, SRM Nagar, Kattankulathur, Chennai - 603203, India

ABSTRACT

Asthma is a condition where the patient's airways swell and produce extra mucus, which makes breathing difficult resulting in wheezing, coughing, and chest discomfort. It is commonly thought that asthma is a disorder affecting the lungs, but current research suggests that asthma may represent part of a systemic airway disease affecting the entire respiratory tract, as asthma often coexists with other atopic disorders, particularly allergic rhinitis. It is important to note that a lack of asthma control contributes to unnecessary morbidity, limitations in daily activities, and impairments in quality of life in general. Asthma is diagnosed by spirometry, which is a potentially costly and time-consuming procedure, as well as the possibility of incorrect inhalation when performing this test. In order to resolve the above issue, sound sensors were used. There was a total of 50 data points collected, including 20 data points relating to asthma patients and 20 data points regarding health patients. Data points were collected using sound sensors and the results were displayed in the Arduino IDE software, following which a pre-processing step was performed to reduce signal noise. Smoothing was achieved by employing a mean filter. Three types of classification have been implemented using machine learning techniques. Due to minimal dataset all the classifier achieved 100% accuracy.

Keywords: Asthma, Lung disease, Sound sensor

Corresponding Author:
Lakshmi Prabha. P,
Assistant Professor, Department of Biomedical Engineering, SRM Institute of Science and Technology, Potheri, SRM Nagar, Kattankulathur, Chennai - 603203, India.
Email: * lakshmip1@srmist.edu.in

1. INTRODUCTION

Asthma is a long-term condition which cause an air passage in the Lungs and it is increasingly recognized as a heterogenous condition[1]this asthma is the diagnosis for several diseases with common symptoms like cough and wheeze, but they are different in pathogenesis, etiology and responses to treatment[2],[3],[4]–[9]. Asthma variants are named as “asthma endotypes”[10], [11] .According to the study almost 300 million people are suffering with asthma worldwide and it is likely 100 million people affected by 2025.ashma related mortality is more identified in low middle income countries[12].These leads breathing difficulties.Usually child patients who undergoing asthma, have function of air passage and the mucus become over hyperactive. Usually, asthma takes place three sources take places in the air passage. This causes the small way to air pass. This small air passage may lead to shortness of breath and the oxygen level become low. The risk of lung disease asthma includes no proper sleep,maximal energy level and so on. Hence it is important to implement the device to detect and identify the lung disease in the early stage.

2. MATERIALS

For this study, both hardware parts and software techniques are used and mentioned below.

2.1. Hardware Requirements

- Sound sensor
- Arduino nano
- Connecting wires

2.2. Software Requirements

- Arduino software
- Python

2.1.1. Sound sensor

In this sound sensor LM393 module is used ,which easily capture the sound signal .Sound sensor is a small board with microphone and the processing circuit reverse the sound signal into electrical signal.[13] the output will beboth analog and digital output (***Fig:2.1).***

Figure 2.1. sound sensor

2.1.2. Arduino nano

In this Arduino nano is based on the ATmega328 which works with mini-b USB cable instead of a standard one. The Arduino nano can be programmed by Arduino software. Each and every Arduino board will be able to accessboth in online and offline mode (***Fig:2.2).***

2.2. Software Requirements

The software technique used in this project are Arduino IDE software and python. Arduino IDE software fordisplaying the output of hardware (sound sensor). python for signal processing and classification of asthma patients and healthy human.

2.2.1 Arduino ide software

Arduino software is generally used for texting the code, to plot the signals and with many functions. It is an open-source software. Generally used to text and display the code to the boards. This software is suitable for operating systems such as Windows, Linux and Mac OS X. In this article the Arduino software is connected to the hardwarepart with the help of USB connection.

2.2.2 PYTHON

Python is a computer programming language and used in this study to get the proper accuracy of the sound sensor[13].

3. METHODOLOGY

By using the sound sensor, the sound signals are collected from the asthma patients and health humans by placing the sensor on the throat[14]. The collected signals are processed and displayed in the Arduino software. this data is processed in python software. The noise from the sound signals is removed by using mean filter. After smoothening GLCM features are extracted. With these features the data is classified[15]–[17]

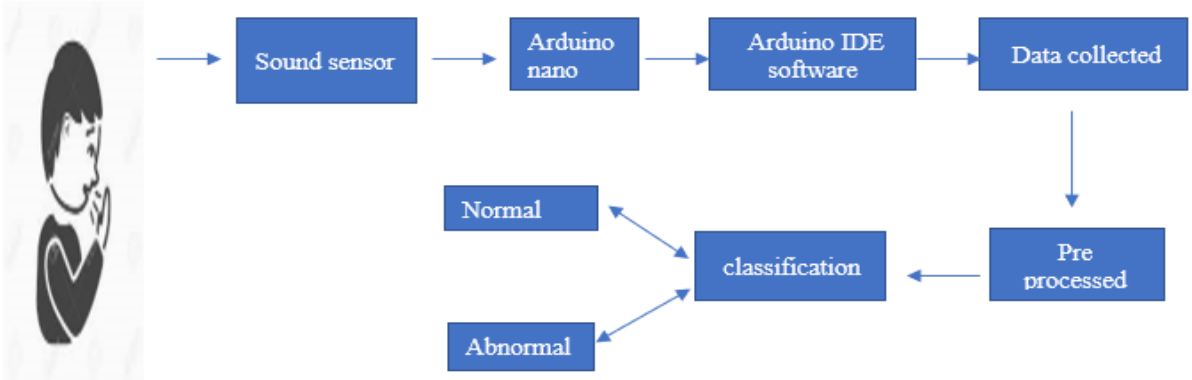

Figure3.1. Block diagram

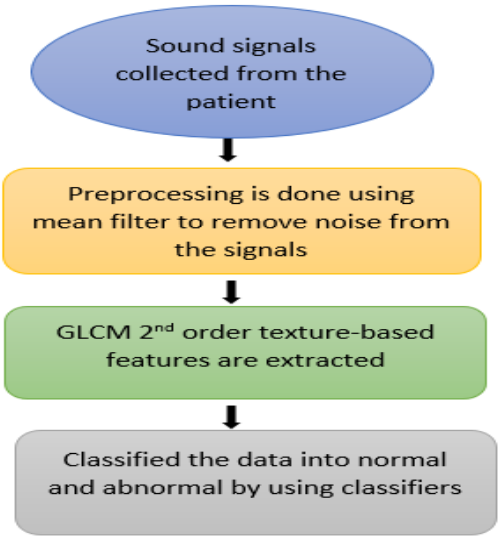

Figure 3.2. flow of the study

3.1. Data Collection

Data is collected by using sound sensor and the values are displayed in the output window of Arduino IDEsoftware.

3.2. Dataset

The acoustic signals from the asthma patients are acquired by using sound sensor and compared with the acoustic signal of the healthy subjects. This data set includes 20 asthma subjects and 20 healthy subjects.

3.3. Preprocessing

The recorded biological signal called lung sound recordings generally have acoustic noise caused by ambient noise, background voice, electronic interference, or any displacement of the sound sensor position. therefore, is very important to pre-process the collected acoustic signals for smoothening prior to any feature extraction procedure.

3.4. Mean Filter

Mean filter is a type of filter that replaces the value of each and every pixel by averaging the pixel values of local neighborhood pixel values. The output signal of health subjects (Fig:3.4) and the asthma patients(fig:3.5).

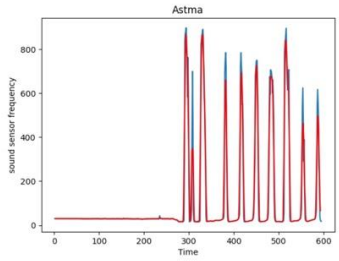

Figure 3.4. sound signal ofhealthy subject

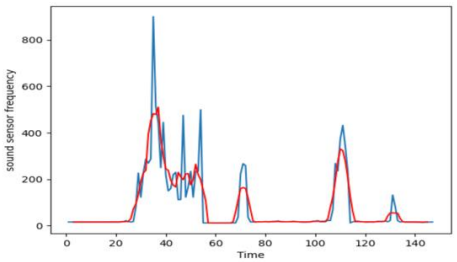

Figure 3.5. sound signal of asthma patient

3.5 Feature Extraction

In this study, audio features are extracted, and it is necessary step in audio signal processing. explains processing of acoustic signals of asthma patients. The method of feature extraction used in this study are texture features called gray level cooccurrence matrix method (GLCM) For both healthy and asthma subjects. The GLCM features called Entropy, Kurtosis, Mean, Std deviation, Median, skewness is extracted from the sound signals. Entropy is finding the width and uniformity of the acoustic signal and it distinguish the communication signals by representing distribution state characteristics of the acoustic signals. Kurtosis is a type of feature extraction which explains the sharpness of the peak of the curve called curve in sound signals. Mean, Median and

the standard deviation of the sound waves are also extracted. Skewness is measuring the asymmetry of the distribution of sound waves. All the above-mentioned features are extracted from both asthma patients and healthy human andthe results are compared. (fig 3.4)

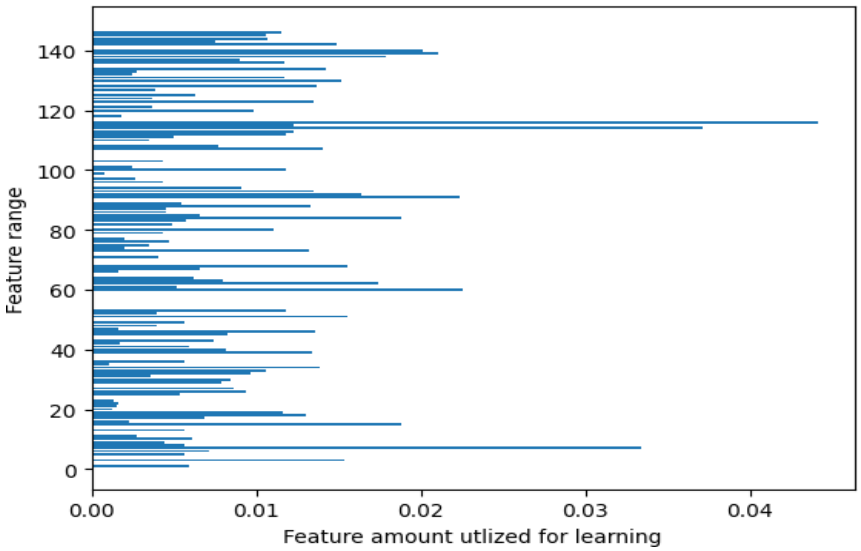

Figure 3.6. feature extraction range**.**

While extracting the features from the data the ranges were plotted which mentioned above figure (fig:3.6).

Table3.1. Average feature extraction values of asthma patient and healthy human

Features	Abnormal	Normal
Entropy	3.463	4.109
Kurtosis	30.203	20.066
Mean	88.86	80.90
Std deviation	139.755	96.88
Median	25.194	24.944
Skewness	1.05	1.24

Data of 50 people were collected in that 25 normal and 25 abnormal. The features from the acquired data extracted for both conditions. The extracted values of the features were averaged and mentioned (table no:3.1) Entropy and skewness is higher in normal people than asthma people. Median, Mean, kurtosis and standard deviation is higher in asthma people than in normal people.

3.6 Classification

The three different machine learning classifiers are used in this study. They are Random Forest classifier,Decision tree, Logistic regression and the accuracy is compared.

Random Forest classifier This type of classifier contains different series of decision trees on diverse subsets of the given dataset (sound signal features). this classifier uses the average to improve the accuracy of the given dataset.

Random forest classifier takes the prediction from each tree in the forest instead of depending on one decision treeand based on the greater number of votes of predictions, this classifier predicts the final output[20]–[22].

Decision tree This classifier has tree structure in which internal nodes indicates the dataset features. branches indicate the rules of decisions and each leaf node indicates the final output of the classifier.as the name suggests just like tree it starts from the root node, further expands on branches and finally construct a tree like structure[23], [24].

Logistic regression Logical regression classifier is a most popular machine leaning classifier and it is Supervised Learning technique.

4. RESULTS

The data from patients are collected, reprocessed and extracted GLCM features. Based on the features extractedthe data is classified by using 3 different machine learning classifiers called Random Forest classifier, Decisiontree classifier, logical regression classifier. all the three classifiers performed well and achieved 100% accuracywith minimal dataset.

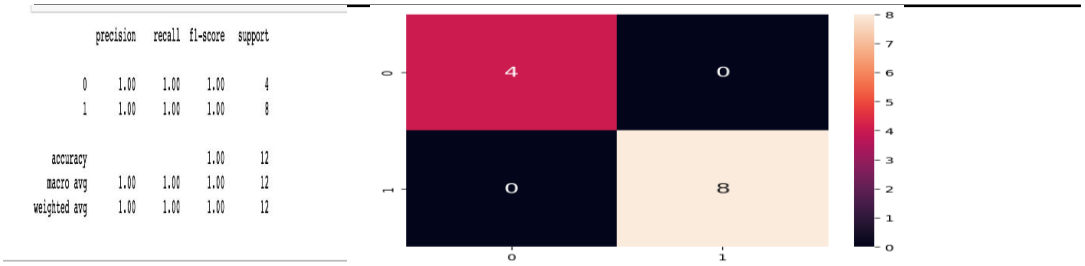

	precision	recall	f1-score	support
0	1.00	1.00	1.00	4
1	1.00	1.00	1.00	8
accuracy			1.00	12
macro avg	1.00	1.00	1.00	12
weighted avg	1.00	1.00	1.00	12

Figure 4.1. Accuracy and Confusion matrix of the data using random forest classifier

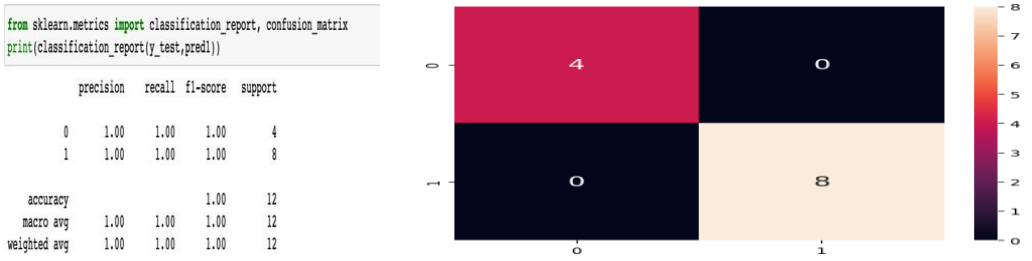

```
from sklearn.metrics import classification_report, confusion_matrix
print(classification_report(y_test,pred1))
```

	precision	recall	f1-score	support
0	1.00	1.00	1.00	4
1	1.00	1.00	1.00	8
accuracy			1.00	12
macro avg	1.00	1.00	1.00	12
weighted avg	1.00	1.00	1.00	12

Figure 4.2. Accuracy and Confusion matrix of the data using Decision tree classifier

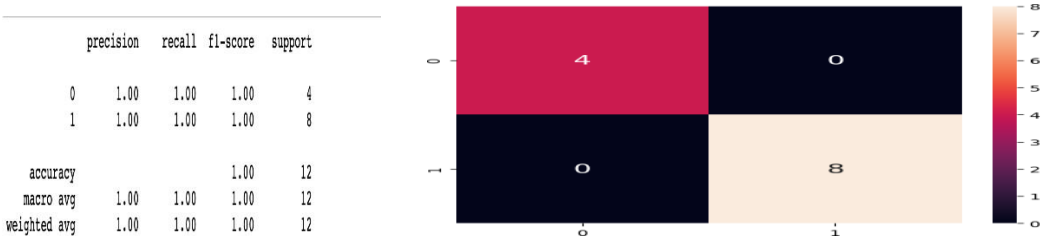

	precision	recall	f1-score	support
0	1.00	1.00	1.00	4
1	1.00	1.00	1.00	8
accuracy			1.00	12
macro avg	1.00	1.00	1.00	12
weighted avg	1.00	1.00	1.00	12

Figure 4.3. Accuracy and Confusion matrix of the data using logical regression classifier

The data of 12 subjects are used for training the classifier in which 4 patients are asthma patients and 8 arenormal. All the three classifiers give 100 percent accuracy.

5. DISCUSSION AND CONCLUSION

This is the study to diagnose asthma just by placing the sound sensor on the throat which is easy, comfortable to the patient and we get accurate results. The traditional test used to diagnose the asthma are FeNO test, Spirometry and the peak flow test. FeNO test is used to calculate the nitric oxide level in patient's breath. This nitric oxide is the sign of lung information and it cannot used for children under 5 years of age .in spirometry test patient blow into the machine and we can measure how fast the patient is breathing out and the air holding capacity of the lungs. Patient may feel dizziness or shortness of breath for a moment and should not performed who had people recent heart attack or any other heart problems.in peak flow test patient is asked to blow into a handheld device to measure how fast the patient is breathing out. While undergoing test patient may feel cough. This study replaces all these tests and it overcome with the problems faced during FeNO test, the spirometry test and peak-flow test. Data collected from both asthma affected patients and healthy human for comparison and classification by referring asthma patients are abnormal and healthy patients are normal. By using the sound sensor, the vibrations and sounds produced while breathing is collected and these sound signals converted into electronic signals by analog to digital converter in Arduino nano microprocessor. These electric signals are displayed in the form of graph on the ARDUINO IDE SOFWARE output window. These signals are collected and saved in a folder. Using python language, the data in the folder is filtered to remove noise and for

classification. Data is preprocessed using mean filter that reduces the background noise, other muscle noise in the patient, electronic interference, displacement of placing the sensor etc. After removing noise, the GLCM features are extracted which are texture based second order statistical features. All the required features of the data are collected for classification.by using these features we trained the classifier and tested the data. All the three classifiers used in this study are random forest, decision tree and logical regression gave 100 percent accuracy.

REFERENCES

[1] The Lancet, "A plea to abandon asthma as a disease concept," *The Lancet*, vol. 368, no. 9537, p. 705, Aug. 2006, doi: 10.1016/S0140-6736(06)69257-X.
[2] P. Haldar *et al.*, "Cluster Analysis and Clinical Asthma Phenotypes," *Am. J. Respir. Crit. Care Med.*, vol. 178, no. 3, pp. 218–224, Aug. 2008, doi: 10.1164/rccm.200711-1754OC.
[3] J. Henderson *et al.*, "Associations of wheezing phenotypes in the first 6 years of life with atopy, lung function and airway responsiveness in mid-childhood," *Thorax*, vol. 63, no. 11, pp. 974–980, Nov. 2008, doi: 10.1136/thx.2007.093187.
[4] W. C. Moore *et al.*, "Identification of Asthma Phenotypes Using Cluster Analysis in the Severe Asthma Research Program," *Am. J. Respir. Crit. Care Med.*, vol. 181, no. 4, pp. 315–323, Feb. 2010, doi: 10.1164/rccm.200906-0896OC.
[5] J. A. Smith, R. Drake, A. Simpson, A. Woodcock, A. Pickles, and A. Custovic, "Dimensions of Respiratory Symptoms in Preschool Children: Population-based Birth Cohort Study," *Am. J. Respir. Crit. Care Med.*, vol. 177, no. 12, pp. 1358–1363, Jun. 2008, doi: 10.1164/rccm.200709-1419OC.
[6] N. G. Papadopoulos *et al.*, "International consensus on (ICON) pediatric asthma," *Allergy*, vol. 67, no. 8, pp. 976–997, Aug. 2012, doi: 10.1111/j.1398-9995.2012.02865.x.
[7] D. C. Belgrave, A. Custovic, and A. Simpson, "Characterizing wheeze phenotypes to identify endotypes of childhood asthma, and the implications for future management," *Expert Rev. Clin. Immunol.*, vol. 9, no. 10, pp. 921–936, Oct. 2013, doi: 10.1586/1744666X.2013.836450.
[8] D. Belgrave, A. Simpson, and A. Custovic, "Challenges in Interpreting Wheeze Phenotypes: The Clinical Implications of Statistical Learning Techniques," *Am. J. Respir. Crit. Care Med.*, vol. 189, no. 2, pp. 121–123, Jan. 2014, doi: 10.1164/rccm.201312-2206ED.
[9] S. E. Wenzel, "Asthma: defining of the persistent adult phenotypes," *The Lancet*, vol. 368, no. 9537, pp. 804–813, Aug. 2006, doi: 10.1016/S0140-6736(06)69290-8.
[10] J. Lötvall *et al.*, "Asthma endotypes: A new approach to classification of disease entities within the asthma syndrome," *J. Allergy Clin. Immunol.*, vol. 127, no. 2, pp. 355–360, Feb. 2011, doi: 10.1016/j.jaci.2010.11.037.
[11] G. P. Anderson, "Endotyping asthma: new insights into key pathogenic mechanisms in a complex, heterogeneous disease," *The Lancet*, vol. 372, no. 9643, pp. 1107–1119, Sep. 2008, doi: 10.1016/S0140-6736(08)61452-X.
[12] T. To *et al.*, "Global asthma prevalence in adults: findings from the cross-sectional world health survey," *BMC Public Health*, vol. 12, no. 1, p. 204, Dec. 2012, doi: 10.1186/1471-2458-12-204.
[13] W. F. Holmgren, R. W. Andrews, A. T. Lorenzo, and J. S. Stein, "PVLIB Python 2015," in *2015 IEEE 42nd Photovoltaic Specialist Conference (PVSC)*, New Orleans, LA, Jun. 2015, pp. 1–5. doi: 10.1109/PVSC.2015.7356005.
[14] H. P. da Silva, A. Fred, and R. Martins, "Biosignals for Everyone," *IEEE Pervasive Comput.*, vol. 13, no. 4, pp. 64–71, Oct. 2014, doi: 10.1109/MPRV.2014.61.
[15] Priyanka and D. Kumar, "Feature Extraction and Selection of kidney Ultrasound Images Using GLCM and PCA," *Procedia Comput. Sci.*, vol. 167, pp. 1722–1731, 2020, doi: 10.1016/j.procs.2020.03.382.
[16] T. Sutojo, P. S. Tirajani, D. R. Ignatius Moses Setiadi, C. A. Sari, and E. H. Rachmawanto, "CBIR for classification of cow types using GLCM and color features extraction," in *2017 2nd International conferences on Information Technology, Information Systems and Electrical Engineering (ICITISEE)*, Yogyakarta, Nov. 2017, pp. 182–187. doi: 10.1109/ICITISEE.2017.8285491.
[17] Ş. Öztürk and B. Akdemir, "Application of Feature Extraction and Classification Methods for Histopathological Image using GLCM, LBP, LBGLCM, GLRLM and SFTA," *Procedia Comput. Sci.*, vol. 132, pp. 40–46, 2018, doi: 10.1016/j.procs.2018.05.057.
[18] J. Shedbalkar, K. Prabhushetty, and A. Inchalc, "A Comparative Analysis of Filters for Noise Reduction and Smoothening of Brain MRI Images," in *2021 6th International Conference for Convergence in Technology (I2CT)*, Maharashtra, India, Apr. 2021, pp. 1–6. doi: 10.1109/I2CT51068.2021.9417979.
[19] A. A. Kumar, N. Lal, and R. N. Kumar, "A Comparative Study of Various Filtering Techniques," in *2021 5th International Conference on Trends in Electronics and Informatics (ICOEI)*, Tirunelveli, India, Jun. 2021, pp. 26–31. doi: 10.1109/ICOEI51242.2021.9453068.
[20] A. T. Azar, H. I. Elshazly, A. E. Hassanien, and A. M. Elkorany, "A random forest classifier for lymph diseases," *Comput. Methods Programs Biomed.*, vol. 113, no. 2, pp. 465–473, Feb. 2014, doi: 10.1016/j.cmpb.2013.11.004.
[21] M. Belgiu and L. Drăguţ, "Random forest in remote sensing: A review of applications and future directions," *ISPRS J. Photogramm. Remote Sens.*, vol. 114, pp. 24–31, Apr. 2016, doi: 10.1016/j.isprsjprs.2016.01.011.
[22] D. Petkovic, R. Altman, M. Wong, and A. Vigil, "Improving the explainability of Random Forest classifier – user centered approach," in *Biocomputing 2018*, Kohala Coast, Hawaii, USA, Jan. 2018, pp. 204–215. doi: 10.1142/9789813235533_0019.
[23] S. B. Kotsiantis, "Decision trees: a recent overview," *Artif. Intell. Rev.*, vol. 39, no. 4, pp. 261–283, Apr. 2013, doi: 10.1007/s10462-011-9272-4.
[24] S. R. Safavian and D. Landgrebe, "A survey of decision tree classifier methodology," *IEEE Trans. Syst. Man Cybern.*, vol. 21, no. 3, pp. 660–674, Jun. 1991, doi: 10.1109/21.97458.

Rehabilitation of Lumbago and Cervicalgia Using Tens Unit Pads on a Wearable Coat

Jason Anthony J[1], Sharan G.V[2], Mohamed Sabir Hussain[3], Anandha Krishnan M[4], S. Sakthivel[5]
[1,2,3,4]III Year Biomedical Engineering Students, SRMIST, Ramapuram, Chennai, India,
[5]Assistant Professor, Department of Biomedical Engineering, SRMIST, Ramapuram, Chennai, India

ABSTRACT

Lumbago (Lower back pain) and Cervicalgia (neck discomfort) are one of the most common disorders largely experienced by people all over the world. Bad posture, physical body strain, Accidents, herniated disks, arthritis and osteoporosis, lordosis, kyphosis, scoliosis are all some of the widely experienced causes. These musculoskeletal disorders affects more than half the population of the world. Lower back pain and neck pain are one of the main contributors to the overall burden of musculoskeletal conditions where Lower back pain has 570 million prevalent cases worldwide and Neck pain affects more than 300 million people worldwide. As the patients have to try 10 to 15 treatments to figure out which works for them, which gets a bit expensive for most people, this paper has attempted to place the underlying nerve stimulator (TENS pads) into a coat in which the patient can rehabilitate oneself by simply wearing it and using it whenever necessary and continuing with their daily activities. This leads to a huge reduction in the time, money and energy used unnecessarily for travelling and taking various treatments. The suggested prototype compromises physiological muscle functions by disrupting biochemistry and neuronal processes. Healthcare professionals may electronically reactivate those inactive physiological processes by maintaining their action potentials up to -60 mV with the help of the proposed technology. This can help reduce pain signals that reach the brain and spinal cord, which may help with pain relief and muscle relaxation.

Keywords: Cervicalgia, Lumbago, Kyphosis, Electric stimulation therapy, Wearable coat

Corresponding Author:
Jason Anthony J,
SRM Institute of Science and Technology, India,
Email: jj7278@srmist.edu.in

1. INTRODUCTION

Neck pain and lower back pain are unusual pathologies that affect people in their later stages of life around 35 - 40 years of age. It's the two most common and largely prevalent disorders in the world. Numerous studies indicate that pain in the neck and lower back pain diminish the ability to work, limits physical exercise, results in disability, and leads to work absence. Very bad posture, traumatic accidents, arthritis, osteoporosis, lordosis, kyphosis, scoliosis, lifting heavy weights are all possible causes. Transcutaneous electrical nerve stimulation (TENS) is a device which uses electrical stimulation to diminish the patient's pain by placing electrodes on the outside of the pores and skin.

It blocks the propagation of sensory pulse stimulation to the nerve or might stimulate endorphin release. It is important to distinguish a TENS unit from other types of electric stimuli such as neuromuscular stimuli that can be used to rapidly activate bulk and other engine nerves. Electrical stimulation of the muscles (EMS), also known as neuro-muscular stimulation with electricity (NMES), is the use of electric-fueled impulses to cause muscle choking. Due to its ability to be used as a training tool for athletes and healthy topics, EMS has attracted more focus in recent years. The apparatus produces the impulses that are delivered to the different muscle groups via sensors placed on the skin to activate the muscles. An action potential that causes a muscular contraction is being released by the brain and spinal cord. The padding that the electrodes are made of sticks to the epidermis and pores. Studies have shown that EMS, which has long been used in physical therapy, is capable of helping, improving, and toning muscle tissues, though ideally to a positive degree.

Garaud et al. conducted a randomised research to determine the effects of a therapeutic education programme on patients receiving transcutaneous electrical nerve stimulation for chronic low back pain. The study assessed TENS' effectiveness for treating LBP when combined with a restorative education programme(TEP). Despite the fact that patients benefitted from a rehabilitative education programme provided by a pain resource nurse, this evidence does not support the application of TENS in the rehabilitation of patients with chronic LBP.

The effectiveness of TENS for treating persistent low backache regardless of radicular pain was improved by A. Buchmuller et al. To assess the effectiveness of active versus sham TENS, the researcher

performed a random, peer reviewed study on adult patients with persistent LBP who visited French pain clinics. They came to the conclusion that TENS pads can only briefly reduce pain and cannot treat persistent lumbago.

Transcutaneous electric nerve stimulation (TENS) was developed by Ana Luiza C. Martimbianco et al. to treat persistent neck discomfort. They comprised randomised controlled studies (RCTs) comparing Tms either by itself or in combination with various therapies to either inactive or active treatments in persons with persistent neck pain. This review discovered extremely weak evidence that TENS and fake TENS vary in their ability to relieve neck discomfort.

TENS for Pain Management was used by Carol GT Vance et al. to update the body of research. When used at a strong, painless intensity, High - frequency and Low-Frequency TENS have been found to specifically offer analgesia, and High frequency Tens may be more efficient for those taking opioids. If High-frequency or Low-frequency TENS are applied repeatedly each day, the formation of resistance to TENS may reduce the effectiveness of analgesia for illnesses with chronic pain.

Sakthivel Sankaran et al designed and Developed muscle stimulation for cervicalgia patients using wearable coats. Electrical stimulation of the underlying nerves of cervicalgia prone region using Tens unit Pads. On the negative side, it focuses only on the cervicalgia region

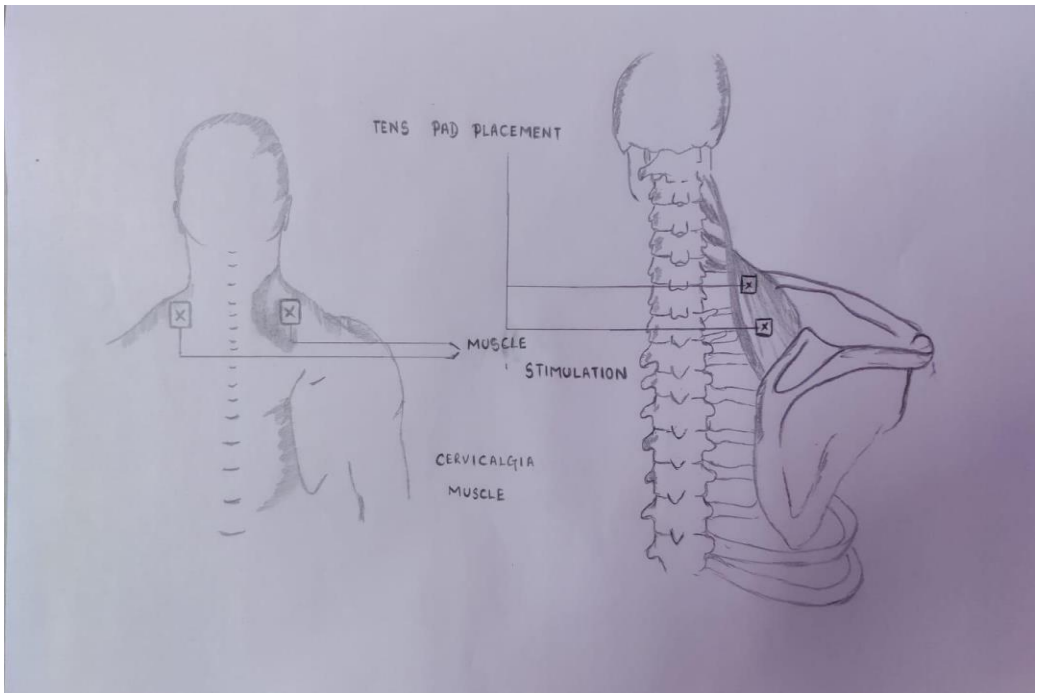

Figure 1. Shows The region of the body's central support structure prone to cervicalgia and the TENS pads are placed on the shoulder region. One of the tens pads is placed on the bulk of the muscle closer to the neck region and the other one is placed on the edge of the shoulder. Few microamperes of electrical impulse is then sent through the cervicalgia region for stimulation

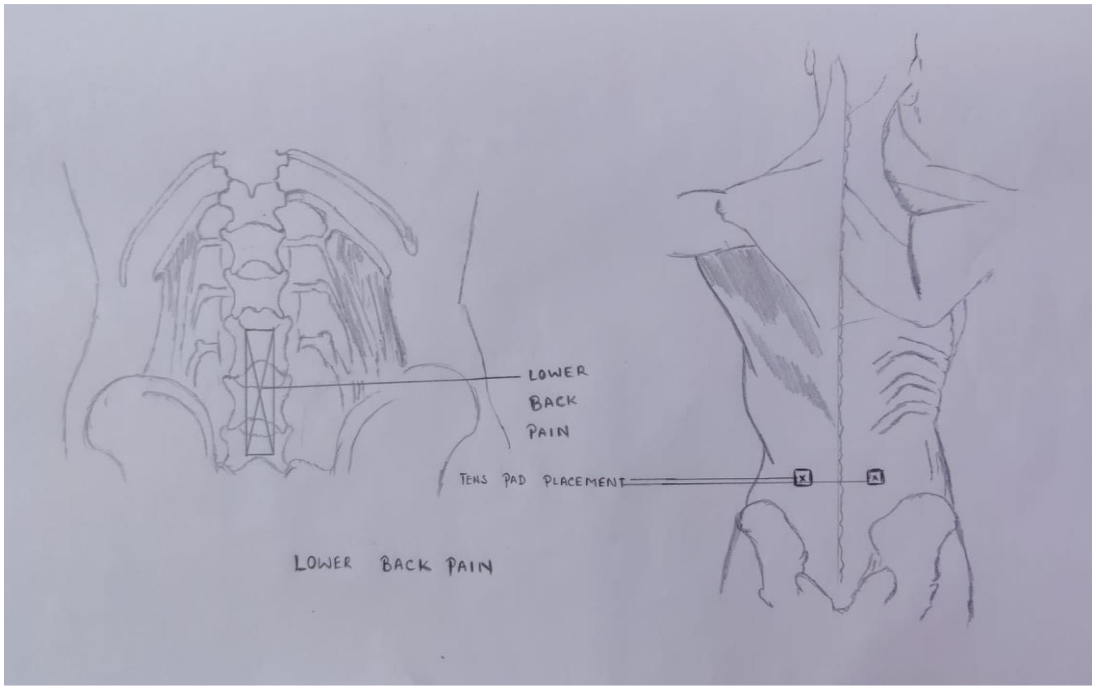

Figure 2. The region of the body's central support structure prone to lumbago. Here, two pairs of electrode pads are present, where one of the pair is above the pain afflicted muscle region. The other pair is placed parallel below the pain afflicted region

2. METHODOLOGY

Upper plane and lower plane are two sided routes or lines that are associated with a two-fold PCB. Since circuitry on a single side of the circuit board are frequently connected to circuits on the opposing side of the board with the help of holes drilled in the board, it is very helpful in many electronic applications. The high power and low current inducement on the transformer's alternative side replaces the reduced voltage and elevated current on the transformer's critical side. The microcontroller (Atmega328) outperforms the CPU as a low voltage regulator.

Customising is the main thing to do right now. Regulator essentially runs the programme that we supply at any time. A circuit or component utilised for controlling a different circuit or component is known as an interface; examples include a potent semiconductor, a resistor, and numerous other components. Using an electrical stream sent by a device to vivify the nerves for medicinal purposes is known as TENS (transcutaneous electrical nerve induction). Darlington semiconductor screens with high voltage and current are used in amplifier IC (ULN2003A) components. The primary source of power for all components is provided by batteries. It has a 500mAH maximum capacity and a recharge cord that aids in battery recharging.

The system currently has just three buttons on the coat that are used to regulate the electrical impulses of the electrodes that make up the TENS pads. Switch number one is a restart switch, switch number two is an incrementing switch, and switch number three is a decrementing switch. The current method only treats the area that is prone to Cervicalgia.

Our suggested system concentrates upon the treatment of the lumbar region of our spine, which is most susceptible to lumbago disorder, as well as the regions exposed to cervicalgia. These two conditions are the most prominent and common musculoskeletal disorders, affecting more than half of the global population and having recurrent cases that cause various complications in the workplace and daily activities. In this technique, we create a lightweight, wearable electrical coat for patients with lumbago and cervicalgia. In this experiment, an Arduino with an ATmega328 microcontroller and a ULN2003A amplifier IC is utilised. Only microamperes or less are used for electrical stimulus. The highest amount of stimulation that can be applied without endangering the patient is 0.4 A. There are 7 buttons in this system that are used to regulate the electrical impulses of the electrodes on the TENS pads. In the event that we need to abruptly halt the electrical stimulation for the patient's convenience we have the restart switch, which is the first switch. The second switch is the cervicalgia switch used to provide electrical stimulation to that region alone without activating the lumbar part. It also has an increment and decrement switch on either side of it to increase and decrease the amount of electrical stimulation given to it. In a similar way the third switch is for the lumbar region where lumbago occurs and it also has an increment and decrement switch to control the amount of electrical stimulation given to it. This way we can choose to provide electrical stimulation to both the lumbago and cervicalgia prone regions at the same time or

separately according to the needs of the patient. The system is portable and very convenient to use and has multiple advantages and can be made even more convenient and comfortable to use with further enhancements.

3. BLOCK DIAGRAM

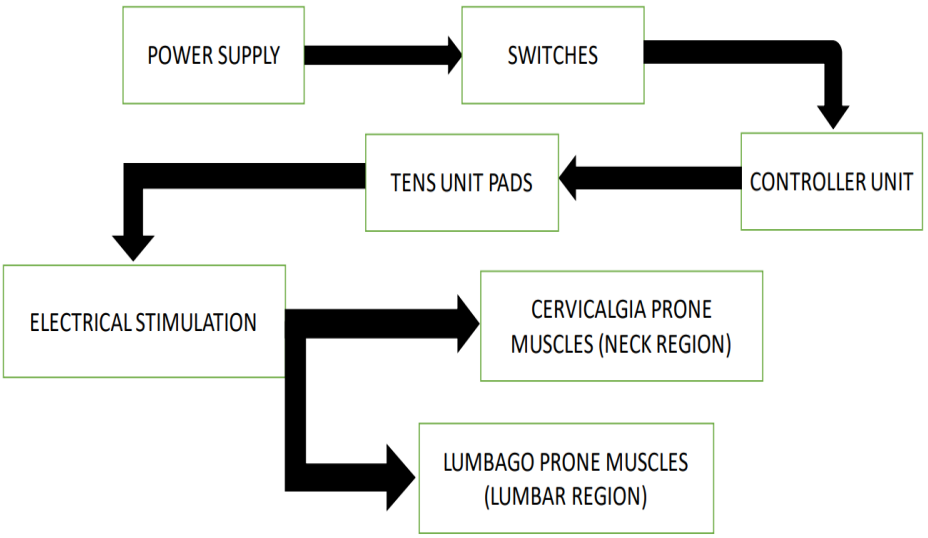

Figure 3. The main power supply for the system comes from a 500mAH rechargeable battery which is used to operate the whole system. The commands from the switches that the patient applies are sent to the controller unit which in turn sends the signal to the corresponding TENS unit pads placed inside the coat . Then the TENS pads then deliver the electrical stimulation to the corresponding regions which is either cervicalgia prone region or the lumbago prone region or both depending on the necessity of the patient.

4. RESULTS AND DISCUSSION

Initially Researchers have used vibrational and heat therapy to try and help with the rehabilitation of pain. Overworked areas and muscle spasms that are common to happen are relaxed through pattern stimulation of vibration and heat in most specific areas such as the lower back, shoulder and knees. Heat and vibration therapy works to release lactic acids that are built up during delayed onset muscle soreness and loosen stiff areas so you can receive the full benefits of total body recovery. Vibration pattern stimulation helps in improved circulation and muscle recovery helps maintain skeletal integrity to help prevent needless injuries. Percussive movements create gentle stretching in muscles, connective tissues, ligaments, and tendons to help bring back your range of motion. With different levels of heat and vibration patterns, your body's muscles and connective tissues release and begin to instantly improve blood flow and reduce soreness in your target areas. Although these two methods have a lot of advantages, they have major disadvantages respectively too.

Due to the fact that vibration cannot pass via the layer of skin and that intense heat energy effects the skin, it is unable to stimulate the nerves or lessen pain. But it is shown in this paper that electrical muscle stimulation temporarily relieves pain in both cervicalgia and lumbago-prone regions without causing any harm to the patient, which is a huge advantage because it is a harmless, mobile, secure to use, convenient, comfortable system and significantly reduces the pain and rehabilitates the individuals, allowing them to continue with their daily activities without any difficulties.

Figure 4. Front view of the patient wearing the wearable coat incorporated with the tens pad. Switches are front-faced in the above mentioned figure to make it convenient for the user to operate according to their needs and adjust the size of the wearable coat to their likeness.

Figure 5. Back view of the patient wearing the wearable coat incorporated with the tens pads. This part of the coat contributes to the stability of the coat and imparts electrical impulses in a smooth manner. It is a convenient mechanism to keep the coat held on to the patiently conveniently for longer duration

5. CONCLUSION

By using tens of cushions that deliver electrical impulses to the aforementioned areas, this research paper aims to design a wearable coat that is dependent on the microprocessor and microcontroller embedded within it. This will help with pain relief and rehabilitation. In doing so, it will benefit people with cervicalgia and lumbago physically and help save time and money that would otherwise be required. The freshly created electrical muscle stimulation coat reduces pain in a therapeutic way, includes both the musculoskeletal regions of the body, and offers improved outcomes. Compared to other techniques, it is much safer and more cost-effective. Researchers have previously used vibration or thermal energy to treat pain. Even though these techniques have their benefits, there are also drawbacks. For example, using vibration won't get rid of the discomfort as it can't penetrate the epidermis. Additionally, intense heat energy has an impact on the epidermis and fails to activate the nerves to lessen pain. However, the clinical trials show that the stimulation of the electrical muscles through the electrodes placed inside the coat used in the technique suggested in this article reduces pain. Devices for electric muscular stimulation are used in a variety of medical treatments. However, they require future improvements and additional rational investigations to remain viable.

6. FUTURE ENHANCEMENTS

The proposed method has great potential of advancement as it can be made in a way that can be controlled and accessed through the mobile phone through Bluetooth or with the use of Wi-fi module which will make the process of rehabilitation through the TENS pads on the wearable coat even more convenient and makes everyday activities so much easier and reduces pain for the patients and provides a way better future with no drawbacks and back pain which can be reduced and rehabilitated in the most safe, comfortable and convenient way. It can also be developed in the upcoming years to even be made as clothes with inbuilt TENS pads which provides electrical stimulation to every part of the body which it is needed for, which will revolutionise the world and help with the major disorders of the human body which more than half the population of the world experience and suffer from. In the future, we can create a smart coat with a heart Rate Sensor, pressure sensors, thermistor, and glucose sensor that can be used to monitor a patient's health. This device will be based on a microprocessor chip and microcontroller.

REFERENCES

[1] Jayjeet Sarkar, Avik Bhattacharya, Abritti Sinha, Arka Dutta, Development of a Pulsed Electromagnetic Field based TENS device using Bluetooth® Communication, IEEE 2017; 978-1- 5090-3239-6/17.
[2] Karl Lorenz Konrad, Jean-Pierre Baeyens, Christof birkenmaier, Anna Helena Ranker, Jonas Widmann, Johannes leukert, lisa Wenisch, Eduard Kraft, Volkmar Jansson, Bernd Wegener, The effect of whole- body electromyostimulation (WBEMS) in comparison to a multimodal treatment concept in patients with non-specific chronic back pain- A prospective clinical intervention study, PLOS ONE 2020;10.1371.
[3] Luke Osborn, Matthew Fifer, Courtney Moran, Joseph Betthauser, Robert Armiger, Rahul Kaliki, Targeted Transcutaneous Electrical Nerve Stimulation for Phantom Limb Sensory Feedback, IEEE 2017;978-1-5090-5803-7/17.
[4] Mayank Lokhande, Muscle Stimulation, International Journal of Care Engineering & Managements (IJCEM) 2014;2348 9510.
[5] M F Azman and A W Azman, The effect of electrical stimulation in improving muscle tone, International conference on mechatronics 2020;1088/1757-899X/260.
[6] Peter Kroling, Anita Gross, Charles H goldsmith, Stephen J Burnie, Ted Haines, Nadine Graham, Aron Brant, Electrotherapy for neck pain, Cochrane Database System 2013;10.1002/14651858.CD004251.pub5.
[7] Sakthivel sankaran, Pallikonda Rajasekaran Murugan, Divya Chandrasekaran, Vijayalakshmi Murugan, Preethuika Immaculate Britto, Vishnuvarthanan Govindaraja, Design of IoT based healthcare monitoring systems using raspberry Pi: A review of the latest technologies and limitations, International conference on communication and signal processing IEEE 2020;978-1-7281-4988-2/20.
[8] Sakthivel Sankaran, Pallikonda Rajasekaran Murugan, Preethika Immaculate Britto, Arunprasath Thiyagarajan, Vishnuvardhanan Govindaraj, A guidance system to read and analyse the traffic rules for the visually impaired human, Electronic Devices, Circuits, and Systems for Biomedical Applications Elsevier 2021;10.1016/B978-0-323-85172-5.00003-4.
[9] Sankaran S, Pradeep Kumar M, Geetha Anandhi C, An Automatic Cardiopulmonary Resuscitator – A Device for People Affected with Cardiac Arrest. In: Sharma T.K., Ahn C.W., Verma O.P., Panigrahi B.K. (eds) Soft Computing: Theories and Applications. Advances in Intelligent Systems and Computing, Vol 1381. Springer, 2021;10.1007/978-981-16- 1696-9_42
[10] Alana Biggers, Aaron Kandola, Cervicalgia and its treatment, Medical news today, 14(5): e0217231/2019.
[11] Fadi Al-Hadidi Isamn Bsisu Saif aldeen AlRyalat Belal AlZu bi, Rasha Bsisu, Mohammad Hamdan, Association between mobile phone use and neck pain in university students: A cross- sectional study using numeric rating scale for evaluation of neck pain, Plos one 2019;10.1371/ journal.pone.0217231.
[12] Gozde Goncu Berk, Design of a wearable pain management system with embedded TENS electrodes, (IJCST) 2017;10.11.08.IJCST-04-2017-0047.
[13] Jayjeet Sarkar, Design and Fabrication of a T.E.N.S pain relief unit, IEEE 2015;978-1-4799-4445-3/15.
[14] Subarna Shakya, Computational Enhancement of Wearable Healthcare Devices on Pervasive Computing System, Journal of Ubiquitous Computing and Communication Technologies 2020;2582-337X.
[15] Tabata Cristina do Carmo Almeida, Francisco Winter dos Santos Figueiredo, Valter Cordeiro Barbosa Filho, Luiz Carlos Abreu, Fernando Luiz Affonso Fonseca and Fernando Adami, BioMed central, Effects of transcutaneous electrical nerve stimulation (TENS) on proinflammatory cytokines: protocol for systemic review 2017;10.1186/s13643-017-0532-5

Fabricating Hydrogels to Emulate Brain Matter to Model and Study Brain Injuries

Shonelle Andrea Morais[1], Jason Anthony J[2], Dr. S. Sakthivel[3]
[1,2]Third year students, Department of Biomedical engineering, SRM Institute of Science and Technology, Ramapuram, Chennai, India
[3]Assistant professor, Department of Biomedical engineering, SRM Institute of Science and Technology, Ramapuram, Chennai, India

ABSTRACT

The objective of this research is to create a soft hydrogel with mechanical characteristics that closely resemble brain tissue.. The accurate in vitro brain model that will be produced by this biomimetic idea will aid in the study of diverse traumatic brain injuries. The suggested design is a hydrogel made of gelatin and alginate that is both natural and biocompatible. To create a hydrogel that replicates the linear and non-linear viscoelastic properties of brain matter as studied in the literature, different amounts of gelatin and alginate are used in this model. Testing for rheology will assist in comparing the hydrogels' mechanical characteristics to those of brain tissue. Consequently, this design will offer an accurate three-dimensional (3D) in vitro brain tissue model that may be used by subsequent researchers to analyse the cellular response of the brain to various stresses similar to those that result in traumatic brain injuries [1,2].

Keywords: Fabricate, Hydrogels, Biocompatible, 3D model, Brain injuries

Corresponding Author:
Shonelle Andrea Morais,
SRM Institute of Science and Technology, India
Email: sm6771@srmist.edu.in

1. INTRODUCTION

The development of materials that mimic the central nervous system is crucial for a number of emerging technologies. To be effective, brain proxies, brain organoids, psychological bioengineering scaffolds, and neuro probes in central nervous system interactions must accurately mimic the physical characteristics of brain tissue. In several in-vivo applications, a biomechanical fit between prostheses and the underlying brain tissue can reduce immune response and rejection of implant. Neural and glial cells need to have their living environment reproduced in-vitro for their regular distinctiveness, motility, function, and multiplication. This is true whether the objective is to boost the quantity of cells for medical strategies or to investigate cellular functions to chemical messengers and innovative therapies in-vitro.[9].

The brain is an anisotropic, extraordinarily delicate tissue that is highly complicated. When something is squishy, engineering the materials might be challenging. Because brain tissues are rather soft, it has proven to be difficult for material scientists to create functional biomaterials that resonate with them. The brain responds mechanically as a viscoelastic substance that is highly porous due to its distinctive architecture.[10].

Standard simulation techniques have difficulty adequately simulating the rigidity of the brain tissue due to its low elastic modulus. Recently, a variety of experimental methods have been applied both in vivo and ex vivo, in dry and moist settings, with different boundary and strength qualities, including microscopy with atomic forces, micro indentation, viscoelasticity, and magnetic resonance elastography. Then, it is established what the brain tissue's young ’s modulus is and is to be between a few hundred Pa and kPa upon use of various techniques. Although different experimental techniques are used and settings are established to carry out these tests differently from lab to lab, the results vary, causing a high degree of variability[10]. The mechanical characteristics of the various brain regions are also still being studied and are not yet fully characterised. There is still debate over whether white or grey matter is stiffer because the findings of many investigations are inconclusive. For the science to advance, detailed studies characterising the stiffness of brain tissue from the bulk to the nanoscale and under physiological settings are crucial. In order to enable accurate comparisons between research, it is also critical for the field to unite around standard approaches for characterisation at these different scales.

Severe neurological injuries are a significant source of mortality and incidence as well as a serious public health issue on a global scale. Those who have survived a TBI usually face incapacitating long-term changes to their personalities, motor skills, and cognitive abilities.. Recently, a spike in brain injuries has created a significant challenge for medical healthcare systems due to the rapid growth of the auto industry and the

inadequate development of the traffic infrastructure in low- and average-income countries. The development of models to simulate the incident under controlled circumstances has been a key step in understanding TBI and delivering better therapy. Understanding brain injury and its capacity to simulate the mechanical forces that compress, strain, and twist the brain tissue that results in damage, ranging from temporary to fatal, is also crucial[11].

2. METHODOLOGY

2.1. Algin/Gelatin hydrogels

The natural polysaccharide is known as alginate, which is composed of -D-mannuronic acid (the "M" residues) and -L-guluronic acid, is produced by brown algae and some microorganisms (the "G" residues). Cross-linking of intra- and interchain cations, most typically Ca2+, frequently results in the hydrogel. Because of their biological compatibility and ability to degrade, glycerin hydrogels produced via collagen dissolution are frequently employed in healthcare and pharmaceutical applications. Since they can promote cell adhesion and proliferation, gelatin-based hydrogels are employed in tissue engineering and drug delivery. The effects of alginate hydrogels with stiffness (elastic modulus) values on the growth and division were examined.

More than the others, the most flexible hydrogel induced cell division and proliferation. Alginate's antioxidant properties were investigated using the NT2 cell line (human NPCs), and it was discovered that alginate could protect cells from H2O2 by attempting to prevent caspase-3 activation and increasing the production of the thermal shock polypeptides . In vitro, alginate displayed a cytoprotective effect by preventing amyloid formation. Flexible alginate biomaterials cross-linked with sub-stoichiometric Ca2+ concentrations have been observed to promote neural adhesion and neurite growth similarly to non-functionalized alginate. Since alginate has antioxidant neuroprotective effects, neurons prefer a supple matrix.[6,7].

Polymeric hydrogels can imitate the asymmetric, conditioned, deformation, and asymmetrical behaviour of brain tissue when they are connected. We show that hydrogel incubation and concentration enable precise control of stiffness and particular stress relaxation behaviour for each loading mode. Higher hydrogel percentages and prolonged incubation times result in stiffer materials. We additionally see a slower release of stress after a protracted incubation. Our methodical approach emphasises the necessity of single-component, multi-modal mechanical examination of hydrogels in order to completely comprehend the particular structure-mechanics relationship of each hydrogel element and ultimately imitate the response of real tissues.

2.2. Properties of the soft hydrogels

1. Expansive properties: Hydrogel is capable of rapid and irreversible change in response to minute environmental changes. The physical texture of the hydrogel can be impacted by changes in environmental factors such as electrical impulses, acidity, humidity, and the inclusion of enzymatic reactions or other ionic species.

2. Properties of the substance: By adjusting the crosslinking level, the hydrogel's necessary mechanical properties may be obtained. A stronger hydrogel might be produced by enhancing bridging because doing so reduces the hydrogels' elongation percentage and makes their structure more brittle.

3. By adjusting the crosslinking level, the hydrogel's necessary mechanical properties may be obtained. A stronger hydrogel might be produced by enhancing bridging because doing so reduces the hydrogels' elongation percentage and makes their structure more brittle.[12].

2.3. Characterization of hydrogels

1.pH: To determine the pH of hydrogels, a digital pH tester is employed. Before usage, a pH gauge needs to be calibrated.

2. SEM Technology: SEM can be used to examine samples to determine their composition, surface topography, and other characteristics including electrical conductivity. SEM allows for adjustments in magnification up to many orders of magnitude, or around tens to hundreds

3.FTIR Spectroscopy: This method is effective for figuring out a substance's molecular make-up. It is predicated on the idea that chemical bonds, the fundamental constituents of a substance, have the ability to excite and absorb infrared light at wavelengths specific to chemical bonds.

4.Measurement of swelling : Currently, there are three techniques available for measuring swelling in hydrogels:-

Technique A: On a roller mixer, the desiccated hydrogel is put before being immersed in deionized water for 48 hours at room temperature. The hydrogel is filtered after swelling via a stainless steel net with many pores. A growth calculation is given below. Ws and Wd stand for the weight of hydrogels in their expanded and dry forms, respectively, swelling is denoted as WS-Wd/Wd.

Technique B: For 48 hours at room temperature, the desiccated hydrogel was combined with a sufficient amount of water in a volumetric receptacle. The mixture is then centrifuged to separate the layers of water-bound substance from the free, unabsorbed water. After the free water has been removed, the enlargement is evaluated using the above mentioned method

Technique C: In method C, the dried gel is submerged for 16 hours at room temperature in deionized water. After swelling, the hydrogel needs to be forced through a 100 degree mesh stainless steel mesh net (149 m). The following factors affect swelling: Swelling is calculated as C100/B, where B is the weight of the insoluble component following water extraction and C is the quantity of the dried hydrogel.

5. X-ray chromatic aberration: Diffraction studies are used to determine whether a substance is solid or amorphous. It is used to determine whether the polymers deform during the pressurisation procedure or maintain their crystalline structure. The diffraction research is a frequently used study method for polymer morphological evaluation.

6. In-vitro drug release studies are conducted to understand the process of freedom over time because drug molecules are contained within hydrogels, which are enlarged polymeric networks. The variables are contrasted with the traditional plot to ascertain the equivalency of the medication solutions.

7. Rheology: At a specific temperature of 4°C, a conical plate-style viscometer is used to determine the viscosity of hydrogels. The viscometer used to measure viscosity is quite accurate. A straightforward formula of the inclination of repose, which also yields the values for height and length, defines the viscosity.

8.Spreadability study: The device was made of two microscopic slides with a pan fixed on a pulley and a wood block with a scale. In order to contrast the formulation and obtain consistent thickness, extra formulation was placed between two microscopic slides, and a 100 g weight was then left on the upper glass slide for five minutes. Weight can be increased, and the amount of time needed to spread the two plates apart was estimated. $S= (m \times l) / t$ Where l is the distance of the microscope slide, t is the time in seconds, m is the weight fastened to the upper slide, and S is the spreadability.

9. X-ray diffraction: This technique is used to check if polymers retain their crystalline structure after being pressurised.

10. Network pore size: Pore size is measured using a variety of techniques, including mercurial porosimetry, electron microscopy, and others.

2.4. Design parameters

Table 1. Design parameters and specifications

PARAMETERS	SPECIFICATIONS
1.Temperature	The hydrogel must ensure to be kept stable at 37^0 C
2. Gas Levels	The hydrogel must ensure to be kept stable at 5% CO2
3. Humidity	The hydrogel must ensure to be kept stable at 85-95%
4. pH	The hydrogel must ensure to be kept stable at 7.2pH

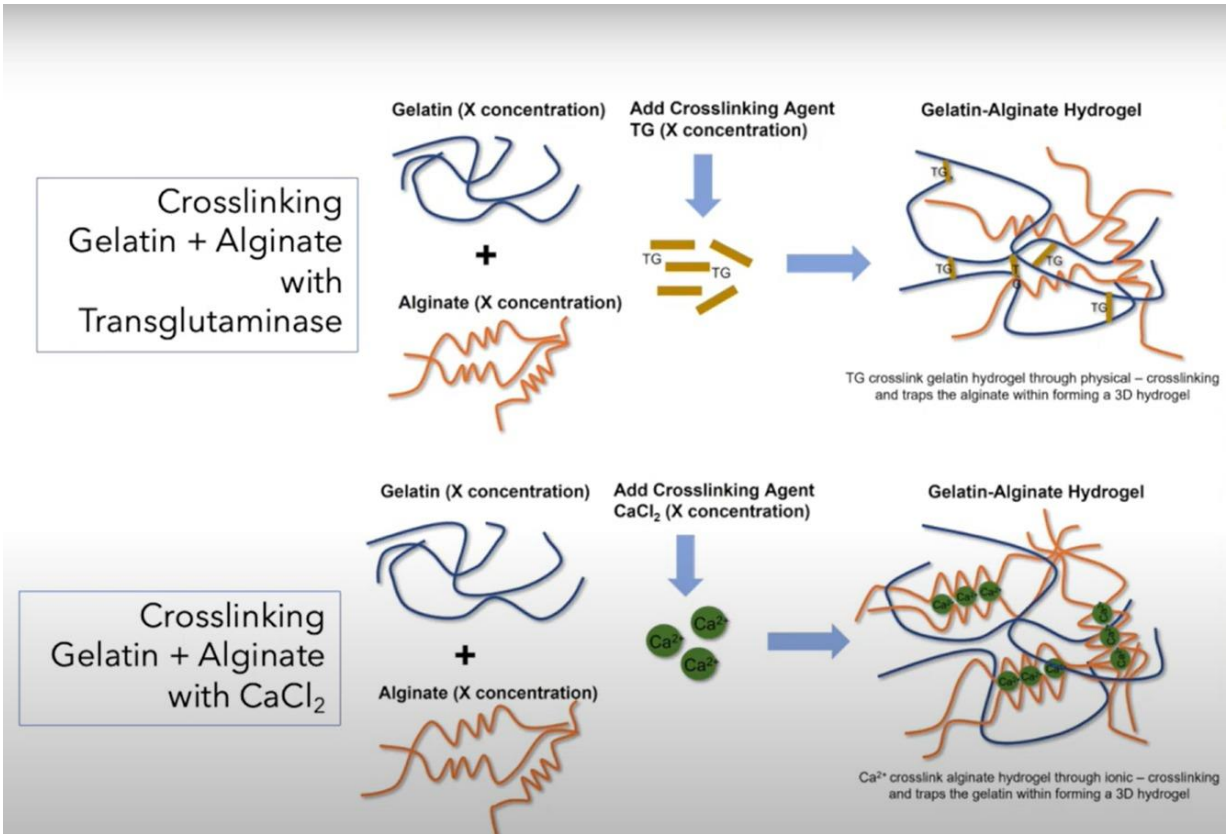

Figure 1. Heterogeneous crosslinking brought on by fast hydrogel + "egg-box" production during CaCl2 diffusion obstructs further Ca2+ diffusion. Therefore, increasing the Ca2+ content is an underutilised method for enhancing the properties of hydrogels, such as self-healing (dynamic ionic bonding of alginate-Ca2+), structural rigidity (dynamic ionic bond formation of Ca2+ and carboxyl groups), anti-freezing (depression of the freezing point in the presence of Ca2+), and high electrical conductivity (basic characteristics of Ca2+), especially opening up a variety of applications in reduced environments. Here, we synthesise an alginate-gelatin imine-based (CaAG) polymer with high Ca2+ bridge by mixing an ald-alginate and gelatin solution to generate an AG hydrogel. This AG hydrogel is then immersed in a CaCl2 solution that has excellent Ca2+ solubility and good dispersion.

3. LITERATURE REVIEW

Table 2. Synthesis of Review for Related Work

No	Author (Year)	Title	Methodology	Findings/Advantages	Drawbacks
1.	Vladimir A. Kornev et al., (2018)	Hydrogel-assisted neuro-regeneration approaches towards brain injury therapy: A state-of-the-art review	Hydrogel polymers are used for neuroregeneration	Rarely are simple hydrogel matrices sufficient for the engineering of brain tissue..	Even modified hydrogels infused with cells have drawbacks, including insufficient neurogenesis direction, poor integration, a potential for side effects, and additional clinical problems such the emergence of the epileptic centre.
2.	Yang Chen et al., (2022)	A Prosperous Application of Hydrogels with Extracellular Vesicles Release for Traumatic Brain Injury (TBI)	The evaluation of the combined use of exosomes and hydrogels for TBI rehabilitation.	Significant benefits include direct access to the lesion, cyst cavity filling, and editability..	Although hydrogels have many benefits, they may also have negative effects such as immunological reaction, infection, mechanical damage to the brain tissue around them, and the fact that injectable hydrogels can only be utilised during surgery.
3.	Tatiana A. Mishchenko et al., (2022)	3D-printed hyaluronic acid hydrogel scaffolds impregnated with neurotrophic factors (BDNF, GDNF) for post-traumatic brain tissue reconstruction	Hyaluronic acid scaffolds are created via 3D extrusion printing for the healing of injured tissue.	The scaffolds are compatible with nervous system cells and may help in the improvement of methods for restoring the morphology and functionality of nerve tissue following traumatic brain injury.	They demonstrate difficulties in minimally invasively implanting the scaffold at the location of the deficiency and limits in simulating the cellular matrix of brain tissue.
4.	Satoshi Tanikawa et al., (2022)	Engineering of an electrically charged hydrogel implanted into a traumatic brain injury model for stepwise neuronal tissue reconstruction	Using electrically charged hydrogels made of cationic and anionic monomers in a 1:1 ratio, neuronal tissue engineering (C1A1 hydrogel)	On the C1A1 gel, neural stem cells (NSCs) were able to adhere and multiply with efficiency.	Although briefly adhering to ionised hydrogels, NSCs eventually detached from them and died, but they did not adhere to highly reactive hydrogels, where they could consolidate and form aggregation.

4. RESULTS AND DISCUSSION (FINDINGS OF THE STUDY)

Due to their simplicity in processing, nanosize, viscoelasticity, swelling ability, high drug encapsulation efficiency, and low toxicity, hydrogels have become more and more common in the medical industry. We made

an effort to cover all of the hydrogel brain applications in this review, including 3D printing, local and remote medication delivery, approaches for treating brain tumours, and brain mapping. Hydrogel has been found to be a potential substance for application in the brain. In order to investigate possible opportunities in the field of medicine, research in this area is still ongoing at a rapid pace.

By simply combining protein and polysaccharides (alginate) components, we showed that the intricate mechanical properties of native brain tissue, such as non - linearity, repeatability, conditioning, and compression-tension imbalance, may be qualitatively recreated. We were able to create a blend mixture with the required mechanical properties thanks to the complex chemical assessment of the individual hydrogel constituents in compressive, stiffness, and torsional shear.

In this study, we characterised the complicated mechanical behaviour of hydrogels made of an alginate-gelatin blend under a variety of loading circumstances, including compression, tension, and torsional shear. By carefully planning a blend of alginate and gelatin hydrogels as an efficient replacement material, We have shown that the complex nonlinear and moment mechanical characteristics of pig brain tissue may be reproduced.

After many iterations, a stable optimised hydrogel model was created in which the concentrations of sodium alginate and gelatin can be altered to best replicate the properties of brain matter. Transglutaminase and calcium chloride dihydrate were used to cross link the proteins. Initially, we focused on structural integrity, and we discovered that 1% sodium alginate with 0.5% gelatin in the presence of calcium chloride dihydrate for 1 hour and transglutaminase for 24 hours produced promising findings.

Table 3. Functions and specifications of each mechanical parameters of the hydrogel

FUNCTIONS	**SPECIFICATIONS**
1. Maintenance of structural integrity	The hydrogel must ensure maintaining the proper shape at 37^0 C
2. Matching Loss modulus of brain matter	The hydrogel must ensure to not exceed or fall below a storage modulus of 2.7kPa - 3.1kPa and a loss of modulus of 2.5kPa when 0.01mN is applied during Rheology experiments.
3. Matching Elastic modulus	The hydrogel must ensure to not exceed or fall below 70+/- 44MPa when 0.01mN is applied during Rheology experiments
4. Control porosity	Target pore size should be above 100 micrometres when measured using Scanning Electron Microscopy(SEM)
5. Matching Maximum strain	The hydrogel must ensure not to fall below 11 +/- 3% when 0.01mN is applied during rheology experiments

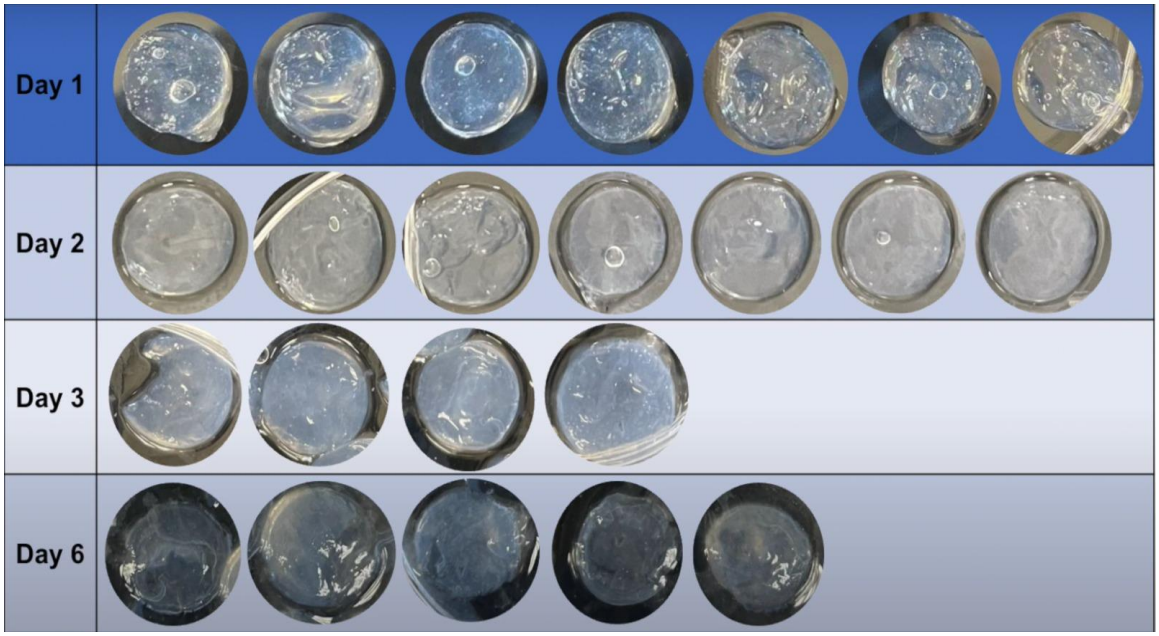

Figure 2. Findings of the study over the course of 5 days with 1% sodium alginate with 0.5% gelatin in the presence of calcium chloride dihydrate for 1hr and transglutaminase for 24hrs

5. FUTURE ENHANCEMENTS

A tissue-engineering construction (scaffold, SC) with certain biochemical capabilities is thought to be the most important building block for brain tissue repair after damage, which is a long-standing difficulty in neuro transplantology[3]. By applying the photopolymerization approach, brain-rich endogenous hyaluronan which has been glycidyl methacrylate altered can be used to create these three-dimensional (3D) polymer scaffolds. Here, we developed 3D hydrophilic scaffolding for cell culture that are impregnated with neurotrophins and have Young's elastic modulus and swelling ratios

The process of neural regeneration is incredibly challenging. The shrinkage of the brain tissue volume in brain injuries caused by trauma inhibits neuronal regrowth. In this study, electrically charged hydrogels called C1A1 hydrogels that had both anionic and cationic monomers in a 1:1 ratio were used to construct neurons. These hydrogels worked well as scaffolding for neural stem cells to connect to (NSCs). NSCs were able to develop into neuroglial cells thanks to the pore-filled C1A1 hydrogels created by cryogelation. In a rodent trauma injury model, the C1A1 permeable hydrogel was transplanted into abnormalities in the brain. VEGF promoted the infiltration of macrophages/microglia, astrocytes, and a host-derived vascular network into the C1A1 porosity hydrogel.

Consecutive implantation of NSCs that were GFP-labelled aided in the promotion of glial and neuronal cell differentiation. As a consequence, this two-step strategy for neural regeneration might someday emerge as a cutting-edge method for the healing of damaged brain tissue.

6. CONCLUSION

Any device incorporating the gelatin-alginate based hydrogel is probably 5 to 10 years away from being used in people because it has not yet received FDA approval. Currently, this study suggests using hydrogel scaffolds to build laboratory models of the brain that could illuminate the process of cell differentiation, such as how neurons establish connections with other types of supporting cells. As we apply a drug or simulate a brain injury to see how these networks of cells are affected and then how we could recover them, we eventually expect that these brain models will supplant animal testing. In vitro testing of medicines in plastic frequently results in drug failures when tested on animals. The cells develop very similarly to how they would in the body because the polymer closely resembles the characteristics of the brain. We come to the conclusion that the best location to test and then transition these drugs is in this scaffold model of the brain made of gelatin and alginate.

REFERENCES

[1] Vladimir A. Kornev et al., “Hydrogel-assisted neuro-regeneration approaches towards brain injury therapy: A state-of-the-art review,” Comput Struct Biotechnol J. 2018; 16: 488–502.

[2] Yang Chen et al., “A Prosperous Application of Hydrogels with Extracellular Vesicles Release for Traumatic Brain Injury (TBI),” Front Neurol., 2022; 13: 908468.

[3] Tatiana A. Mishchenko et al., "3D-printed hyaluronic acid hydrogel scaffolds impregnated with neurotrophic factors (BDNF, GDNF) for post-traumatic brain tissue reconstruction,"Front. Bioeng.Biotechnol., Volume 10 - 2022 | https://doi.org/10.3389/fbioe.2022.895406
[4] Satoshi Tanikawa et al., "Engineering of an electrically charged hydrogel implanted into a traumatic brain injury model for stepwise neuronal tissue reconstruction,"Now published in Scientific Reports doi: 10.1038/s41598-023-28870-z.,2022.
[5] W.M. Tian et al.," Hyaluronic Acid–Poly-D-Lysine-Based Three-Dimensional Hydrogel for Traumatic Brain Injury," Mary Ann Liebert, Inc.,3 May 2005,https://doi.org/10.1089/ten.2005.11.513
[6] Yi Chaiet al.,"Structural alignment guides oriented migration and differentiation of endogenous neural stem cells for neurogenesis in brain injury treatment,"Elsevier Ltd.,https://doi.org/10.1016/j.biomaterials.2021.121310.
[7] Kun Zhang et al.,"Potential application of an injectable hydrogel scaffold loaded with mesenchymal stem cells for treating traumatic brain injury,"Journal of materials Chemistry B., Issue 19,2018.
[8] Rodrigo Lozano et al., "3D printing of layered brain-like structures using peptide modified gellan gum substrates,"ScienceDirect.,Volume 67, October 2015, Pages 264-273
[9] Michael L. Shuler et AL., "Toward in vitro models of brain structure and function," PNAS.,September 5, 2014/111 (38) 13682-13683/https://doi.org/10.1073/pnas.1414484111.
[10] Qing Li et al., "Recent trends in the development of hydrogel therapeutics for the treatment of central nervous system disorders,"NPG Asia Materials.,Volume 14, Article number: 14 (2022).
[11] Mihyeon Bae et al., "Neural stem cell delivery using brain-derived tissue-specific bioink for recovering from traumatic brain injury,"Mihyeon Bae et al 2021 Biofabrication 13 044110.
[12] Anindya Sundar Adak et al., "Extracellular Matrix (ECM)-Mimicking Neuroprotective Injectable Sulfo-Functionalized Peptide Hydrogel for Repairing Brain Injury,"https://doi.org/10.1021/acsbiomaterials.9b01829.
[13] Shanshan Ma et al., "Sodium alginate/collagen/stromal cell-derived factor-1 neural scaffold loaded with BMSCs promotes neurological function recovery after traumatic brain injury,"ScienceDirect.,Volume 131, 1 September 2021, Pages 185-197
[14] Christopher T. Tsui et al., "Applying a novel 3D hydrogel cell culture to investigate activation of microglia due to rotational kinematics associated with mild traumatic brain injury,"ELSEVIER.,https://doi.org/10.1016/j.jmbbm.2020.104176.
[15] Wei-Hong Jian., "Glycosaminoglycan-based hybrid hydrogel encapsulated with polyelectrolyte complex nanoparticles for endogenous stem cell regulation in central nervous system regeneration,"ELSEVIER.,https://doi.org/10.1016/j.biomaterials.2018.05.009
[16] Qavia S, Pourmahdian S, Eslamia H. Acrylamide Hydrogels Preparation via Free Radical Crosslinking Copolymerization: Kinetic Study and Morphological Investigation, Journal of Macromolecular Science, Part A: Pure and Applied Chemistry. 2014; 51:842-848.
[17] Rana P, Ganarajan G, Kothiyal P. Review on Preparation and Properties Hydrogel Formulation, World Journal of Pharmacy and Pharmaceutical Sciences. 2015; 4(12):1069-1080.
[18] Tan H, Marra KG. Injectable, biodegradable hydrogels for tissue engineering applications. Materials. 2010; 3:1746-1767.

Stress Strain Measurement of Dental material using Laser Speckle Imaging

Jeffry J[1], Lakshmi Parvathi M[2], Abira Bright B[3], Vani Damodaran[4]
[1,2,3,4]SRM Institute of science and technology, Kattankulathur, Chengalpattu

ABSTRACT

Grinding of teeth exerts excess stress on dental material, which eventually leads to the gradual wear and tear of the enamel. Laser speckle imaging (LSI) has been proven to be a sensitive technique for detecting changes induced by pressure. The purpose of this study is to measure dental material stress and strain using LSI. To achieve this, the blurring effect of the speckle pattern is analysed to determine the imaging modality for LSI. The paper describes the implementation of laser speckle interferometry for assessing the strain developed on dental material due to an applied stress. Dental samples are subjected to pressure to develop stress, and the resulting strain is measured through analysis of the captured speckle images.

Keywords: Laser Speckle Imaging, Calcium Phosphate, Graphite, Load cell

Corresponding Author:
Dr. Vani Damodaran,
Assistant Professor, SRM Institute of Science and Technology, Kattankulathur, Chengalpattu
Email: vaind@srmist.edu.in

1. INTRODUCTION

The tooth is under constant stress due to biting and chewing actions. Certain medical conditions make people bite hard and this affects the tooth after a certain period of time. The study of the applied stress and the resulting strain can clearly help in studying the tensile strength of the material (Kinney et al, 2003). The formation of a cavity leads to filling made of composites, ceramics, etc. The study of the tensile strength of such material helps in further understanding how long it would last.

A speckle pattern, also referred to as a random interference effect, is produced when laser light impacts a diffuse objects. The interference pattern known as "laser speckle" is created when light is reflected or scattered from various locations on the lighted surface (De la Torre, et al 2016). The superposition of waves that comes at a particular spot-on image determines the intensity that results there. If the resulting amplitude is zero, at the point, a black speckle can be seen since each individual wave cancels out; if the waves come at the phase point, the highest intensity can be visible which was discussed by (Briers, David, et al 2013). This technique has also been used in ophthalmology, dermatology, and neurology, biomedical applications.

The speckle pattern varies when the object is moving. These variations may reveal details about the movement (Bazylev et al, 2009). The simplest technique to obtain this data to capture upon exposure, a speckle pattern duration higher than the shortest time scale for speckle fluctuations; these fluctuations blur the speckle, lowering the local contrast of the speckles (Kong et al 2018). As a result, differences in speckle contrast are used to code velocity distributions. The Doppler effect can be used to gather the same data, however creating a two-dimensional Doppler map involves either scanning the laser beam or high-speed camera imaging (Vaz, Pedro G et al, 2016)

Laser speckle imaging is a non-invasive method which studies the speckle pattern to measure the effect of stress applied on tooth material. It is a diagnostic method that studies the properties of scattered coherent light (Zaslansky et al 2005). A diffuse pattern image, which at first glance appears as noise, actually contains details of microstructure and small changes of a tissue (Zaslansky et al., 2006). By statistically analysing the light's temporal and spatial fluctuations separated by microstructure dynamics and heterogeneities, it is able to learn more about the dynamics.

This paper reports the stress and strain pattern observed in calcium phosphate-based fillings. A small block of calcium phosphate is subjected to manual stress and the resulting strain or deformation is measured from the out-of-plane displacement using laser speckle imaging.

2. METHODOLOGY

The process of stress-strain analysis for dental filling material involves laser speckle imaging, the process is explained in Figure 1. First to select the material required for the dental filling and with the selected

materials the dental block is developed, which will then be used for laser speckle analysis. Calcium phosphate (4 gms) and graphite (0.5 gms) are mixed together with water to create a stronger material for a dental filling, as shown in Figure 2 where the preparation process is illustrated.

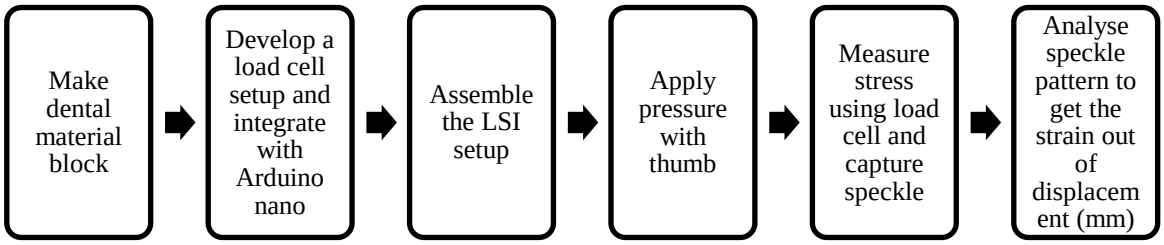

Figure 1. Laser Speckle Imaging process

An Arduino Nano is connected to a load cell with a capacity of 3kg, and this, in turn, is connected to an LCD display which displays the pressure that is given during analysis. The laser speckle imaging setup is built and pressure is applied using the thumb gradually from 0 gms to 1000 gms. The resulting image is displayed on the LCD display. In addition, Stress is measured through a load cell, while the speckle is captured with the use of an ESP32 camera module. Finally, the analysis of the speckle pattern helps to determine the strain from the displacement of the targeted object, in millimeters.

2.1. Materials

2.1.1 Calcium Phosphate

$Ca_3(PO_4)^2$ materials have attracted more scientific attention recently for bones and teeth. They are sought biomedical materials with great biocompatibility and non-harmful chemical components. The two types of calcium phosphates that are utilised the most are hydroxyapatite and tricalcium phosphate. One category of bioactive synthetic materials is calcium phosphates. Because of their crystalline, osteoconductive, and chemical closeness to bone tissue. Tricalcium phosphate are biodegradable materials which can be used to replace normal bone which is has good tolerance by both hard and soft tissues. Their "restorability," or the degree of breakdown in vivo, is used to categorize them. Tricalcium phosphate is said to be "resorbable," but hydroxyapatite is said to be "non-resorbable." (Nery et al. 1975) initial dental application was disclosed a "tricalcium phosphate reagent," which was later shown to be a mixture of hydroxyapatite and tricalcium phosphate rather than the authors' initial description of it as "tricalcium phosphate".

2.1.2 Graphite

Carbon atoms with a hexagonal crystal structure are piled into stacked sheets composed into minerals known as graphite. Under normal circumstances, purest carbon is the most stable. The characteristics of graphite include extreme softness, low specific gravity, minimal reactivity, and high electrical and thermal conductivity. Graphite has a greasy sensation due to its high softness and ability to that readily slide into another. Other allotropes, or forms, of carbon, exist in nature, each with a unique crystal structure. One type is hexagonally arranged carbon atoms. Graphite has recently been drawing attention as biomaterials which have good biocompatibility, and antibacterial effects, particularly against dental pathogens (Hyung-Jin Nam et al. 2019). Graphene has been used for bone replacement, bone regeneration due to its mechanical strength to improve osteogenesis.

2.2. Dental Block Preparation

The dental material that is utilized for measuring stress-strain properties comprises Calcium Phosphate (4gms) blended with Graphite (0.5gms) and distilled water (3ml). After mixing the ingredients, the mixture is placed in a mould with dimensions of 2cm x 2cm x 2cm and pressure is applied to distribute it evenly. The mixture is then subjected to a temperature of 60°C and kept in a hot air oven for a period of one day, following which it is heated in a ceramic bowl in a furnace at a temperature of 1000°C to enhance its strength.

Figure 2. Process of making dental sample

The addition of graphite to the material enhances its strength, and subjecting it to heat treatment further increases its durability (Karahan et al 2018). The primary goal of adding graphite is to ensure that the material is resistant to breaking or damage. In line with this, a dental block with dimensions of 2cm x 2cm x 2cm was prepared. The process of creating the dental block is depicted in Figure 2.

2.3. Arduino Nano

The Arduino Nano module, which is a self-contained device, is a small and comprehensive piece of technology that is similar in features to other Arduino products, despite arriving in a different package. In this particular application, a 3kg load cell has been connected to the Arduino Nano and programmed to display values in grams on an LCD screen when pressure is applied. It is possible to program the Arduino Nano using the Arduino software.

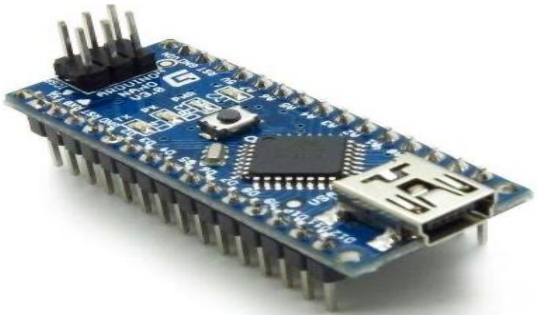

Figure 3. Arduino Nano

2.4. Load cell setup

The load cell with a weight capacity of 3 kg is linked to an Arduino nano board in a manner that enables the display of applied pressure on the Liquid Circuit Display (LCD) screen. The pressure applied on the load cell is measured and communicated to the LCD screen through the nano board. A comprehensive schematic diagram showing the load cell, Arduino nano board, and the LCD is illustrated in figure 4. This arrangement enables the precise determination and display of the pressure applied to the load cell through the LCD screen.

Figure 4. Load cell

2.5. ESP 32 Camera Module

The ESP32 microcontrollers are small, inexpensive devices that come with both Wi-Fi and Bluetooth integrated into them. One particularly competitive example of these microcontrollers is the ESP32 CAM WiFi Module Bluetooth, paired with an OV2640 Camera Module capable of taking 2-megapixel images as shown in figure 4. This module not only includes processors, but also wireless networking capabilities, peripheral ports, and power management features. In short, the ESP32 CAM module is a versatile and cost-effective solution for integrating wireless networking and camera functionality in a small package.

Figure 5. ESP 32 Camera Module

2.6. FTDI Programmer

FTDI is the abbreviation for Future Technology Devices International Limited, a privately owned Scottish company specializing in Universal Serial Bus (USB) technology. The company provides programming for the ESP 32 camera module, which captures and records the video or image in a computer. This process is done in a particular way that allows for efficient and effective transfer of data between the camera module and the computer.

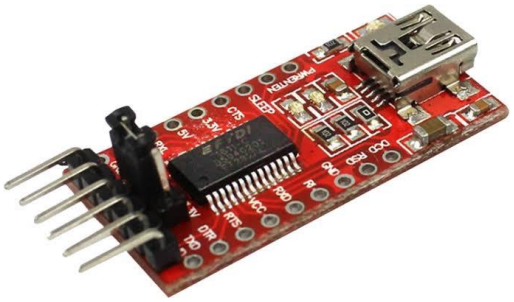

Figure 6. FTDI Programmer

2.7. LSI Assembly

The setup of the Laser Speckle Imaging involved assembling a dental block onto a Load Cell. This setup was further enhanced by placing a red laser pointer and an ESP32 camera module on the opposite side of the dental material, at a distance of 23 cm from the camera lens, which acts as the focal point. To capture the images, the camera is connected to FTDI, which supports modern systems by converting the serial transmission to and from a USB signal. The laser was positioned in such a way that the light is focused on the block and the camera captures images of the block. The list of components used for assembling the system can be found in table 1. Figure 7 displays the final setup for the Laser Speckle Imaging system.

Table 1. The components for the setup

Sl.No	Materials	Quantity
1	ESP 32 Camera Module	1
2	Dental Material	1 Block
3	Laser Pointer	1
4	Load cell	1
5	FTDI Programmer	1
6	Arduino Nano	1
7	LCD display	1

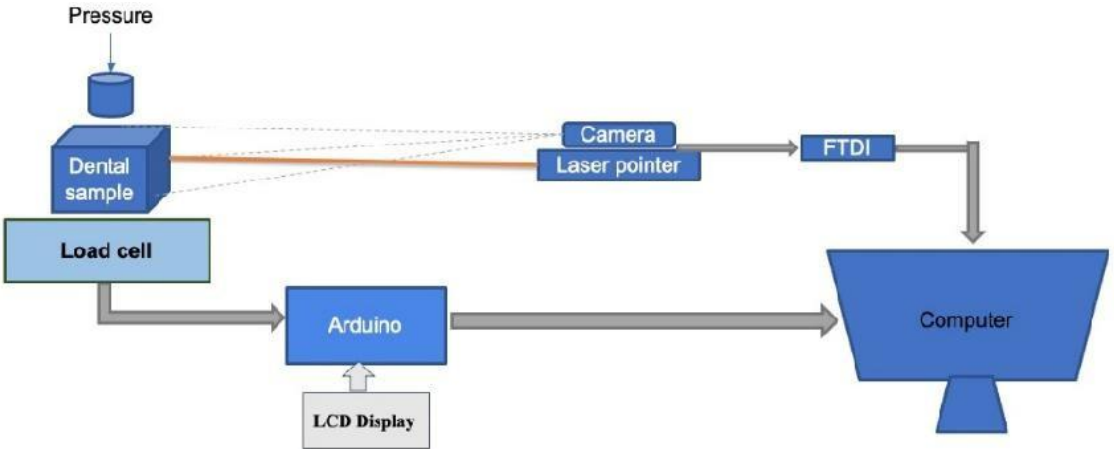

Figure 7. LSI Setup

2.8. Working

The laser is powered on and the camera is activated through the FTDI programmer to capture video. The dental material is placed slightly away from the focal length of the lens in order to detect the out-of-plane displacement. The pressure is manually applied on the block using the thumb. The roughness of the dental material causes a speckle pattern formation when illuminated with laser light. The pressure applied on the material leads to deformation and bulging. The deformation along the side where the laser is pointed is measured by capturing images of the speckle pattern. The consecutive speckle images are analysed to see the intensity variation with increasing pressure.

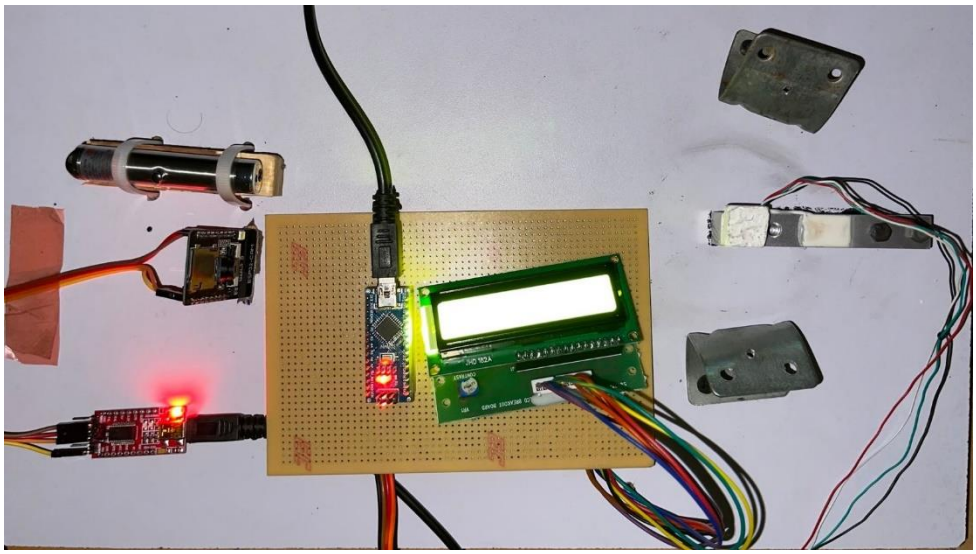

Figure 8. Working LSI Setup

As the sample is initially kept slightly away from the focal point, the increasing pressure and deformation will lead to the speckle pattern getting in focus and thereby an increase in pixel intensity. A video is recorded as the pressure is applied and is processed in MATLAB R2021B. The individual frames are extracted from the video and the difference in the speckle pattern intensity among consecutive frames is obtained. The change is graphically represented as pressure vs intensity plot. The working setup is shown in figure 8.

3. RESULTS AND DISCUSSION

Utilizing both graphite and calcium phosphate, the dental block was developed, and the hardware setup is made for the LSI system. The pressure applied to the dental block with the thumb is measured and displayed on the LCD screen in grams. The pressure applied causes variation in speckle pattern. The speckle variation is shown in figure 9.

Figure 9. Speckle pattern changes with varying applied pressure

By processing the speckle image in MATLAB, the graph was plotted for the pressure (grams) vs the mean intensity variation as shown in figure 10. The mean intensity variation is obtained by taking the mean of the difference between the consecutive frames. The dental block is initially placed out of focus by a few micron meters, the increase in pressure causes out of place displacement which causes the deformation closer to focus. As a result, the mean intensity variation of the speckle increase as the pressure increase.

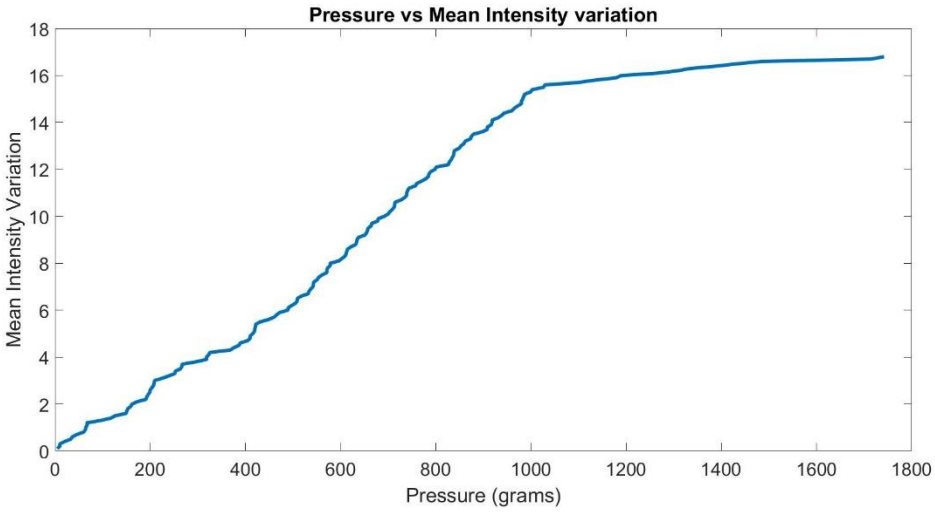

Figure 10. Graphical Outputs

4. CONCLUSION

In this paper, an LSI system was developed, to detect the stress applied to the dental block and to analyse the strain or the deformation caused, by measuring the out-of-plane displacement. Pressure is applied on the dental material, the speckle pattern on the illuminated side surface is acquired and analyse to measure strain. The pressure causes the speckle pattern to change. By analysing the change in the mean intensity between consecutive speckle images, the out of plane displacement can be observed. Future work involves an automatic stress-inducing mechanism and testing of other dental materials.

REFERENCES

[1] Koshoji, Nelson H., Sandra K. Bussadori, Carolina C. Bortoletto, Renato A. Prates, Marcelo T. Oliveira, and Alessandro M. Deana. "Laser speckle imaging: a novel method for detecting dental erosion." *PloS one* 10, no. 2: e0118429(2015)

[2] Briers, David, Donald D. Duncan, Evan Hirst, Sean J. Kirkpatrick, Marcus Larsson, Wiendelt Steenbergen, Tomas Stromberg, and Oliver B. Thompson. "Laser speckle contrast imaging: theoretical and practical limitations." *Journal of biomedical optics* 18, no. 6; 066018-066018 (2013)

[3] Chang Liu, Kıvılcım Kılıç, Sefik Evren Erdener, David A. Boas, and Dmitry D. Postnov, "Choosing a model for laser speckle contrast imaging," Biomed. Opt. Express 12, 3571-3583 (2021)

[4] Briers, J. David. "Laser speckle contrast imaging for measuring blood flow." Optica Applicata 37 (2007).

[5] Boas, David A., and Andrew K. Dunn. "Laser speckle imaging in biomedical optics." *Journal of biomedical optics* 15, no. 1 ;011109-011109 (2010)

[6] Vaz, Pedro G., Anne Humeau-Heurtier, Edite Figueiras, Carlos Correia, and Joao Cardoso. "Laser speckle imaging to monitor microvascular blood flow: a review." *IEEE reviews in biomedical engineering* 9: 106-120(2016)

[7] Bazylev, N. B., and S. P. Rubnikovich. "Investigation of the stressed-strained state of cermet dentures using digital laser speckle-photographic analysis." Journal of Engineering Physics and Thermophysics 82: 789-793 (2009).

[8] Postnov, Dmitry D., Xiaojun Cheng, Sefik Evren Erdener, and David A. Boas. "Choosing a laser for laser speckle contrast imaging." *Scientific reports* 9, no. 1; 2542(2019)
[9] Kong, Tae Hoon, Sunkon Yu, Byungjo Jung, Jin Sil Choi, and Young Joon Seo. "Monitoring blood-flow in the mouse cochlea using an endoscopic laser speckle contrast imaging system." *PloS one* 13, no. 2: e0191978(2018)
[10] Kinney, J. H., S. J. Marshall, and G. W. Marshall. "The mechanical properties of human dentin: a critical review and re-evaluation of the dental literature." Critical Reviews in Oral Biology & Medicine 14, no. 1: 13-29 (2003).
[11] Nery, E. B., K. L. Lynch, W. M. Hirthe, and K. H. Mueller. "Bioceramic implants in surgically produced infrabony defects." Journal of periodontology 46, no. 6: 328-347(1975)
[12] Nam, Hyung-Jin, You-Min Kim, Yong Hoon Kwon, In-Ryoung Kim, Bong-Soo Park, Woo-Sung Son, Seung-Min Lee, and Yong-Il Kim. "Enamel surface remineralization effect by fluorinated graphite and bioactive glass-containing orthodontic bonding resin." Materials 12, no. 8 :1308(2019).
[13] Karahan, Hüseyin Enis, Christian Wiraja, Chenjie Xu, Jun Wei, Yilei Wang, Liang Wang, Fei Liu, and Yuan Chen. "Graphene materials in antimicrobial nanomedicine: current status and future perspectives." Advanced healthcare materials 7, no. 13: 1701406 (2018).
[14] Zaslansky, Paul, Ron Shahar, Asher A. Friesem, and Steve Weiner. "Relations between shape, materials properties, and function in biological materials using laser speckle interferometry: in situ tooth deformation." Advanced Functional Materials 16, no. 15 : 1925-1936 (2006).
[15] De la Torre, I. Manuel, María del Socorro Hernández Montes, J. Mauricio Flores-Moreno, and Fernando Mendoza Santoyo. "Laser speckle based digital optical methods in structural mechanics: A review." Optics and Lasers in Engineering 87 : 32-58 (2016).
[16] Zaslansky, Paul, John D. Currey, Asher A. Friesem, and Steve Weiner. "Phase shifting speckle interferometry for determination of strain and Young's modulus of mineralized biological materials: a study of tooth dentin compression in water." Journal of biomedical optics 10, no. 2: 024020-024020 (2005).

Generation of Optimal SURF Descriptor Codebook for ANA Pattern Classification

Jeevitha Kora Naidu[1], Janani Arulmani[2], Kanchana Devanathan[3]
[1,2,3]Department of Biomedical Engineering, SRM Institute of Science & Technology. Kattankulathur, Chennai, India

ABSTRACT

Indirect immunofluorescence analysis of human epithelial type 2 cells is the gold-standard method for diagnosing autoimmune diseases. (HEp-2). This study is focused on optimizing the codebook size of dictionary learning to increase the classification accuracy of example images The "Task 2 Sample Classification" dataset from his ICPR competition in 2016 was used in this study. The top-hat transform is used for the illumination correction of sample images. As further preprocessing, anisotropic diffusion filtering followed by pixel normalization is performed. SURF feature descriptors are obtained from preprocessed images. Vector quantization using the k-means algorithm is performed to generate codebooks of sizes 8, 16, 32, 64, 128, 256, and 512. Support vector machine (SVM), naive bayes (NB) classifier, random forest (RF), and logistic regression (LR) are the four classifiers that have developed codebooks that are provided. The results show that 100% average accuracy of within-class classification is achieved with codebook sizes of 512 and 32 for uniform and speckled patterns, respectively. HF classifiers perform well among other classifiers. Observation of codebook size allows us to choose the optimal codebook size for dictionary learning in HEp-2 cell image analysis. Analysis of classifier performance is useful for further investigating the relationship of classification accuracy with respect to codebooks.

Keywords: Indirect Immunofluorescence, Human Epithelial Type-2 (HEp-2) cells, autoimmune diseases, codebook, Top-hat transform, Anisotropic diffusion filtering, Logistic Regression, Naïve Bayes, Random Forest, Support Vector Machiner

Corresponding Author:
Dr. Kanchana Devanathan,
Assistant Professor,Deaprtment of Biomedical Engineering
SRM Institute of Science & Technology. Kattankulathur, Chennai, India
Email:kanchand2@srmist.edu.in

1. INTRODUCTION

Antinuclear antibody (ANA) screening by indirect immunofluorescence (IIF) is a typical technique in contemporary autoimmune disease diagnostic methods [1, 15]. Fluorescence microscopy is frequently used to test grown cells of the HEp-2 cell line. The perceived strength of the fluorescent signal and the type of staining pattern is used to make a diagnosis [2,6]. Medical professionals and lab professionals may accurately recognize patients by understanding the significance of various patterns [3, 4].

The visual analysis of enormous quantities of picture data is a time-consuming and tedious procedure that necessitates the time and efforts of highly specialized and trained operators, resulting in more extraordinary expenditures on healthcare [2]. Variability is caused by factors such as slide preparation, conjugate specificity, the effectiveness of the fluorescence microscope, and the reader's expertise [3, 5, 7, 8].

Specific Different types of autoimmune disorders are shown by specific staining patterns. As a result of this, a clear description of them is essential for making a diagnosis [2, 14]. Diffuse interphase nuclear staining and chromatin staining of mitotic cells help identify a homogeneous pattern. The difference between a speckled pattern and interphase cell nuclei is nuclear staining [5,6,7].

Pre-processing of original images is essential to enhance the cell nucleus, remove the artifacts and enhance the nucleus boundaries and extracting useful features [5]. Non-uniform illumination over the specimen is a major artifact induced due to improper placement of the light source. Morphological operations-based techniques are found to be effective in overcoming this artifact. Top hat transform with large structuring element is considered to pre-process the green channel images [16].

Anisotropic diffusion filter has been implemented on the brightness channel of HSB and cyan component CMYK to reduce noise and simultaneously preserve the shape and contrast of the cell structures [17]. To enhance the edges with region specific filtering anisotropic diffusion filter has been attempted with

satisfactory result [18].

The Hessian matrix is the foundation of the Speeded-up Robust Features (SURF) detector. SURF employs box filters to approximate the second order Gaussian derivatives, in contrast to SIFT, which approximates the Laplacian of Gaussian (LoG) with Difference of Gaussians (DoG).The ability to swiftly calculate different descriptors is one of SURF's key features. Additionally, the SURF descriptor is unaffected by typical picture alterations including rotation, scaling, lighting, and slight changes in perspective. [9]

Image descriptors extracted are used to construct the Bag-of-words framework. The visual words are used to build a dictionary, which correspond to the essential description of the image and are commonly used in object recognition. Building a BoW model has been attempted with various types of image descriptors for HEp-2 images [10, 11].

The Input vector quantization (VQ) algorithms are based on the shortest Euclidean distance between an input vector and all words in a codebook (also called a template). A bag of words is constructed based on term frequency, which represents the number of times each template is repeated throughout the document [12]. In this work, we use an approach known as K-means to generate codebooks.

To generate VQ's codebook, each training image has been divided into M rectangular pieces. Each block is transformed into a vector and the vectors of all the training images are concatenated to produce the training set. Mathematically, a subset of the vectors in the training set is selected. The vectors that were selected are all collected in the first codebook. Each vector is known as a "codeword" in the original codebook. The original codewords in the final codebook are progressively updated to form the final codebook. [13]

The automated classification of the staining pattern based on standardized and measurable picture components collected using image processing techniques may aid in the resolution of repeatability and dependability difficulties. Furthermore, computer-aided systems can interpret vast amounts of visual data quickly, needing little or limited input from human operators [2, 16].

2. METHODOLOGY

2.1. Database Description

The ICPR 2016 I3A Task 2 training set includes 1008 images from 252 samples.This data set was obtained in 2013 from the Sullivan Nicolaides Institute of Pathology, Australia. It was extracted from the sera of 1001 patients diagnosed as ANA-positive.

Each patient's serum was diluted to a concentration of 1:80 before imaging with a monochrome camera attached to the microscope. Each sample was taken of her four times, resulting in four alternate playback positions of her for each sample. Among those seven pattern classes in the collection include uniform, speckle, nucleolus, centromere, nuclear envelope, Golgi apparatus, and the mitotic spindle. The last three classes are less common, while the first four categories are typical ANA patterns.

All images are available in monochrome, uncompressed format with 1388 x 1040 pixel resolution and manually created cell masks. For HEp-2 images, MATLAB 2017a is used for preprocessing and SURF feature extraction.

2.2. Illumination Correction

A top-hat transform (THT) is used to increases the illumination of HEp-2 image. Compute the morphological opening of the image using the structuring element and subtract the result from the original image [19]. It is defined by the following formula:

$$\boldsymbol{THT}(\boldsymbol{x},\boldsymbol{y}) = \boldsymbol{f}(\boldsymbol{x},\boldsymbol{y}) - \boldsymbol{foB}(\boldsymbol{x},\boldsymbol{y}) \qquad \text{eq.1}$$

Where THT (x, y) is the top-hat transform at pixels x, and y, f(x, y) is the position of the matched images, foB(x, y) is performed using the structuring element Morphological opening operation.

2.3. Filtering

Anisotropic Diffusion Filter (ADF) is a nonlinear filter based on Partial Differential Equation [20]. These filters may successfully decrease noise and smoothen image while taking into consideration region borders and minor features [21].The PDE for smoothing the object area while preserving the edges obtained through edge detection is given by equation 2.

$$\begin{aligned} \boldsymbol{I_t} &= \boldsymbol{div}(\boldsymbol{c}(\boldsymbol{x},\boldsymbol{y},\boldsymbol{t})\boldsymbol{\nabla I}) \\ &= \frac{\boldsymbol{\partial}}{\boldsymbol{\partial x}}(\boldsymbol{c}(\boldsymbol{x},\boldsymbol{y},\boldsymbol{t})\boldsymbol{I_x}) + \frac{\boldsymbol{\partial}}{\boldsymbol{\partial y}}\big(\boldsymbol{c}(\boldsymbol{x},\boldsymbol{y},\boldsymbol{t})\boldsymbol{I_y}\big) \end{aligned} \qquad \text{eq.2}$$

Where c is the conduction diffusion coefficient that conducts the smoothing operation on the picture, *Ix* and *Iy* are image intensities in the *x* and *y* directions, represents the gradient of the brightness function, t represents time, and I represents image. The conduction diffusion coefficient *c* is considered as a function of magnitude of gradient of image brightness function. It is expressed by the equation 3.

$$\boldsymbol{c(x,y,t) = f(\|\nabla I(x,y,t)\|)} \qquad \text{eq.3}$$

Proper selection of the function f is vital to preserve and sharpen the edges. The magnitude of the gradient is larger on the edge of the images, while the magnitude of function f is lower on the edge of each image. Popular choice of function *f* is given by the equation 4.

$$\boldsymbol{f(\|\nabla I(x,y,t)\|) = \exp\left(-\left(\frac{\|\nabla I\|}{K}\right)^2\right)} \qquad \text{eq.4}$$

Where, *K* is a constant which indicates the edge strength threshold. *K* can be tuned for specific applications.

2.4. Contrast Enhancement

Intensity adjustment is a technique for converting the intensity values of an image to a different range. The image's contrast is increased by remapping the data values to span the whole intensity range [0, 255]. The imadjust function in MATLAB is used to improve the contrast of HEp-2 pictures.

2.5. SURF Keypoint Extraction

SURF derived some inspiration from SIFT, which uses integrated visuals. The integral image is made up of all the pixels in input image I that are included within a rectangular region extending from (0, 0) to (x, y) [23].

$$\boldsymbol{I_{\sum(x,y)} = \sum_{i=0}^{x}\sum_{j=0}^{y} I(x,y)} \qquad \text{eq.5}$$

In order to quickly analyse the scale space, the integral image-based filter sizes are scaled up. The choice for interest point identification depends on which determinant of the Hessian matrix has the highest determinant value. The Hessian matrix H(f(x),) in x at scale is defined as follows [23], where I is an image and f(x) = (x, y) is a point.

$$\boldsymbol{H(x,\sigma) = \begin{bmatrix} L_{xx}(f(x),\sigma) & L_{xy}(f(x),\sigma) \\ L_{xy}(f(x),\sigma) & L_{yy}(f(x),\sigma) \end{bmatrix}} \qquad \text{eq.6}$$

where *Lxx(f(x), σ* is the convolution of the Gaussian second-order derivative with the image I at point (x, y), and Lxy(f(x),σ) and Lyy(f(x),σ) are equivalent.

A 32-dimensional vector made up of the 2D Haar wavelet responses produced in 44 sub-regions around each interest point is then used to construct the orientation-dependent descriptors. A 64-dimensional vector is formed [22] when information on the polarity of the intensity changes is taken into consideration.

2.6. Codebook Generation

In order to identify interest regions in training photos and categorise related qualities, a vector quantization approach is used to create a visual codebook. The learned cluster centers, or "codewords," for each group serve as its representation. How many clusters are found using the clustering approach determines the size of the codebook. The entire patches of an image are then mapped into a fixed-length feature vector [22] by quantizing each interest point of an image in the dataset to its nearest codeword in the codebook. The procedure's algorithm is as follows: [24]

Step 1: Select k random vectors from the training set and call it as code vectors.
Step 2: Find the squared Euclidean distance of all the training vectors with the selected k vectors
Step 3: A training vectors Xj is put in ith cluster if the squared Euclidean distance of the Xj
Step 4: IfXjis minimum for more than one codevector then Xj is put in any one of them.
Step 5: Compute centroid for each cluster.
Step 6: Centroids of each of cluster form set of new codevectors
Step 7: Centroids are taken as input to K-Means algorithm for the next iterations.
Step 8: Compute MSE for each of k clusters and net MSE.
Step 9: Replace initial code vectors by the centroids of each cluster respectively.
Step 10: Repeat the steps 4 to 7 till the two successive net MSE values are same.

3. RESULTS AND DISCUSSION

The HEp-2 images of homogeneous and speckled patterns are subjected to pre-processing. The representative images of the specimen with 3-D plot of pixel intensity before and after pre-processing are shown in the Figure1.

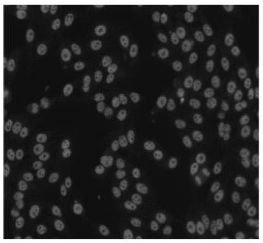

(a) Original Image

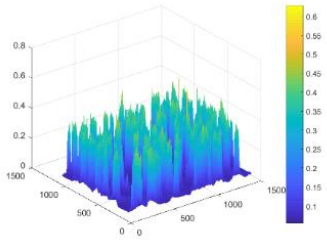

(b) 3D Intensity profile of Original Image

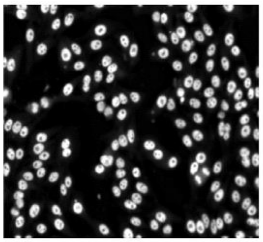

(c) Pre-processed Image

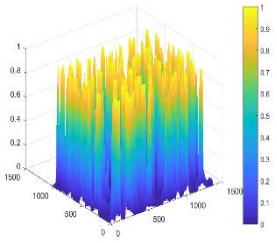

(d) 3D Intensity profile of Pre-processed Image

Figure 1. Original and Pre-processed images with respective 3-D intensity plots

Once pre-processing of the images are performed, the SURF keypoints are extracted from the images. The keypoint descriptor is further extracted forming a 64-dimensional vector for each image. The representative patterns considered in this study along with extracted SURF keypoints are shown in the Figure 2.

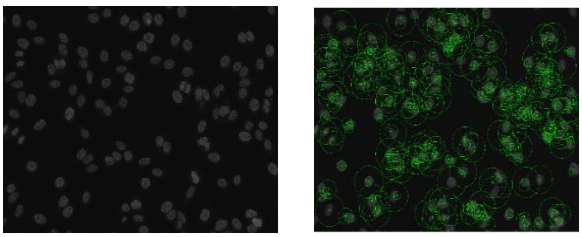

(a) Homogeneous Intermediate Intensity

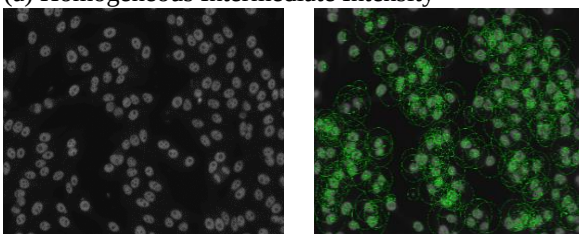

(b) Homogeneous Positive Intensity

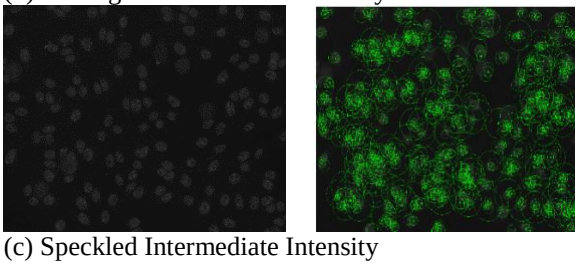

(c) Speckled Intermediate Intensity

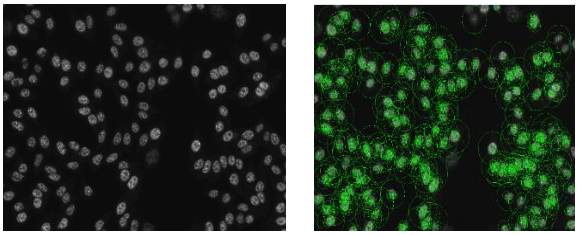

(d) Speckled Positive Intensity

Figure 2. Representative HEp-2 Specimen Images and respective SURF Key points

Table 1 summarizes the various codebook sizes experimented to analyze the performance of the classifiers to distinguish the homogeneous intermediate and positive patterns. The performance of the classifiers for classifying speckled intermediate and positive patterns is summarized in Table 2.

Table 1. Homogenous – Intra Class Accuracy (%)

Codebook	LR	SVM	RF	NB	Mean Accuracy
CB = 8	99.88	99.88	100.00	97.29	99.26
CB = 16	100.00	99.97	100.00	97.70	99.42
CB = 32	99.94	99.96	100.00	97.00	99.22
CB = 64	99.93	99.99	100.00	98.07	99.50
CB = 128	99.99	100.00	100.00	98.13	99.53
CB = 256	100.00	100.00	100.00	98.17	99.54
CB = 512	100.00	100.00	100.00	98.42	**99.60**

Table 2. Speckled – Intra Class Accuracy (%)

Codebook	LR	SVM	RF	NB	Mean Accuracy
CB = 8	99.94	99.94	100.00	92.73	98.15
CB = 16	99.94	100.00	100.00	93.21	98.29
CB = 32	99.99	99.97	100.00	99.02	**99.74**
CB = 64	99.88	99.98	100.00	98.45	99.58
CB = 128	99.98	100.00	100.00	97.90	99.47
CB = 256	99.98	100.00	100.00	98.67	99.66
CB = 512	99.99	100.00	100.00	98.53	99.63

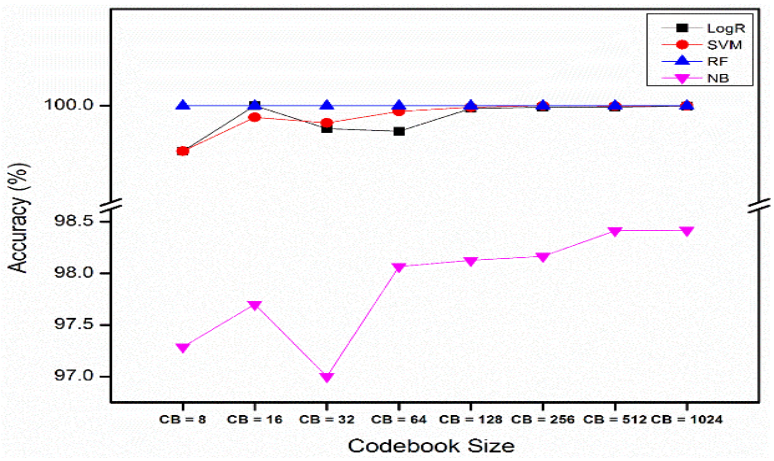

Figure 3. Homogeneous pattern - Intra-class Classifier performance

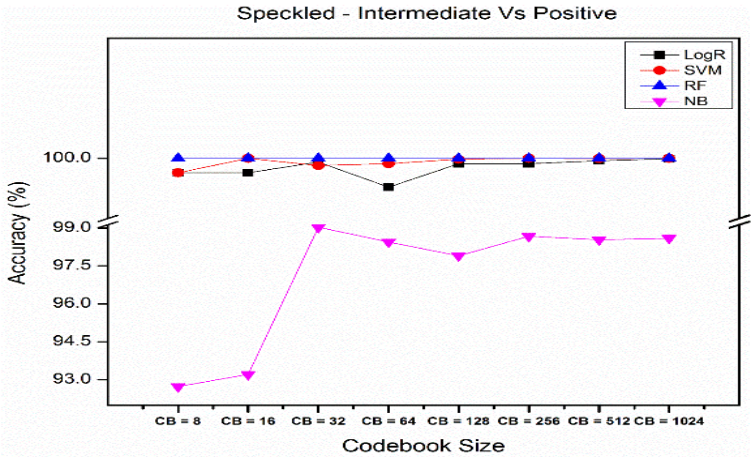

Figure 4. Speckled pattern - Intra-class Classifier performance

From Figure 3 and 4, it is observed that the codebook size has significant effects on the performance of the classifiers. For both patterns, codebook size 32 changes the trend of the accuracy vs codebook size plot. NB classifier has comparatively less significant output than the other classifiers. RF classifier is found to provide best classification performance for the intra-class analysis of homogeneous and speckled patterns. The codebook size 512 and 32 are found to be effective among all the classifiers. Table 3 highlights the performance comparison of the various classifiers for the inter-class classification of the patterns.

Table 3. Homogeneous Vs. Speckled - Inter Class Accuracy

Codebook	LR	SVM	RF	NB	Mean Accuracy
CB = 8	99.88	99.881	98.24	88.04	96.51
CB = 16	99.52	99.76	98.01	88.44	96.43
CB = 32	99.91	99.90	99.57	98.62	**99.50**
CB = 64	99.78	99.81	99.38	93.02	98.00
CB = 128	99.94	99.94	98.98	89.80	97.16
CB = 256	99.40	99.37	98.63	85.64	95.76
CB = 512	99.66	99.66	99.44	88.33	96.77

When multi-class classification is performed, the LR and SVM are found to provide equivalent results. Codebook size of 64 can be useful for multi-class classification and the results are as follows:

Table 4. Multiclass Classification

Codebook	LR	SVM	RF	NB	Mean Accuracy
CB = 8	99.91	99.82	96.01	81.37	81.37
CB = 16	99.81	99.63	96.90	82.13	82.13
CB = 32	99.64	99.81	98.73	89.48	89.48
CB = 64	99.89	99.94	99.25	97.54	**97.54**
CB = 128	99.94	99.93	98.57	95.36	95.36
CB = 256	99.90	99.79	98.44	92.99	92.99
CB = 512	99.89	99.80	99.12	91.98	91.98

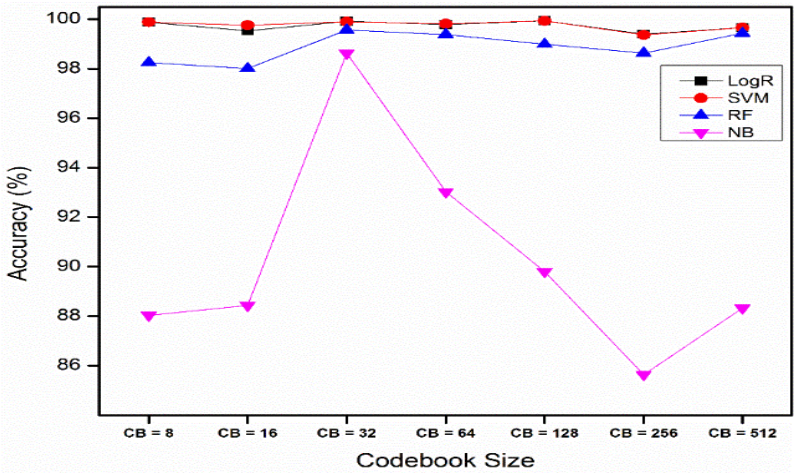

Figure 5. Homogeneous Vs Speckled - Inter-class classifier performance

In Figure 5, it can be observed that the classifier performance is highly unstable with the increase in the codebook sizes. Among all the codebook sizes, 32 is considered to be optimal since the classifiers' performance are satisfactory. In Figure 6, it is shown that the codebook size of 64 has significant classification accuracy when compared to other sizes among all the classifiers. LR and SVM are found to be having similar performance in classification of multi-class patterns.

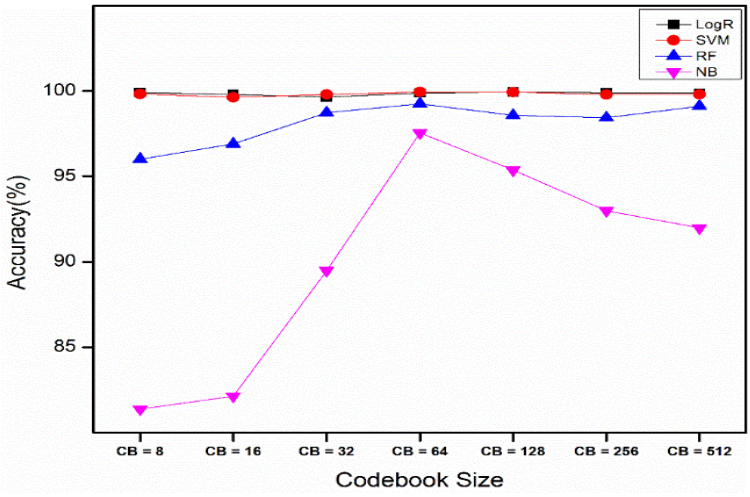

Figure 6. Homogeneous Vs Speckled – Multi-class classifier performance

4. CONCLUSION AND FUTURE SCOPE

In this research, an attempt has been made to optimize the selection of codebook size for classification of HEp-2 staining patterns. Homogeneous and speckled patterns with positive and intermediate intensity are considered for this study. 420 specimen images from the ICPR 2016 Task 2 training set are taken for experiments. Pre-processing followed by SURF keypoint extraction is performed. Codebooks are generated for various sizes using k means algorithm.

The results have indicated that there is a significant impact of codebook size on the classification performance of the staining patterns under intra, inter and multi-class scenarios. Other dictionary learning methods can be implemented in future to compare the performance of the vector quantization. Further research could be carried out in tuning of codebook parameters such as length, computational time and efficiency for the improved classification of HEp-2 staining patterns.

REFERENCES

[1] Hobson, P., Lovell, B. C., Percannella, G., Saggese, A., Vento, M., &Wiliem, A, "HEp-2 staining pattern recognition at cell and specimen levels: datasets, algorithms and results", *Pattern Recognition Letters*, Vol. 82, pp. 12-22, 2016.

[2] Di Cataldo, S., Bottino, A., Ficarra, E., &Macii, E, "Applying textural features to the classification of HEp-2 cell

patterns in IIF images", *In 21st International Conference on Pattern Recognition (ICPR)*, pp. 3349-3352, 2012.
[3] Buchner, C., Bryant, C., Eslami, A., &Lakos, G, "Anti-nuclear antibody screening using HEp-2 cells", *Journal of visualized experiments: JoVE*, Vol. 88, 2014.
[4] Larsen, A. B. L., Vestergaard, J. S., & Larsen, R, "HEp-2 cell classification using shape index histograms with donut-shaped spatial pooling", *IEEE transactions on medical imaging*, Vol. 33, No.7, pp. 1573-1580, 2014.
[5] Foggia, P., Percannella, G., Soda, P., & Vento, M, "Benchmarking HEp-2 cells classification methods", *IEEE transactions on medical imaging*, Vol. 32, No.10, pp. 1878-1889, 2013.
[6] Chan, E. K., Damoiseaux, J., Carballo, O. G., Conrad, K., de Melo Cruvinel, W., Francescantonio, P. L. C., ... & von Mühlen, C. A, "Report of the first international consensus on standardized nomenclature of antinuclear antibody HEp-2 cell patterns 2014–2015", *Frontiers in Immunology*, Vol. 6, pp. 412, 2015.
[7] Hobson, P., Lovell, B. C., Percannella, G., Vento, M., &Wiliem, A, "Classifying anti-nuclear antibodies HEp-2 images: A benchmarking platform", *In 2014 22nd International Conference on Pattern Recognition (ICPR)*, pp. 3233-3238, 2014.
[8] Soda, P. and G. Iannello, "A Multi-Expert System to Classify Fluorescent Intensity in Antinuclear Autoantibodies Testing", *Computer-Based Medical Systems*, pp. 219-224, 2006.
[9] Hwang, S, "Bag-of-visual-words approach based on SURF features to polyp detection in wireless capsule endoscopy videos", *ISVC*, Vol. 11, pp. 320-7, 2011.
[10] Joachims, Thorsten, "Text Categorization with Support Vector Machines: Learning with Many Relevant Features", *Machine Learning*, Vol. 1398, pp. 137-142, 1998.
[11] Xu, X., Lin, F., Ng, C., & Leong, K. P, "Automated classification for HEp-2 cells based on linear local distance coding framework", *EURASIP Journal on Image and Video Processing*, Vol. 13, 2015.
[12] Schmitt, M., & Schuller, B, "OpenXBOW: introducing the passau open-source crossmodal bag-of-words toolkit", *The Journal of Machine Learning Research*, Vol. 18, No. 1, pp. 3370-3374, 2017.
[13] Shahid, H., & Ward, R. K, "Codebook design for vector quantization using hexagonal partitioning", *In 2016 IEEE Canadian Conference on Electrical and Computer Engineering (CCECE)*, pp. 1-6, 2016.
[14] Pollard, K. M, "Autoantibodies and Autoimmunity: Molecular Mechanisms in Health and Disease", 2005.
[15] Elbischger, P., S. Geerts, K. Sander, G. Ziervogel-Lukas and P. Sinah, "Algorithmic Framework for Hep-2 Fluorescence Pattern Classification to Aid Auto-Immune Diseases Diagnosis", *Proceedings of the International conference on Symposium on Biomedical Imaging: From Nano to Macro*, pp. 562-565, 2009.
[16] Tonti, S., S. D. Cataldo, A. Bottino, and E. Ficarra, "An Automated Approach to the Segmentation of HEp-2 Cells for the Indirect Immunofluorescence ANA Test", *Computerized Medical Imaging and Graphics*, Vol. 40, pp. 62-69, 2015.
[17] Huang, Y. L., Y. L. Jao, T. Y. Hsieh, and C. W. Chung, "Adaptive Automatic Segmentation of HEp-2 Cells in Indirect Immunofluorescence Images", *IEEE Explore*, pp. 418-422, 2008.
[18] Cheng, C. C., J. S. Taur, T. Y. Hsieh, and C. W. Tao, "Segmentation of Anti-Nuclear Antibody Images Based on the Watershed Approach",*In Industrial Electronics and Applications*, Taichung, June, 1695-1700, 2010.
[19] Hassanpour, H. and N. Samadiani, "Using Morphological Transforms to Enhance the Contrast of Medical Images", *Egyptian Journal of Radiology and Nuclear Medicine*, 46(2), 481-489, 2015.
[20] Perona, P. and J. Malik, "Scale-Space and Edge Detection Using Anisotropic Diffusion", *IEEE Transaction on Pattern Analysis and Machine Intelligence*, Vol. 12, No.7, pp. 629-639, 1990.
[21] Tsiotsios, C. and M. Petrou, "On the Choice of the Parameters for Anisotropic Diffusion in Image Processing", *Pattern Recognition*, Vol. 46, No.5, pp. 1369-1381, 2012.
[22] Mayurathan, B., Ramanan, A., Mahesan, S., &Pinidiyaarachchi, U. A. J, "Speeded-up and compact visual codebook for object recognition", *International Journal of Image Processing (IJIP)*, Vol/ 7, No.1, pp. 31, 2013.
[23] Jiang, P., Zhao, S., & Cheng, S, "Rotational invariant LBP-SURF for fast and robust image matching", *In 2015 9th International Conference on Signal Processing and Communication Systems (ICSPCS)*, pp. 1-7, 2015.
[24] Kekre, H. B., &Sarode, T. K, "Vector quantized codebook optimization using k-means", *International Journal on Computer Science and Engineering (IJCSE)*,Vol. 1, pp. 283-290, 2009.

Prediction and Diagnosis of Cardio Vascular Diseases using Machine Learning Techniques

Ravipati Naga Deepthi[1], Uddanti Sri Sai Ramya[2], Ramana Venkata Rami Reddy[3], Nakka Soma Sekhar[4], VBKL Aruna[5]
[1,2,3,4,5]Department of Electronics and Communication Engineering,Velagapudi Ramakrishna Siddhartha Engineering College, Kanuru, Vijayawada, Andhra Pradesh

ABSTRACT

Cardiovascular disease is one of the most hazardous conditions impacting people nowadays and significantly changes current lifestyle. One of the most lethal human diseases, cardiovascular disease has a detrimental impact on processing.Further health evaluations, treatments, and innovative characteristics are still required from the patient to the distant hospital. A precise and speedy verification of cardiovascular events is crucial for the early diagnosis and treatment of heart failure. It's frequently believed that the ritualistic medical history is spectacularly ineffective at diagnosing cardiovascular diseases. With non-invasive methods like machine learning, it may be possible to distinguish between healthy people and people with heart disease with precision and efficiency. There are numerous machine learning strategies for CVD prediction. The most complete and effective strategy, however, is determined by the data set being used. One of the deadliest human ailments is cardiovascular disease, which has a terrible impact on processing methods. The data is first pre-processed using data from before coronary artery disease. Then, we can anticipate CVDs early on by applying machine learning methods. Naive Baye's, SVM,Random, Forest,Gradient Booster and Logistic Regression are the most often used algorithms. Large data sets are suited for Random forest. The publicly accessible Kaggle database, which was integrated with Google Collaboratory and a PYTHON programme, can be used as the input database. We shall categorise a person's heart ailment into phases after classifying heart diseases. Based on the likelihood of developing a heart block, there are four categories. Arterial blockage is the stage 1 and stage 2 condition, while chronic heart disease is the stage 3 and stage 4 condition.

Keywords: CVDs, Machine Learning, Google collaboratory, Classification, Data preprocessing.

Corresponding Author:
Ravipati Naga Deepthi,
Department of Electronics and Communication Engineering,Velagapudi Ramakrishna Siddhartha Engineering College, Kanuru, Vijayawada, AndhraPradesh
Email: deepthiravipati7@gmail.com

1. INTRODUCTION

Cardiovascular disease (CVD), a chronic and complicated disease resulting from heart and vascular conditions, is currently the main cause of chronic disability and early mortality on a global scale. The usual methods of treatment are medical and surgical ones. Yet, these treatments are unable to reverse CVD. The quality of life for those with CVD is also considerably improved by these medicines. As a result, the primary focus of contemporary CVD care is prevention measures. According to recent studies, early intervention could save nearly 80% of CVD-related premature deaths. Moreover, CVD has a slow onset and a long incubation period; as a result, it is frequently diagnosed at a more advanced stage. Thus, early recognition of high-risk groups for CVD is essential for its management and prevention.

The use of Csk prediction models to identify high-risk populations that could benefit from early intervention to reduce their likelihood of developing CVD has been supported by an increasing number of CVD prevention and control guidelines. The majority of the current risk prediction models for CVD were built using conventional statistical methods. A model is deemed to be established if it meets the independence and linearity requirements. This has an effect on both the use of external verification and the precision of the prediction model because it is unable to adequately represent the intricate interaction between variables.

The machine learning (ML) algorithm, a well-known statistical method, can successfully handle non-linearity, variable redundancy, and inter-variable interactions. It is frequently utilised in the field of CVD prevention and control because it may be used to explore potential risk factors for CVD in order to improve its prediction performance. Notwithstanding its advantages, there are still concerns about its ability to predict CVD. According to related studies, ML algorithms perform more accurately when making predictions than traditional

statistical methods. In contrast, study found that the predictive performance of logistic regression (LR) was comparable to that of machine learning techniques.

According to this study, there is a direct link between high CVD incidence and high prevalence of the disease's risk factors, such as metabolic syndrome, hypertension, and obesity. The majority of these models are based on a feature screening strategy, despite the fact that Chinese researchers have lately produced prediction models based on Cox regression and ML algorithms.

According to this study, there is a direct link between high CVD incidence and high prevalence of the disease's risk factors, such as metabolic syndrome, hypertension, and obesity. The majority of these models are based on a feature screening strategy, despite the fact that Chinese researchers have lately produced prediction models based on Cox regression and ML algorithms.

2. RELATED WORKS

Clinicians should focus on tracking changes in NT-proBNP, Ddimer, Killip, cTnI, and LDH in order to enhance the clinical results of ACS patients.This suggestion is supported by research on models for patients with acute coronary syndrome that use machine learning to predict in-hospital mortality. The methodologies employed in this paper are the study's design and the patient variables and definition, building a model to predict hospital mortality risk for ACS patients, statistical investigation.

Muktevi Sri Venkatesh proposed a method for anticipating cardiovascular illness using machine learning techniques including K-Nearest Neighbour (KNN), Support Vector Machines (SVM), Logistic Regression (LR), Naive Bayes (NB), and Random Forest (RF). Patients with chronic CVD infection and healthy individuals can be predicted using a few learning calculations employing KsssNN, SVM, LR, NB, and RF[1]. The Logistic Regression classifier demonstrated its prowess in forecasting with the greatest outcomes in terms of precision and quickest execution time, according to the reenactment's results.

For the purpose of predicting the risk of developing heart disease, Ibomoiye Domor Mienye and Yanxia Sun[8] proposed a method based on an enhanced ensemble learning approach that uses techniques such as logistic regression (LR), l k nearest neighbour (KNN), support vector machine (SVM), linear discriminant analysis (LDA), classification and regression tree (CART), gradient boosting (GB), and random forest (RF). The proposed technique performed best with precision of 96%, sensitivity of 91%, accuracy of 93%, and F1 score of 93%.

In January 2022, A. Reyana, Sandeep Kautish, and Rajkumar Gangappa Nadakinamani[5] developed an approach for analysing clinical data in order to forecast cardiovascular illness using machine learning methods. This approach makes use of M5P Tree, Random Tree, REP Tree, Linear Regression, J48, JRIP, and Naive Bayes algorithms. Two datasets—Statlog (heart) and Hungarian—are made available in this study for machine learning classification techniques such Naive Bayes, Linear Regression, Random Tree, REP Tree, J48, and JRIP. To select the best machine learning model, the performance of the proposed CDPS was evaluated using a number of variables. When it comes to the prediction of patients with cardiovascular illness, the Random Tree model performed amazingly well, with the best RMSE of 0.0231, accuracy of 100%, the lowest MAE of 0.0011, and the quickest prediction time of 0.01 (secs).

In December 2021[12], M. D. Amzad Hossen, Tahia Tazin, and Sumiaya Khan published a method for supervised machine learning-based cardiovascular disease analysis and prediction that makes use of methods like Random Forest (RF), Logistic Regression (LR), and Decision Tree (DT). The goal of this research was to determine which machine learning classifier would be most effective in predicting heart disease given the dataset provided. Three distinct classifiers' results were compared. The logistic regression technique performed better than the other two classifiers, with an accuracy of 92%.

A method on Early and Accurate Prediction of Heart Disease Using Machine Learning Model was proposed in 2021[3] by B Padmaja, Chintala Srinidhi, Kotha Sindhu, and Kalali Vanaja. It uses methods like Random Forest (RF), Logistic Regression (LR), K-Nearest Neighbor (KNN), Support Vector Machine (SVM), Decision Tree (DT), Gradient Boosting, and Naive Bayes. A variety of data mining techniques are used for classification.The random forest data mining classification algorithm was used with a minimum set of 14 required characteristics, and it generated good results.

Apurb Rajdhan, Milan Sai, and Avi Agarwal[7] proposed a method for applying machine learning to detect heart illness in April 2020. Decision Tree (DT), Logistic Regression (LR), Random Forest (RF), and Naive Bayes are employed in this method (NB).The goal of the study was to identify the most efficient ML algorithm for heart disease diagnosis.

The accuracy score of various machine learning algorithms for heart disease prediction is evaluated in this work using data from the UCI machine learning repository[10].The Random Forest algorithm, with an accuracy score of 90.16%, is the best algorithm for foretelling heart disease, according to the study's findings.Weicheng Sun and Ping Zhang proposed a method for the prediction of cardiovascular disorders using machine learning in May 2021, which uses methods such as Support Vector Machine (SVM), Logical Regression

(LR), and Random Forest (RF).The results show that the SVM-based method can provide an average area under the ROC curve of 78.84%, proving that SVM outperforms LR & RF for our data.

3. METHODS

To finish our work, we used a heart disease dataset that we acquired from Kaggle. As seen in table 1, this dataset contains 917 instances of 9 different variables, including age, sex, cp, trestbps, chol, fbs, restecg, thalach, and exang. The dataset is initially cleaned up and processed using pre-processing techniques. The total number of patient records showed was 917.The data scientist can have a better knowledge of the dataset's validity with the use of data visualization tools. Five machine learning classifiers are exposed to the dataset: Logistic Regression (LR, SVM, GB, RF), Gradient Booster, Random Forest, Naive Bayes, and SVM (GB).The most accurate classifier can be used to determine which one is the best. The trends connected to diseases are separated by datasets. From the data, a training dataset and a testing dataset are produced.920 records in total, together with 76 medical-related features, were obtained. The list of 9 qualities that the system is based on is displayed in the table below.

Table 1. Dataset attributes

S.No	Attributes	Value type
1.	Age	Numerical
2.	Sex	Numerical
3.	Cp	Numerical
4.	Trestbps	Numerical
5.	Cho	Numerical
6.	Fbs	Numerical
7.	Restecg	Numerical
8.	Thalach	Numerical
9.	Exang	Numerical

4. DESIGN PROCESS

A-Data Collection

- The quality and amount of our data have an impact on the precision of our model.
- Typically, the result of this stage is a data representation Guo condenses it as a table that we will utilise for training.
- Previously gathered data can still be used at this level by using datasets like Kaggle, UCI, etc.

B-DATA PREPARATION

- Acquire data and make it training-ready. reasonable train/evaluation split? Depending on the field, the accessibility of the data, the specifics of the dataset, etc., 80/20, 70/30, or anything comparable may be appropriate.
- Clean anything that may need to be cleaned (remove duplicates, correct errors, deal with missing values, normalisation data type conversions, etc.)
- The impacts of the specific order in which we gathered and/or otherwise prepared our data are eliminated by randomizing the data.
- Use data visualisation to uncover pertinent associations between variables or gaps between classes (bias alert!), or carry out more exploratory investigations.
- Group the sets according to training and assessment purposes.

C- CHOOSE A MODEL

- Chosen the most effective technique for the job at hand. Many algorithms exist.

D. TRAIN THE MODEL

- To respond or forecast accurately as often as is practical is the goal of training.
- Linear regression example: The computer software would need to learn the values of m(orW) and b. (x is input,y is output)

- Each step of the procedure involves training.

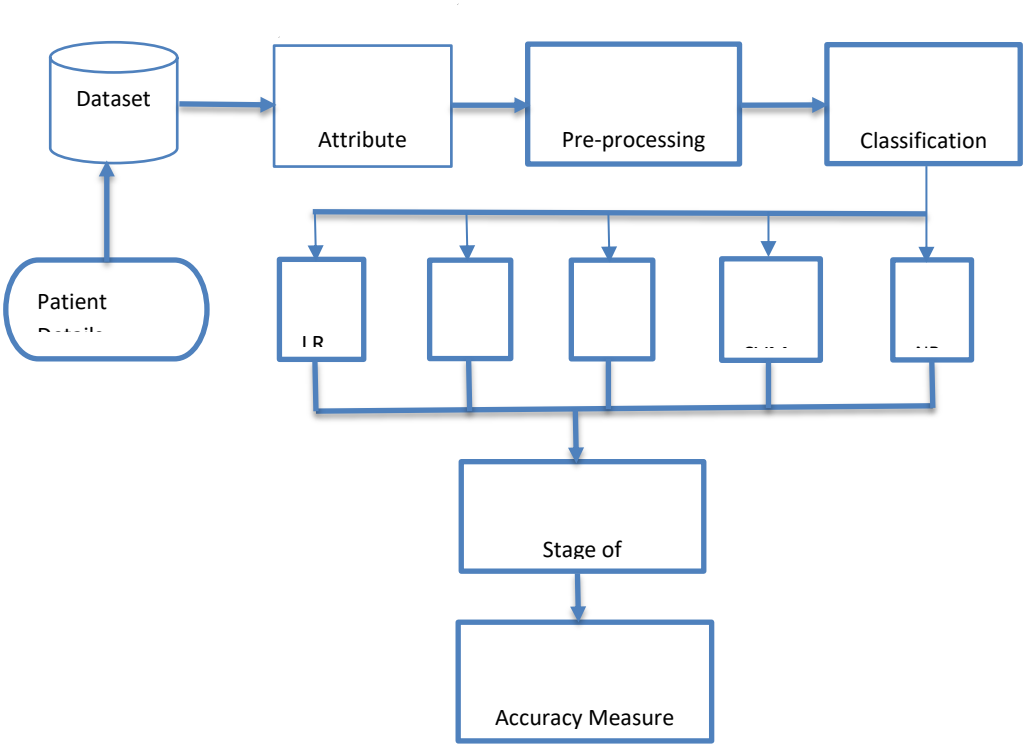

Figure 1. Flowchart Model

Algorithms used:

A. Random Forest:

Random Forest techniques are used in both regression and classification.Predictions are made based on a tree-like organisation of the data.When used on large data sets, the Random Forest approach may still produce the same findings even when a significant portion of record values are missing.

B. Logistic Regression:

Typically, the logistic regression approach is used for binary classification problems. The logistic regression technique uses the logistic function to restrict the output of a linear equation to the range between 0 and 1, as opposed to fitting a straight line or hyperplane.

C. Naive Bayes:

The Nave Bayes algorithm is a supervised learning method for classification issues that is based on the Bayes theorem.It is mostly employed in text categorization with a large training set.Being probabilistic classifier, it makes predictions based on the likelihood that an object will occur.

D. SUPPORT VECTOR MACHINE(SVM):

The vector machine, which can be used to address both classification and regression problems, is one of the most well-liked supervised learning techniques. According to the SVM approach,n-dimensional space can be classified by drawing the best line or decision border.

E. *Gradient Booster(GB):*

Gradient booster is a method that stands out for its prediction speed and accuracy, especially with large and complex datasets.Bias errors and variance errors are the two types of errors. Using gradient boost method, we may lessen the bias error of the model.

5. RESULTS

- Information on 917 patients was included in the dataset that was used for this inquiry.By using algorithms like Logistic Regression, Gradient Booster, SVM, Naive Bayes, and Random Forest, we can determine whether a person has CVD or not.The evaluation metric used in this inquiry was accuracy.
- The classification of heart disease is done using machine learning algorithms
- The one who has no heart disease,the model will predict it as ‘0’,which implies the person has no chance of getting heart disease.
- The one who has heart disease,the model will divide the stages of disease into 4 types based on chance of getting heart blockage.

- Based on the severity of arterial blockage, heart disease can be divided into 4 phases (stages 1 through 4).
- Artery blockage>50% indicates presence of heart disease. The stage of cardiac disease increases with the size of the obstruction.
- Heart attacks can occur at any time in people with stage 3 and stage 4 chronic heart disease.

Accuracy

It is defined as the ratio of accurate predictions to all predictions made by the classification algorithm.

$Accuracy = TP + TN/(TP + TN + FP + FN)$.

- Collected dataset from kaggle.

Table 2. Accuracy values

Algorithms	Accuracy
Logistic Regression	0.804878
SVM	0.707317
Random Forest	0.985366
Naïve Bayes	0.780488
Gradient Booster	0.964321

- Logistic Regression, SVM, Naive Bayes, Gradient Booster, and Random Forest are the algorithms.
- Nave Bayes, SVM, Gradient Booster, and Logistic Regression all have accuracy values of 0.780488, 0.804878, 0.707317, and 0.964321 respectively. The Random Forest algorithm, which has an accuracy of 0.985366, is the most accurate of these five algorithms.

REFERENCES

[1] Ke J., et al. machine learning-based approaches for predicting in-hospital mortality for patients with acute coronary syndrome. 2022 Mar 1;53:127-34 the Emergency Medicine American Journal.
[2] Stevens BR and CJ Pepine emerging importance of machine learning in research and application of cardiovascular disease. Cardiology Research and Practice, American Heart Journal Plus, 2021 November 1, 11:100050.Early and accurate cardiac disease prediction using machine learning model.
[3] Padmaja, B., et al. TURCOMAT 12.6 (2021): 4516-4528 Turkish Journal of Computer and Mathematics Education.
[4] Fernandez-Cabo, E. Lara-Pezzi, X. Rossello, V. Fuster, F. Benito, J. P. Manzano, J. C. Silla, & (2020). The definition of cardiovascular risk in young, asymptomatic people is improved by machine learning. Journal of the American College of Cardiology, 76(14), 1674-1685.
[5] Zhou, Y., et al. (2019). cardiovascular event prediction for percutaneous coronary intervention using machine learning. 73(9S1), 127–127. Journal of the American College of Cardiology.C Tangiographydata. *International Journal of Cardiology*, *335*, 130-136.
[6] "Detection of Cardiovascular Disease Using Machine Learning Classification Models," Hana H. Allawi and S. Alsuwat Manal. The International Journal of Engineering Research & Technology's ISSN (2021) is 2278-0181.
[7] Manasa Gummalla, Yiye Zhang, Kelly Michalak, Evan Sholle, Zhuoran Xu, Ashley N. Beecy, and others. Predicting heart failure all-cause mortality or 30-day unplanned readmission using machine learning and electronic health data 1, no. 2 (2020): 71–79 in the Journal of Cardiovascular Digital Health.
[8] Wang, Z., Sun, Y., and Mienye, I. D. (2020). An improved ensemble learning approach for predicting the risk of heart disease. Unlocked Medical Informatics, 20, 100402.
[9] W. Benjamins, M. W. Yeung, T. Maaniitty, A. Saraste, R. Klén, P. van der Harst, et al (2021). utilising machine learning to enhance clinical and coronary data integration to better identify patients for advanced cardiac imaging data froma CT angiogram. 335, 130–136, International Journal of Cardiology.
[10] Kim, Y., et al. cardiovascular risk assessment based on deep learning and employing retinal image-based coronary artery calcium scores. e306-e316 in The Lancet Digital Health, 3(5).
[11] R.G. Nadakinamani et al., 2022. Analysis of Clinical Data for Prediction of Cardiovascular Disease Using Machine Learning. Cognitive neuroscience and machine learning, 2022.
[12] "Supervised analysis and prediction of cardiovascular illness using machine learning." M. D. Hossen et al. Issues in Engineering Mathematics 2021 (2021)
[13] Ramalingam VV, Dandapath A, Raja MK. Heart disease prediction using machine learning techniques: a survey. Int J Eng Technol. 2018;7(2.8):684–7.
[14] Shah, Devansh, Samir Patel, and Santosh Kumar Bharti. "Heart disease prediction using machine learning techniques." *SN Computer Science* 1 (2020): 1-6.

The Preliminary Study of Upper Arm Movements Using Wearable Sensors For The Use of Exercise In Post-Stroke Patients

Gokul Raj G[1], D. Ashok Kumar[2], Varshini Karthik[3]
[1,2,3]SRM Institute of Engineering and Technology, Kattankulathur

ABSTRACT

The study aims to investigate the upper arm movements of post-stroke patients using surface electromyogram (EMG) signals. The exercise and regular rehabilitation of the subjects will improve their health conditions and support the therapeutic medical condition. The movements of the upper arms while performing specific workouts like crawling stretches and weight training at the elbows. These exercises are trials with normal subjects in the age range of 20 to 24. The muscles that respond to these exercises are the deltoid, biceps, and triceps. The EMG data were collected using the Delsys Trigno wireless EMG and statistically analyzed. The muscle responses of the post-stroke patients will be lower than those of the other normal subjects. The statistical analysis of mean, maximum, minimum, and T-test revealed activation changes in the muscles. It has been found that post-stroke rehabilitation using these exercises will improve the patient's overall health condition.

Keywords: Neuromuscular disease, Post-stroke, Virtual Reality, EMG.

Corresponding Author:
Dr.Varshini Karthik, Professor, Department of Biomedical Engineering
SRM Institute of Engineering and Technology, Kattankulathur
Email: varshinikps@gmail.com

1. INTRODUCTION

(Feigin et al. 2021) Stroke is one of the leading causes of death and disability in the world. Strokes leave people with long-term physical and cognitive impairments. Smoking, drinking, an irregular lifestyle, a lack of sleep, and hypertension are all factors that contribute to strokes. This study looks at the effects of a stroke. The patients are very concerned about regaining control of their body movements. Recent advanced technologies enable patients to resume their normal lifestyles. The neuromuscular system is critical to human daily activity. But it damages the cells of the neurons and affects electrical signals from the brain. Neuromuscular diseases damage the nerves that govern voluntary muscles and sensory nerves. Neurons transmit and receive electrical signals to regulate voluntary muscles. When neurons are sick or die, nerves and muscles can't communicate and Muscles deteriorate (atrophy). From 1990 to 2019, A high body mass index, hyperglycemia, bad cholesterol, nephropathy, a dietary deficiency in red meat, alcohol consumption, and exposure to tobacco smoke contributed to smoking, and a diet limited in fruits and vegetables investigated stroke-related disability-adjusted life years. (Mugnosso et al., 2017) Robotic devices, for example, assist the disabled and people with neuromuscular disorders with rehabilitation practices. According to the EMG signals and data analysis, subjects with muscle fatigue or a neuromuscular disease are more sensitive, the mean frequency decreases, and the RMS values decrease. (Akbari and Talasaz 2014) The connection between the movements and activity of the upper human muscles when the elbow becomes stretched. a nonlinear autoregressive exogenous (NARX) model of the recurrent neural network (RNN) kind to identify the EMG signals of the triceps brachii based on the datasets of the other two muscles (deltoid and pectoral major). Using the NARX model, the R-values and mean square error values show how EMG signals from other arm movements can be used to find the lost functions of an arm that has been cut off above the elbow. (Feigin et al., 2021) As a significant and frequent cause of disability globally, stroke is one of the most common chronic conditions. According to recent data, there are already 650 million people worldwide, many of whom are 60 or older, and by 2050, that number will reach 2 billion. (Chaze et al. 2022) The most recent technological advancements, such as virtual reality (VR) and video gaming, provide patients with a visual therapeutic strategy that supports their recovery. One of the technologies that are used to immerse users in a depiction of the actual world that is customized to rehabilitation activities is virtual reality (VR).

2. LITERATURE REVIEW

Neurological problems may decrease motor function and life quality. Researchers are trying to rehabilitate the nervous system and minimize neurological and cognitive problems in stroke, spinal cord injury, and clinical disease patients. Neurorehabilitation treatments include robot- and VR-assisted single-player games.

Recently, multiplayer games may boost the effectiveness of robot- and VR-assisted neuromuscular rehabilitation. (Brazalovich, Philip, et al. 2022). Gaming is the best way to communicate to distract from the pain, respond to the therapy, and increase the effort put into the work. (P. Sweetser and P. Wyeth, 2005) The robot assists in rehabilitation. Used after neurologic damage to assist repetitively and follow mobility recovery. Robots can haptically measure sensorimotor function, give instruction, and enhance motor recovery. Robotic paradigms may enhance muscle strength and healing over standard training mechanisms. The kinematics of the movement of particular daily tasks were compared with the parameters of the upper limb kinematics during exercises using the Neuroforma system. [7] Manual muscle testing (MMT) is a tool to identify a stroke patient's rehabilitation by measuring and analyzing position changes in the shoulders, elbow, forearm, and wrists. (Nadinne Alexandra Roman, et al.,2022) By using the IMU sensors and creating VR environments for monitoring the frozen shoulder movements of rehabilitation patients. (Jianjun Cui et al., 2019) Angles are measured from the seven basketball players using the IMU sensors, and it compares the analysis with 3D motion analysis. Mareike Roell, et.al 2019) The triceps brachii, biceps brachii, the clavicular region of the pectoralis major, and the anterior, middle, and posterior deltoid are the muscles that are responsible for movement. The study has been based on the function of the muscles while driving a car. The steering wheel is one of the car's control components that turns in both clockwise and anti-clockwise directions. (Y. Liu, X, 2012)

3. METHODOLOGY

Electromyography (EMG) measures how a nerve stimulates a muscle's electrical activity. The data collected from an EMG are often required to assist in the diagnosis or exclusion of several conditions, including but not limited to:

- Muscle disorders such as muscular dystrophy and polymyositis are examples of these conditions.
- A disease called myasthenia gravis is one example of a condition that affects the connection that exists between the nerve and the muscle.
- Peripheral neuropathies and carpal tunnel syndrome are examples of disorders that affect the nerves located outside the spinal cord and are referred to as "peripheral nerves."
- ALS, also known as amyotrophic lateral sclerosis, and polio are two examples of diseases that damage the motor neurons in the brain and spinal cord.
- A herniated disc in the spine is one example of a condition that might harm the nerve root.

When brain clots break and hemorrhage or causes a blockage in the blood flow to the brain, the natural consequence is a stroke. The brain's tissues die from the absence of oxygen and blood because of the hole or obstruction. Stroke symptoms can include:

- Monoplegia (weakness of a single limb)
- Lack of feel or weakness in the arm, face, and leg, particularly on one side; problems communicating or

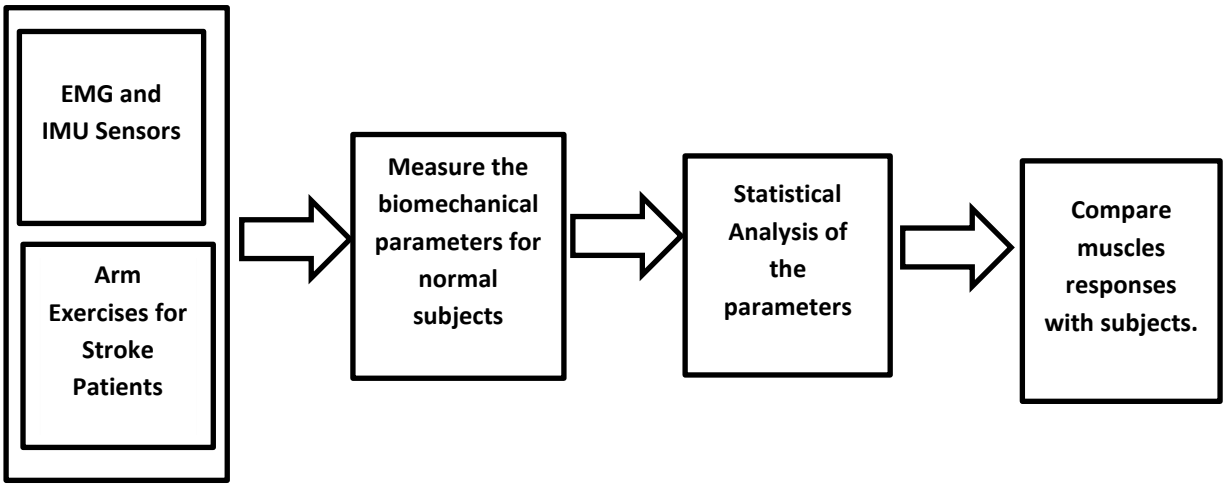

understanding others' stammered speech, confusion, disorientation, or a failure to respond.

- unexpected mood changes notably increased agitation.
- vision issues, including hazy or darkened vision in one or both eyes.

Post-stroke rehabilitation is the therapy that helps patients recover from abnormal activity. It depends on the different parts of the brain that have been damaged by the stroke. The ability to walk, speak, build strength, and perform everyday activities are also all domains that could benefit from rehabilitation. Physical activity includes rehabilitation,

- range-of-motion psychotherapy,
- constraint-induced psychotherapy,

- mobility exercises, and
- Fitness levels target muscle strength.

Functional electrical stimulation, robotics, wireless networks, and virtual reality are all examples of recent technologies that may be used to support the physical rehabilitation of stroke patients. Some examples of cognitive and emotional activities that would be included in rehabilitation are therapy for psychological issues, therapy for communication issues, psychological investigation and treatment, and drug therapy. The patients' recovery time will differ from person to person, and it cannot be predicted. Generally, some factors are involved in rehabilitation: physical factors, emotional factors, social factors, and therapeutic factors. The level of recovery is usually the fastest in the weeks and months after a stroke. There is evidence, however, that performance may improve even 12 to 18 months after a stroke.

In neuromuscular treatment, the use of robotics and virtual reality Neurological deficiencies may weaken a person's motor function, which might have a critical effect on their quality of life. In patients who have suffered a stroke, a spinal cord injury, or a traumatic brain injury, researchers investigated the effects of their efforts on attempting to repair the nervous system and lessen the severity of neurological deficits. The Fugl-Meyer Assessment, the Frenchay Arm Test, the Motor Assessment Scale, the Action Research Arm Test, the Box, and Block Test, and the Nine-Hole Peg Test are ancient tests for the neuromuscular disorder subject that show the quality of upper arm movements based on observational investigations. (Gil-Agudo et al. (2011)

Occupational and physical therapy also moved into new areas of life to help stroke patients regain control of their upper bodies. Most stroke patients go through different phases. The seven-phase methodology uses spastic and involuntary muscular activities that can help in rehabilitation. A stroke might leave a patient unable to lift their arm forward or grip and release objects. Stroke survivors may be able to get their arms to work normally again with home exercises, ongoing medical care, and Saebo products. Simbarashe Shahwe, the team lead physiotherapist at Boston Physiotherapy Ltd., recommends exercise for stroke rehabilitation. Shahwe has encouraged stroke patients to concentrate on simple arm exercises to improve strength and reestablish muscle-to-mind connections. Once you begin healing from a stroke, the neurological impairment will affect your quality of life. You can teach the brain to compensate for impairment, but you must use the damaged muscles. Exercises at the fundamental level assist in the rehabilitation of neuromuscular disorders. the movements of the upper arms while performing specific workouts like crawling stretches and weight training at the elbows. The ulnar muscles, axillary nerves, and musculocutaneous nerves are all innervated during every activity. At first, the preliminary trials of these exercises were used to acquire the EMG responses of the chosen muscles in normal subjects between the ages of 20 and 25.

3.1. Exercises

3.1.1 Elbow stretch:

The primary goal of the elbow stretch is to increase the range of motion in the elbow joint. You may do this workout either while seated or while standing (Fig1). Maintain the arm in the position that is most comfortable for you, and then lightly bend and straighten the elbows in the manner that you would while curling a dumbbell. The muscles responsible for the elbow stretch were the biceps and triceps. The biceps muscle is responsible for flexion and supination (backward rotation) of the forearm. The action was innervated by the musculocutaneous nerves C5, C6, and C7. Distal nerve transfer may reinnervate the triceps. The flexor carpi functional fascicle of the ulnar nerve and the posterior axillary nerve are often employed for reinnervation. Both nerves restore triceps function. This reflex mostly evaluates spinal nerve C7. The patient's shoulder and elbow are stretched 90 degrees to evaluate reflexes and the triceps nerve is then tapped proximal to the ulnar nerve.

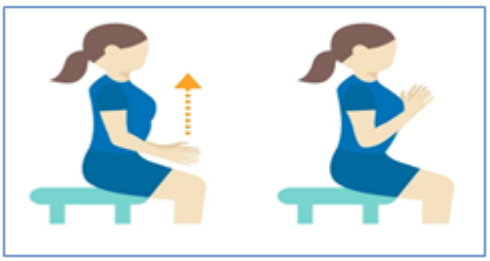

Figure 1. The action of elbow stretch

3.1.2 Elbow weight stretch:

These exercises show that the next level of patients can handle the activities. In a standing or sitting position, hold a small weight in your hand. Gently bend and straighten the elbow (Fig 2). Repeat to your endurance point. Over time, increase repetitions as the elbow strengthens. The biceps and triceps are the muscles that respond to

this exercise. The biceps muscle controls forearm flexion and supination (backward rotation). The action was innervated by the musculocutaneous nerves C5, C6, and C7. Distal nerve transfer may reinnervate the triceps. The flexor carpi functional fascicle of the ulnar nerve and the posterior axillary nerve are often employed for reinnervation. Both nerves restore triceps function. This reflex mostly evaluates spinal nerve C7. The patient's shoulder and elbow are stretched 90 degrees to evaluate reflexes. The triceps nerve is then tapped proximal to the ulnar nerve.

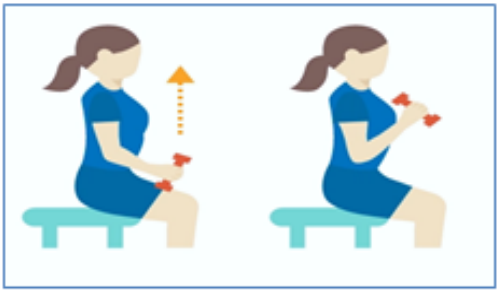

Figure 2. The action of elbow weight stretch

3.1.3 Crawling stretch:

Take up a crawling position with your elbows straight. Gently lean your body backward, keeping your arm position, until you feel a stretch on your inner arm (Fig 3). Hold the position and repeat. Crawling stretches are responsive to the forearm and deltoid muscles. The deltoid muscle is responsible for the innervation of an axillary nerve between C5 and C6. It also provides stability to the shoulder joint.

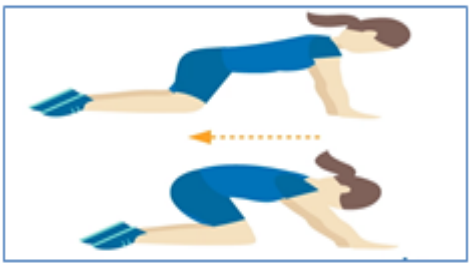

Figure 3. The action of crawling Stretch

4. DATA COLLECTION

Delsys software's wireless EMG sensors were used to collect EMG data (fig 4). These sensors were linked to the WIFI module, and EMG signals were sent to the Delsys base station. Lab Chart third-party software was used to integrate the system**.** Lab Chart is the software to acquire physiological signals and perform analog transduction, signal conditioning, data recording, and validation (fig 5). The study's subjects were drawn from a pool of healthy people. These studies used subjects between the ages of 20 and 24.

The sensors were placed on the belly part of the biceps and triceps muscles using a double-sided adhesive skin interface. Based on the choice of exercises, elbow, crawling, and elbow weight stretch trigger the muscle's activations. For exercises 1 and 2, the first sensor is placed on the belly muscles of the biceps, and the second sensor is placed on the belly muscles of the triceps. Then the subjects can perform the elbow stretch and elbow weight stretch continuously five times. For this exercise 3, sensors 1 and 2 were placed on the left and right sides of the deltoid muscles, respectively. The subject can carry out the exercises a total of five times. The EMG signals were recorded and saved as CSV files for later analysis.

Figure 4. EMG sensors

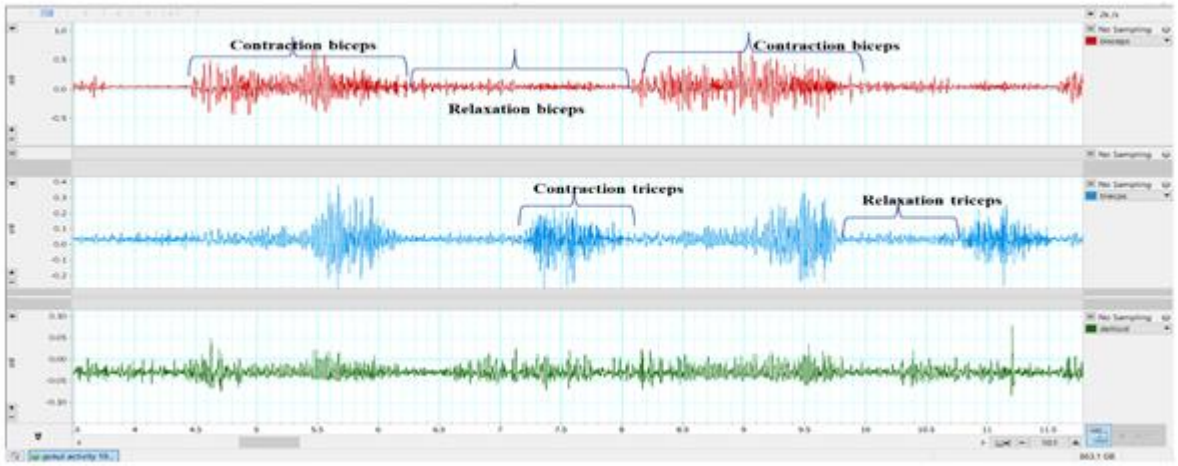

Figure 5. Data acquisition using lab chart software

5. DATA ANALYSIS

The electrical activity of the subject is acquired using EMG sensors. The sensors are connected through the WIFI to the base station and the EMG signal with 48 milliseconds of the time delay accelerometers time delay was 96 milliseconds. The exported data has a sampling rate of 1 m/s, a bandwidth of 10–850 Hz, and an input range of sensors selected between 22 mV and 11 mV. The EMG data are exported then it can be calculated the mean, standard deviation, maximum, and minimum.

The EMG signals were analyzed in terms of average, standard deviation, root mean square, AND t-Test obtained by using the statistical equation as follows:

verage (avg) $(x) \quad = 1/N \sum_{k=0}^{n} xi$

Standard deviation (SD) $(\partial) = \sqrt{\frac{1}{N}\sum_{i=1}^{N}(xi - x)\text{^}2}$

Root means square (RMS)= $\sqrt{\frac{\int_{t1}^{t2}[F(t)]^2 dt}{(t2-t1)}}$

RMS reflects the average EMG signal's power over time. The signal's amplitude is measured operating in a different time, so it's a time domain variable. The standard deviation is calculated as the square root of variance by determining each data point's deviation relative to the mean.

6. RESULT

In this study, EMG signals from ten healthy subjects were collected during various exercises. The movement of particular muscles results in the contraction of the muscles and motor nerves. When the continuous movements of a specific muscle vary from the first time to the final time, it indicates that information from the brain has reached the muscles. EMG signal data are analyzed using the means and standard deviations of the biceps, triceps, and deltoid muscles.

The upper limb movements differ for every subject based on their muscle growth, physiology condition, muscle strength, and muscle fatigue. For the results, EMG signals show increasing muscle contraction while performing the particular exercises. To verify the improvement in muscle strength and the improvement of the proper activations of the nerves by the statical analysis.

Table 1. Comparison of the maximum value of elbow weight stretch exercise

Exercises	**Left elbow weight stretch 1**		**Left elbow weight stretch 5**		**Right elbow weight stretch 1**		**Right elbow weight stretch 5**	
Muscles	Biceps	Triceps	Biceps	Triceps	Biceps	Triceps	Biceps	Triceps

	(mV)	(mV)	(mV)	(mV)	(mV)	(mV)	(mV)	(mV)
Mean	0.0185	0.0425	0.0188	0.04255	0.01761	0.421	0.01856	0.04184
Standard deviation	0.1232	0.01847	0.01809	0.0249	0.3088	0.02795	0.3168	0.02516
Minimum	-0.670	-0.0481	-1.2636	-0.0965	-2.0793	-0.0446	-1.7624	-0.0336
Maximum	0.803	0.1832	1.3801	0.188	1.9525	0.1227	2.7276	0.12821

From Table 1, Subjects performed maximum elbow weight stretch exercises. The table results show that the maximum contraction of the muscles increased from the first to the last count. The left biceps muscle contraction at the initial count was 0.803 mV, then the final count was 1.38 mV. The musculocutaneous nerves C5, C6, and C7 were the ones that innervated these actions. Similarly, the right biceps muscle contraction at the initial count was 1.95 mV, then the final count was 2.72 mV. The musculocutaneous nerves C5, C6, and C7 were the ones that innervated these actions. The mean and standard deviation reflect the overall performance of the exercises, and there is some variation in the values. The mean and SD for the left biceps muscle at the initial count were 0.018±0.12 and 0.042±0.018 for the triceps muscle. The initial count means and SD for the right biceps muscle were 0.018±0.03 and 0.421±0.02 for the triceps muscle, respectively.

Table 2. Comparison of the maximum value of elbow stretch exercise

Exercises	**Left elbow stretch 1**		**Left elbow stretch 5**		**Right elbow stretch 1**		**Right elbow stretch 5**	
Muscles	Biceps (mV)	Triceps (mV)	Biceps (mV)	Triceps (mV)	Biceps (mV)	Triceps (mV)	Biceps (mV)	Triceps (mV)
Mean	0.0193	0.04254	0.01852	0.04266	0.0177	0.04173	0.01789	0.04305
Standard deviation	0.2935	0.04655	0.2634	0.04379	0.4257	0.1598	0.4737	0.1511
Minimum	-1.2519	-0.2718	-1.5836	-0.145	-2.1065	-0.2533	-1.7118	-0.265
Maximum	1.4183	0.21965	1.562	0.2248	2.8318	0.2629	2.4605	0.2505

From Table 2, Subjects performed maximum elbow stretch exercises. The table results show that the maximum contraction of the muscles increased from the first to the last count. The left biceps muscle contraction at the initial count was 1.41 mV, then the final count was 1.56 mV. The musculocutaneous nerves C5, C6, and C7 were the ones that innervated these actions. Similarly, the right biceps muscle contraction at the initial count was 2.86 mV, then the final count was 2.46 mV. The musculocutaneous nerves C5, C6, and C7 were the ones that innervated these actions. The mean and standard deviation reflect the overall performance of the exercises, and there is some variation in the values. The mean and SD for the left biceps muscle at the initial count were 0.019±0.29 and 0.042±0.046 for the triceps muscle. The initial count means and SD for the right biceps muscle were 0.017±0.42 and 0.041±0.15 for the triceps muscle, respectively.

Table 3 Comparison of the maximum value of crawling stretch exercise

	Left crawling stretch		**Right crawling stretch**	
	Deltoid 1 (mV)	**Deltoid 5 (mV)**	**Deltoid 1 (mV)**	**Deltoid 5 (mV)**
Mean	0.179	0.01838	0.04216	0.04198
Standard deviation	0.01829	0.01149	0.0303	0.0237
Minimum	-0.0639	-0.0292	-0.05018	-0.0543
Maximum	0.11034	0.099	0.15743	0.1674

From Table 3, Subjects performed maximum crawling stretch exercises. The table results show that the constant contraction of the muscles was maintained from the first to the last count. The left deltoid muscle

contraction at the initial count was 0.11 mV, then the final count was 0.099 mV. The axillary nerve between C5 and C6 was the one that innervated these actions. Similarly, the right deltoid muscle contraction at the initial count was 0.157 mV, and the final count was 0.16 mV. The axillary nerve between C5 and C6 was the one that innervated these actions. The mean and standard deviation reflect the overall performance of the exercises, and there is some variation in the values. The mean and SD for the left deltoid muscle at the initial count were 0.017±0.018 respectively. The mean and SD for the left deltoid muscle at the final count were 0.018±0.011 respectively. The initial count means and SD for the right deltoid muscle was 0.042±0.03respectively. The final count means and SD for the right deltoid muscle was 0.041±0.023 respectively.

Table 1-3 shows the innervation of the axillary nerves, musculocutaneous nerves, and ulnar nerves by performing the exercises. The daily practice of this exercise will improve muscle strengthening, and regular activation of the nerve also helps recovery from the stroke.

This analysis of all 10 normal subjects and the comparison between subjects show an improvement in the activation of the nerve and muscles. This exercise will aid in post-stroke rehabilitation and the recovery of patients suffering from other neuromuscular disorders. Through this exercise, the affected motor neurons and another sensory nerve also receive the impulse from the brain. Thus, engaging these mechanisms provides a potential strategy to enhance plasticity for stroke recovery.

Table 4. Mean EMG variations across 5 repetitions for left & right elbow weight exercise

	Left elbow weight stretch 1		**Left elbow weight stretch 5**		**Right elbow weight stretch 1**		**Right elbow weight stretch 5**	
subjects	**Biceps (mV)**	**Triceps (mV)**	**Biceps (mV)**	**Triceps (mV)**	**Biceps (mV)**	**Triceps (mV)**	**Biceps (mV)**	**Triceps (mV)**
1	0.0185	0.0425	0.0188	0.04255	0.01761	0.421	0.01856	0.04184
2	0.017	0.04187	0.01729	0.04221	0.0176	0.04197	0.0176	0.0421
3	0.017	0.0419	0.015	0.0418	0.0169	0.099	0.0168	0.0449
4	0.0415	0.033	0.0412	0.0339	0.0416	0.0335	0.411	0.0334
5	0.042	0.0449	0.049	0.0339	0.0165	0.01852	0.0188	0.04254
6	0.024	0.04115	0.026	0.142	0.0174	0.01706	0.01729	0.04151
7	0.0233	0.0419	0.0263	0.052	0.018	0.0171	0.015	0.0419
8	0.0163	0.0335	0.0178	0.0389	0.0177	0.0415	0.0412	0.0335
9	0.036	0.034	0.0366	0.0344	0.023	0.0129	0.049	0.0498
10	0.031	0.034	0.0301	0.0398	0.0175	0.0165	0.026	0.0412
AVG	**0.02666**	**0.03887**	**0.027809**	**0.05014**	**0.02038**	**0.07190**	**0.063125**	**0.04127**

Table 4 shows that the overall action is elbow weight stretch in the normal subjects. The mean values of the biceps and triceps muscles of both hands have developed the muscles and connected the nervous system to the brain. These exercises aid in the neuromuscular disorder patient's rehabilitation.

Table 5. Mean EMG variations across 5 repetitions for left & right elbow exercise

	Left elbow stretch 1		**Left elbow stretch 5**		**Right elbow stretch 1**		**Right elbow stretch 5**	
subjects	**Biceps (mV)**	**Triceps (mV)**	**Biceps (mV)**	**Triceps (mV)**	**Biceps (mV)**	**Triceps (mV)**	**Biceps (mV)**	**Triceps (mV)**
1	0.0193	0.04254	0.01852	0.04266	0.0177	0.04173	0.01789	0.04305
2	0.0171	0.04151	0.01706	0.04157	0.0175	0.0423	0.0175	0.0421
3	0.0174	0.0419	0.0171	0.04177	0.0169	0.0421	0.0168	0.4199
4	0.0412	0.0335	0.0415	0.034	0.0412	0.0334	0.0412	0.033
5	0.0123	0.0498	0.0129	0.0413	0.01852	0.0419	0.0412	0.034
6	0.0162	0.0412	0.0165	0.0442	0.01706	0.033	0.0123	0.0413
7	0.0175	0.0335	0.0174	0.0382	0.0171	0.0449	0.0162	0.0442
8	0.0177	0.0429	0.018	0.0399	0.0415	0.04115	0.0175	0.0382
9	0.0195	0.0447	0.0177	0.0406	0.0129	0.0419	0.0177	0.0399

10	0.0184	0.0312	0.023	0.0333	0.0165	0.0473	0.0188	0.0457
AVG	**0.01966**	**0.04027**	**0.019968**	**0.03975**	**0.021688**	**0.04096**	**0.021709**	**0.07813**

Table 5, from the mean value of the elbow stretch, shows the constant contraction of the biceps and triceps muscles. The initial activity for the post-stroke patient should be a flexible exercise to engage the physiotherapist and interact with the rehabilitation process. These exercise innervation of the musculocutaneous nerves C5, C6, and C7.

Table 6. Mean EMG variations across 5 repetitions for left & right crawling exercise

	Left crawling stretch 1		**Right crawling stretch 5**	
subjects	**Deltoid 1 (mV)**	**Deltoid 5 (mV)**	**Deltoid 1 (mV)**	**Deltoid 5 (mV)**
1	0.0179	0.01838	0.04216	0.04198
2	0.01744	0.0178	0.042058	0.042098
3	0.0173	0.177	0.0418	0.04186
4	0.0789	0.0578	0.10877	0.11705
5	0.0187	0.0182	0.0789	0.0145
6	0.01257	0.0115	0.0187	0.0201
7	0.0177	0.0153	0.0145	0.0123
8	0.07899	0.0823	0.0178	0.0169
9	0.0144	0.0159	0.177	0.0253
10	0.0145	0.01753	0.0578	0.0499
AVG	**0.02884**	**0.043171**	**0.059949**	**0.038199**

According to Table 6, the deltoid muscles on the left hand are the most contracted, while the deltoid muscles on the right hand are less contracted. This causes the body's weight to be balanced on the left hand while making the movements repeatedly. From these mean values, we adopted the T-test to perform paired samples of the elbow weight stretch, elbow stretch, and crawling stretch.

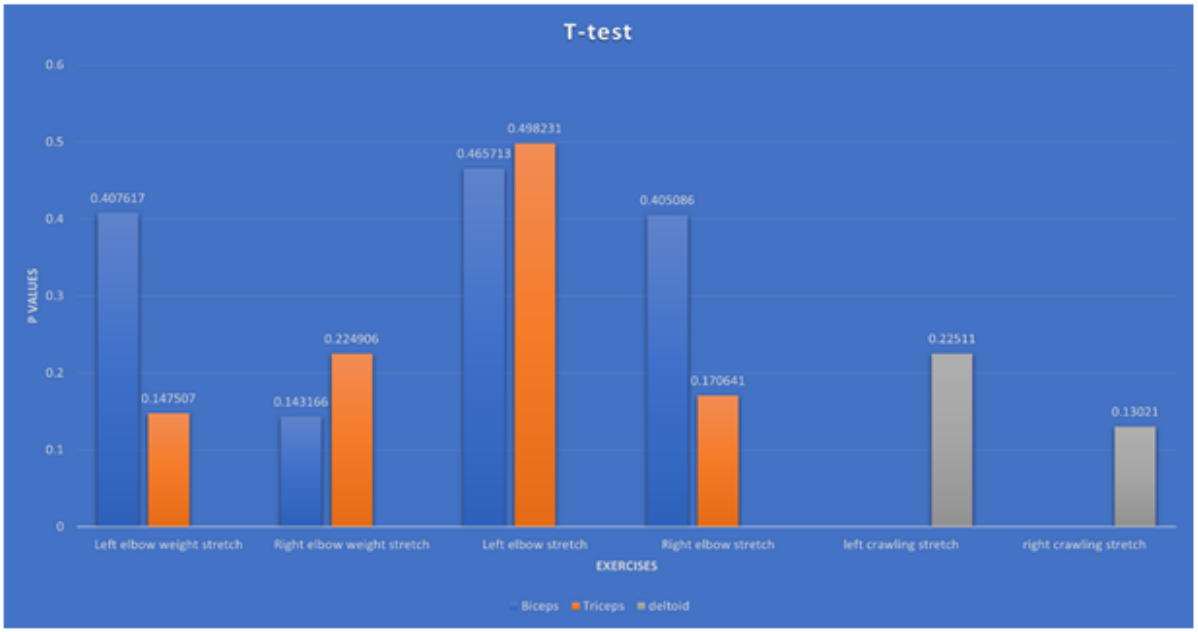

Figure 6. Results showing P>0.05 which inference in EMG difference with exercises.

Figure 6 shows that the p-values for the elbow weight stretch, crawling stretch, and elbow stretch exercises were greater than 0.05. Thus, the contraction of the initial action of the muscles differs from the final contractions. It demonstrates that no significant differences exist.

7. CONCLUSION AND FUTURE WORK

The movement of the upper limb has an impact on the motor performance of post-stoke patients and focuses on motor recovery. In this study, the deltoid muscles, biceps muscles, and triceps muscles pair that can produce the same movements action of exercise. The results show the normal subject's action of the muscles with innervated ulnar nerves, musculocutaneous nerves, and axillary nerves. The mean and standard deviation values show the overall activation of the muscles in repetitive performance of the movements. And T-test was also performed and the p values of the exercises are greater than 0.05 and there is no significant difference.

From this study, the EMG data analysis for 10 normal subjects and confirming the activation of the muscles like the biceps, triceps, and deltoid for elbow stretch, elbow weight, and crawling stretch exercises. These exercises should be practiced by post-stroke patients or neuromuscular patients will help improve their health conditions and feel free from pain. Recent advanced technology like robotics, virtual reality, and argument are immersed with EMG sensors that will help recover neuromuscular disorder patients. This system can be used to reduce the clinical burdens of therapists and extend the treatment into the patient's home, facilitating home-based healthcare. These exercises are done by using VR to do the activity or play the game in a virtual environment for rehabilitation post-stroke patients. It reduces the risk to the patients and expenses associated with training as well as the number of errors.

REFERENCES

[1] V. L. Feigin *et al.*, "Global, regional, and national burden of stroke and its risk factors, 1990–2019: a systematic analysis for the Global Burden of Disease Study 2019," *Lancet Neurol.*, vol. 20, no. 10, pp. 795–820, Oct. 2021, doi: 10.1016/S1474-4422(21)00252-0.

[2] M. Mugnosso, F. Marini, M. Gillardo, P. Morasso, and J. Zenzeri, "A novel method for muscle fatigue assessment during robot-based tracking tasks," in *2017 International Conference on Rehabilitation Robotics (ICORR)*, London, Jul. 2017, pp. 84–89. doi: 10.1109/ICORR.2017.8009226.

[3] A. Akbari and M. Talasaz, "Prediction of Above-elbow Motions in Amputees, based on Electromyographic (EMG) Signals, Using Nonlinear Autoregressive Exogenous (NARX) Model," *Iran. J. Med. Phys.*, vol. 11, no. Issue 2,3, Aug. 2014, doi: 10.22038/ijmp.2014.3095.

[4] F. Chaze *et al.*, "Virtual reality and well-being in older adults: Results from a pilot implementation of virtual reality in long-term care," *J. Rehabil. Assist. Technol. Eng.*, vol. 9, p. 205566832110723, Jan. 2022, doi: 10.1177/20556683211072384.

[5] P. Brazalovich, J. E. Simon, C. R. Criss, J. P. Yom, and D. R. Grooms, "The effects of virtual reality immersion on drop landing mechanics," *Sports Biomech.*, pp. 1–17, Feb. 2022, doi: 10.1080/14763141.2022.2035427.

[6] P. Sweetser and P. Wyeth, "GameFlow: a model for evaluating player enjoyment in games," *Comput. Entertain.*, vol. 3, no. 3, pp. 3–3, Jul. 2005, doi: 10.1145/1077246.1077253.

[7] N. A. Roman, R. S. Miclaus, C. Nicolau, and G. Sechel, "Customized Manual Muscle Testing for Post-Stroke Upper Extremity Assessment," *Brain Sci.*, vol. 12, no. 4, p. 457, Mar. 2022, doi: 10.3390/brainsci12040457.

[8] J. Cui, S.-C. Yeh, and S.-H. Lee, "Wearable Sensors Integrated with Virtual Reality: A Self-Guided Healthcare System Measuring Shoulder Joint Mobility for Frozen Shoulder," *J. Healthc. Eng.*, vol. 2019, pp. 1–6, Apr. 2019, doi: 10.1155/2019/7681237.

[9] M. Roell, H. Mahler, J. Lienhard, D. Gehring, A. Gollhofer, and K. Roecker, "Validation of Wearable Sensors during Team Sport-Specific Movements in Indoor Environments," *Sensors*, vol. 19, no. 16, p. 3458, Aug. 2019, doi: 10.3390/s19163458.

[10] Y. Liu, X. Ji, H. Ryouhei, M. Takahiro, and L. Lou, "Function of shoulder muscles of driver in vehicle steering maneuver," *Sci. China Technol. Sci.*, vol. 55, no. 12, pp. 3445–3454, Dec. 2012, doi: 10.1007/s11431-012-5045-9.

[11] A. Gil-Agudo, A. del, A. de los Reyes-Guzman, A. Bernal-Sahun, and E. Roco, "Applications of Upper Limb Biomechanical Models in Spinal Cord Injury Patients," in *Biomechanics in Applications*, V. Klika, Ed. InTech, 2011. doi: 10.5772/19920.

A Smart Alert System to Ensure Sterile Workspace in a Clinical Laboratory

Vincy Shamley Eben[1], D. Kathirvelu[2*]
[1,2]SRM Institute of Engineering and Technology, Kattankulathur

ABSTRACT

Saliva is a biological fluid and a medium for disease transmission as it contains various combinations of pathogens, antigens, and antibodies that may induce illnesses. Saliva can act as a diagnostic tool and as it is a host defensive agent. Sputum is a thick, transparent mucus produced by the lower respiratory tract that contains pathogens that can induce sickness. Aim: The purpose of this research is to design an alert system and to maintain a sterilized workspace to offer protection for clinical professionals and patients. Methodology: There are 20 subjects involved in this study. They were divided into two groups of 10 with mean age of (33.7±9.26). Group 1(N=15) consists of infected patients, whereas Group 2(N=15) consists of non-infectious people. The samples were gathered by swap test and incorporated into the developed alert system, which is made up of sensors that function on the resistance principle. The sensor measures the humidity level of the sample and amplifies the collected signal. The microcontroller is programmed to generate a buzzer sound to alert the surroundings and additionally, it illuminates infectious places with the LED light so that the place might be sterilized. The Wi-Fi module will display the values in the cloud and store the data in the smartphone. Result: comparatively sputum has less moist content than saliva the resistance value will be less than 400 ohms and it illuminates the red color LED with the buzzer. The resistance value of saliva will be more than 400 and less than 600 ohms and it will blink yellow color LED with the buzzer. The green LED will indicate when there is no moisture content in the fabricated sensor. Conclusion: These results will indicate and identify the hazardous pathogens that cause diseases in the clinical and working environment by using saliva and sputum as samples.

Keywords: Saliva Sputum, Harmful pathogen, Sterile workspace, Contagious diseases

Corresponding Author:
D. Kathirvelu
SRM Institute of Science and Technology, Kattkankulathur
Email: kathir297@gmail.com

1. INTRODUCTION

Saliva is a diagnostic and extracellular fluid that is consistently secreted by the salivary glands of humans, namely the parotid, submandibular, and sublingual glands. These glands provide 90% of total saliva production, with the remaining 10% produced by the other minor salivary glands. Saliva is defined as the total saliva produced by the major and minor glands. Saliva is composed of 98.5% water and 1.5% acquired organic and inorganic components, such as enzymes, protein, mucin, and urea created by the human body. Saliva includes inorganic components such as electrolytes like potassium, calcium, chloride, phosphate, and sulfate (Dave et al., 2021). Saliva has a significant role in healing intraoral diseases caused by a variety of pathogenic bacteria and chemical or enzymatic sensitivities, as well as in improving the body's ability to lubricate and digest(Slots & Slots, n.d.). For diagnosing and prognosing the illness, saliva was utilized to detect diseases such as dental caries, periodontal disease, cancer, and diabetes mellitus. Saliva includes virus-transmitting risk factors such as rabies, the common cold, SARS-COV19, polio, and HIV (Human Immunodeficiency Virus). It is non-invasive and painless, and it can be used instead of a blood serum or urine test for diagnosis. (Zhang et al., 2016). A disease like covid-19 is an airborne illness, and it is transmitted by saliva aerosols or droplets generated from the infected human's respiratory system while sneezing, coughing, or speaking. Whether it is a huge or little droplet, it will be polluted or include one or two germs that will transfer the illnesses. (Reyes et al., 2021). as well as Sputum is a thick, transparent mucus that contains some saliva and is infected with bacteria and viruses. The colors can be used to analyze the sputum with the naked eye. Sputum is a Bronchoalveolar Lavage Fluid (BALF) and epithelium lining fluid, and it is a better sample to diagnose infections than nasal swabs. It is often referred to as a respiratory viral agent(Humes et al., 2022). Sputum contains infection-causing microorganisms and is utilized to identify pathogens and suspect antibacterial activity(Shrestha & Rajbhandari, 2018). Microbiological pathogens in the sputum samples may induce airborne infections via aerosols and saliva

droplets. Pathogens like Rhinovirus and streptococcus cause the common cold and asthma and cause a wide range of human illnesses, from minor skin problems and throat disorders (mononucleosis or strep throat) to serious invasive infections, rheumatic fever, and scarlet fever(Iorgulescu, n.d.). Many articles published in the last 10 years have suggested that saliva and sputum are the key ways to transmit viral and bacterial diseases. Human viral infections can spread in a variety of ways. Aerosols and saliva particles are produced while sneezing or coughing vigorously(Corstjens et al., 2015). The common cold and influenza are both viral infections that can affect humans but are seldom harmful. They are spread by an airborne sickness for which there is no vaccination, and numerous bacteria in the oral cavity cause a variety of human diseases. The bacterium streptococcus causes a mild illness that affects the skin and throat. It is also one of the most common illnesses discovered in saliva. Streptococcus pyogenes, the organism that causes strep throat, is found in 10% of adults and 25% of children. Both saliva and sputum are acidic in nature, which can lead to several oral health problems; These samples also contain a wide range of biological and analytical basic information.(Strazdins et al., 2005) as well as physical and chemical characteristics to determine the ph. level (Kubala et al., 2018). Several studies have proved that oral fluids like saliva and sputum were used to diagnose viral and bacterial infections but could not distinguish the differences between the infections and corstijen et al designed a point-of-care device to get an immediate result that is compared with a laboratory test. The saliva-based test will target the actual analyte testing for the antibody to specify the pathogens(Corstjens et al., 2015). The identification of hazardous infections utilizing oral secretions will be accurate, and the presence of microorganisms will be easy to identify. Initially, the sensors will use the potentiometric approach to detect the moisture content in the surroundings. (Rumenjak et al., 1996; Urbanowicz et al., 2019). So, the aim of the current research is to design a smart alert system to ensure a sterile workspace in a clinical environment using saliva and sputum as a specimen.

2. MATERIALS AND METHODOLOGY

2.1. Population study

The study population consists of 30 subjects within the age group of 20 to 45 years. They were separated into 2 groups and each consisting of 15. Whereas subjects in group A is an infected subject and group B consists of non-infectious persons. Infectious subjects have generalized respiratory problems, common colds, strep throat, etc(Baliga et al., 2013).

2.2. Sample collection

Saliva is a diagnostic oral fluid that is simple to collect, non-invasive, and economical to diagnose viral infections quickly utilizing the point of care equipment**.** The international medical organization WHO protocol was followed for collecting the saliva and sputum samples. The individuals should refrain from consuming any form of food or beverages before taking the sample, which should be taken in the early morning following an overnight fast. The first instruction given to the individuals was to rinse their mouths with water without swallowing. Then they were instructed to spit out their saliva and sputum after a 5-minute mouth rinse. Conversely, instruct the person to lower their head and allow their saliva naturally flow. The participants were instructed to take a deep breath before coughing and to collect their sputum (Baliga et al., 2013; LAM Corstjens et al., 2012).

2.3. Methodology

For the purpose of this endeavor, various subjects were selected. samples were gathered from people in assorted age categories. This study implements both infectious and non-infectious individuals. Laying the samples of sputum and saliva on sensors. The sensor is nickel-coated and works on the resistivity principle. Furthermore, it calculates the moisture content of the samples using the analog output and displays the results digitally. It measures the resistance value based on the quantity of samples collected by the sensor. The resistance value measured is inversely proportional to the sample content. The higher the moisture level in the sensor, the better the resistivity, resulting in a low resistance value. The lower the moisture content in the sensor, the lower the resistivity, resulting in a high resistance value. The operational amplifier receives the signal from the acquired signal. It makes the weak signal stronger. The amplified signal will be received by the microcontroller Arduino, which will then be programmed to produce a buzzer sound to alert the patients and the physicians. LED lighting provides an additional technique of alerting. If there is no moisture content in the sensor, there will not be a signal, and the green LED light will remain on. When the subject's saliva droplets or aerosols are detected in the air or on the job site and the resistance value is greater than 400 but less than 600, the sensor will sound an alarm and flip on a yellow LED light. If the infected subject's sputum has just spread there and the resistance value is less than 400, the sensor will additionally sound an alarm and flash a red LED light to alert you. As a result of being a combination of pathogens and analytes, the sputum will have a low moisture content. And the foundation of the ideals is resistance. If we notice any alerts or detect any yellow or red lights flickering. The infected region must be sterilized. The MCU ESP 8266 WIFI module node will retain the

information and display the values in the cloud, separately. The overall working methodology of the proposed system is outlined in **Fig.1.**

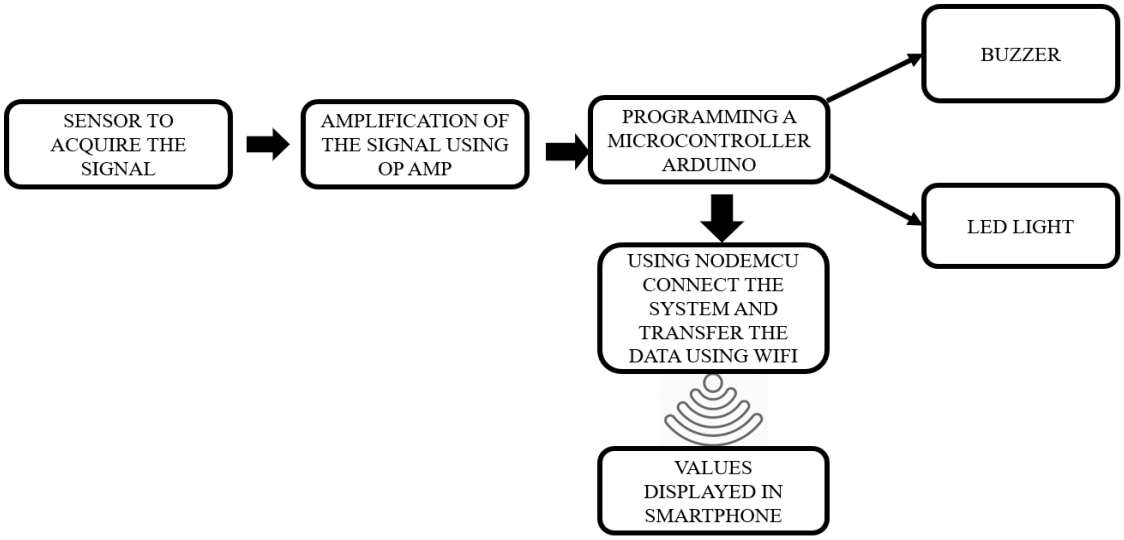

Figure 1. Block diagram of the proposed system

2.4. Statistical analysis

The acquired data were analyzed and classified based on total population studies, with the total population categorized into two groups: infectious and non-infectious. Group A includes the whole population (n=30, age = 33.79.26, overall moisture content of sputum =333.06± 33.17, and saliva moisture content =171.4 ±56.23). The T-test was used to compare infectious and non-infectious samples (age, sputum, saliva). The statistical performance of saliva for the sensitivity confidence interval (CI) (38.38% to 88.18%) and sputum (CI) (32.9% to 83.66%) and specificity value for both sputum and saliva is 93.33%.

A receiver operating characteristic (ROC) study has been conducted to establish the outcome of the designed alert system and if it produces acceptable and precise data.

2.5. Performance assessment: -

It is critical to evaluate the degree of sensitivity, specificity, precision, and accuracy of the developed alert system outputs. True positive (TP) means an accurate test result for a sick subject, false positive (FP) implies a positive diagnosis for a non-infected individual, true negative (DN) represents an inaccurate response for a non-infected person, and false negative (FN) denotes a negative response for an infected person. Specificity represents the correct forecast of the circumstances, whereas sensitivity indicates the actual prediction of the typical study population. The accuracy of the warning system relates to how effectively it forecasts the true status of the samples.

3. RESULT

The resistance value is determined by measuring the moisture content in samples such as saliva and sputum, which is integrated into the specified alarm system (ohm). This project's outcome includes 30 subjects. Sputum has a mean average and standard deviation of (333.06± 33.17), whereas saliva has a mean and standard deviation of (171.4 ±56.23). The general population's characteristics are recorded in (Table-1).

Table 1. Characteristics of the total population

Characteristics	**Mean ± Standard deviation**
Age (years)	33.7 ± 9.26
Sputum (moisture content) (Ω)	333.06 ± 33.17
Saliva (moisture content) (Ω)	171.4 ± 56.23

Table 2 illustrates the T-Test values for normal and infected samples. For normal participants, the sputum includes (356.5 ±22.6) and for people with the disease, the t -value is (0.00). Normal and sick participants' saliva moist content is (532.2± 47.5), (456.6 ±35.074) t value (0.00).

Table 2. T-Test between the normal and diseased subjects

Characteristics	**Normal**	**Diseased**	**T-Value**
Age(years)	34.1±10.3	33.2±8.43	< 0.80
Sputum (moist content) (Ω)	356.5±22.6	309.6±24.1	< 0.00
Saliva (moist content) (Ω)	532.2±47.5	456.6±35.074	< 0.00

The receiver operational analysis (ROC) provides the true positive, false negative, false positive, and true negative results. We define a threshold value for both sputum (320) and saliva (470), and we determine the true positive and false positive rates for both. **Table 5** outlines the ROC analysis.

Table 5 ROC analysis

Total number of population (N=30)

Characteristics	**Sputum values**	**Saliva values**
True- positive	9	10
False-negative	6	5
True positive rate	0.6	0.66
False-positive	1	1
True-negative	14	14
False positive rate	0.06	0.06

The performance statistics of the collected sputum samples the sample's true prediction of diseases is (60.00%), and the confidence interval value is 95%; the specificity evaluates the true prediction of diseases in normal persons (93.33%). The positive predictive value is 90.00%, whereas the negative predictive value is 70.00%. The accuracy for illness prediction utilizing the designed alert system is (76.67%), and the sensitivity rate (66.67%) specificity rate is (93.33%) for saliva. **Table 3** summarises the sputum performance statistics.

Table 3. Performance characteristics of sputum

Statistics	**Value**	**95% CI**
Sensitivity	60.00%	32.29% to 83.66%
Specificity	93.33%	68.05% to 99.83%
Positive likelihood ratio	9.00	1.30 to 62.51
Negative likelihood ratio	0.43	0.23 to 0.81
Diseases prevalence	50.00%	31.30% to 68.70%
Positive predictive value	90.00%	56.44% to 98.43%
Negative predictive value	70.00%	55.30% to 81.48%
Accuracy	76.67%	57.72% to 90.07%

According to Table 3, the designed alert system predicts the outcome of the collected sputum samples based on the tabulated values. The disease prevalence is speculated to be 50.00%. The precise positive likelihood ratio is 9.00, with a negative likelihood ratio of 0.43%. The performance statistics value of saliva samples for disease prediction or sensitivity rate is (66.67%). The specificity percentage is (93.33%). The method's positive predictive value is (90.91%), its negative predictive value is (73.68%), and its accuracy for disease prediction is (80.0%). The condition prevalence rate is 50.00%, with a positive likelihood ratio of 10.00 and a negative likelihood ratio of 0.36. The saliva value is summarized in **Table 4**

Table 4. Performance characteristics of saliva

Statistics	**Value**	**95% CI**
Sensitivity	66.67%	38.38% to 88.18%
Specificity	93.33%	68.05% to 99.83%

Positive likelihood ratio	10.00	1.46 to 68.69
Negative likelihood ratio	0.36	0.17 to 0.74
Diseases prevalence	50.00%	31.30% to 68.70%
Positive predictive value	90.91%	59.28% to 98.57%
Negative predictive value	73.68%	57.48% to 85.30%
Accuracy	80.00%	61.43% to 92.29%

4. LIMITATIONS

Though this work appears easier, this has some limitations which must be overcome. Collection of the infectious sample may lead to contagious disease spread to a normal subject. While collecting the samples we wanted to follow all the safety measures.

5. CONCLUSION

We are developing a smart alert system to find hazardous microorganisms that cause diseases in the clinical and working environment by using saliva and sputum as samples. The device will notify you and provide a response via LED lights, as well as display the resistance value in the IoT technology and record the data for later use. According to the statistical analysis, the designed alert system will give us accurate and precise values between the normal and diseased subjects Future work can be centered on developing a sensor that directly recognizes infections, and we can focus on developing a sensor module that is used to identify the different types or the specified diseases causing pathogens. Using other body fluids, we can identify the pathogens. The variation between the saliva and sputum can be analyzed.

REFERENCES

[1] Dave, P. K., Rojas-Cessa, R., Dong, Z., & Umpaichitra, V. (2021). Survey of saliva components and virus sensors for prevention of COVID-19 and infectious diseases. In *Biosensors* (Vol. 11, Issue 1. MDPI.
[2] Slots, J., & Slots, H. (n.d.). *Bacterial and viral pathogens in saliva: disease relationship and infectious risk*.
[3] Zhang, C. Z., Cheng, X. Q., Li, J. Y., Zhang, P., Yi, P., Xu, X., & Zhou, X. D. (2016). Saliva in the diagnosis of diseases. In *International Journal of Oral Science* (Vol. 8, Issue 3, pp. 133–137). Sichuan University Press.
[4] Reyes, J., Fontes, D., Bazzi, A., Otero, M., Ahmed, K., & Kinzel, M. (2021). Effect of saliva fluid properties on pathogen transmissibility. *Scientific Reports*, *11*(1).
[5] Humes, S. T., Iovine, N., Prins, C., Garrett, T. J., Lednicky, J. A., Coker, E. S., & Sabo-Attwood, T. (2022). Association between lipid profiles and viral respiratory infections in human sputum samples. *Respiratory Research*, *23*(1).
[6] Shrestha, D., & Rajbhandari, P. (2018). Prevalence and associated risk factors of tooth wear. *Journal of the Nepal Medical Association*, *56*(212), 719–723.
[7] Iorgulescu, G. (n.d.). Saliva between normal and pathological. Important factors in determining systemic and oral health. In *Journal of Medicine and Life* (Vol. 2, Issue 3).
[8] Corstjens, P. L. A. M., Abrams, W. R., & Malamud, D. (2015). *Saliva and viral infections*. www.CDC.
[9] Strazdins, L., Meyerkort, S., Brent, V., D'Souza, R. M., Broom, D. H., & Kyd, J. M. (2005). Impact of saliva collection methods on sIgA and cortisol assays and acceptability to participants. *Journal of Immunological Methods*, *307*(1–2), 167–171.
[10] Kubala, E., Strzelecka, P., Grzegocka, M., Lietz-Kijak, D., Gronwald, H., Skomro, P., & Kijak, E. (2018). A Review of Selected Studies That Determine the Physical and Chemical Properties of Saliva in the Field of Dental Treatment. In *BioMed Research International* (Vol. 2018).
[11] Corstjens, P. L. A. M., Abrams, W. R., & Malamud, D. (2015). *Saliva and viral infections*.
[12] Rumenjak, Vlatko, et al. "Determination of Electrolyte Concentration in Saliva by Potentiometrie Method." *Acta stomatologica Croatica: International journal of oral sciences and dental medicine* 30.3 (1996)
[13] Urbanowicz, Marcin, et al. "A miniaturized solid-contact potentiometric multisensor platform for determination of ionic profiles in human saliva." *Journal of Solid State Electrochemistry* 23 (2019)
[14] Baliga, S., Muglikar, S., & Kale, R. (2013). Salivary pH: A diagnostic biomarker. *Journal of Indian Society of Periodontology*, *17*(4), 461–465.
[15] LAM Corstjens, P., professor, A., & Malamud, D. (2012). *Detecting viruses by using salivary diagnostics*.

Design of NonInvasive Multimodal Glucose Monitoring System Through Sweat and Infrared Light

Pooja B[1], Bhargavi Haripriya A[2], Anitha G[3]
[1,2,3]SRM Institute of Science and Technology, Kattkakulathur

ABSTRACT

Diabetes mellitus is a condition where there is an abnormality in the blood glucose and insulin level that leads to irregularities in the metabolism of the body. Determining blood glucose level is crucial as it plays a leading role in the origin of energy for cells to survive and perform regular tasks. This work is about noninvasive method of blood glucose level identification using different parameters namely sweat and infra-red radiation. Sweat analysis is done using the conductivity method. It is observed for diabetes patients, the presence of salt in the sweat is higher than the normal patients. A comparison study was done between the two non-invasive methods and an invasive methods. From this study, it is noted that the value of sweat was accurate when compared to the optical method of measuring blood sugar levels. The approach using sweat and infrared method for measuring blood glucose is effective and painless and the device is low-cost and easy to use.

Keywords: Diabetes, Blood glucose, Non invasive, Sweat, Infrared

Corresponding Author:
Bhargavi Haripriya A,
SRM Institute of Science and Technology, Kattkankulathur
Email:bhargava@srmist.edu.in

1. INTRODUCTION

According to recent studies, diabetes has been raising to a sharp extent due to unhealthy lifestyle and food changes that leads to obesity, hypertension, diabetes, and other complications. It is most prevalent in southern regions and comparatively low in northern regions.[1]. The person who was affected by diabetes has to take the blood glucose value from the blood. This method leads to pain while pricking the fingers so in order to find the easiest way to know blood glucose level, two different methods were chosen, and from that, the most appropriate value of blood glucose is taken. The principle behind measuring glucose using infrared (IR) in the 700 to 1600 nanometer wavelength range. It is based on the absorption of light in the interstitial fluids light is passed through the finger. Blood glucose levels are estimated by detecting the variations in the light intensity caused by the absorption or scattering of glucose molecules to NIR light, which depends on the concentration of the glucose in the tissue(Yadav et al. 2015) [2] and the principle behind the sweat is divided into two types Optical sensing and electro sensing methods. The optical sensing method consists of three types Fluorescent, Colorimetric, and luminescence (Yu and Sun 2020)[3]. This apparatus used the conductivity measurement technique using copper electrodes. Sweat contains ions, which lead to the conduction between the copper electrodes, and this conductivity is converted into voltage value using a voltage divider rule. The normal person will have a conductivity range of 400 to 600 conductivity/second. But the diabetes person will have a conductivity range of above 900 conductivity/second. In infrared radiation, light is passed into the fingertip and it reaches the interstitial fluids and reflects the light and converts it into an electrical signal. This change will happen every 10 seconds. So, a normal person will have a glucose level of below 20 and a diabetes person will have in a range above 60.

2. MATERIALS

The prototype designed uses two sensors and the output is displayed in the IOT software in the Adafruit website.

Below is the detailed description of the hardware components and software used.

2.1. Sweat sensor

The sensor module has a progression of equal presented follows to quantify drops volume to decide the water level, Easy to screen the water level as the yield to simple sign and corresponding to the water level. Simple, ADC, and can be associated with Arduino information pins

2.2. IR sensor

To use a 5mm wide, imported groove optical coupling sensor. It has a light that displays the output level; if the level is too high, the lights are off. If the output is low, it is on. It will output at a high level if it is covered; otherwise, it will output at a low level. With a good waveform and signal, this could operate more than 15 mA. It uses LM393 as a voltage comparator.

2.3. Microcontroller (Arduino Nano)

Based on the ATmega328, the Arduino Nano is a compact, comprehensive, and module is a self-device (Arduino Nano 3.x). It arrives in a different package both as approximately the same features as the other Arduino connector boards. It requires a Mini-B USB cable instead of a standard one to work.

2.4. Wi-Fi module (Node MCU)

The Node MCU Dev Kit/Board integrates the wirelessly ESP8266 chip. The ESP8266Wi-Fi chip with Esp8266 Systems is economical and operates using TCP/IP protocol. To learn more about the ESP8266, use the Wi-Fi Module. There is a Node MCU Development Board v1.0 (Version2), which is offered for the Node MCU Dev Kit.

2.5. Display Unit

The control that the LCD displays that work with the Hitachi HD44780 driver using the Liquid Crystal library. There are numerous of them, and the 16-pin interface is the commonly used.

2.6. Adafruit Website

Ada fruit IO is a platform created to view, respond to, and interact with the data from the project and also protect our data and secure it as private data feeds are private by default.

Figure 1 shows the prototype constructed, with the detailed naming of all the components.

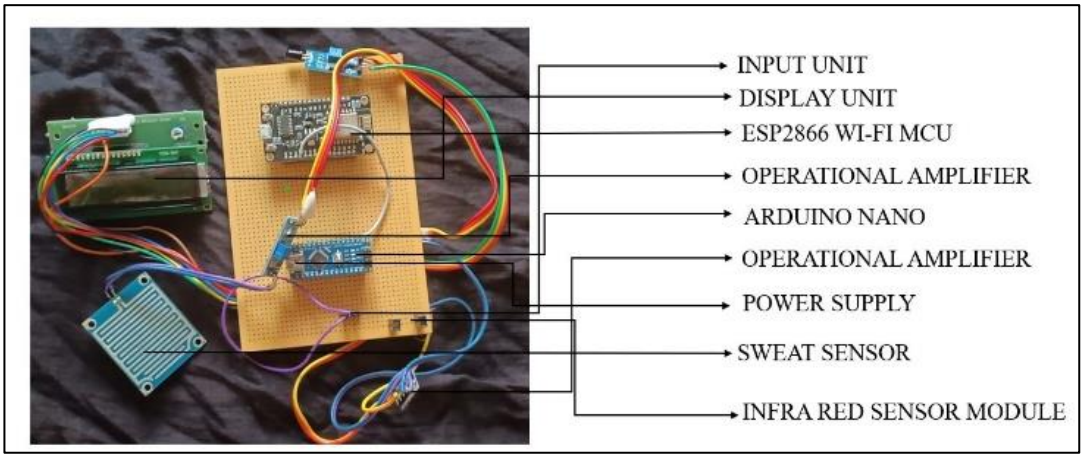

Figure 1. Prototype of non-invasive multimodal glucose monitoring system

3. METHODOLOGY

Various subjects were chosen from different age groups. From the subjects, history of blood glucose level was collected. Two different approaches to measuring blood glucose were chosen: one is using sweat and another is using infrared.

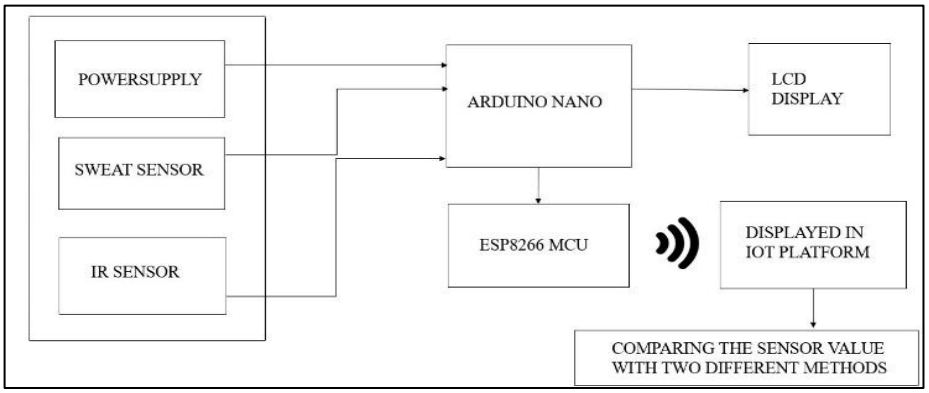

Figure 2. Block Diagram of prototype

For the sweat method, the subjects were asked to perform some activity from that the sample were collected from the patient using a stirrer and sweat is placed on the sensor. For Infrared reading, the subjects were asked to keep their fingers in between the sensors, before that the fingers should be clean and dry. From this, the data was collected and processed in Arduino nano, from one side these values were displayed in LCD display. Data was also transmitted to the ESP8266 Wi-Fi module and the data is received in the IOT platform, from where the value is displayed on a smartphone.

Block diagram of the prototype is shown in Figure 2. Figure 3 shows the methodology of the working of the device.

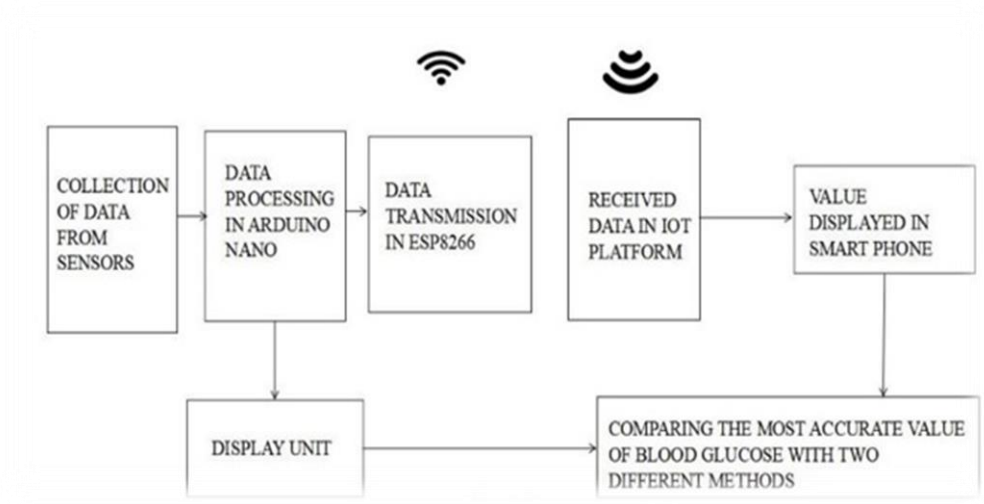

Figure 3. Methodology

4. RESULTS

The non-invasive blood glucose measurement was taken for normal, abnormal and for sports persons. The data were collected from various subjects from various age group and analyzed their health condition and working environment and the values were displayed in IOT platform**.**

The subject results are shown under four groups, namely, normal, abnormal, sports and gestational.

4.1. For Normal Subjects

Table 1. Sweat and Infra-red values for normal subjects

Subject	Sweat Value	Infrared Value	Age	Sex	Indication	Health Condition	Occupation
Subject 1	440	10	51	M	Normal	Nil	Aavin
Subject 2	413	15	25	M	Normal	Nil	Student
Subject 3	423	13	48	F	Normal	Thyroid, Blood pressure	Home Maker
Subject 4	548	10	22	F	Normal	Nil	Student
Subject 5	537	11	21	F	Normal	Nil	Student
Subject 6	438	12	22	F	Normal	Nil	Student
Subject 7	481	15	23	F	Normal	Nil	Student
Subject 8	460	9	22	F	Normal	Nil	Student
Subject 9	487	11	22	F	Normal	Nil	Student
Subject 10	509	13	67	M	Normal	Nil	Business
Subject 11	446	9	62	F	Normal	Nil	Home maker
Subject 12	455	13	27	F	Normal	Nil	Student

From table 1 Twelve subjects were chosen from the age 20 to 70, 9 females and 3 males were chosen and they belong to occupation such as House wife, Student, Business and working person. Overall, their blood glucose was normal with no history of diabetes except one but the blood glucose level was normal in both the methods.

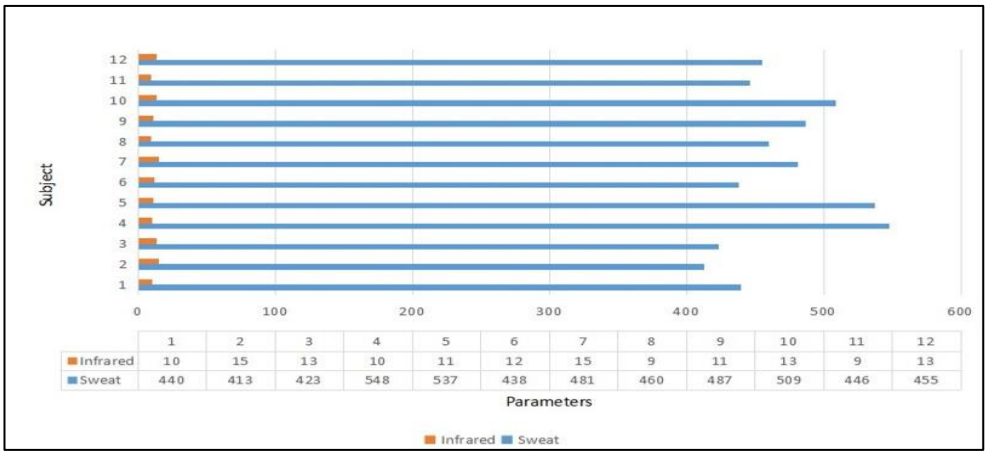

Figure 3. Graphical representation of subjects with normal blood glucose level

4.2. For Abnormal Subjects

Table 2. Sweat and Infra-red values for Abnormal subjects

Subject	Sweat Value	Infrared Value	Age	Sex	Indication	Health Condition	Occupation
Subject ab 1	973	61	65	F	High Sugar	Blood Sugar	House wife
Subject ab 2	977	70	72	F	High Sugar	Blood Sugar	House wife
Subject ab 3	963	68	68	F	High Sugar	Blood Sugar	House wife
Subject ab 4	932	60	60	F	High Sugar	Blood Sugar	House wife
Subject ab 5	915	63	63	F	High Sugar	Blood Sugar	House wife

Subject ab 6	903	67	67	F	High Sugar	Blood Sugar	House wife

From table 2, Six subjects were chosen from the age 60 to 80, 6 females were chosen and they belong to occupation (House wife). Overall, their blood glucose was abnormal with history of diabetes.

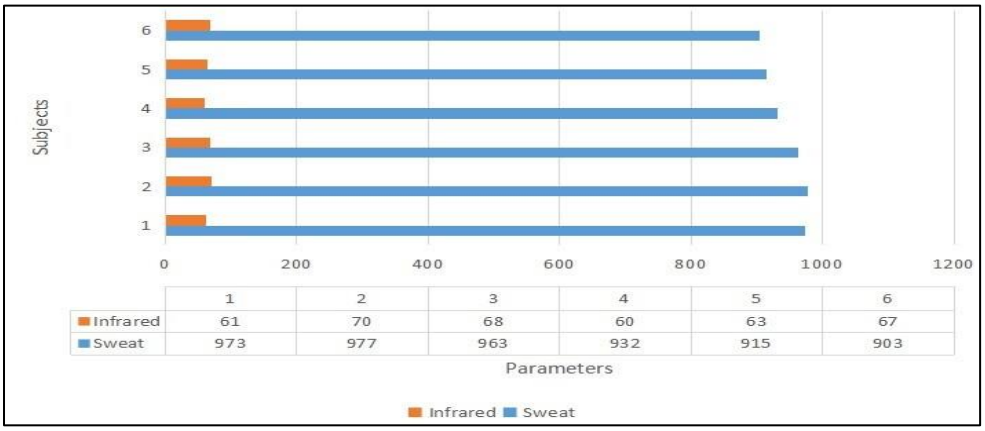

Figure 4. Graphical representation of subjects with Abnormal blood glucose level

4.3. For Sports Subject

Table 3. Sweat and infrared values for Sports subjects

Subject	Sweat value	Infra-red value	Age	Sex	Indication	Health Condition	Occupation
Subject 1	682	20	21	F	Normal	Nil	Student
Subject 2	791	23	20	F	Normal	Nil	Student
Subject 3	761	22	23	F	Normal	Nil	Student
Subject 4	792	18	19	M	Normal	Nil	Student
Subject 5	638	25	22	M	Normal	Nil	Student
Subject 6	649	21	22	M	Normal	Nil	Student
Subject 7	773	19	21	M	Normal	Nil	Student
Subject 8	813	26	19	M	Normal	Nil	Student
Subject 9	615	24	20	M	Normal	Nil	Student
Subject 10	708	23	20	F	Normal	Nil	Student

From table 3, ten subjects were chosen from age 20 to 30, 6 males and 4 females were chosen and they belong to occupation(student). Overall, their blood glucose level was normal and their health condition also in normal range.

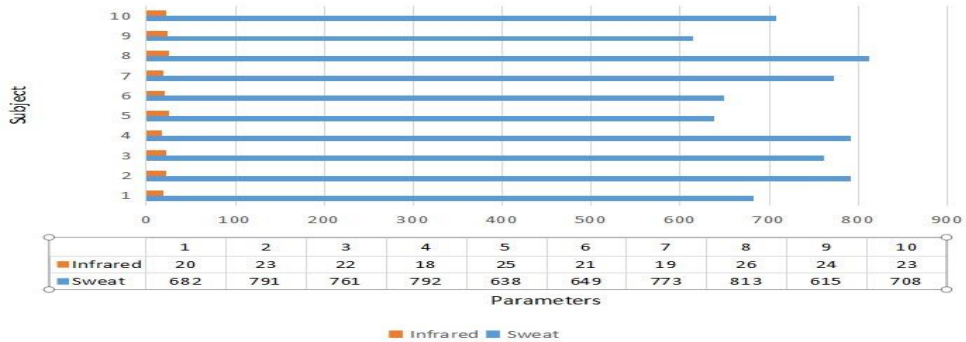

Figure 5. Graphical representation of subjects with gestation period

Table 4. Sweat and infrared values for Gestation subjects

Subject	Sweat value	Infrared value	Age	Sex	Indication	Health Condition	Occupation
Subject 1	520	10	26	F	Normal	Nil	House wife

From table 4, one subject was chosen from age 25 to 30, and they belong to occupation (House wife). Overall, there the blood glucose level for that subject is normal with proper health condition.

4.4. Values Displayed in IOT Platform

From the microcontroller, the data will be transmitted via ESP8266 Wi-Fi module and the data is received and displayed in the IOT website platform.

Figure 6. Sweat value of a normal subject in IOT platform

Figure 7. Infrared value of a gestation subject in IOT Platform

Figure 6 and 7 represents the output of the protype which is displayed in the IOT platform for sweat the value is 537 conductivity/sec which is in the range from (400-600), and for Infra-red the value is 10 nanometers from the range of (10-15).

Figure 8. shows a cumulative display of all the groups sweat and infra-red

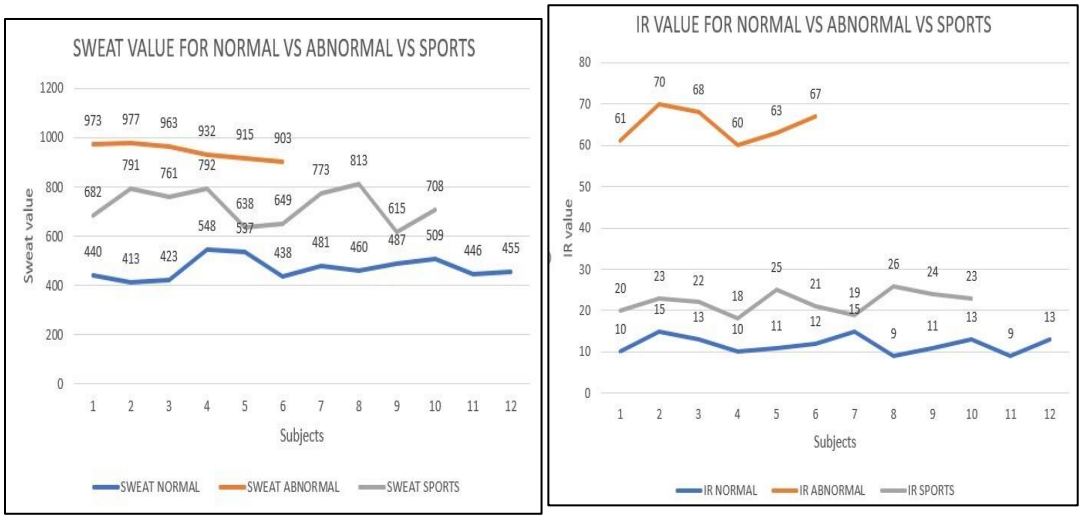

Figure 8. Comparison between a) sweat and b) IR method for blood glucose

5. DISCUSSION

From this different type of subjects were chosen based on various age groups and occupation and evaluation of blood glucose level was concluded. The approach of sweat method was effective when compared to light method. The accuracy of sweat was high due to salt conduction in the body. The accuracy in light method was comparatively low due to external light sources.

6. CONCLUSION

In this project, a model for measuring non-invasive measurement of blood glucose parameters using sweat and blood oxygen content has been designed. Based on the results it can be concluded that, the known diabetic person has an average value of Sweat 943.83conductivity/sec, IR-64.83 nanometers, and for normal Sweat 469.75 conductivity/sec, IR 11.75 nanometers, and for sports Sweat-722.2conductivity/sec, IR-22.1 nanometers in this particular range of sweat (800-1000) and IR (60-80) for known diabetes, for normal Sweat (400-600), IR (10-15) and for sports, Sweat (600-800) and IR (15-25). Values displayed in LCD were changing constantly due to environmental factors, therefore usage of the IoT platform was much constant while displaying the accurate data value and it is easy to use. Overall, from the two non-invasive methods both the values were high for the diabetic persons so this method is easy to identify whether they have high or low blood sugar levels. The data has been collected only for a limited number of persons, In the future, this can be improved by collecting numerous data.

The collection of samples for sweat was difficult from person to person and also varies due to environmental conditions. For measuring Infrared, the device should be kept in dark place to get appropriate values. The excessive salt content in sweat can also predict high glucose value.

REFERENCES

[1] https://www.indiascienceandtechnology.gov.in/featured-science/exploring-diabetes-epidemic-india-Exploring Diabetes epidemic in India
[2] Yadav J, Rani A, Singh V, Murari BM. Prospects and limitations of non-invasive blood glucose monitoring using near-infrared spectroscopy. Biomedical signal processing and control. 2015 Apr 1; 18:214-27.
[3] Yu H, Sun J. Sweat detection theory and fluid driven methods: A review. Nanotechnology and Precision Engineering. 2020 Sep 27;3(3):126-40.
[4] Nivetha K, Ramya N, Thendral R, Gopikrishnan A. Blood glucose measurement by sweat using Arduino. BLOOD. 2018 Jul;4(2).
[5] Kirk JK, Stegner J. Self-monitoring of blood glucose: practical aspects. Journal of diabetes science and technology. 2010 Mar;4(2):435-9.
[6] Phetsang S, Kidkhunthod P, Chanlek N, Jakmunee J, Mungkornasawakul P, Ounnunkad K. Copper/reduced graphene oxide film modified electrode for non-enzymatic glucose sensing application. Scientific reports. 2021 Apr 29;11(1):1-3.
[7] Zafar H, Channa A, Jeoti V, Stojanović GM. Comprehensive review on wearable sweat-glucose sensors for continuous glucose monitoring. Sensors. 2022 Jan 14;22(2):638.
[8] Dhiman TK, Poddar M, Lakshmi GB, Kumar R, Solanki PR. Non-enzymatic and rapid detection of glucose on PVA-CuO thin film using ARDUINO UNO based capacitance measurement unit. Biomedical Microdevices. 2021 Sep;23(3):1-1.
[9] Thevenot DR, Toth K, Durst RA, Wilson GS. Electrochemical biosensors: Recommended definitions and classification. Biosens. Bioelectron. 2001; **16:121**–131.
[10] Bruen D, Delaney C, Florea L, Diamond D. Glucose sensing for diabetes monitoring: Recent developments. Sensors 2017;**17**(8):1866. https://doi.org/10.3390/s17081866.
[11] Xuan X, Yoon HS, Park JY. A wearable electrochemical glucose sensor based on simple and low-cost fabrication supported micro-patterned reduced graphene oxide nanocomposite electrode on flexible substrate. Biosens. Bioelectron. 2018; **109:75**–82. https://doi.org/10.1016/j.bios.2018.02.054
[12] Zhuang JC, Jiang XH, Wang JJ et al. Stretchable electrode composed of carbon nanotube-SBS hybrid film and its application on biosensor. J. Electrochem. Soc. 2017;**164**(14):H1028–H1032. https://doi.org/10.1149/2.0741714jes
[13] Tomasz Kossowski, Rsyzard Stasinski "IR attenuation measurement for non-invasive glucose level analysis", 23rd International conference on Signals, systems and Image processing, 2016.
[14] Komal Lawand, Mahesh Parihar, Shital N. Patil, "Design and Development of Infrared LED Based Non Invasive Blood Glucometer",IEEE INDICON 2015
[15] Sibylle Fallet, Leila Mirmohamadsadeghi, Virginie Moser,Fabian Braun,Jean-Marc Vesin, "Real-time approaches for heart rate monitoring using image photoplethysmography", Computing and Cardiology Conference,2016.

Medical Assist Robot for Isolated Ward Patient in Hospitals

K. Prakash[1], K. Santhiya Devi[2], K. Tamilarasi[3], R. Yogalakshmi[4]
[1]Assistant Professor, BME Department, Kings Engineering College, Irungattukottai, Chennai, India
[2,3,4]IV Year, BME Department, Kings Engineering College, Irungattukottai, Chennai, India

ABSTRACT

Robots in medicine help by relieving medical personnel from routine tasks that take their time away from more pressing responsibilities, and by making medical procedures safer and less costly for patients. They can also perform accurate surgery in tiny places and transport dangerous substances. Due to the pandemic situation many people are forced to isolate to control the spreading disease. This project focus on designing a robot for the isolated patients there by reducing the spreading of disease. The proposed system helps the patient to take care of them such as taking food and medicine on time without any medical assistants support. The patient will be monitored by using the IoT in that hospital.

Keywords: Robots, Pandemic Disease, IoT

Corresponding Author:
K.Prakash,
Assistant Professor, BME Department, Kings Engineering College, Irungattukottai, Chennai, India.
Email: kprakashvinoth@gmail.com

1. INTRODUCTION

The aim of this project work is to design of a medical prototype robot for nurse assistance. Robotics in the medical field is an ongoing trend in both research and commercial sectors. Robots are used in every hospital department for assistance in delivering things, surgery, checking vital signs, telepresence, etc...,

Medical prototype robot is a scenario based assistive robot with a customized design to help the hospital staff fight against Covid-19(corona virus disease) outbreak, ensuring social distancing. It has basic features like delivering medicine and small handheld devices, remote temperature sensing using IR (infrared) and UVC (ultraviolet type C) disinfection unit.

In hospital and other medical facilities, an isolation ward is a separate ward used to isolated patients with infectious diseases. Several wards for individual patients are usually placed together in an isolation unit.

An isolation facility aims to control the airflow in the room so that the number of airborne infectious particles is reduced to a level that ensures cross-infection of other people within a healthcare facility is highly unlikely. At State level, a minimum of 50 bed isolation ward should be established.

Corona virus disease 2019 (COVID-19) has now been characterized as a pandemic by the World Health Organization. Strict measures have been taken by hospitals worldwide to isolate patients diagnosed or suspected of COVID-19. Throughout hospitalization in the isolation wards, patients are not allowed to have visitors, and the only contact they have with their family members is *via* mobile devices.

It is well-documented that patients who were isolated experience stress that leads to behavioural or emotional manifestations. Isolation leads to the removal of everyday items and routines which may induce fear, anxiety, depression and hasty mood changes.

Figure 1. Robot nurse helps to isolation patient

The main aim of this prototype is to make the nurse not to handle the devices which was handled by the patients in which we can convey the information through an audio system (which is already available in the hospital) or a nurse will be assisting the initial instructions required (by ensuring the social distance) that is in the isolated ward so that the patient can do the task properly. For this prototype, we are using the basic microcontroller, that is, Arduino UNO. We were successful in taking readings with the help of a temperature sensor and were able to supply power to the UVC lamp in which it sterilized the objects inside the unit when it was exposed for 2-3 minutes. And finally, the robot was able to move successfully with the help of Arduino and Bluetooth setup.

2. LITERATURE SURVEY

1. Steeve Shibu Chempolil, Renie Melvinia Basaiawmoit, Sneha Saji,Karthik Raj V, "Design of a Medical Prototype Robot for Nurse Assistance", 2021

Robotics in the medical field is an ongoing trend in both research and commercial sectors. Robots are used in every hospital department for assistance in delivering things, surgery, checking vital signs, telepresence, etc. Medical prototype robot is a scenario-based assistive robot with a customized design to help the hospital staff fight against Covid19 (Coronavirus disease) outbreak, ensuring social distancing. It has basic features like delivering medicine and small handheld devices, remote temperature sensing using IR (infrared) and UVC (ultraviolet type C) disinfection unit. The main aim of this prototype is to make the nurse not to handle the devices which was handled by the patients in which we can convey the information through an audio system or a nurse will be assisting the initial instructions required that is in the isolated ward so that the patient can do the task properly.

2. Kamran Hammed, "An Approach to design Human Assisting Prototype Robot for providing Fast and hygienically secure environment to Clinical professionals in order to fight against COVID19 in Hospitals", 2021.

In the current era robots play vital role in several industries, hospitals, and research organizations etc. In hospitals robots support and nursing staff currently may also use in this era during COVID19 Pandemic to transport such patient sample or dispose of their usage belonging to avoid spreading of this pandemic to clinical staff. From making deliveries, dispensing medication, visiting patients to aiding surgeries, robots are improving the way hospitals function. Central Sterilization Supply Department (CSSD) offers sterilization amenities to Outpatient Department (OPDs), wards and operation theatre (OT) of hospitals. It provides facilities to receive, clean, pack, disinfects, sterilizes, store and distribute instruments, in accordance with well-delineated protocols and standardizes procedures. An alarming boost in Hospital Ac-quired Infections (HAI) demonstrates the necessity of a well-organized CSSD to prevent surge in HAI. Although quality assurance procedures are followed to ensure safety and efficiency at all levels: appropriate handling of contaminated items, decontamination, proper cleansing, and instrument care, but the necessity of human presence to implement these procedure in-creases the threat of HAI.

3. Jianmin Li,Kang Kong, "System Design of a Novel Minimally Invasive Surgical Robot That Combines the Advantages of MIS Techniques and Robotic Technology"',2020.

Existing minimally invasive surgical (MIS) robots are generally large, complex and expensive, which greatly increases the operation cost and limits the applications of MIS robot technology. To solve these problems, a small table- attached MIS robot that combines the high efficiency of the traditional MIS technique and the dexterity of robotic operations is proposed in this paper. The master and slave manipulators of the new robot are integrated, which allows the surgeon to manipulate the robot next to the operation table. Moreover, the novel design can be used with existing MIS instruments, providing surgeons dexterous operation and intuitive motion control with guaranteed operation efficiency. To simplify the structure of the robotic system, a multistage cable transmission structure is established. In addition, to reduce the difficulty of operations, especially suturing operations, a novel surgical instrument is developed with a ''roll-pitch-distal roll'' wrist and a quick-exchange interface.

4. Sachie Yamada, Tatsuya Nomura, Takayaki Kanada, "Healthcare Support by a Humanoid Robot", 2019.

A series of studies were conducted as an exploratory survey to examine the possible roles of a robot as a partner in healthcare. The results show that Japanese people are willing to use a humanoid robot as an exercise partner in variety of usage scenarios. In particular,a walking robot was found to be useful for socially anxious individuals, in that it can serve as a safe partner that is not evaluates.

5. Matthias Rehm, Antonia L. Krummheuer, and Kasper Rodil "Developing a New Brand of Culturally-Aware Personal Robots Based on Local Cultural Practices in the Danish Health Care System", 2018.

In earlier work it has been shown how culture can be used as a parameter influencing human robot interaction in general. While this is a good starting point, in our work with concrete application fields we encounter that culture in its usual definition as national culture is too general a concept to be useful in these concrete applications. Thus, we shifted our focus instead to a concept of local cultural practices, which is derived from situated practices as in Wengers communities of practice and grounded loosely in Sperbers idea of an

epidemiology of representations, i.e. culture or rather cultural practices as an emergent phenomenon from learning processes in a given group.

6. Kosta Jovanovic, Andrea Schwier, Eloise Matheson, Michele Xiloyannis, "Digital Innovation Hubs in Health-Care Robotics Fighting COVID-19", 2021.

The use of robotics in health care has seen a recent rise in interest due to its potential for use during the SARS-CoV-2 pandemic. The transmission rate of COVID-19 has meant that health-care workers are under increasing pressure, risks, and workload to manage the requirements of personal protective equipment, strict disinfection procedures, and the heightened medical needs of patients. Patients are suffering from isolation, and not just in hospitals: higher-risk individuals must shelter, meaning social interactions, particularly in care homes, are limited. Robots can help by providing disinfection and logistics services that support patients and health-care professionals, by acting as devices to be used for rehabilitation at home (for both pre-existing conditions and for COVID-19-related treatment), and via interventional systems that can widely distribute future vaccinations.

7. Geng Yang, Honghao Lv, Zhiyu Zhang,. Liu Yang, Deng Jia. "Keep Healthcare Workers Safe: Application of Teleoperated Robot in Isolation Ward for COVID-19 Prevention and Control". 2021

At the time of writing, the coronavirus disease (COVID-19) has affected 212 countries and territories across the globe. According to the world health organization (WHO), a total number of 4,735,622 confirmed cases, including 316,289 deaths was reported. In the fight against COVID-19, nurses, doctors, and other healthcare workers are in the front line of the battle bearing the higher risk of infection. The International Council of Nurses (ICN) gathered further information to suggest that more than 90,000 healthcare workers have been infected worldwide. Personal protective equipment (PPE) shortage is one of the key factors increasing the infection risk for the medical staffs. Therefore, finding alternative ways to lower the infection risk has become an urgent problem to be solved.

Using robotic technology and telemedicine to help with the combat of COVID-19 outbreak has gained a great attention for good reasons: more robots and virtual meetings in the field means less person-to-person contact, thus, lower risk of infection for healthcare workers. Using robots can also reduce community transmission and PPE consumption.

8. Shengzheng Wu, Dudu Wu, Ruizhong Ye, Keyan Li, Yuehua Lu. "Pilot Study of Robot-Assisted Teleultrasound Based on 5G Network: A New Feasible Strategy for Early Imaging Assessment During COVID-19 Pandemic".2020

Early diagnosis is critical for the prevention and control of the coronavirus disease 2019 (COVID-19). We attempted to apply a protocol using tele ultrasound, which is supported by the 5G network, to explore the feasibility of solving the problem of early imaging assessment of COVID-19. Four male patients with confirmed or suspected COVID-19 were hospitalized in isolation wards in two different cities. Ultrasound specialists, located in two other different cities, carried out the robot-assisted tele ultrasound and remote consultation in order to settle the problem of early cardiopulmonary evaluation. Lung ultrasound, brief echocardiography, and blood volume assessment were performed. Whenever difficulties of remote manipulation and diagnosis occurred, the alternative examination was repeated by a specialist from another city, and in sequence, remote consultation was conducted immediately to meet the consensus. The ultrasound specialists successfully completed the telerobotic ultrasound. Lung ultrasound indicated signs of pneumonia with varying degrees in all cases and mild pleural effusion in one case. No abnormalities of cardiac structure and function and blood volume were detected. Remote consultation on the issue of manipulation practice, and the diagnosis in one case was conducted. The cardiopulmonary information was delivered to the frontline clinicians immediately for further treatment. The practice of tele ultrasound protocol makes early diagnosis and repeated assessment available in the isolation ward. Ultrasound specialists can be protected from infection, and personal protective equipment can be spared. Quality control can be ensured by remote consultations among doctors. This protocol is worth consideration as a feasible strategy for early imaging assessment in the COVID-19 pandemic.

9. Jing wang MD, Chengzhong peng MD, Yan zhao MD "Application of a Robotic Tele-Echography System for COVID-19 Pneumonia".2020

To date, coronavirus disease 2019 (COVID-19) has infected millions of people worldwide. Ultrasound plays an indispensable role in the diagnosis, monitoring, and follow-up of patients with COVID-19. In this study, we used a robotic tele-echography system based on a 5G communication network for remote diagnosis. The system has great potential for lung, heart, and vasculature information, medical staff protection, and resource sharing, can be a valuable tool for treating patients during the pandemic, and can be expected to expand to more specialized fields.

10. ValeriaSeidita, FrancescoLanza,Arianna pipitone, Antonio Chella."Robots as intelligent assistants to face COVID-19 pandemic". 2020

The epidermic at the beginning of this year due to a new virus in the corona virus family, is causing many deaths and is bringing the world economy to its knees. Moreover, situation of this kind are historically cyclinical. The symptoms and treatments of infected patients are, for better or worse even for new virus, always

the same: more or less severe flu sysmptoms, isolation and full hygiene. By now man has learned how to manage epidemic situation,but deaths and negative effects continue to occur.

3. METHODOLOGY

The outbreak of novel coronavirus pneumonia (COVID-19) has significantly and continuously impact to the entire world. Until March 2021, there were more than 120,000,000 diagnosed cases globally. Referring to the Interim Guidelines for Collecting and Handling of Clinical Specimens for COVID-19 Testing (Interim Guidelines), Real-Time Reverse Transcription Polymerase Chain Reaction (RT-PCR) of respiratory specimens (oropharyngeal and nasopharyngeal swabs, bronchoalveolar lavage, tracheal aspirate) is the gold standard test for detection of COVID-19 infection. As a common respiratory tract infection sampling method, oropharyngeal swab sampling is widely used in the diagnosis of COVID-19. Patients are supposed to open their mouths properly, and then medical staff scratches the epidermal cells on the patients' pharyngeal mucosal tissue with a pharyngeal swab. In this process, medical staff exposes themselves to the droplets from patients' respiratory tracts, which means a high risk of infection.

In this system we use ARDUINO UNO microcontroller as the brain of this proposed system so that all program coding is stored in it. Bluetooth is used to give directions to the robot. The Transmitter (mobile) will send the data to the receiving side. On the other hand, the receiving side has a robotic chase and a receiver (HC-05). The receiver will get the signal and send it to the controller and the controller will send the data to the motor driver. RTC is used to monitor the time and give medicine to the patient on the scheduled time. If scheduled time occurs, buzzer will alarm. APR module is the pre-recorded voice module used to play voice for the patient about medicine in the speaker. All the information is displayed in the LCD. IOT is communication device, then patient given medicine data stored. The ESP32 CAM Wi- Fi Module Bluetooth with OV2640 Camera Module 2MP for patient Face recognition and patient moment check has a very competitive small-size. The IOT are used to monitoring the updated information to the cloud. The EPS32 are used to survey the isolated ward in hospital. There are four modules are used to this robot.

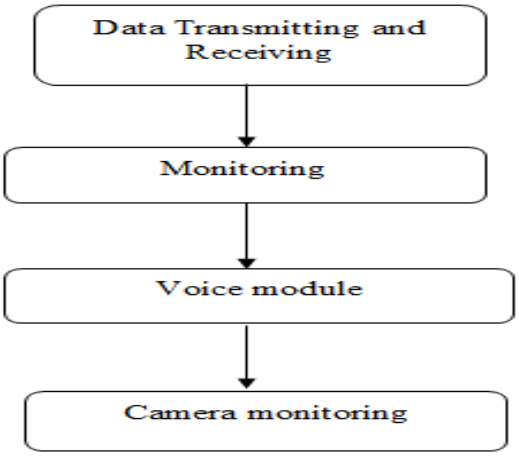

Figure 2. Flow Chart (Work Flow)

Figure 3. Isolation Patient Care

3.1. Data transmitting and receiving

Data transmission is the process of sending digital or analog data over a communication medium to one or more computing, network, communication or electronic devices. It enables the transfer and communication of devices in a point-to-point, point-to-multipoint and multipoint-to-multipoint environment.

The robot receives direction commands through Bluetooth. Data is sent from the transmitter (mobile) to the receiving side. To run the chase, we employ the four commands LEFT, RIGHT, FORWARD, and BACKWARD. To steer the robotic pursuit, we use a mobile app.

There is a robotic chase and an HC-05 on the receiving side. The transmitter side signals will be received by this receiver, which will then communicate them to the controller, which will then transmit the data to the motor driver. The chase will be redirected in accordance with the Bluetooth order.

3.2. Monitoring

In order to administer medication to the patient at the appointed time, Real Time Clock (RTC) is utilised to keep track of the time. Buzzer will sound an alarm if the time is as scheduled. In accordance with the deadline, the patient must take the medication. The alarm buzzer will sound if the time restriction is surpassed.

In a wide range of applications, Real Time Clock's are essential for accurately recording the current time. They also offer alarm, timer, and interrupt features, as well as helping to cut down on power usage.

3.3. Voice module

The Audio Playback Recorder (APR) is a single chip voice recorder and playback device with 8 channels. Each channel can store up to 1.3 minutes speech message and total 11 minutes speech can be recorded and stored in all the channels .The APR module, a pre-recorded voice module, is used to play a voice message informing the patient of their medication through the speaker.

An LCD (Liquid Crystal Display) is a kind of flat panel display that operates primarily with liquid crystals. Given that they are frequently utilised in cell phones, televisions, computer monitors, instrument panels, and other products, LEDs offer a wide range of applications for consumers and organisations. The LCD shows all of the information. When the time limit is up, the APR Voice command for the medications is issued.

3.4. Camera monitoring

The ESP32-CAM is a full-featured microcontroller that also has an integrated video camera and micro SD card socket. It is inexpensive and easy to use, and it is perfect for IOT devices requiring a camera with advanced functions like image tracking and face recognition.

The ESP32 CAM Wi-Fi Module Bluetooth with OV2640 Camera Module 2MP for patient face recognition and patient movement checking. It is competively small in size. It is suitable for home smart devices, industrial wireless control, wireless monitoring, and other IOT applications. The Internet Of Things (IOT) are used to monitor the updated information through the cloud.

4. RESULTS AND DISCUSSION

Experiment results show that the sampling robot can effectively to give the medicines and food without infection risks. The hybrid force/position controller of the robot guarantees the consistency of the leader-follower operation and keeps the operation force within the expected threshold range. The trajectory required for sampling robot is an interesting issue. To obtain enough mucosal epithelial cells, the swab needs to slide the different areas of the rear pharyngeal wall and ensure continuous sampling. There is no specification and related research on the sampling trajectory. Z-shaped trajectory is used for robotic sampling in the clinical trial, fully validated in manual sampling. We also provide another typical trajectory form, "O" trajectory, to test the sampling robot. To achieve autonomy and standardized sampling in the future, a universal and effective trajectory is the primary premise. According to the results of clinical trials, there is no positive correlation between the contact force and the CT value of the sample.

Figure 4. The Robot

This conclusion contradicts the conventional experience that more epithelial cells could be scraped off with a stronger contact force. The possible reason is that the tip area of the swab is limited, and it is impossible to load more cells after crossing a certain area mucosal layer. If more cells are needed, the shape of the tip of the swab can be reshaped to increase the contact area between the swab and the mucosal layer. Before the clinical application, the medical devices need to meet the protection and sterilization standards, especially related to infectious diseases. In our clinical application, we adopted two sets of isolation covers and combined them with alcohol and ultraviolet light to avoid the spread of viruses. There is no standard of isolation and sterilization against infectious diseases for the robot to follow. So, it is necessary to carry out research on the robotic isolation method and the level of protection which is of great significance to large-scale applications in the future.

In the process of prevention and control of COVID-19, a variety of robotic applications, including consultation, disinfection, and distribution services, have fully demonstrated the value of robots in emergent public health events. The robot that completes the services of patient is needs to be in close contact with humans, especially interacting with human tissues, which involves risking the safety and effectiveness of the operation. With the spread of this pandemic, the emergence of asymptomatic infections, and the recent public health events of infections such as COVID-19, humans have started expecting more from robots. Their expectations involve unattended operation in the isolation area and the integration and unmanned operation from interrogation and sampling. It will demand higher requirements for the robot's operating abilities.

In the future, it will be important to conduct in-depth research on the expansion of robots' operational capabilities, improvement of intelligence, and multi-robot collaboration.

According to the world health organisation, a total number of deaths for disease. The disease affected by the human all are isolated by the hospitals. In fight against the disease, nurses, doctors, and other healthcare workers are in the front line of the battle bearing the higher risk of infection. The international council of nurses (ICN) gathered further information to suggest that more than 90,000 healthcare workers have been infected worldwide. Personal protective equipment (PPE) shortage is one of the key factors increasing the infection risk for the medical staffs.

Using robotic technology and telemedicine to help with the combat of COVID-19 outbreak has gained a great attention for good reasons; more robots and virtual meetings in the field means less person-to-patient contact, thus, lower risk of infection for healthcare workers. Using robots can also reduce community transmission and PPE consumption.

5. CONCLUSION

This project presented the tray carrying robot for hospital use. The tray carrying robot goes back and forth between a patient and the tray rack located in a corner of a hospital ward. The robot movement was controlled by the line trace control algorithm using the single and multiple guide lines. Using the line trace of the multiple guide lines, one robot can serve more than one user. Also, the guide line attached to the ceiling of a hospital ward was also proposed to prevent the guide tape from getting dirty.

REFERENCES

[1] COVID-19 Dashboard by the Centre for Systems Science and Engineering (CSSE) at Johns Hopkins University (JHU) (ArcGIS, Johns Hopkins Univ., 2020)
[2] Centre of Disease Control and Prevention. Interim Guidelines for Collecting, Handling, and Testing Clinical Specimens for COVID-19. May 22. Available at: https://www.cdc.gov/coronavirus/2019-ncov/lab/guidelinesclinicalspecimens.html.
[3] Special Expert Group for Control of the Epidemic of Novel Coronavirus Pneumonia of the Chinese Preventive Medicine Association. "An update on the epidemiological characteristics of novel coronavirus pneumonia (COVID-19)." Chinese Journal of Epidemiology 41.02(2020):139–144.
[4] G.-Z. Yang et al., "Combating COVID-19-The role of robotics in managing public health and infectious diseases," Science Robotics, vol. 5, no. 40, Mar 25 2020, Art. no. eabb5589.
[5] J. Sea, S. Shim, H. Park, J. Beak, J. H. Cho, and N.-H. Kim, "Development of Robot-Assisted Unfact Swab Sampling System for Upper Respiratory Disease," Applied Sciences-Basel, vol. 10, no. 21, Nov 2020, Art. no. 7707.
[6] C. Li, X. Gu, X. Xiao, C. M. Lim, X. Duan, and H. Ren, "A Flexible Transoral Robot Towards COVID-19 Swab Sampling," Frontiers in robotics and AI, vol. 8, pp. 612167-612167, 2021 2021.
[7] Y. Hu et al., "Design and Control of a Highly Redundant Rigid-flexible Coupling Robot to Assist the COVID-19 Oropharyngeal-Swab Sampling," Yee Robotics and Automation Letters, vol. 7, no. 2, pp. 1856-1863, Apr 2022.
[8] S. Wang, K. Wang, H. Liu, and Z. Hou, "Design of a Low-cost Miniature Robot to Assist the COVID-19 Nasopharyngeal Swab Sampling," 2020.
[9] S.-Q. Li, W. L. Guo , H. Liu et al., "Clinical application of an intelligent oropharyngeal swab robot: implication for the COVID-19 pandemic," European Respiratory Journal, vol. 56, no. 2, Aug 1 2020, Art. no. 2001912.
[10] G. S. Fischer et al., "MRI-compatible pneumatic robot for transperineally prostate needle placement," Elease Transactions on Mechatronics, vol. 13, no. 3, pp. 295-305, Jun 2008.

Prediction of Sleep Apnea based on Respiratory Flow Analysis

A.R. Reshma Ruth Pauline[1], Dr. T. Jayanthi[2]
[1,2]SRM Institute of Science and Technology, Chennai

ABSTRACT

A potentially serious disorder called sleep apnea causes frequent breathing pauses and restarts during sleep. Obstructive Sleep Apnea (OSA), which is more common, is a type of sleep apnea brought on by relaxed throat muscles. Although OSA is most common in older men, it can affect both sexes and children. Symptoms include snoring, noticed breathing stopping, wheezing, or air choking while sleeping at night, increased sleepiness during the day, poor memory, and frequent mood swings. OSA increases the risk of occupational fatal accidents, automobile accidents, severe depression, and in most cases, cardiac and cerebrovascular disease, as well as shorter survival times if it is not treated. Polysomnography (PSG), a lab-based overnight sleep study, is the most accurate method for identifying obstructive sleep apnea. This type of test, though, can be more expensive, and the electrodes attached not be comfortable. The primary goal of this study is to develop hardware that will enable respiratory flow analysis to diagnose obstructive sleep apnea. It uses a Mass Air Flow (MAF) sensor to measure the inspiratory and expiratory flows. This data is collected for 5-8 hours and then analyzed. The findings will aid in a quicker and more precise diagnosis of obstructive sleep apnea.

Keywords: Obstructive sleep apnea, Inspiratory flow, Expiratory flow, Mass flow sensor

Corresponding Author:
Dr.T. Jayanthi,
SRM Institute of Science and Technology
Email: jayantht@srmist.edu.in

1. INTRODUCTION

Sleep is as essential to a high quality of life as eating wholesome, natural food is to people because it fulfills a basic human need. The effects and challenges of various clinical conditions on treating doctors and patients still need to be explained to the public. In turn, this profoundly impacts human breathing patterns, gas exchange, and ventilation. Sleep disorders change the nature of sleep. Amplifying the underlying diseases could increase the impact of the disease. A person spends almost 30% of their time sleeping, and the quality of their sleep dramatically impacts how they feel. The hallmarks of breathing-related sleep disorders include anomalies in the rhythm of breathing or the amount of aeration during sleep (C. Doukas, T.Petsatodis, C.Boukis, I.Maglogiannis, 2012). It has been viewed as a chronic condition that requires ongoing care and management. Sleep apnea may be present in someone who snores loudly and still feels exhausted after a whole night's sleep. Major breathing-related sleep disorders like obstructive sleep apnea (OSA) are characterized by a complete or partial obstruction of the higher airline during sleep, which can cause frequent oxyhemoglobin desaturations and fragmented sleep. In addition to having an impact on people's health and occasionally leading to nocturnal deaths, OSA is a significant risk factor for cardiovascular disease (C.A.Kushida,2006), (N.Takama, M.Kurabayashi,2009). Although it can affect anyone, especially children, OSA is most common in older men. OSA can increase the risk of workplace accidents, auto accidents, despair, and in most cases, cardiac illness, as well as shorter survival times if it is not treated in a timely manner. The sleep respiratory rate, for detecting obstructive sleep apnea, is a parameter that is used as an important indicator for complex diseases. In a relaxed state, a healthy adult breathes 12–20 times per minute. When OSA is present, the respiratory rate becomes abnormal, and the rate of breathing while sleeping becomes slow or occasionally comes to a complete stop due to apnea. So, a crucial and early indicator for OSA monitoring is respiratory rate while you sleep.

Due to the rising prevalence of OSA, the challenging setup, and concerns that PSG testing is expensive, alternative testing methods, like portable HSAT, have become more popular recently (P.E.Peppard, T.Young, J.H.Barnet, M.Palta, E.W.Hagen, K.M.Hla, 2013) (J.A.Walsleben, 2004). The HSAT is more practical and affordable and can be completed at the patient's house. The HSAT will record several factors: respiratory effort, airflow, heart rate or ECG, arterial oxygen saturation, snoring, body positions, and movements. The increased diagnostic precision of more recent equipment and the widespread validation of many devices

against PSG (N.A. Collop, 2011) has made a more usable and affordable diagnostic option available. Since a night-to-night fluctuation is said to be a characteristic of OSA and is typically more pronounced in those with acceptable conditions, the ability of HSAT to record multiple sleep periods is helpful (L.R.A. Bittencourt, 2001). HSAT is convenient, but frequently underestimates the AHI, increasing the possibility of a false-negative result because it cannot measure total sleep duration (TST) or recognize arousal (M.R.Zeidler, V.Santiago, J.M.Dzierzewski, M.N.Mitchell, S.Santiago, J.L.Martin, 2015). The HSAT is not recommended by the American Academy of Sleep Medicine (AASM) for population screening, but it is recommended for the diagnosis of OSA in certain populations.

In this study, a device that uses respiratory flow analysis to diagnose OSA was developed. It uses a mass airflow sensor to measure the flow rates during inhalation and exhalation. The benefit of this method is that it allows for movement. When compared to conventional tests, which call for various electrodes to be attached to various body parts, it is more comfortable. Data is collected for 8 hours and analyzed. The findings will contribute to a quicker and more precise diagnosis of obstructive sleep apnea.

2. METHODOLOGY

A CPAP mask has been used for this study in order to fit our needs. A PCB has been designed and used. The ESP32 serves as the PCB's primary component. The rate of inhalation and exhalation have been sensed and detected using a Mass Air Flow (MAF) sensor. The AF3000 sensor is the one utilized for obtaining flow rates. The mass flow sensor is ideal for demanding applications like respiratory and medicinal aeration because of the unique way the mass flow sensor channel is designed to cause a low-pressure decrease through the body of the sensor. The modified CPAP mask has this PCB installed on it. It is powered by a 2000 mAh lithium polymer rechargeable battery with a voltage of 3.7V. It will take 8 hours to collect the flow data. examined, too.

The flow data collected has been analyzed using Matlab and peak detection has been done. Using the peak count, the data can be observed as normal and abnormal data.

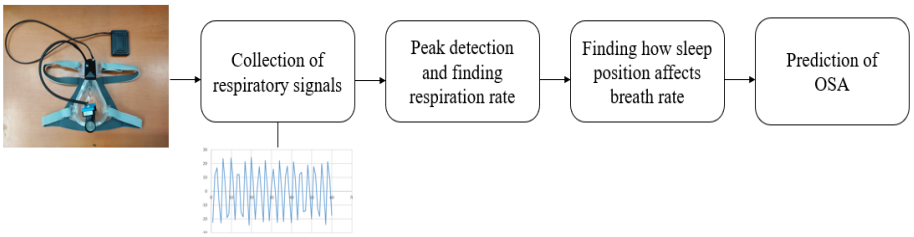

Figure 1. Methodology Flowchart

3. RESULTS

Data were gathered for both regular breathing and breath with a pause. The peaks were identified using Matlab.

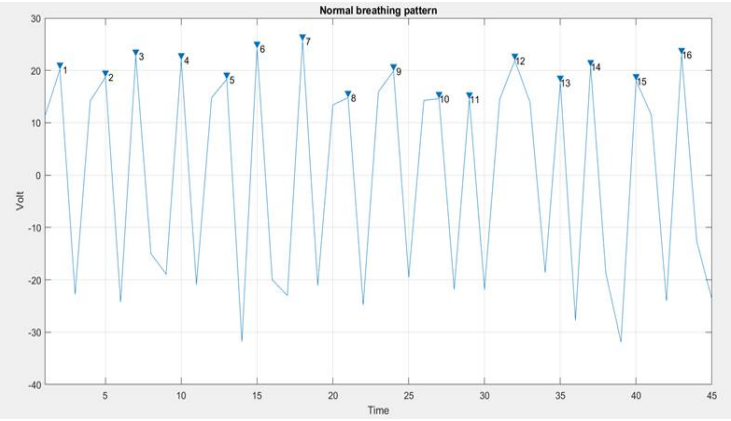

Figure 2. MAF sensor output - Normal breathing (1 min).

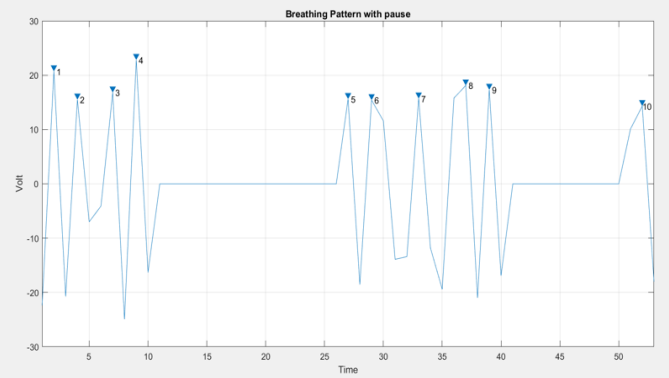

Figure 3. MAF sensor output - Breathing with pause (1 min).

Figures 2 and 3 show how many peaks are detected in both signals, 16 in normal breathing and 10 in breathing with a pause. These counts show the number of breaths taken in a minute. The average respiratory rate for a typical subject is 12-20 breaths per minute. Anything below 12 and above 20 is considered abnormal.

4. CONCLUSION

The modified CPAP mask was used for eight hours to measure the breath flow rate. The obtained data was then graphed to display the flow rate. To diagnose OSA, this will be examined later using specialized tools. This device's advantage is that it is wireless and straightforward to use. The MAF sensor's high accuracy contributes to the accuracy's high level. So, a tool for diagnosing obstructive sleep apnea has been created that is simple to use and comfortable to handle. For the purpose of diagnosing OSA, the data has been observed, gathered, and analyzed. In the future, this technique may be used in conjunction with snore detection and snore intensity measurement to assess a person's potential level of sleep apnea.

ACKNOWLEDGMENT

For their support, a heartful thank and gratitude to MedCuore Medical Solutions Pvt. Ltd.

REFERENCES

[1] C. Doukas, T. Petsatodis, C. Boukis, and I. Maglogiannis, “Automated sleep breath disorders detection utilizing patient sound analysis,” *Biomed. Signal Process. Control*, vol. 7, no. 3, pp. 256–264, May 2012.

[2] C. A. Kushida *et al.*, “Practice Parameters for the Use of Continuous and Bilevel Positive Airway Pressure Devices to Treat Adult Patients With Sleep-Related Breathing Disorders,” *Sleep*, vol. 29, no. 3, pp. 375–380, Mar. 2006.

[3] N. Takama and M. Kurabayashi, “Influence of Untreated Sleep-Disordered Breathing on the Long-Term Prognosis of Patients With Cardiovascular Disease,” *Am. J. Cardiol.*, vol. 103, no. 5, pp. 730–734, Mar. 2009.

[4] P. E. Peppard, T. Young, J. H. Barnet, M. Palta, E. W. Hagen, and K. M. Hla, “Increased Prevalence of Sleep-Disordered Breathing in Adults,” *Am. J. Epidemiol.*, vol. 177, no. 9, pp. 1006–1014, May 2013.

[5] J. A. Walsleben *et al.*, “Sleep and Reported Daytime Sleepiness in Normal Subjects: the Sleep Heart Health Study,” *Sleep*, vol. 27, no. 2, pp. 293–298, Mar. 2004.

[6] N. A. Collop *et al.*, “Obstructive Sleep Apnea Devices for Out-Of-Center (OOC) Testing: Technology Evaluation,” *J. Clin. Sleep Med.*, vol. 07, no. 05, pp. 531–548, Oct. 2011.

[7] L. R. A. Bittencourt *et al.*, “The variability of the apnoea-hypopnoea index,” *J. Sleep Res.*, vol. 10, no. 3, pp. 245–251, Sep. 2001.

[8] M. R. Zeidler, V. Santiago, J. M. Dzierzewski, M. N. Mitchell, S. Santiago, and J. L. Martin, “Predictors of Obstructive Sleep Apnea on Polysomnography after a Technically Inadequate or Normal Home Sleep Test,” *J. Clin. Sleep Med.*, vol. 11, no. 11, pp. 1313–1318, Nov. 2015.

Study and Analysis of Sitting Posture Using Emg and Accelerometer Sensor

Yugendhar R[1], Anitha G[2]
[1,2]SRM Institute of Engineering and Technology, Kattankulathur

ABSTRACT

The study aimed to identify and analyze the sitting posture using EMG and accelerometer sensor, whether the muscle gets strained during computer operation, resulting in an increase in the neck-shoulder area and upper trapezius muscle, acromion, during the computer work. Ten subjects were asked to participate to perform the computer work. All subjects are asked to have their proper sitting posture at 90◦ to the adjustable chair.EMG muscle sensors are placed at the selected position neck-shoulder area and upper trapezius muscle and acromion at the same time accelerometer sensor is placed in the head, y- direction to measure the angle changes during computer operation. The result of the study shows that during computer operation muscles get strained compared to a normal sitting posture. The upper trapezius muscle and acromion are getting more strained.

Keywords: EMG, Accelerometer sensor, Trapezius muscle, Acromion

Corresponding Author:
Anitha G,
SRM Institute of Engineering and Technology, Kattankulathur
Email: anithag@srmist.edu.in

1. INTRODUCTION

According to the report, 25-76% of virtual display unit operators are affected by musculoskeletal discomfort. This cause is because more populations got affected by multifactorial and complex. The most important factor that affects muscle load is caused by poor work posture, a large number of work tasks, and eye strain. Such disorders are affected not only by poor posture, a large number of tasks, as a result of prolonged sitting computer work. In recent years, mounting evidence has pointed to prolonged sitting workers having a high chance of the risk factors (WRNULD). As a result, prolonged sitting increases the risk of developing upper respiratory symptoms Aras et al., 1997. In addition to the survey, there is a relationship between poor posture and prolonged sitting posture, it determines the risk of shoulder and neck pain for working more than five hours. The commonly used "forward head posture" employed by office workers entails a head posture back side of the neck and "rounded shoulders" which causes work-related disorders. Understanding the development of WRNULD requires postures of the neck and shoulder movements to be recorded for posture correction. Therefore, prolonged sitting office workers cause a high chance of risk disorder.

2. LITERATURE REVIEW

Previous research has shown a positive relationship between upper trapezius muscle activation and cervical spine muscle flexion during computer operation. The relaxed sitting posture causes increased strength in the disc pressure and flexion relaxation. As a result, poor sitting posture causes some risk and ideal sitting posture will cause an increased amount of pressure, therefore research has been done on poor and ideal posture. To recent findings, there is difficult to maintain the ideal posture in day-to-day life. After sitting in an ideal posture there are changes in the posture after some work or without work. According to O'Sullivan et al. (2011), there will be no difference between the ideal and clinically ideal postures. Most of the research is focused based on the findings on muscle activity and kinematics.

Recent research has defined it as the biofeedback of the effect of posture correction for prolonged sitting posture correction, there will be increasing the upper trapezius muscle. Vested et al. (2011) proposed that in the targeted muscle area during the computer operation, there are changes in the upper trapezius muscles, which slightly increase when the muscles get strained. As a result, here wireless Emg muscle sensor is used to place at the identified shoulder region, head-neck position, upper trapezius muscle, and acromion.

3. METHODOLOGY

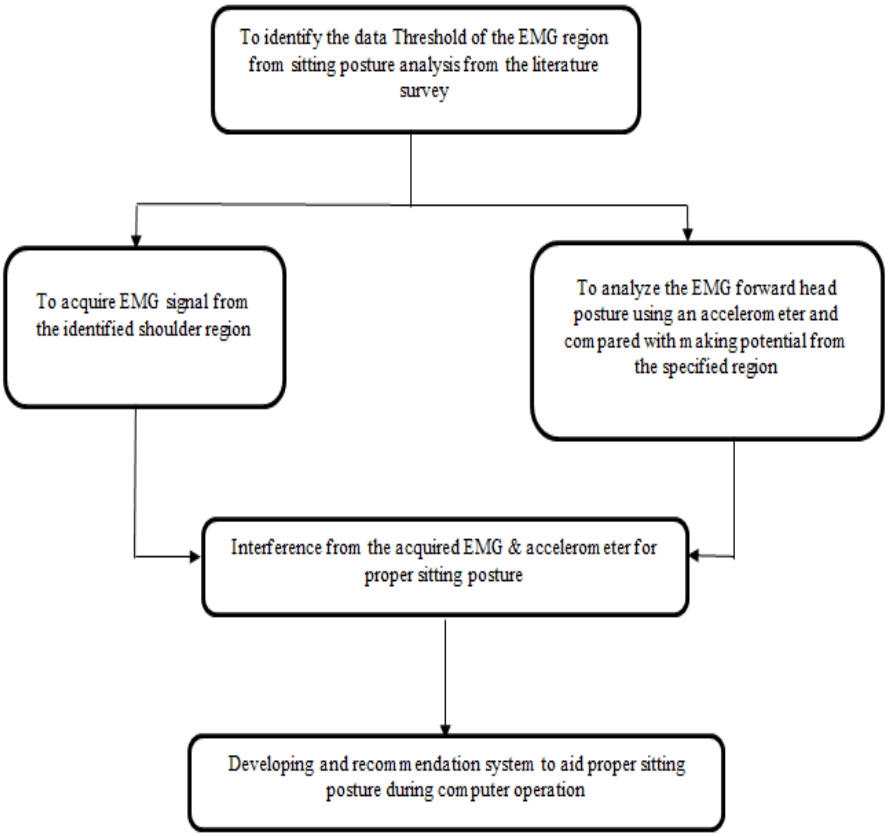

Based on the methodology, the identified threshold of the EMG from sitting posture analysis from the literature survey, to acquire EMG signal from identified shoulder region. Three positions were chosen to place the EMG sensor neck-shoulder area and upper trapezius muscle and acromion. At the same time, an accelerometer sensor is placed at the neck position to analyze the forward head posture. Interference from acquired EMG data and accelerometer for proper sitting posture. Finally developing and recommendation system to aid proper sitting posture during computer operation. Electromyography (EMG) measures how a nerve stimulates a muscle's electrical activity. The data was collected from an EMG during the sitting posture.

4. DATA COLLECTION

Delsys software's wireless EMG sensors were used to collect EMG data. The sensors were linked to the WIFI module, and EMG signals were sent to the Delsys base station. The trigno EMG sensors from Delsys are used to measure and wirelessly transmit(40m) surface EMG (sEMG) signals to the Trigno wireless foundation system. Lab Chart software and a Trigno wireless device enabler will measure these signals in real time. A Delsys EMG sensors also have a three-axis accelerometer that can be used to analyze the motion. All the signals are streamed (40 m) to the Trigno base station(receiver)for freedom of movement. The Trigno sensor delivers signals to a base station utilizing a time-synchronized wireless protocol that reduces data delay.

Figure 1. Delsys EMG wireless sensor

4.1 Lab Chart Software

Lab chart supports data collection systems' high-speed integration of analog transduction, signal conditioning, data recording, and validation. Lab chart provides researchers and educators with advanced data collection software that integrates with AD instruments modular DAQ gear. Data recording, processing, and display are simplified with LabChart DAQ software. High-quality graph generation is built into software packages. Peak analysis, spike histograms, and dose-response curves may be created using both computer programs. Users may also see data in four formats and curve fits using the data plot API. In total, AD Instruments DAQ software packages are vital to every DAQ system.

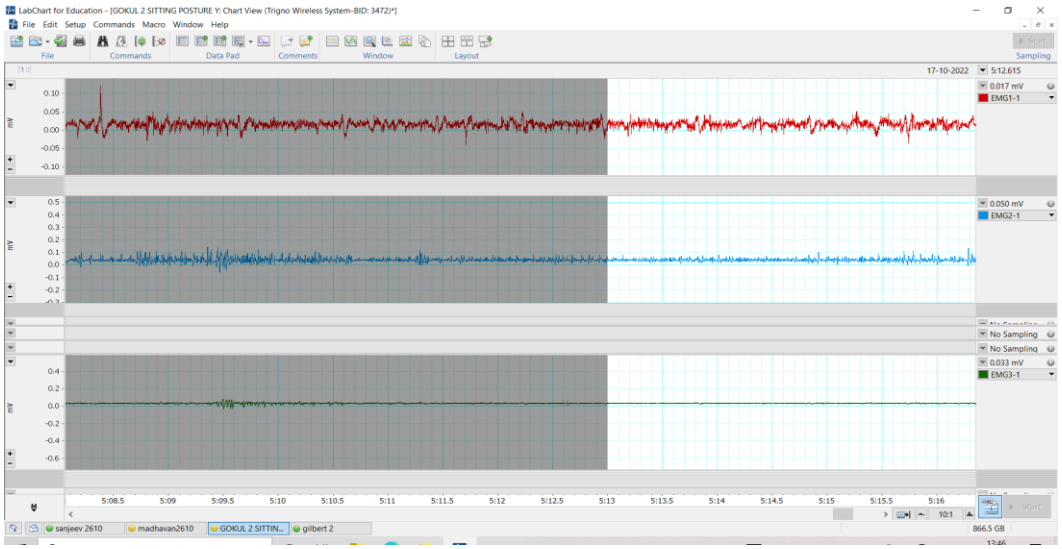

Figure 2. Data acquisition using lab chart software

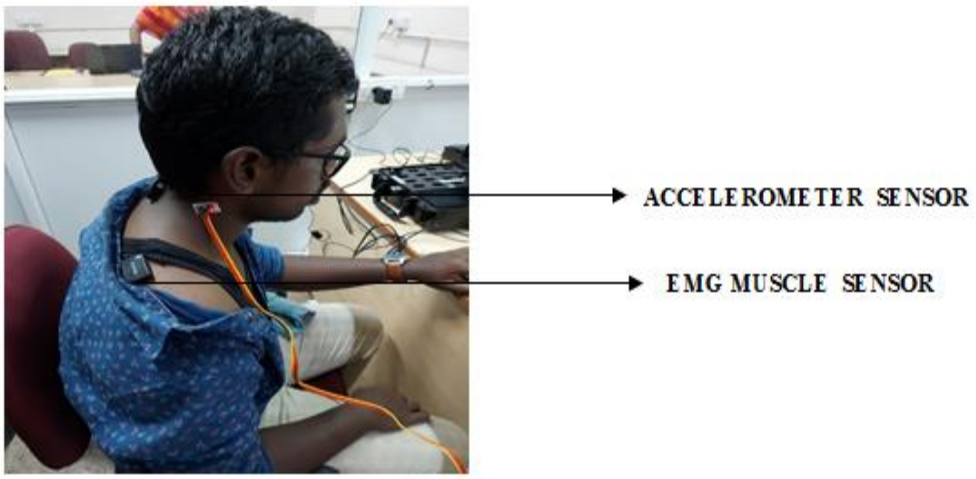

Figure 3(a). placement of accelerometer sensor and muscle sensor

5. DATA ANALYSIS

The electrical activity of the subject is acquired using EMG sensors. The sensors are connected through the WIFI to the base station and the EMG signal with 48 milliseconds to the time delay accelerometers time delay 96 milliseconds. The exported data has a sampling rate of 1 m/s, a 10-850 Hz bandwidth, and an input range of sensors selected between 22 mV and 11 mV. The EMG data are exported then the mean, standard deviation, maximum, and minimum can be calculated. The EMG signals and accelerometer sensor were analyzed in terms of the average, correlation of the EMG and accelerometer sensor.

Average (avg) = $1/N \sum^{n}_{k=0} xi$

correlation $r = \frac{\sum(x_i-\bar{x})(yi-\bar{y})}{\sqrt{\sum(x_i-\bar{x})\hat{2}(yi-\bar{y})\hat{2}}}$

6. RESULT

This study uses EMG sensors to acquire EMG signals from normal subjects. Muscle activation is acquired at the particular muscles. At the same accelerometer sensor is placed in the neck that measures the angle of movement.

Table 1. Acquired Angle Ideal Posture and Computer Work

POSITION	SUBJECT1	SUBJECT 2	SUBJECT 3	SUBJECT 4	SUBJECT 5
Sitting Posture angle using an accelerometer (ideal Posture)	88.23	83.26	84.38	86.12	85.36
Sitting Posture angle using an accelerometer (computer work)	37.35	45.1	54.5	43.1	48.31

Table 2. Acquired EMG (Ideal Posture)

	EMG-1 (mv) (HEAD-NECK)	EMG-2 (mv) (UPPER TRAPEZIUS)	EMG-3 (mv) (ACROMION)
SUBJECT 1	0.01609	0.0403	0.0324
SUBJECT 2	0.01406	0.0406	0.0330
SUBJECT 3	0.01580	0.0399	0.0337
SUBJECT 4	0.01423	0.0455	0.0355
SUBJECT 5	0.0189	0.0545	0.0321

The above table acquired EMG during the ideal posture in front of the computer. For each subject ask to work on the computer for 15 to 30 mins. Subject 1 for each position 0.01609 mV for head and neck position,0.0403 mV for upper trapezius muscle,0.0324 mV for acromion. At the same EMG acquired during the task, there will be changes.

Table 3. Acquired EMG (After Computer Work)

	EMG-1(HEAD-NECK)	EMG-2(UPPER TRAPEZIUS	EMG-3 (ACROMION)
SUBJECT 1	0.3446	0.6205	0.7569
SUBJECT 2	0.5144	0.6474	0.8506
SUBJECT 3	0.6387	0.8485	0.7615
SUBJECT 4	0.4232	0.5265	0.6557
SUBJECT 5	0.5452	0.7252	0.7215

Here we can see that compared to ideal posture and after computer work, there will be slight changes compared to ideal posture. For subject 2 and subject 3, there will be changes in the upper trapezius muscle. At the same time acromion position is also highly acquired compared to the upper trapezius muscles. By comparing and correlating the acquired EMG and accelerometer angle value we can get the threshold value.

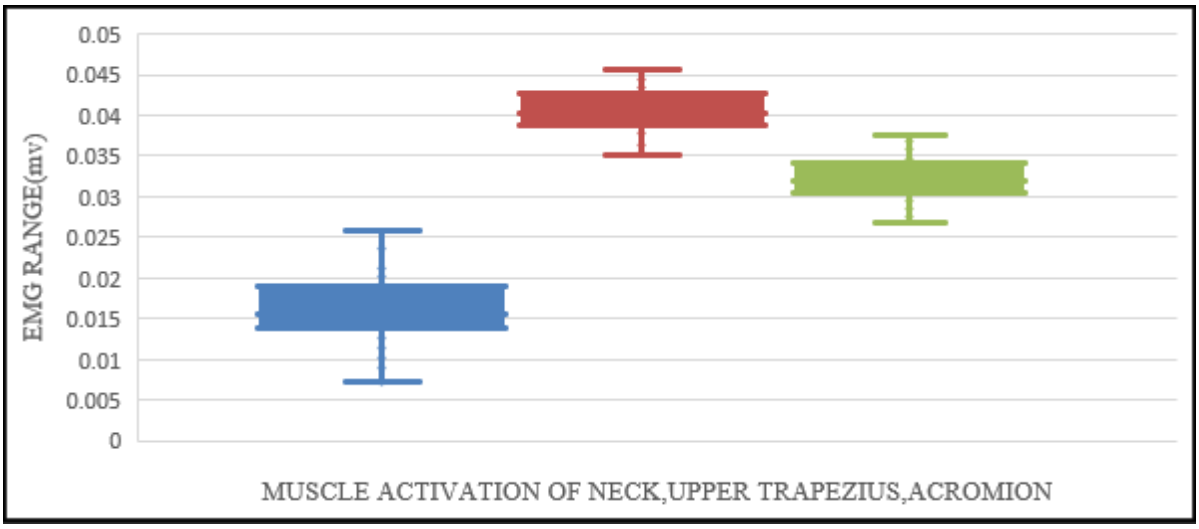

Figure 4(a). Representation of EMG acquired while ideal posture

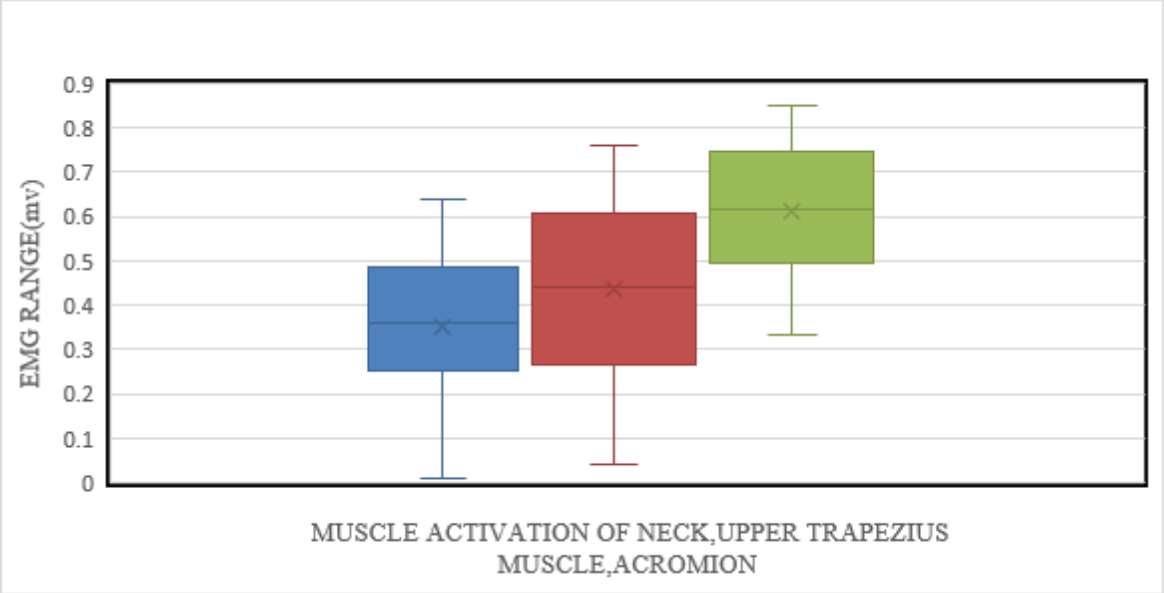

Figure 4(b). Representation of EMG-acquired sitting while doing a computer task

The above figure shows that's representation of muscle activation from the acquired dataset, whereas the bar graph shows that during the ideal posture, the upper trapezius muscle is highly acquired, after the computer task, the muscles get strained and it shows that slightly all the three muscles getting more strained. We can see in the above figure after the muscle getting strained neck, upper trapezius muscles, and acromion were get strained, like wise for each subject after the muscle getting strained we can ably identify the muscle getting more strained. The above figure represents subject 1. After getting all the subject data correlating the angle value and EMG value, where we can get the threshold value.

Table 4. Correlation of Posture Angle and Acquired EMG Data

	NECK&SHOULDER REGION	**TRAPEZIUS MUSCLE**	**ACROMION**
POSTURE ANGLE OCCURRED DURING MUSCLE STRAINED	44.1 Degree	40.1 Degree	37.35 degree
EMG OCCURRED WHILE MUSCLES GET STRAINED	0.5646mv	0.6325mv	0.7645mv

Here, correlating by the posture angle and acquired EMG data we can say the Neck and shoulder region during the posture angle occurred during muscle strain at 44.1 degrees, while the same EMG occurred while muscles get strained at 0.5646 mV. For the Trapezius muscle, we can get 40.1 degrees for posture angle and 0.6325 mV for EMG muscles. For the Acromion muscle 37.5 degrees for posture angle and 0.7645 mV for EMG muscles. So, we can see that Acromion must get more strained at the same time the posture angle of the neck posture has changed.

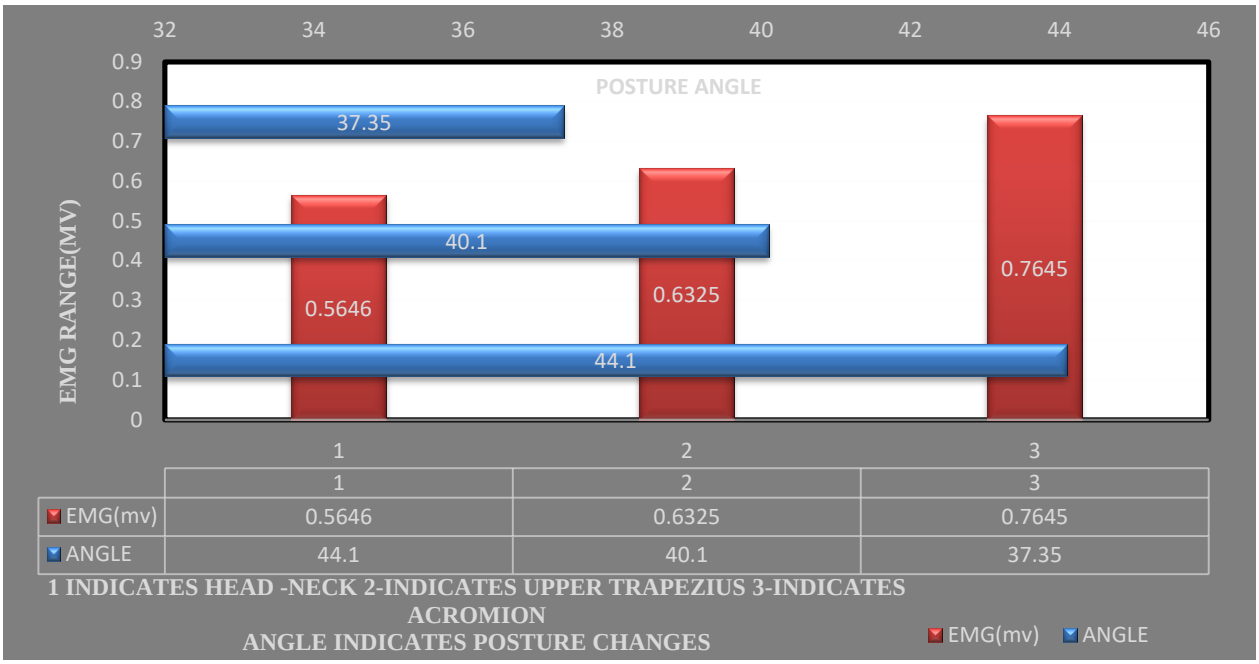

Figure 5. Representation of posture angle changes when muscle getting strained

7. CONCLUSION AND FUTURE WORK

According to a current report, Musculoskeletal discomfort is reported to affect 25-76% of the virtual display unit operators, it is caused due to work posture, work tasks, and poor lighting strain. It may affect musculoskeletal disorders, not only occur due to this specifically related disorder. It will affect prolonged sitting posture during computer operation. The present study aimed to determine the kinematic changes in the angle posture during computer operation. This study was also designed to investigate the muscles that get strained while performing the task, and the angle from the normal sitting posture changes during computer operation. Although the importance of ergonomic chair design, back and armrests, and well-designed workstations is recognized, these settings have limitations in reflecting individual differences and producing constant attention to one's posture. This shows that prolonged sitting muscle activation gets more strained while performing the task. In this study, the upper trapezius muscles and acromion are getting more strained.

REFERENCES

[1] Fogleman M, Lewis RJ. Factors associated with self-reported musculoskeletal discomfort in video display terminal (VDT) users. Int J Ind Ergo 2002; 29: 311–8.
[2] Nakazawa T, Okubo Y, Suwazono Y, et al. Association between duration of daily VDT use and subjective symptoms. Am J Ind Med 2002; 42: 421–6
[3] Tittiranonda P, Remple D, Armstrong T. Effect of four computer keyboards in computer users with upper extremity musculoskeletal disorders. Am J Ind Med 1999; 35: 647–61
[4] Mork PJ, Westgaard RH. Back posture and low back muscle activity in female computer workers: a field study. Clin Biomech (Bristol, Avon) 2009;
[5] Szeto GP, Straker LM, Raine S. A field comparison of neck and shoulder postures in symptomatic and asymptomatic office workers. Appl Ergon 2002; 33: 75–84
[6] Chiu TT, Ku WY, Lee MH, et al. A study on the prevalence and risk factors for neck pain among university academic staffing in Hong Kong. J Occup Rehabil 2002; 12: 77–91
[7] Szeto GP, Straker L, O'Sullivan P. A comparison of symptomatic and asymptomatic office workers performing monotonous keyboard work — 2: neck and shoulder kinematics. Man Ther 2005; 10: 281–91
[8] McLean L. The effect of postural correction on muscle activation amplitudes recorded from the cervicobrachial region. J Electromyogram Kinesiol 2005; 15: 527–35
[9] Enwemeka CS, Bonet IM, Ingle JA, Prudhithumrong S, Ogbahon FE, Gbenedio NA. Postural Correction in Persons with Neck Pain (II. Integrated Electromyography of the Upper Trapezius in Three Simulated Neck Positions). J Orthop Sports Phys Ther 1986; 8: 240–2
[10] O'Sullivan PB, Kendell M, Möller NE. The effect of different standing and sitting postures on trunk muscle activity in a pain-free population. Spine 2002; 27: 1238–44.
[11] Amick, B.C., Robertson, M.M., DeRango, K., Bazzani, L., Moore, A., Rooney, T., Harrist, R., 2003. Effect of office ergonomics intervention on reducing musculoskeletal symptoms. Spine 28, 2706–2711.
[12] Hartvigsen, J., Leboeuf-Yde, C., Lings, S., Corder, E.H., 2000. Is sitting while at work associated with low back pain? A systematic, critical literature review. Scand. J. Public Health 28, 230–239

[13] Hartvigsen, J., Lings, S., Leboeuf-Yde, C., Bakketeig, L., 2004. Psychosocial factors at work in relation to low back pain and consequences of low back pain; a systematic, critical review of prospective cohort studies. Occup. Environ. Med. 61
[14] Jull G, Kristjansson E, Dall'Alba P. Impairment in the cervical flexors: a comparison of whiplash and insidious onset neck pain patients. Manual Therapy 2004;9:89–94
[15] Nederhand MJ, Ijzerman MJ, Hermens HJ. Cervical muscle dysfunction in chronic whiplash-associated disorder grade II (WAD II). Spine 2000;25(15):1938–43.

Assessment of Lower Limb Movement to Develop Strength and Stability in the Foot for Football Sport Game Players

Gilbert L. Sangu[1], Jaison Jacob Mathunny[2], Varshini karthik[3], Ashokkumar Devaraj[4]
[1,2,3,4]SRM Institute of Science and Technology, India

ABSTRACT

This study aims to assess the effect of mountain climber exercises on lower limb strength and stability. The goal is to develop strength and stability in the leg for footballers, thereby, helping to prevent acute ankle sprains. Thirty footballers of the same average age of 20 years old were divided into two groups either a control group (n=15) or an experimental group (n=15), Height and weight of each subject were obtained and an average BMI was calculated as a normalized value. The experimental group was instructed to perform mountain climber exercises, including toe walk, marching form drill, up with one down with two, and up with two, down with one. These exercises were performed for seven days, with an eighth day for resting, before EMG values were taken. The EMG values were taken to measure muscle activation in the Tibialis anterior muscle (TAM) and gastrocnemius muscle (GM) on both left and right legs during various exercises. The effects of both exercise normal footballer exercise and mountain climber exercise were assessed and Descriptive statistical analysis was performed on the data obtained from the test in this research. This involved the calculation of summary measures of mean and root mean square (RMS), of the electromyography (EMG) signals obtained from the Tibialis anterior muscle (TAM) and gastrocnemius muscle (GM) on both left and right legs during various exercises. The findings from this research showed that all exercises activated both muscles, with some variation between left and right legs. This study provides practical evidence that performing the mentioned exercises can improve the strength and stability of football players.

Keywords: Surface EMG Gastrocnemius Tibia Anterior Football game sport, biomechanics

Corresponding Author:
Varshini karthik,
Srm Institute of Science and Technology, India
Email:varshini.varshinikps@gmail.com

1. INTRODUCTION

Football is a team sport that has two eleven-person teams battling it out with a spherical ball. Players pass the ball to one another and attempt to score goals by kicking the ball into a huge net. Because of the frequent use of contact moments in football, a player's foot stability and strength are of utmost importance [1].

The player's lower limbs, namely the muscles, tendons, and bones that connect them, play a key role in maintaining balance and stability [2] Muscle weakness and instability can lead to dislocations or even fractures in a football player's lower extremities [3].

As a result, increasing your muscular strength via exercise is crucial for maintaining and enhancing your lower body's range of motion [4]. Stability of the lower extremities can be attained through doing different exercise and each exercise tend to have effect on particular area of muscles Therefore a focus on the muscle stability is more important especially for the football player simply it can result to injury the study in the article of Prevention of sport injury which says 80% of the study are focusing on the contact game which means the game with movement collision hence state that Acute injuries in collision and contact sports are the primary focus of intervention research, with just 20% of studies devoted to non-contact sports [5]. The muscles in the body plays a major rule simply through strengthening the muscle by doing various exercise one can be able to archive strength and stability focusing on exercising a particular targeted body area soccer players' physical performance was shown to improve more after 8 weeks of contrast strength training (CST) than after 8 weeks of plyometric training, according to research comparing the two types of training for explosiveness and directional change in the lower limbs (PT) [6].

There have been a lot of studies done recently on the issue of lower limb muscular asymmetries and muscular imbalances to try to figure out what role they play as risk factors in injuries and re-injuries in various team sports. [7] In another research, teenage football players were split into two groups for a period of six weeks: those working on core stability, and a control group that did not. Both the core stability training and the regular warm-up were given the same amount of volume in training [8] so that the overall benefits of each could be compared.

In spasticity, the muscles become rigid and tight, limiting the patient's ability to move freely and fluidly. Spasticity is assessed as muscular activity during stretch, during passive and active movement, and is characterized by the muscles' continued contraction and resistance to being stretched, which has adverse effects on movement, speech, and gait [9]. Damage or disturbance to the brain or spinal cord region that regulates muscle and stretch responses is the most common cause of spasticity. Those findings suggest that muscle strength asymmetry in the ankle joint may lead to counterbalancing muscle strengthening in the knee joint to maintain the centre of body mass[10], based on a publication examining the effects of left-right asymmetry in muscle strength on the isokinetic strength of the knee and ankle joints as a function of athletes' levels of performance. There has been a lot of research done on the importance of lower-body strength and strength balance to injury prevention and performance in soccer players, but most of that research has focused on just two muscles: the quadriceps and the hamstrings. The results of this study show that the hamstrings-to-quadriceps ratio does a poor job of distinguishing between the backgrounds of soccer players and provides little predictability for injury prevention and performance [11].

A 12-week eccentric hamstring strengthening programme increased strength and sEMG to a similar magnitude regardless of its scheduling relative to the football training session [12]. This study was conducted by comparing a control group and an experimental group who performed exercises before or after training. The physical features of the lower limbs, including strength, endurance, and range of motion, balance, and discomfort during adductor squeeze and other exercise, were reported in a Cross-sectional investigation by other researchers [13].

The aim of this study is to assess lower limb movement through number of exercises to develop strength and stability in the foot for football sport game players hence help in preventing acute ankle sprain

2. MATERIAL AND METHODOLOGY

2.1. Participant

Thirty male football players, all SRM University students, volunteered to take part in the study. All players have at least eight years of football practise and four years of competitive experience in various football events. Participants (Table I) were randomly assigned to one of two groups: the experimental group training programme (EG, n = 15) or the control group training programme (CG, n = 15). Prior to performing the study, groups were matched based on the players' normalised strength values, muscular fitness, and body mass index, as well as their years of practise. A blocked restricted randomised procedure was employed for the subject group fitting. This procedure, which was carried out using a computer random number generator, produced balanced randomisation while also ensuring that both groups had equivalent mean values for each parameter. All participants in this trial were healthy, had no history of serious lower limb injuries, and were not given any medication. Following a verbal discussion of the possible risks and advantages of participating in this study, each participant provided written informed permission. The research was carried out in accordance with the Helsinki Declaration.

Table 1. Anthropometric characteristics of the participants.

Variables	Group	n	Mean	Std Deviation
Age	C	15	20.4000	.91026
	E	15	20.2000	1.14642
Height	C	15	171.2667	5.35146
	E	15	169.2667	6.26175
Weight	C	15	60.6667	6.92528
	E	15	58.7933	7.27122
Fat Mass	C	15	7.4733	2.72357
	E	15	8.1000	2.10034
Muscle Mass	C	15	50.9600	4.27030
	E	15	48.9133	5.12792
BMI	C	15	20.4667	.91235
	E	15	20.4200	.85624
Football Experience	C	15	4.2000	.56061
	E	15	4.1333	.63994

Notes: Data shown as mean ± SD for control (C, n = 15) and experimental (E, n = 15) groups.

2.2. Design

A randomised-controlled trial design was used to assess lower limb mobility utilising a range of exercises to assist football players in developing foot strength and stability, hence reducing acute ankle sprains during football games. Sensor placement; Proper signal detection is of most important simply position of the sensor on the intended muscle help to yield good results based on EMG activation Figure1.

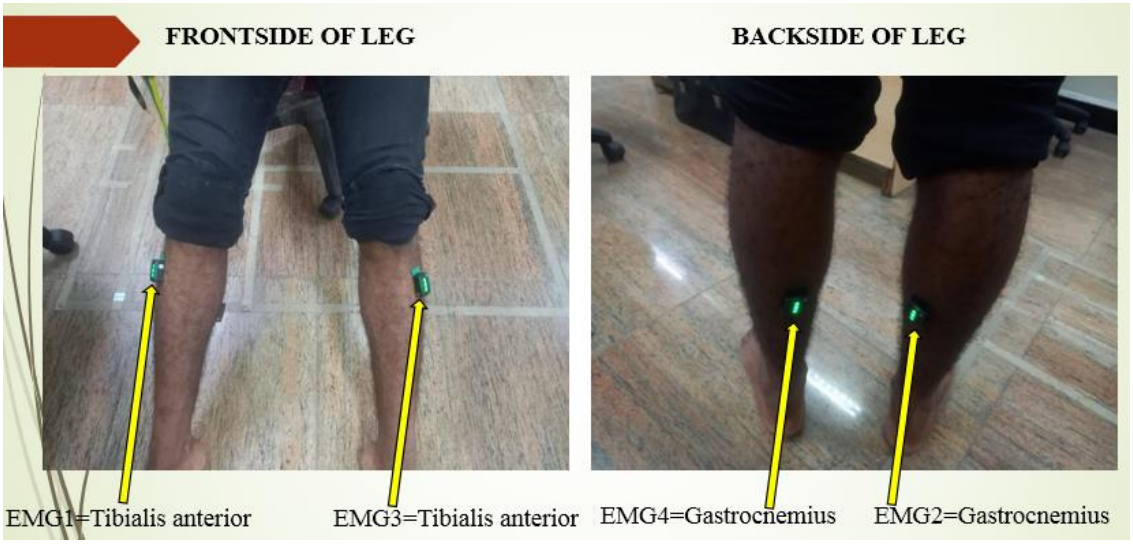

Figure 1. Wireless EMG Sensor placement

2.3. Lab Chart Software

Lab Chart, a computer programme used for creating lab charts, is used to record and analyse many kinds of experimental information. Is it the most adaptable way to transform your chart view's time-based raw data and calculations into discrete numbers for use in statistical testing? An individual's medical history is documented on a medical chart. A whole image of the patient may be gleaned from an accurate medical record. Further, the record contains crucial data that helps doctors make educated decisions about patients' treatment.

2.4. Delsys Kit

This is the kit which tend to act as the independent module for wireless system it has also the charging slot for charging the wireless EMG from this kit a USB cable is connected to the lap top which will be having a trigno software for activating the wireless EMG sensor. The Delsys kit can be shown on figure2.

2.5. Delsys Trigno Software

The Delsys Trigno Wireless System is the best starting point for building a custom EMG setup for your wireless physiological measuring requirements in the field of movement science. Because of this programme, you may connect your wireless EMG to your EMG set. Delsys trigno software can be shown on figure 3.

2.6. Wireless Emg Sensors

Get hold of some cordless EMG sensors and freely monitor your muscle's electrical activity. Wireless electromyography (EMG) has several potential uses in the field of exercise physiology. Capturing muscle contractions and electrical muscle activity without restricting your customers' range of motion is possible with wireless EMG. On the place where it was implanted, this sensor also helps in identifying the contractions of skeletal muscles.

2.7. Methodology

Subject was asked to do number exercises which are grouped into three groups' early steps exercises, Intermediate steps exercises and advanced steps exercises in barefoot. In each group there are number of exercises a Subject has to perform the exercises were performed sequentially based on training Programme Table 2. These activities was conducted within two weeks in each steps and acquire some biomechanical parameters This study aims to assess the effect of mountain climbers' exercise on lower limb movement to develop strength and stability in the leg for footballers hence helping in preventing acute ankle sprain. Thirty Footballers of the same average age of 20 years old were divided into two groups either a control group (n=15) or an experimental group (n=15), Height and weight of each subject were obtained and an average BMI was calculated as a normalized value. The control group was left to continue with their usual physical exercise which are termed as warm up football normal exercise while the experimental group was told to perform some numbers of exercises which are toe walk, marching form drill, up with one down with two and up with two down with one as exercise used by mountain climbers for 14 days as mentioned on the training programme Table 2. The exercises were performed for seven days repeatedly then the eight day was left as a resting day and after seven exercise days, the EMG value was taken based on the exercise performed and targeted muscles

being activated. The effect of both exercise normal footballer exercise and mountain climber exercise were assessed by performing the EMG test using Delsys IMU kit with wireless EMG sensors placed on TAM and GM on both left and right leg data obtained from the test a statistical analysis was performed.

Table 2. Training Programme

s/no	**Exercises**	**Guidelines**	**Weeks 1-2**
	Part I		
1.	Toe splay	Sit on a chair with your feet flat on the ground. Spread your toes apart as far as you can and hold for 2 seconds.	2 sets of 15 reps (perform each rep for 2 seconds)
2.	Ankle alphabet	Sit on a chair with your feet flat on the ground. Lift one foot off the ground and trace the alphabet in the air with your toes. Repeat with the other foot.	2 sets of 10 reps (perform each rep slowly and with control)
3.	Towel Grab	Sit on a chair with a towel on the ground in front of you. Place your foot on top of the towel and scrunch your toes to grab the towel.	2 sets of 10 reps (hold each rep for 5 seconds)
4.	Toe and heel walks	Stand with your feet hip-width apart. Walk forward on your toes for 10 steps, then walk back on your heels for 10 steps.	2 sets of 10 reps (walk back and forth for 2 minutes)
	Part II		
5.	UP with one, down with two	Stand with your feet hip-width apart and lift one foot off the ground. Slowly lower your foot back down, touching your toes to the ground first, then your heel. Repeat for 10 reps on one foot, then switch to the other foot.	2 sets of 10 reps (perform each rep slowly and with control) Cool-down: 5 minutes of stretching
6.	UP with two, down with one	Stand with your feet hip-width apart and lift both feet off the ground. Slowly lower one foot back down, touching your toes to the ground first, then your heel. Repeat for 10 reps on one foot, then switch to the other foot.	2 sets of 10 reps (perform each rep slowly and with control) Cool-down: 5 minutes of stretching
7.	Marching form drill	Stand with your feet hip-width apart and your arms at your sides. Lift one knee up to hip level while swinging the opposite arm forward. Lower your leg and repeat with the other leg and arm.	2 sets of 20 reps (perform each rep for 2 seconds) Cool-down: 5 minutes of stretching

3. STATISTICAL ANALYSIS

Descriptive statistical analysis was used in this research. This involved the calculation of summary measures of mean and root mean square (RMS), of the electromyography (EMG) signals obtained from the Tibialis anterior muscle (TAM) and gastrocnemius muscle (GM) on both left and right legs during various exercises. The primary aim of the descriptive statistical analysis was to provide a quantitative summary of the data and to facilitate an understanding of the pattern of muscle activation during different exercises. It is worth noting that this type of analysis did not involve any hypothesis testing or inferential statistics for making generalizations about the population.

Table 3. Synthesis of Review for Related Work

No	Author(year)	Purpose	Method	Findings	Similarity	Differences

1	J. Yu, D. Park, and G. Lee, Jan. 2013	Improvements in pain, muscle strength, endurance, and functional fitness	Experimen tal analysis	Effectiveness of eccentric strengthening exercises as a non-invasive and low-cost treatment option	Makes good use of exercises	patients with Achilles tendinopathy
2	G. L. Lentell, L. Katzman, Jun. 1990	Importance of muscle function in maintaining ankle stability	Experimen tal analysis	Interventions aimed at improving muscle function may be beneficial for preventing ankle injuries and improving rehabilitation outcomes.		ankle stability and various measures of muscle function
3	N.Trajković, Ž. Kozinc, Jun. 2021	Importance of ankle strength and range of motion for postural stability	Experimen tal analysis	improving ankle strength and range of motion may be beneficial for enhancing postural stability	Makes good use of exercises	ankle strength and range of motion, and postural stability
4	P. Zaki, S. Khakimov, May 2020	Improved injury prevention strategies and management	Experimen tal analysis	Fractures of the femur, tibia, and fibula accounted for a substantial proportion of soccer-related injuries	soccer-related injuries	reduce fractures soccer players

4. RESULTS AND DISCUSSION (FINDINGS OF THE STUDY)

The RMS value for the activation of the gastrocnemius muscle on the right leg (0.08510 mV) was higher than that of the Tibialis anterior muscle (0.03455 mV), whereas on the left leg, both muscles showed relatively similar activation values (TAM: 0.04315 mV and GM: 0.04926 mV).During the heel walk exercise, the RMS value for the activation of the Tibialis anterior muscle was higher on both legs (left: 0.16074 mV, right: 0.09158 mV) compared to the gastrocnemius muscle (left: 0.03120 mV, right: 0.04154 mV).For the marching form drill exercise, the RMS value for the activation of the gastrocnemius muscle was significantly higher (left: 1.32667 mV, right: 0.10763 mV) than that of the Tibialis anterior muscle (left: 0.14344 mV, right: 0.03319 mV).During the "up with two, down with one" exercise, the RMS value for the activation of the Tibialis anterior muscle was higher on the left leg (up with two, down with one: 0.10424 mV) compared to the right leg (up with one, down with two: 0.05430 mV). However, the RMS value for the activation of the gastrocnemius muscle was higher on the right leg (up with one, down with two: 0.05988 mV) compared to the left leg (up with two, down with one: 0.08142 mV). The opposite pattern was observed when the exercise was performed in reverse.

Table 4. Muscle activation data for Experimental group Using wireless EMG Sensors

Exercise	**Left Leg EMG values**		**Right Leg EMG values**	
	Muscles Activated	**RMS(mV) Mean**	**Muscles Activated**	**RMS (mV) Mean**
Toe walk	Tibialis anterior	0.04315	Tibialis anterior	0.03455
	Gastrocnemius	0.04926	Gastrocnemius	0.08510
Heel Walk	Tibialis anterior	0.16074	Tibialis anterior	0.09158
	Gastrocnemius	0.03120	Gastrocnemius	0.04154
Marching form drill	Tibialis anterior	0.14344	Tibialis anterior	O.03319
	Gastrocnemius	1.32667	Gastrocnemius	0.10763

Up with one, Down with two (up with left leg)	Tibialis anterior	0.05233	Tibialis anterior	0.04267
	Gastrocnemius	0.03341	Gastrocnemius	0.15049
Up with one, Down with two (up with right leg)	Tibialis anterior	0.05430	Tibialis anterior	0.04478
	Gastrocnemius	0.05983	Gastrocnemius	0.05988
Up with two, Down with one (Down with left leg)	Tibialis anterior	0.10424	Tibialis anterior	0.02449
	Gastrocnemius	0.08142	Gastrocnemius	0.12806
Up with two, Down with one (Down with right leg)	Tibialis anterior	0.13382	Tibialis anterior	0.06615
	Gastrocnemius	0.07592	Gastrocnemius	0.14679

Note: Tibialis anterior = EMG1 for Right Leg and EMG3 for Left leg. Gastrocnemius = EMG2 for Right Leg and EMG4 for Left leg considering image on Fig1.Only muscle contraction values were taken. Randomly EMG window selection was applied. Three data from sensor were taken and averaged. The RMS were calculated followed by mean calculation. Wireless EMG sensor placed at the particular targeted muscle. Each muscle is activated the most based on the exercise being performed. Compare left leg EMG values based on TAM vs. GM similarly to the right leg. EMG Data collection trends tells about improvement. Data collected from Strength and stability test followed by t-test analysis helped on comments on exercise effectiveness between EG and CG.

Figure 2. Delsys EMG kit

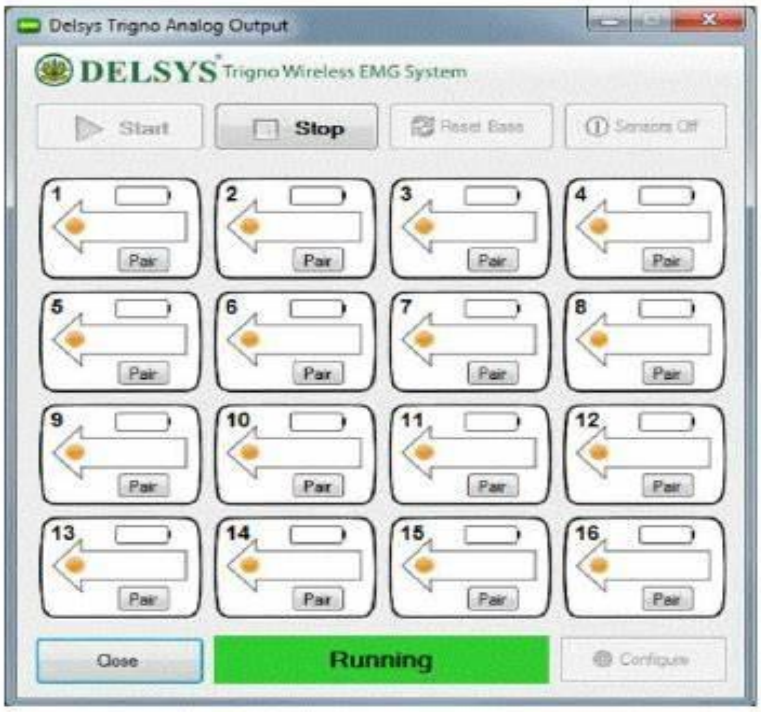

Figure 3. Delysys Trigno Software

The aim of this research work was to assess lower limb movement to develop strength and stability in the foot for football sport game players. The data was collected through electromyography (EMG) to measure the activation of Tibialis anterior muscle (TAM) and gastrocnemius muscle (GM) during different exercises including toe walk, heel walk, marching form drill, and up with two, down with one.

The results of the study showed that the TAM and GM muscles were both activated during all the exercises, indicating that these exercises could be effective in developing muscle strength and stability in football players. The TAM and GM on the left leg were relatively similar during the toe walk, whereas in the right leg, the GM seemed to be more activated than the TAM. During the heel walk, the EMG value of TAM on both legs was more activated as compared to the EMG value of GM of the left and right leg.

The marching form drill exercise seemed to activate more GM on both legs as compared to TAM. During the up with two, down with one exercise, the TAM of the left leg was more activated than GM on the same leg, whereas the TAM of the right leg was less activated as compared to the GM of the same leg. The values showed a mirror reflection when the same exercise was performed in the reverse way by starting with the other leg.

Tibialis anterior and Gastrocnemius muscles are vital for ankle stability and control and are frequently addressed in ankle sprain prevention therapies. The Tibialis anterior is responsible for ankle dorsiflexion and foot inversion, whereas the gastrocnemius is responsible for ankle plantar flexion and knee stability during movement. Single-leg balancing exercises and calf raises are examples of exercises that target the Tibialis anterior and gastrocnemius muscles. Athletes can lower their risk of ankle sprains by strengthening these muscles and increasing their proprioceptive control.

However, the study had some limitations, including the lack of pickup volume of the surface electrode, which could have led to additional muscles contracting in a way that interferes with the targeted muscle if the fiber of a synergetic antagonistic muscle is included. Additionally, the self-exercise initiative performed by some individuals in the control group may have altered the final results.

4.1. Research Gap

The research gap that prompted the conduct of this study was lack of evidence-based interventions to prevent acute ankle sprains in footballers. Acute ankle sprains are a common injury among football players, and

they can have significant negative effects on their performance and career. Therefore, there is a need for effective preventive measures to reduce the incidence of ankle sprains in footballers. The study aimed to fill this research gap by investigating the effects of mountain climber exercises on lower limb strength and stability, which are essential for preventing acute ankle sprains in footballers based on Tibialis anterior and Gastrocnemius muscles.

By considering above mentioned gap found from literature review, current study has been performed to fill above mentioned gap.

4.2. Future Trends of the Study

Future work should include more participants, pickup volume of the surface electrode, assessing the strength and stability of the same exercises using a force plate which is the gold standard for testing muscle strength and stability involving many force related parameters and further investigations into other muscles involved in lower limb movement.

5. CONCLUSION

In conclusion, based on the data obtained, it can be concluded that the TAM and GM muscles are being activated during exercises aimed at developing muscle strength and stability in football players. The study findings provided practical evidence that these exercises can improve the strength and stability of football players and thus contribute to preventing ankle sprains.

ACKNOWLEDGMENT

Special thanks goes to all the footballers who volunteered for this study, my guide Dr. Varshini karthik (PhD) for her care and support and last but not least the SRMIST for providing the facilities to conduct this research

REFERENCES

[1] J. Yu, D. Park, and G. Lee, “Effect of Eccentric Strengthening on Pain, Muscle Strength, Endurance, and Functional Fitness Factors in Male Patients with Achilles Tendinopathy,” Am. J. Phys. Med. Rehabil., vol. 92, no. 1, pp. 68–76, Jan. 2013, doi: 10.1097/PHM.0b013e31826eda63.

[2] G. L. Lentell, L. L. Katzman, and M. R. Walters, “The Relationship Between Muscle Function and Ankle Stability,” J. Orthop. Sports Phys. Ther., vol. 11, no. 12, pp. 605–611, Jun. 1990, doi: 10.2519/jospt.1990.11.12.605.

[3] P. Zaki, S. Khakimov, J. Hess, and W. Hennrikus, “Femur, Tibia, and Fibula Fractures Secondary to Youth Soccer: A Descriptive Study and Review of the Literature,” Cureus, May 2020, doi: 10.7759/cureus.8185.

[4] N. Trajković, Ž. Kozinc, D. Smajla, and N. Šarabon, “Relationship between ankle strength and range of motion and postural stability during single-leg quiet stance in trained athletes,” Sci. Rep., vol. 11, no. 1, p. 11749, Jun. 2021, doi: 10.1038/s41598-021-91337-6.

[5] K. McBain et al., “Prevention of sport injury II: a systematic review of clinical science research,” Br. J. Sports Med., vol. 46, no. 3, pp. 174–179, Mar. 2012, doi: 10.1136/bjsm.2010.081182.

[6] M. Hammami, N. Gaamouri, R. J. Shephard, and M. S. Chelly, “Effects of Contrast Strength vs. Plyometric Training on Lower-Limb Explosive Performance, Ability to Change Direction and Neuromuscular Adaptation in Soccer Players,” J. Strength Cond. Res., vol. 33, no. 8, pp. 2094–2103, Aug. 2019, doi: 10.1519/JSC.0000000000002425.

[7] K. Fousekis, E. Tsepis, and G. Vagenas, “Lower limb strength in professional soccer players: profile, asymmetry, and training age,” J. Sports Sci. Med., vol. 9, no. 3, pp. 364–373, 2010.

A. Dello Iacono, J. Padulo, and M. Ayalon, “Core stability training on lower limb balance strength,” J. Sports Sci., vol. 34, no. 7, pp. 671–678, Apr. 2016, doi: 10.1080/02640414.2015.1068437.

[8] J. F. M. Fleuren, G. J. Snoek, G. E. Voerman, and H. J. Hermens, “Muscle activation patterns of knee flexors and extensors during passive and active movement of the spastic lower limb in chronic stroke patients,” J. Electromyogr. Kinesiol. Off. J. Int. Soc. Electrophysiol. Kinesiol., vol. 19, no. 5, pp. e301-310, Oct. 2009, doi: 10.1016/j.jelekin.2008.04.003.

[9] K. Jeon, S. Chun, and B. Seo, “Effects of muscle strength asymmetry between left and right on isokinetic strength of the knee and ankle joints depending on athletic performance level,” J. Phys. Ther. Sci., vol. 28, no. 4, pp. 1289–1293, Apr. 2016, doi: 10.1589/jpts.28.1289.

[10] M. Beato, D. Young, A. Stiff, and G. Coratella, “Lower-Limb Muscle Strength, Anterior-Posterior and Inter-Limb Asymmetry in Professional, Elite Academy and Amateur Soccer Players,” J. Hum. Kinet., vol. 77, pp. 135–146, Jan. 2021, doi: 10.2478/hukin-2020-0058.

[11] R. Lovell, M. Knox, M. Weston, J. C. Siegler, S. Brennan, and P. W. M. Marshall, “Hamstring injury prevention in soccer: Before or after training?,” Scand. J. Med. Sci. Sports, vol. 28, no. 2, pp. 658–666, Feb. 2018, doi: 10.1111/sms.12925.

[12] B. F. Mentiplay et al., “Lower limb musculoskeletal screening in elite female Australian football players,” Phys. Ther. Sport, vol. 40, pp. 33–43, Nov. 2019, doi: 10.1016/j.ptsp.2019.08.005.

Monitoring Magnetic Resonance Imaging Coldhead by Using Sound Selectivity Method

Upendo S. Busanya[1], Varshini Karthik[2], Ashokkumar. D[3]
[1,2,3]Department of Biomedical Engineering, SRM Institute of Science and Technology, Tamilnadu, India

ABSTRACT

The study is intended to design a system for detecting the on and off states of Magnetic resonance imaging coldhead using sound selectivity method, which will help to monitor the coldhead at a distant range and hence protect the machine from helium lose due to any malfunction of cooling system. The sound sensor detects the sound given by the coldhead during the on state and process in the microcontroller, the processed signal when sound is heard is considered as coldhead is on, while the signal at no sound condition is considered as coldhead is off and at this point the alarm alerts and the message is sent o respondent service engineer through GSM mode. The alarm from the designed system alerts the technician near the place, and the GSM sends message to the Site Engineer who will reach at field area and take the logs from the designed system through the IOT as well as reset the system again after resolving the coldhead problem. The designed system help to prevent an event that the machine is too hot and too much helium evaporates due to off state of the coldhead which may cause the magnet to quench if further actions are not taken in time, this is done by using Sound selectivity device which will capture the sound of the coldhead and monitor it's condition in 24/7 and send immediate information about the coldhead state to a respondent engineer.

Keywords: Resonance imaging (MRI), Coldhead, Sound selectivity method

Corresponding Author:
Dr. Ashokkumar D,
Associate Professor, Department of Biomedical Engineering
SRM Institute of Science and Technology, Kattankulathur, 603203, Tamil Nadu, India
Email: ashokd@srmist.edu.in

1. INTRODUCTION

MRI imaging equipment is complex in both mechanics and computer technology, but is, very basically, a machine that scans the body using radio waves, and uses electromagnetic field data to create images of different parts of the body. Magnetic Resonance Imaging machines require quite a bit of energy, a specially designed containment area, and climate control in order to work properly and reach their optimal life spans.

The MRIs cooling system is a helium-based system that keeps the magnet cool during imaging. The magnet works with a superconductive coil which requires near zero temperature to create an electromagnetic field. In order to keep the magnet cool, it is constantly bathed in liquid helium at -452.4ºC. The liquid helium is constantly boiling, and will quickly begin to evaporate if exposed to too much heat, so the cold head works to eliminate this excess heat. The cold head is used to re-condense gaseous helium that has evaporated from the liquid helium inside. Once re-condensed, it can be added back to the supply of liquid helium

The state from which the coldhead is on by giving out sound is not always known to customers. Hence the conditions for rise in temperature or its stability, water flow and helium level are observed by the factory responsible. This important state of coldhead on or off may bring a lot of problems to the machine, unfortunately the user may not have the technical knowledge, and in that case monitoring of MRI coldhead is required to alert the service engineer of such occurrences at site location. [1].

The mechanical activity of the coldhead leads to vibrations, that vibration creates sound which can be heard from inside the magnet and outside throughout the filter panel and quench pipe hence the monitoring of coldhead activity by recording the audible signal is possible outside the RF cabin.In this study, the designed system is purposely monitoring the MRI coldhead based on audible characteristics of the coldhead and perform the following two main tasks (i) Detect the coldhead audible signal and process the on and off state ,(ii) Inform the surrounding user with alarm signal and send message to respondent engineer for the off condition of the coldhead in order to arrive at site location without delay and resolve the problem.

2. LITERATURE REVIEW

Beyer J, et al (2017) have studied the mechanical activity of the Magnetic resonance imaging and used the knowledge of vibrations related to coldhead to monitor any problem that may occur to endanger the coldhead activity and by doing so provides sufficient information if there is any failure on MRI coldhead which may cause it to stop and the helium heats to gas increasing pressure and leave from open valve throughout the quench pipe, hence helium loss. The study was possible by analyzing the noises and vibrations due to mechanical activity of the coldhead and used piezoelectric sensor to monitor these condition and the measurements was taken in all locations while the operating procedure is taken and while not in different scenario and the working of coldhead was determined. In this case the monitoring was able to be done without coming in contact with a scanner and designed system was accuracy to forecast the failure of MRI's coldhead by means of vibrations details received [1].

F. Steinmeyer, et al (2002) explained about the circular process on the system to maintain the cryogenic fluid which must be useful as a cooling system of Magnetic resonance imaging (MRI) systems all over the world and many machines has been ramp up and shim for imaging using this technology in many health care centers and hospitals. The audible sound of coldhead has been the mark for its activity to work as the cooling system where the field engineer will detect the condition from its sound this is an importance task for maintaining the superconductor magnetic state which requires a very cold state of nearly to zero. The process of refilling is done through the open valves near the quench pipe. [2].

Richard B. Buxton (2009) Reminds of the important tasks performed by Magnetic resonance imaging in a field of health care department where a lot of medical diagnosis are done especially one based on soft tissues and hence become a major medical device all over the world. The knowledge of Magnetic resonance imaging has made the work of many specializations easily not only in radiology department but also other departments [3].

Shafiya Sabah, et al (2022) explains why it is necessary to provide preventive maintenance and corrective maintenance to medical devices for their sustainability and also the regular inspections of these machines is needed with respect to safety check and services, the upgrading and care handling of medical

systems should be followed by all medical centers and hospital before they bring to huge damage and brought to higher cost or perhaps loss of an equipment. In that case the study has given more information on systematic procedures based on research and experiences from different hospital and health centers. The descriptions are very important for increasing the life span of the machine and hence beneficial for the merit purpose of an institution providing health service [4].

3. MATERIALS AND METHODOLOGY

This part explains about the development of sound sensor hardware and microcontroller with signal analysis and data processing bus, transmission and acquisition system. The sound detection is done by sound sensor and the audible signal is processed by a microcontroller and sent to informative destination by the use of GSM mode.

Sound Sensor

A sound detected via microphone; affects the diaphragm made of magnets warped with a metal wire, the effect of sound signals causes the magnets to vibrate at once current excited from the coils. The volume of sound has set point adjusted via an on board potentiometer. It can be used to set a required range of decibels and frequency heard at the filter panel and when the amplitude of sound reaches exactly range the output counts LOW, or else HIGH.

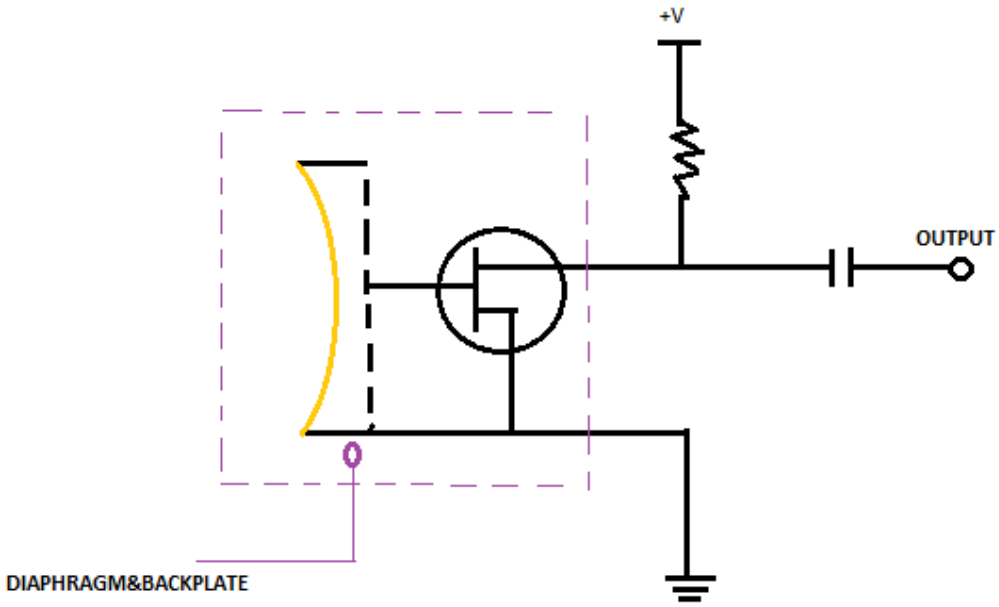

Figure 4.1. Sound Sensor diagram

Figure 4.1.Sound Sensor diagram**,** Shows when the couldhead sound reaches into the microphone it generates sound waves that strike the diaphragm causing it to vibrate, the vibrations at the diaphragm by sound waves leads to displacement and changes at the capacitance are produced. As the result electrical signal and output is generated, which can be measured and determine the amplitude of the sound. The voltage terminal and output terminal connects to the microcontroller for signal processing.

3.1 Signal Processing

The mechanical activity of the coldhead gives rise to vibrations. The vibrations create sound which can be heard at the filter panel outside the RF cabin where the sound sensor is located and receive these sound waves. The voltage is generated and signal acquired by the 8-bit micro-controller ATmega328P. If the sound sensor detects a volume range as adjusted by the potentiometer, the counts goes to LOW. However, we must ensure that the sound is caused by cold head and not by background noise. Therefore, we wait for 1000

milliseconds or 1 second after the output goes low. If the output remains LOW, the message "COLD HEAD ON" is printed on a display. When the sound goes off and there is no detection by the sound sensor, the microcontroller updates the false changes and output goes to HIGH. Similarly the to make sure that there is no sound signal the void count waits for 3minutes before replacing the message to "COLD HEAD OFF" and send to respondent person's mobile while displaying and give alert for the user around.

3.2 Measurement setup

The measurement was conducted on 3T MRI System (Magnetom Spectra, Siemens, Germany). The Sound sensor was positioned at the filter panel where the helium cables to the compressor pass through and the disconnected shim cable leaves a little space to help an audible sound detection from outside the RF cabin possible by the microphone at a minimum range of 40 to 50dB and 1 KHz.

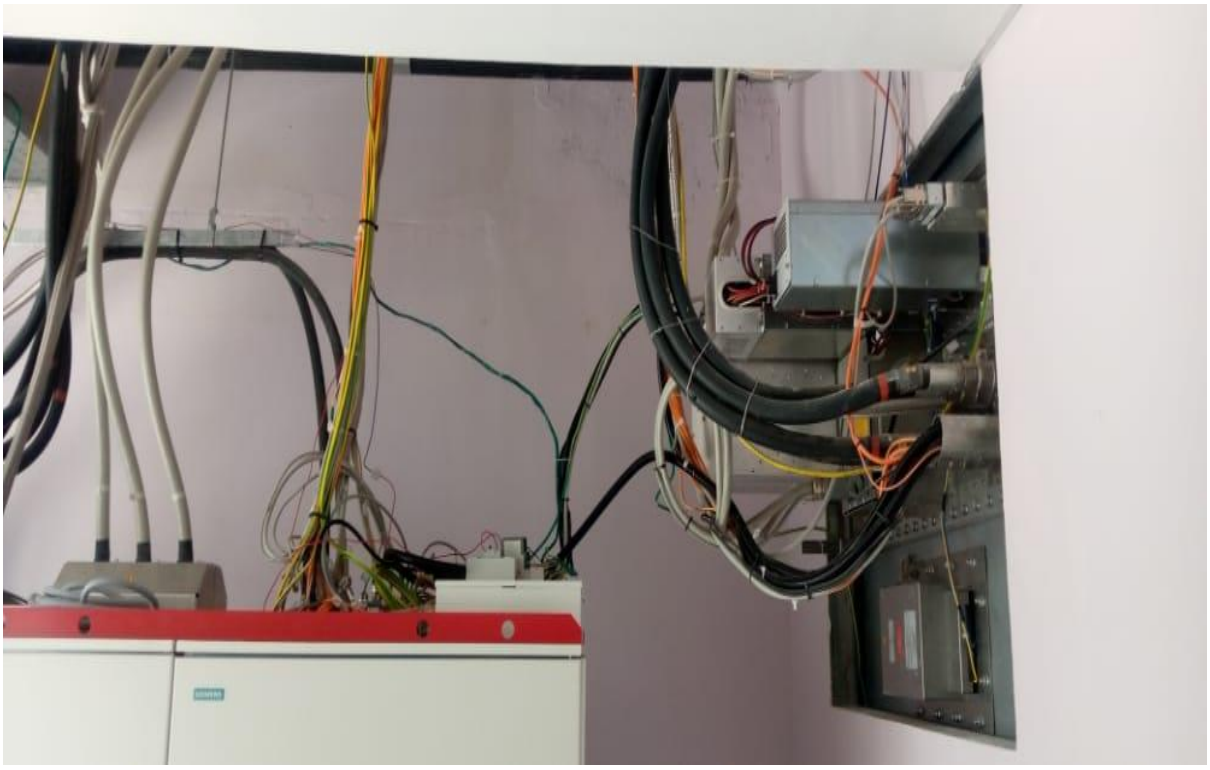

Figure 4.2. MRI filter panel

From the Figure 4.2.MRI filter panel the continuously sound is audible at constant range in such that the sound sensor is adjusted to it throughout potentiometer.

3.3 Block diagram

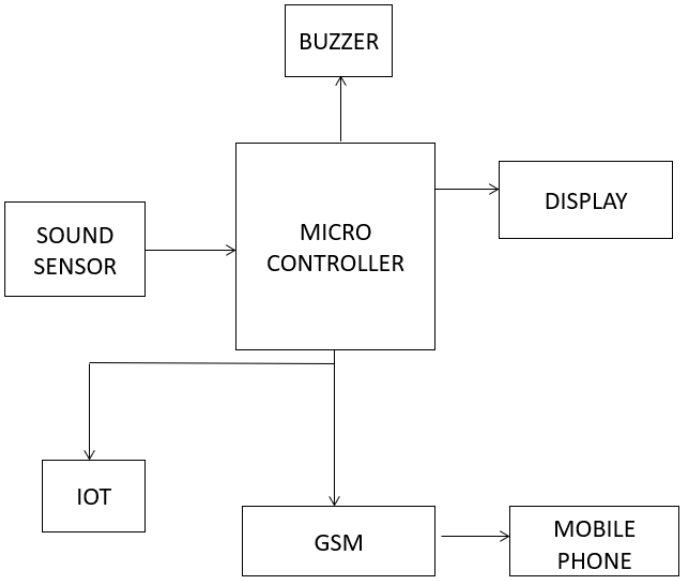

Figure 4.3. The block diagram of the MRI coldhead monitoring system using sound selectivity method.

Figure 4.3.The block diagram of the MRI coldhead monitoring system using sound selectivity method, shows a schematic signal analysis steps from the detection at sound sensor where the analogue signal is converted to electrical signal and processed in a micro-controller in a low and high conditions, the false signal which is considered as void count will change the output informative message to the user throughout GSM as "COLD HEAD OFF" and alert the surrounding while displaying on digitizer. The alarm sounds through the buzzer.

3.4. Circuit diagram

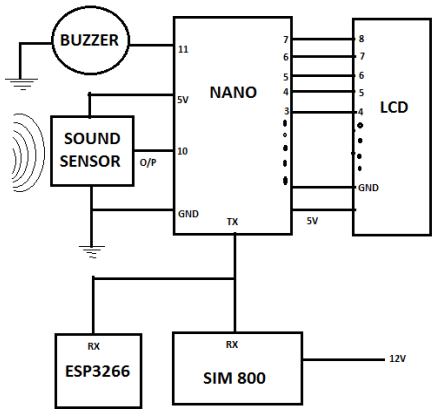

Figure 4.4. The circuit diagram for the MRI coldhead monitoring system using sound selectivity method.

Figure.4.4.the circuit diagram for the MRI coldhead monitoring system using sound selectivity method, shows the circuit diagram from which the sound signal detected from the sound sensor is sent to the Nano throughout the output and 5v terminal and is processed by this microcontroller to count on the true and false updates for the analysis, depending on the output the displays on the LCD and the sound may alert on buzzer connected to Nano terminal for the false signal. Sim 800 is connected to transmitter terminal of the micro-controller in which the message to inform the user or respondent person is sent. The ESP8266 receives data from Nano for log in purpose.

3.5. Arduino nano

Arduino Nano is the micro-controller used in this project to integrate with other device, It is processing device programmed with necessary configurations to count the input signal from the sound sensor and connect to other components with necessity commands to give out feedback for the monitoring purpose. It is very small based on ATmega328P powered by USB cable under 9V.

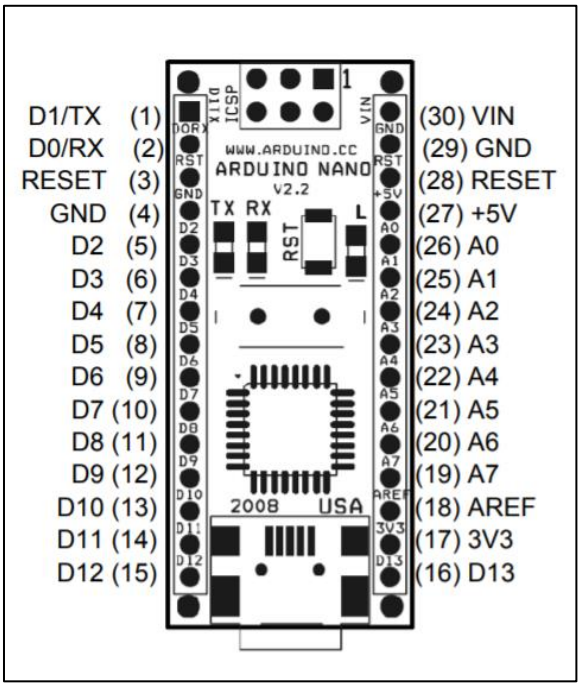

Figure 4.5. Arduino nano

3.6 Buzzer

The general-purpose buzzer is commonly used in alarm and indication applications by converting signal to sound. It can operate from 6V to 12V and hence can be used in a wide range of systems. It sounds when the false count signal is received as the result of cold head off.

3.7 LCD

The LCD is used to interface with any kind of microprocessor target boards such as 8051, AVR, Arduino, and any other processors. The board comes with 4-bit data and 3-bit control pins. The board has to be powered with +5V. This breakout board helps bring up a family of monochrome graphic LCDs. By breaking the ZIF tail of the compatible displays out to a 16-position 0.1" header connecting the display is a breeze.

3.8 SIM 800

SIM800 is another important device connected to our monitoring system, its aim is to send message to the respondent person about the current status of the MRI coldhead and alert when the coldhead is off. SIM800 is a GSM/GPRS module which supports quad-band: GSM850, EGSM900, DCS1800 and PCS1900 networks that can be used all over the world.

The voltage operating range from 3.4v to 4.4v and it has necessity pins which can be connected to micro-controller by UART with baud rate from 1200bps to 115200bps.

Figure 4.6. Buzzer

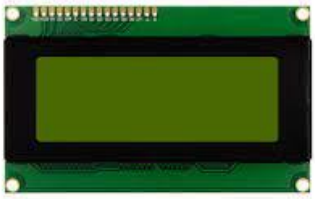

Figure 4.7. LCD

Figure 4.8. SIM 800

3.9 Data storage and accessibility

The output data is collected from the device by means of internet of things using ESP8266 which can help with exchanging data from the system device to another device by means of internet. The ESP8266 is capable of connecting via Wi-Fi and enable the service engineer to log in the dashboard and collect the update status of recently time and condition of Coldhead. The technology enables designed system to communicate with other systems through network access.

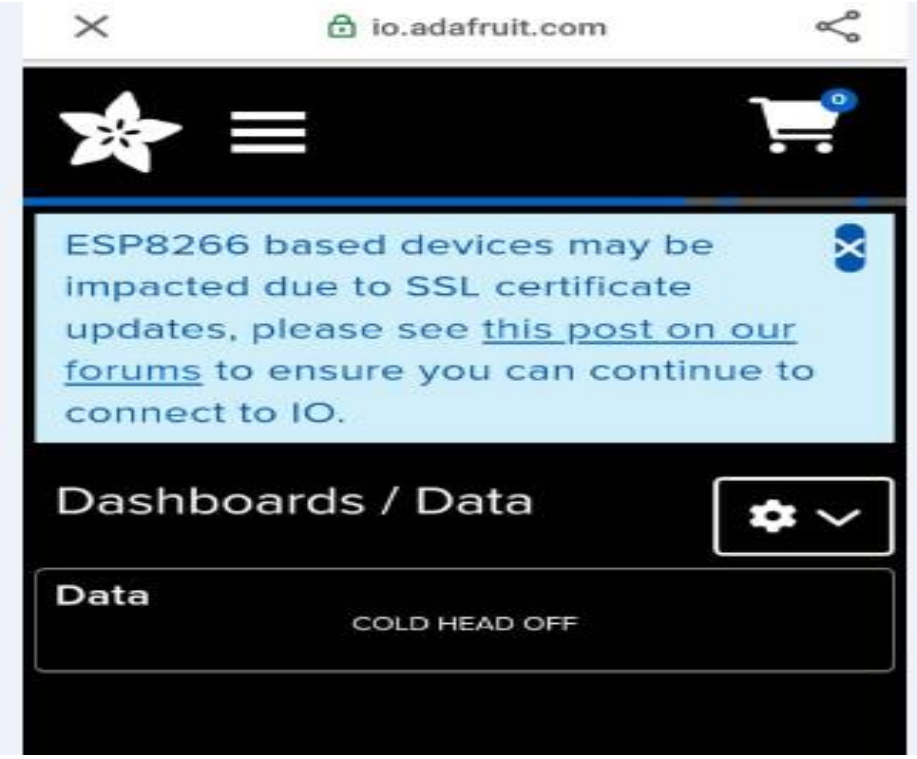

Figure 4.9. Data storage output

4. RESULTS

The audible sound were acquired at the filter panel of the MRI and processed according to the adjusted required range of volume decibels and frequency from the Coldhead and were determined to be the true sound from the MRI coldhead neglecting the interference with the feature mechanical characteristics of MRI coldhead that it must be heard continuously without stopping only to enable the circulation of helium and maintain the cooling system. The output where taken for the false updates where the coldhead sound were not audible to confirm the status event that coldhead should be off when there is no sound, at this condition the informative message is sent to respondent person or user for quick measurements to be taken

5. DISCUSSION AND CONCLUSION

The recording of experimental work for monitoring an MRI's coldhead status was conducted. The audible sound from coldhead mechanical vibrations was detected by the sound sensor positioned at the filter panel at the dB range of 40 to 50 dB and 1 KHz, which was processed by the micro-controller and used to determine the coldhead state as on for true signal and off for false signal.

The method was based on sound selectivity to identify the state of coldhead when it is on and off condition. The auditory frequency selectivity idea as explained by John Foster, et al (1985) gives the wide knowledge on how we may use auditory organ to determine and process sound as well as selecting particularity on identification of place of articulation. [5]

The Study of MRI pulse sequence as written by Bernstein et al (2004) was supportive to know the continuation of pulses as the coldhead changes the gas helium back to its liquid state hence required to be active all the time in 24/7[6] due to the electromagnetic characterization of superconducting radiofrequency coils which requires a very cold state near zero and hence helium preserve it when is in cold liquid state, Sabelle Saniour et al (2020) [7].

The study experiment differs from the one done by Redwane Zaaboul et al (2020) from which they monitored the coldhead by vibration method, the vibrations was monitored from different positions of the MRI scanner which gives out vibration signals and processed for determining the failure of coldhead [8].

6. LIMITATIONS AND FUTURE WORKS

Due to the requirement of the RF cabin, the mostly part of it is covered hence find difficult to access the high range of audible volume dB of the MRI cold head. From this study we have introduces the possibility of accessing the minimum dB that could be heard from the filter panel by adjusting the potentiometer to match the audible range. However further research has been done and developed devices to monitor MRI cold head based on different phenomenon. Either this work can still be supportive since will always find the way to access the sound from outside, e.g from quench pipe which receives the mechanical vibrations from the cold head directly and give it out in form of sound, here we can position our sensor and always receive the sound for monitoring purpose.

ACKNOWLEDGMENT

I would like to sincerely thank the management of SRMIST for providing the research facilities to conduct this study.

REFERENCES

[1] Beyer, J., Krug, J. and Friebe, M. (2017) "Monitoring the Coldhead of Magnetic Resonance Imaging Systems by Means of Vibration Analysis". Journal of Sensor Technology, 7, pp.39-51.
[2] Steinmeyer, F., P. W. Retz, K. White, A. Lang, W. Stautner, P. N. Smith, and G. Gilgrass. (2002) "Towards the invisible cryogenic system for Magnetic Resonance Imaging". Advances in Cryogenic Engineering, 47, pp. 1659–1666.
[3] Buxton, R. (2009) "Introduction to Functional Magnetic Resonance Imaging: Principles and Techniques, Cambridge University Press.
[4] S. Sabah, M. Moussa and A. Shamayleh, (2022) "Predictive Maintenance Application in Healthcare," 2022 Annual Reliability and Maintainability Symposium (RAMS), pp. 1-9.
[5] Summerfield, Q., Foster, J., Tyler, R., & Bailey, P.J. (1985) "Influences of formant bandwidth and auditory frequency selectivity on identification of place of articulation in stop consonants", Speech Commun., 4, pp. 213-229.
[6] Bernstein, MA, King, KF & Zhou, XJ. (2004) "Handbook of MRI Pulse Sequences", Elsevier Inc.
[7] Saniour, I., Geahel, M., Briatico, J. et al. (2020) "Versatile cryogen-free cryostat for the electromagnetic characterization of superconducting radiofrequency coils", EPJ Techn Instrum **7**(3), pp. 1-11.
[8] R. Zaaboul, M. H. El Yousfi Alaoui and S. El Hani, (2020) "Vibration monitoring of the MRI Scanner's cold head," 2020 International Conference on Electrical and Information Technologies (ICEIT), pp. 1-5.

Puducherry - India
www.melangepublications.com

ISSN : 2456 - 1983
www. iirjet.org